University of Alberta

Archean and Proterozoic evolution of the Beaverlodge Belt, Churchill craton, Canada

by

Russell P. Hartlaub ©

A thesis submitted to the Faculty of Graduate Studies and Research in partial fulfillment of the requirements for the degree of Doctor of Philosophy

Department of Earth and Atmospheric Sciences

Edmonton, Alberta

Fall, 2004

Library and Archives Canada

Published Heritage Branch

395 Wellington Street
Ottawa ON K1A 0N4
Canada

Bibliothèque et Archives Canada

Direction du Patrimoine de l'édition

395, rue Wellington
Ottawa ON K1A 0N4
Canada

Your file Votre référence
ISBN: 0-612-95943-0
Our file Notre référence
ISBN: 0-612-95943-0

The author has granted a non-exclusive license allowing the Library and Archives Canada to reproduce, loan, distribute or sell copies of this thesis in microform, paper or electronic formats.

The author retains ownership of the copyright in this thesis. Neither the thesis nor substantial extracts from it may be printed or otherwise reproduced without the author's permission.

L'auteur a accordé une licence non exclusive permettant à la Bibliothèque et Archives Canada de reproduire, prêter, distribuer ou vendre des copies de cette thèse sous la forme de microfiche/film, de reproduction sur papier ou sur format électronique.

L'auteur conserve la propriété du droit d'auteur qui protège cette thèse. Ni la thèse ni des extraits substantiels de celle-ci ne doivent être imprimés ou aturement reproduits sans son autorisation.

In compliance with the Canadian Privacy Act some supporting forms may have been removed from this thesis.

While these forms may be included in the document page count, their removal does not represent any loss of content from the thesis.

Conformément à la loi canadienne sur la protection de la vie privée, quelques formulaires secondaires ont été enlevés de cette thèse.

Bien que ces formulaires aient inclus dans la pagination, il n'y aura aucun contenu manquant.

Canada

Abstract

The Murmac Bay Group of the Beaverlodge Belt, Churchill craton, Canada, formed during continental extension (rifting) of an ancient Meso- to Paleoarchean crustal block. This crustal block is identified on the basis of Nd model ages, xenocrystic zircons, and the 3060 ± 40 and 2999 ± 7 Ma U-Pb crystallization ages for the Lodge Bay and Cornwall Bay granites, respectively. Ancient ca. 3.62 and >3.7 Ga grains dominate the detrital zircon population of the Murmac Bay Group sediments, but deposition occurred after ca. 2.77 Ga, the youngest detrital zircon in this study. The age of the Murmac Bay Group is thus constrained as younger than ca. 2.77 Ga and older than the crosscutting 2631 ± 12 Ma Dead Man and Donaldson Lake granites. The gross lithological and stratigraphic make-up of the Murmac Bay Group closely resembles that of the Prince Albert, Woodburn Lake and Mary River Groups of the northwestern Churchill craton, all three of which have been interpreted as ca. 2.7 Ga continental rift successions. The Murmac Bay Group is interpreted to be correlative with these successions. If correct, the total length of this Neoarchean rift is at least 2000 km and records the break-up of a large Paleo- to early Neoarchean continent (Nunavutia).

The Murmac Bay Group has been invaded by a suite of ca. 2.3 Ga post-orogenic granites. The emplacement of these granites was coeval with middle to upper amphibolite-facies metamorphism and deformation (M_1,D_1) based on ca. 2.3 Ga metamorphic monazite and zircon. Local ca. 2.3 Ga metamorphism, deformation, and magmatism is a small component of regional ca. 2.3 Ga crustal reworking related to the

Blezardian Orogeny. This major magmatic arc and collision zone developed along the western margin of the Churchill craton from ca. 2.4-2.26 Ga.

Ca. 1.98-1.93 Ga crustally derived magmatism in the Beaverlodge Belt, including the Feil Lake and Uranium City granites, is coeval with tight to isoclinal folding (D2) and regional middle amphibolite to granulite facies metamorphism. Ca. 1.9 Ga open-to tight-folding (D_3) coincided with exhumation of high-grade rocks, and may be related to the final phases of Churchill-Slave-Buffalo Head intracontinental deformation.

Acknowledgments

The years of research that are reflected in this manuscript began through a simple invitation by Ken Ashton. Sitting on an outcrop and discussing future plans, Ken asked if I would like to be part of a long-term project to study Precambrian supracrustal rocks in an area that was about as far north as you could go without leaving Saskatchewan. Ken promised spectacular scenery and lots of bedrock exposure. I was hooked. Both the scenery and bedrock were far more spectacular than I had hoped. Ken's enthusiasm for geological discussion helped to keep me focused on improving this work. Thanks Larry, for your eye to detail and for asking all the right questions. Tom, I have learned a lot of positive things from the way you treat your students. I feel truly lucky to have worked with two supervisors who are so good at what they do, who deeply understand the scientific method, and who work so well together. An important contributor to my doctoral experience was Chris Böhm. I already miss our long discussions on Geology, Canadian Culture, and everything else. The Manitoba Geological Survey is lucky to have you.

Danielle Boivin, Colin Card, Erin Chorney, Jeff Coolican, Sarah Ehman, Bryan Hartall, and Robert McFadyen provided invaluable assistance in the field. I would like to thank Bob Macdonald, Charlie Harper, and especially Tom Sibbald for sharing their first-hand knowledge of the Uranium City Area. Tom Sibbald also allowed me to use some of his excellent original maps and field data. Appreciation is extended to Kevin Ansdell, Mel Stauffer, and Julie Bergeron for the geological tour of the Black Bay Fault. A big thank you goes to all the staff of the

Saskatchewan Geological Survey who organized field equipment, arranged field assistants, provided me with base-maps and gave me a venue for scientific discussion at the annual Open House.

Much of my work has been facilitated by the world-class technical staff at the University of Alberta. Mark Labbe and Don Resultay provided ongoing advice and help with thin sections, grain mounts, crushing equipment and more. Sergei Matveev is a master with the electron microprobe. It would be a true accomplishment on my part if I could understand half the technical information that he gave me. Stacey Hagen was not only my aide at the Mass-spectrometer, but a true spirit-inflator. She made my numerous hours in the Lab more enjoyable.

Finally, thank you Valerie for sticking with me right to the end. Your visit to U-city was the highlight of my summer. Without you I would know nothing about libraries, international development, and igneous, err … I mean metamorphic, rocks.

Table of Contents

ABSTRACT

ACKNOWLEDGEMENTS

TABLE OF CONTENTS

LIST OF TABLES

LIST OF FIGURES

CHAPTER 1: Introduction 1

CHAPTER 2: The Archean Murmac Bay Group: evidence for a giant Archean rift in the Rae Province, Canada 9

CHAPTER 3: Ca. 2.3 Ga magmatism in the western Canadian Shield: remnants of an important period of Laurentian accretion 61

CHAPTER 4: Paleoproterozoic metamorphism and deformation of the Archean Churchill craton, Canada: new results from the western Beaverlodge Belt, Saskatchewan 99

CHAPTER 5: An ancient (Meso- to Paleoarchean) crustal block in the Rae Province, Saskatchewan: evidence from Sm-Nd and U-Pb constraints 151

CHAPTER 6: Concluding remarks 182

List of Tables

Table 2-1. Geochemical data table for Murmac Bay Group basalts and gabbros. **56**

Table 2-2. U-Pb data table. **59**

Table 3-1. U-Pb data table **92**

Table 3-2. Whole rock geochemistry of the North Shore Plutons. **94**

Table 3-3. Sm-Nd results for the North Shore Plutons. **98**

Table 4-1. Paleoproterozoic deformation and metamorphic history of the western Beaverlodge Belt. **141**

Table 4-2. Chemical monazite data from EMP analysis. **142**

Table 4-3. U-Pb data table. **148**

Table 4-4. LA-MC-ICPMS results. **150**

Table 5-1. U-Pb data table. **180**

Table 5-2. Sm-Nd data table. **181**

List of Figures

Chapter 1

Figure 1-1. Simplified geology of North America highlighting the Archean Cratons. 8

Chapter 2

Figure 2-1a. General geology of the Rae Province and bounding tectonic entities. 45

Figure 2-1b. Geology of the Beaverlodge Belt. 45

Figure 2-2. Simplified geological map of the Murmac Bay Group on the north shore of Lake Athabasca, Saskatchewan 46

Figure 2-3. Simplified stratigraphy of the lower Murmac Bay Group. 47

Figure 2-4. Geological map of the Elliot Bay Granite (EBG) and the unconformably overlying Murmac Bay Group. 48

Figure 2-5. Photos of the Murmac Bay Group. 49

Figure 2-6. Photos of intrusive rocks. 50

Figure 2-7. Plot of MBG basalts on a basalt discrimination diagram. 51

Figure 2-8. N-MORB normalized plots of selected trace elements for basalts and gabbros from the MBG as well as basalts from two known continental rift settings. 52

Figure 2-9. Concordia diagram for the Lodge Bay Granite. 53

Figure 2-10. Concordia diagram for the Cornwall Bay Granite. 53

Figure 2-11. Concordia diagram for the Donaldson Lake Granite. 54

Figure 2-12. Concordia diagram for the Dead Man Granite. 54

Figure 2-13. Concordia diagram for the Fookes Lake Quartzite. 55

Figure 2-14. Concordia diagram for the Dunbar Bay Psammite. 55

Figure 2-15. Concordia diagram of Ancient detritus from the Fookes Lake Quartzite and the Dunbar Bay Psammite. 55

Chapter 3

Figure 3-1. Map of North America with the study area highlighted. 81

Figure 3-2. Geological sketch map of the western Canadian Shield with southern Paleozoic cover removed 82

Figure 3-3. Simplified geological map highlighting the location of the North Shore Plutons. 84

Figure 3-4. Plane light photomicrograph of zircons from the North Shore Plutons. 85

Figure 3-5. Concordia plots of Macintosh Bay and Gunnar granites. 86

Figure 3-6. Concordia plots of Geebee Lake, Yahyah Lake and Hayter Bay granites. 87

Figure 3-7. Harker variation diagrams for the North Shore Plutons and biotite and hornblende gneiss from basement to the Taltson Magmatic Zone. 88

Figure 3-8. Chondrite normalized REE plot for the North Shore Plutons. 89

Figure 3-9. MORB normalized trace and major element plot of several granitoid suites. 89

Figure 3-10. Nb vs Y discrimination plot of the North Shore Plutons. 90

Figure 3-11. Rb vs Nb + Y discrimination plot of the North Shore Plutons. 90

Figure 3-12. Cartoon diagram displaying Paleoproterozoic tectonic history for northwestern Laurentia. 91

Chapter 4

Figure 4-1. (A) Map of North America. (B) General geology of the Churchill craton and bounding tectonic entities. 126

Figure 4-2. Simplified geological map of the Beaverlodge Belt on the north shore of Lake Athabasca, Saskatchewan. 127

Figure 4-3. Simplified geological map of the study area. 128

Figure 4-4. Metamorphic zonation map of the study area with sketch cross-section. 129

Figure 4-5. Stereonet analysis of F_3 folding in the study area. 130

Figure 4-6. Photographs of field relationships in the western Beaverlodge Belt. 131

Figure 4-7. Plane light and crossed polar photomicrographs of Murmac Bay Group metamorphic mineral assemblages. 132

Figure 4-8. Chemical monazite ages from 5 samples compiled into histogram format with overlapping probability density plots. 133

Figure 4-9. Backscattered electron images of selected monazites from the study area with spot analysis ages overlain. 134

Figure 4-10. Concordia plots of metamorphic zircon from amphibolite and intermediate meta-volcanic rock. 135

Figure 4-11. Concordia plots of metamorphic titanite from lower amphibolite-facies meta-basalt and monazite and zircon from a cordierite-bearing granite neosome. 136

Figure 4-12. Backscattered electron images of selected metamorphic zircon spheres from a cordierite-bearing granite neosome. 137

Figure 4-13. Terra-Wasserburg and relative probability plots of LA-MC-ICPMS zircon data from a cordierite-bearing granite neosome. 138

Figure 4-14. Topo and BSE images of zircon from a cordierite-bearing granite neosome with $^{207}Pb/^{206}Pb$ profiles from spot LA-MC-ICPMS analyses. 139

Figure 4-15. BSE images of zircon from a cordierite-bearing granite with individual LA-MC-ICPMS spot ages overlain. 140

Chapter 5

Figure 5-1. (A) Map of North America. (B) General geology of the Churchill craton and bounding tectonic entities. 171

Figure 5-2. Simplified geological map of northwestern Saskatchewan. 172

Figure 5-3. Concordia diagram of the Prince Lake Granite. 173

Figure 5-4. Backscatter electron images of zircons from the Uranium City and Feil Lake Granites. 174

Figure 5-5. Concordia diagram of the Uranium City Granite. 175

Figure 5-6. Concordia diagram for the Feil Lake and Uranium City granites. 176

Figure 5-7. Nd evolution trend for granitic samples from this study. 177

Figure 5-8. ϵNd plot of granitic and supracrustal samples from this and related studies. 178

Figure 5-9. General geology of the Churchill craton and bounding tectonic entities with areas of probable Meso to Paleoarchean crust highlighted. 179

Chapter 1: Introduction

The Rae and Hearne Provinces (Hoffman, 1988; Fig. 1-1) comprise a remote area of reworked Archean crust that has an exposed extent of > 1 million km^2. Together, these two provinces form the core of the former Archean Churchill Province and were subdivided based on the presence of a major structural break termed the Snowbird tectonic zone (STZ, Hoffman, 1988). This craton scale structure records both Archean and Paleoproterozoic metamorphism and deformation (Hanmer et al., 1994, Baldwin et al., 2003) but whether it represents a Paleoproterozoic suture (Hoffman, 1988, 1989), an Archean suture, or an intracontinental strike-slip shear zone (Hanmer et al., 1994; 1995) remains unclear (Baldwin et al., 2003). The term "Churchill craton" can be considered to refer to those components of the Rae and Hearne that were amalgamated during Archean time, whereas the domain names Rae and Hearne imply regional location with respect to the STZ. The boundary between the Churchill and Slave cratons is generally placed at the 2.0-1.93 Ga Taltson-Thelon Magmatic Zone (Hoffman, 1988). On the eastern margin of the Churchill craton, the Trans-Hudson Orogen marks the 1.9-1.8 Ga closure of the Manikewan Ocean and amalgamation of the Churchill, Superior, and Sask cratons with intervening oceanic arcs and basins (Hoffman, 1988; Lewry and Collerson, 1990; Ashton et al, 1999).

Although the Churchill craton is one of the largest and best exposed Archean cratons in the world, it is also one of the least well studied. The lack of interest in the Churchill craton is derived, in part, from its lack of known major economic mineral deposits and its remote location away from major centres of population and transportation infrastructure. However, the Churchill craton represents a significant

component of Earth's Archean crust, and therefore it presents an important opportunity for study of early Earth evolution and the nature of Paleoproterozoic crustal reworking during assembly of the supercontinent Laurentia.

The western Beaverlodge Belt of northern Saskatchewan (Fig. 1-1) is an ideal location to study the evolution of the Churchill craton. This belt contains a large portion of supracrustal rocks that may be critical to understanding greenstone belt evolution in the Churchill craton. Secondly, early reconnaissance studies suggest that the area has undergone several pulses of magmatism, metamorphism, and deformation. A detailed examination of the conditions and timing of these events could have craton-wide implications for Archean and Proterozoic tectonics. The belt ranges from low to high metamorphic-grade, providing a unique opportunity to study rocks at a variety of crustal levels. In addition, the low grade parts of the belt enable detailed rock descriptions and protolith identification.

Geology of the Beaverlodge Belt

Rocks in the Beaverlodge Belt were initially subdivided by Alcock (1936) into the inferred Archean Tazin Group and the Beaverlodge series of implied Proterozoic age. The lithological similarity between parts of these two groups and the apparent lack of an unconformity between them led Tremblay (1972) to introduce the term "Murmac Bay Formation", which he defined as the "ungranitized" supracrustal rocks that were exposed around Murmac Bay. Later, 1:20 000 scale mapping revealed that the Murmac Bay Group (MBG) (Macdonald, 1983) was a mixed package of Precambrian supracrustal rocks that included quartzite, carbonate, pelite, iron formation, ultramafics, gabbro, and mafic volcanics (Sibbald and Lewry, 1980; Macdonald *et al.*, 1982;

Sibbald, 1982, 1984; Sibbald *et al.*, 1983). Quartzite with a thin basal scour surface and rarely exposed basal conglomerate was suggested to mark the unconformity between the MBG and the ca. 3.0 Ga Lodge Bay and Elliot Bay granites (Persons, 1988).

The MBG has been correlated with the Hurwitz Group (Sibbald and Lewry, 1980; Fig. 1-1), a ca. 2.1 Ga (Heaman and LeCheminant, 1993) package of supracrustal rocks that is exposed in the Hearne Province. A Pb-Pb evaporation study of detrital zircons from MBG quartzite appeared to confirm a Paleoproterozoic depositional age (O'Hanley *et al.*, 1994). However, the presence of quartzite, komatiite, and banded iron formation in the MBG seems better correlated with the Archean Woodburn Lake Group (Ashton, 1988; Zaleski, 1999) and the Prince Albert Group (Shau, 1982) of the northwestern Churchill craton (Fig. 1-1). Both of these latter groups contain quartzite, komatiite and banded iron formation, but are known to be late Archean in age.

The MBG is intruded by granitoid rocks that have been collectively termed the "North Shore Plutons" (Macdonald, 1984). These granites have given a range of U-Pb and Pb-Pb ages between ca. 2.0 and 2.35 Ga (Persons, 1988; O'Hanley *et al.*, 1994). The relatively wide span of granite ages has limited their usefulness for constraining the ages of Murmac Bay Group deposition and later deformation.

Research objectives

The principal research objectives of this work were chosen to improve the understanding of local geology and aid craton- and global-scale correlations which could better constrain Archean and Paleoproterozoic tectonics. The first goal of this work is to recognize and characterize the basement to the Murmac Bay Group. Once the local basement is characterized, the regional extent of Meso- to Paleoarchean basement

in the Churchill craton can be evaluated. Secondly, the age and tectonic environment of Murmac Bay Group volcanism and sedimentation needs to be identified. Only when the setting of the Murmac Bay Group is well constrained will local and global comparisons be made possible. Third, the age of plutonism in the Beaverlodge Belt needs to be better defined. Are the "North Shore Plutons" a single suite of plutons? Are there any Archean granites in the Beaverlodge Belt? The fourth major research objective is to constrain better the nature and age of metamorphism and deformation in the Beaverlodge Belt. The complex geological history of the Beaverlodge Belt may require the utilization of new in-situ geochronological techniques.

Previous work and description of study area

The research presented herein coincides with a 1:20,000 scale bedrock-mapping project conducted by the Saskatchewan Geological Survey, the initial results of which have been reported in Hartlaub and Ashton (1998), Hartlaub (1999), and Ashton et al. (2000, 2001). The study area is approximately 600 km^2 and consists of excellent bedrock exposure (>50% in some areas) that is enhanced by a rugged topography of cliffs and valleys. Portions of this area were previously mapped, at a variety of scales, by Alcock (1936), Jolliffe (1946), Christie (1953), Blake (1955), Macdonald *et al.* (1982), Sibbald (1982), Sibbald *et al.* (1983) and Schwann (1985). Economic interest in the area is high due to the presence of gold in some of the granitoid rocks (Beavan, 1938; Christie, 1953; Sibbald, 1984; and Appleyard, 1990).

References

Alcock, F.J. 1936. Geology of the Lake Athabasca region Saskatchewan. Geological Survey of Canada, Memoir 196: 41p.

Appleyard, E.C. 1990. Petrogenetic aspects of the Goldfields granites, Goldfields area, Saskatchewan. Saskatchewan Geological Survey, Saskatchewan Energy and Mines, Misc. Rep. 90-4: 84-93.

Ashton, K.E., Boivin, D., and Heggie, G. 2001. Geology of the Southern Black Bay Belt, west of Uranium City, Rae Province. Saskatchewan Geological Survey, Saskatchewan Energy and Mines, Misc. Rep. 2001-4.2: 50-63.

Ashton, K.E., Kraus, J., Hartlaub, R.P., Morelli, R., 2000. Uranium City revisited: A new look at the rocks of the Beaverlodge Mining Camp. Saskatchewan Geological Survey, Saskatchewan Energy and Mines, Misc. Rep. 2000-4.2: 3-15.

Ashton, K.E., and Card, C.C. 1998. Rae Northeast: A Reconnaissance of the Rae Province Northeast of Lake Athabasca. Misc. Rep. 98-4, Saskatchewan Geological Survey, Saskatchewan Energy and Mines: 3-16.

Ashton, K.E., Heaman, L.M., Lewry, J.F., Hartlaub, R.P., and Shi, R. 1999. Age and origin of the Jan Lake Complex: a glimpse at the buried Archean craton of the Trans-Hudson Orogen. Canadian Journal of Earth Sciences, **36**: 185-208.

Baldwin, J.A., Bowring, S.A., and Williams, M.L. 2003. Petrological and geochronological constraints on high pressure, high temperature metamorphism in the Snowbird tectonic zone, Canada. Journal of Metamorphic Geology, **21**: 81-98.

Beavan, A.P. 1938. The Geology and Gold Deposits of Goldfields, Lake Athabasca, Saskatchewan. unpublished Ph.D. thesis, Princeton University: 158p.

Blake, D. 1955. Oldman River map-area, Saskatchewan. Geological Survey of Canada, Mem. 279: 52p.

Christie, A.M. 1953. Goldfields-Martin Lake map area, Saskatchewan. Geological Survey of Canada, Mem. 269: 126p.

Cooke, H.C. 1937. Preliminary report, Goldfields area, Saskatchewan. Geological Survey of Canada, Pap. 37-3.

Hanmer, S., Parrish, R., Williams, M., and Kopf, C. 1994. Striding-Athabasca Mylonite Zone - Complex Archean Deep-Crustal Deformation in the East Athabasca Mylonite Triangle, Northern Saskatchewan. Canadian Journal of Earth Sciences, **31**: 1287-1300.

Hanmer, S., Williams, M., and Kopf, C. 1995. Striding-Athabasca Mylonite Zone - Implications for the Archean and Early Proterozoic Tectonics of the Western Canadian Shield. Canadian Journal of Earth Sciences, **32**: 178-196.

Hartlaub, R.P., and Ashton, K.E. 1998. Geological investigations of the Murmac Bay group, Lake Athabasca north shore transect. Saskatchewan Geological Survey, Saskatchewan Energy and Mines, Misc. Rep. 98-4: 17-28.

Hartlaub, R.P. 1999. New insights into the geology of the Murmac Bay Group, Rae Province, Northwest Saskatchewan. Saskatchewan Geological Survey, Saskatchewan Energy and Mines, Misc. Rep. 99-4.2: 17-26.

Heaman, L.M., and LeCheminant, A.N. 1993. Paragenesis and U-Pb Systematics of Baddeleyite (Zro2). Chemical Geology, **110**: 95-126.

Hoffman, P.F. 1988. United Plates of America, the Birth of a Craton - Early Proterozoic Assembly and Growth of Laurentia. Annual Review of Earth and Planetary Sciences, **16**: 543-603.

Hoffman, P.F. 1989. Precambrian Geology and tectonic history of North America, *in* Bally, A.W., and Palmer, A.R., eds., The Geology of North America – An Overview: Geological Society of America, Boulder, p. 447-512.

Jolliffe, A.W. 1946. Summary Report on the Cornwall Bay–Fish Hook Bay Area. Geological Survey of Canada, unpublished manuscript, 7p.

Lewry, J.F. and Collerson, K.D. 1990. The Trans-Hudson Orogen: Extent, subdivision, and problems; *in* Lewry, J.F. and Stauffer M.R., eds., The Early Proterozoic Trans-Hudson Orogen of North America, Geol. Assoc. Can., Spec. Pap. 37, p. 1-14.

Macdonald, R. 1983. Geology and regional context of the Oldman Lake Area. Saskatchewan Geological Survey, Saskatchewan Energy and Mines, Misc. Rep. 83-4: 19-23.

Macdonald, R. 1984. Bedrock compilation, Greater Beaverlodge area (NTS 74N-6 to -11). Saskatchewan Geological Survey, Saskatchewan Energy and Mines, Misc. Rep. 84-4: 42-43.

Macdonald, R., Thomas, M., and Lee, N. 1982. Geology of the Hill Lake area (NTS 74N, CSMA photomap sheet 6500-65900). Saskatchewan Geological Survey, Saskatchewan Energy and Mines, Misc. Rep. 82-4: 8-11.

O'Hanley, D.S., Kyser, K.T., and Sibbald, T.I.I. 1994. The age and origin of the North Shore Plutons in the Rae Province, Goldfields area, Saskatchewan. Canadian Journal of Earth Sciences, **31**: 1397-1406.

Persons, S.S., 1988. U-Pb geochronology of Precambrian rocks in the Beaverlodge area, Northwestern Saskatchewan. Unpublished M.Sc. Thesis, University of Kansas: 68p.

Schwann, P.L. 1985. Geochemistry and Petrology of the Nicholson Bay Ultramafic Complex, Northwestern Saskatchewan. unpublished B.Sc. thesis, University of Regina, 67p.

Sibbald, T.I.I. 1982. Uranium metallogenic studies: Nicholson Bay area. Saskatchewan Geological Survey, Saskatchewan Energy and Mines, Misc. Rep. 82-4: 43-45.

Sibbald, T.I.I. 1984. Gold metallogenic studies, Goldfields area. Saskatchewan Geological Survey, Saskatchewan Energy and Mines, Misc. Rep. 84-4: 116-121.

Sibbald, T.I.I. and Lewry, J.F. 1980. Uranium metallogenic studies: Lodge Bay area, Lake Athabasca. Saskatchewan Geological Survey, Saskatchewan Mineral Resources, Misc. Rep. 80-4: 44-48.

Sibbald, T.I.I., Schwann, P.L., and Dunn, C.E. 1983. Uranium-gold metallogenic studies: Nicholson Bay Ultramafic Complex. Saskatchewan Geological Survey, Saskatchewan Energy and Mines, Misc. Rep. 83-4: 75-79.

Tremblay, L.P. 1972. Geology of the Beaverlodge Mining Area, Saskatchewan. Geological Survey of Canada, Mem. 367: 265p.

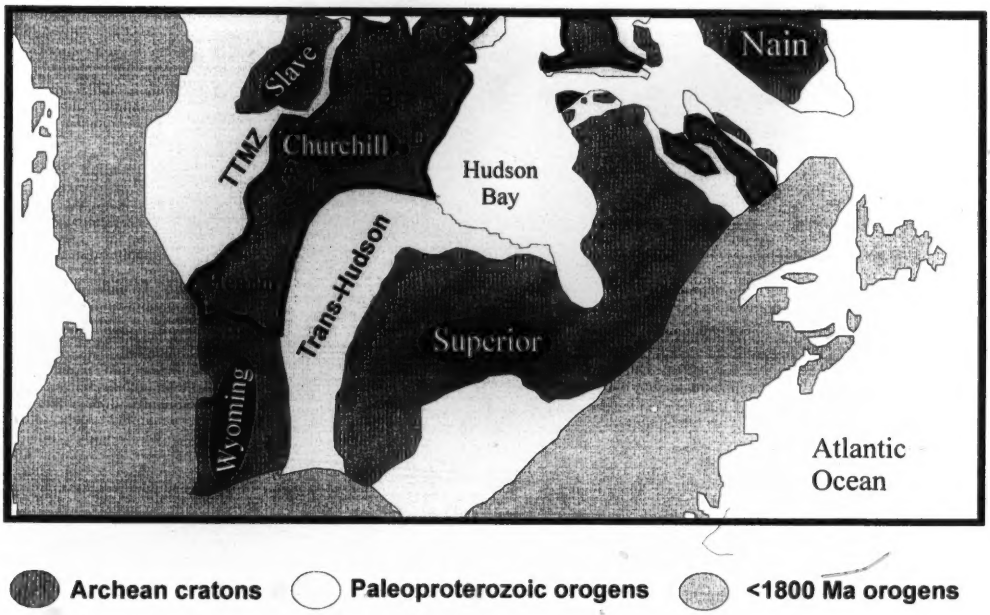

Figure 1-1. Simplified geological map of North America highlighting the major Archean cratons. The Churchill craton is outlined in a thick black line. The approximate locations of important areas discussed in the first chapter are: a, The Beaverlodge Belt; b, The Woodburn Lake Group; c, The Prince Albert Group; and D, The Hurwitz Group. STZ, Snowbird tectonic zone; TTMZ, Taltson-Thelon Magmatic Zone. Figure modified after Hoffman, 1989.

Chapter 2: The Archean Murmac Bay Group: evidence for a giant Archean rift in the Rae Province, Canada

A version of this chapter was accepted for publication in Precambrian Research, July 2003 and is currently in press. Co-authors are L.M. Heaman[a], K.E. Ashton[b], and T. Chacko[a].
[a]Department of Earth and Atmospheric Sciences, 1-26 Earth Sciences Building, University of Alberta, Edmonton, Alta., Canada, T6G 2E3
[b]Saskatchewan Geological Survey, 2101 Scarth St., Regina, Sask., Canada, S4P 3V7

1. Introduction

Many Archean greenstone belts are thought to have formed in oceanic environments, either as ocean floor rocks, oceanic plateau, island arcs or back-arcs (e.g. de Ronde and de Wit, 1994; Jackson et al., 1994; Aspler and Chiarenzelli, 1996). This interpretation is based, in part, on the lack of identifiable sialic continental basement and the preponderance of mafic and ultramafic volcanic rocks exhibiting strong geochemical similarities to those in modern-day oceanic settings. However, some Archean "greenstone belts" are interpreted to have formed by continental extension and rifting. One of the commonly cited examples of this tectonic setting is the Belingwe Greenstone Belt of the Zimbabwe Craton (Bickle et al., 1975; Blenkinsop et al., 1993; Nisbet et al., 1993; Hunter et al., 1998). Other Archean greenstone belts linked to continental extension are reported from the Superior (Wilks and Nisbet, 1988; Thurston and Chivers, 1990; Tomlinson et al., 1999) and Rae provinces (Schau, 1982; Ashton, 1988; Zaleski et al., 2000a) and Slave (Henderson, 1981; Bleeker et al., 1999), Karelian (Thurston and Kozhevnikov, 2000), Yilgarn (Swager, 1997) and Dharwar cratons (Srinvasan and Ojakangas, 1986). The strongest argument for continental rifting in these areas is the presence of old sialic basement that is unconformably overlain by a

package of clastic and/or carbonate sediments with overlying conformable mafic and ultramafic volcanic rocks. Other evidence includes the bimodal nature of volcanic packages (Thurston et al., 1985), crustal contamination (Bickle et al., 1994; e.g. Chauvel et al., 1993; Green et al., 2000) and xenocrystic zircon in volcanic rocks (Bickle et al., 1994; Bateman et al., 2001), and the age and geochemical similarities between basement dykes and flood basalts (e.g. Blake, 2001). In alternative accretionary models, the basal sedimentary members of these supracrustal belts are interpreted as passive margin or rift sequences, whereas the overlying volcanic units are considered obducted ocean floor rocks (Kusky, 1989; Kusky and Kidd, 1992, 1999; Kusky and Hudleston, 1999).

Representative stratigraphic sections for some North American Archean rift sequences (Thurston and Chivers, 1990; Bleeker et al., 2000) are typically floored by small inliers of basement rock that are overlain by rare pockets of polymictic or oligomictic quartz-pebble conglomerate. These conglomerates are directly overlain by a sequence of shallow-water sedimentary rock that is dominated by quartz-rich sandstones. Thick carbonate packages have also been reported (Wilks and Nisbet, 1988). Pillowed to massive mafic volcanic rock with a minor component of komatiitic volcanic and/or intrusive rocks and banded iron formation generally overlie the shallow-water sedimentary rocks. Volcanic rocks have also been reported to lie directly upon sialic basement (Zaleski et al., 2001). This rift sequence is similar to successions of Phanerozoic age that have early rift sediments that are cut by mafic dykes (Sheth, 1999, and references therein) and overlain by a package of interbedded sedimentary and volcanic rocks (e.g. Dunning et al., 2002; MacDonald et al., 2002)

Direct evidence for the aereal extent of Archean extensional systems may place some constraints on the size of Archean continental plates, which is otherwise difficult to determine as older greenstone belts have typically been dissected by faults and deformation zones. Some studies have suggested that Archean oceanic plates were small (Hargraves, 1986), triple junctions were numerous (Drury, 1978), and the volume of continental crust in the early Archean was less than it is today (McLennan and Taylor, 1983; Condie, 1990). The largest area of exposed Archean terrain, the 2×10^6 km^2 Superior Province, is proposed to have formed by subduction-driven amalgamation of numerous small continental plates and intervening oceanic arcs by ca. 2.67 Ga (Card, 1990; Stott, 1997; Percival et al., 2000). De Wit et al. (1992) argued that subduction processes welded numerous sub-domains into the 1.2×10^6 km^2 Kaapvaal Craton between 3.7 and 2.7 Ga. They also argue that a large portion of Archean continental material may have been recycled back into the mantle. This work is in agreement with Armstrong (1981, 1991) and Arndt (1999), who argue that a large volume of continental crust may have already existed by the beginning of the Archean. Thus, we might expect that large continents, or even supercontinents, may also have been present in the Archean.

This paper describes the supracrustal Murmac Bay Group (MBG) and its underlying granitoid basement in the southern Rae Province of the Canadian Shield (Fig. 2-1a). We compare the MBG with the ca. 2.7 Ga Prince Albert (Schau, 1982; Skulski et al., 2002), Woodburn Lake (Ashton, 1988; Zaleski et al., 2000a), and Mary River (Jackson and Taylor, 1972; Bethune and Scammell, 1997) groups, which contain quartzite-basalt/komatiite assemblages that are considered to be broadly correlative and to have

formed by continental extension (Jackson and Taylor, 1972; Jackson and Morgan, 1978; Schau, 1982; Ashton, 1988; Schau and Ashton, 1988; Schau, 1997; Zaleski et al., 2000a, 2001). If the MBG is correlative with these three groups, it would extend this rift assemblage for a total length of >2000 km, and would imply the existence of a large stable >2.7 Ga Archean craton, Nunavutia.

2. Geological setting

The MBG lies within the southern Rae Province of the western Canadian Shield (Fig. 2-1a). The Rae Province is bounded to the southeast by the Hearne Province across the Snowbird Tectonic Zone (Hoffman, 1990). The Rae Province is thought to have a continental affinity ("Nunavutia" of Schau and Ashton, 1988), whereas the Hearne Province may represent amalgamated juvenile oceanic terranes (Aspler and Chiarenzelli, 1996). The Rae Province is separated from the Archean Slave Craton in the west by the 2.0-1.9 Ga Taltson-Thelon orogenic belt (Hoffman, 1988). To the north and east of the study area (Fig. 2-1b), upper amphibolite to granulite facies equivalents of the Murmac Bay Group extend to the margins of the shear zone bounded Nevins Lake Block (Ashton and Card, 1998; Card and Bethune, 1999) for an exposed extent of ~3000 km^2. The Train Lake Domain that bounds the Nevins Lake Block to the north and east is primarily composed of granitic orthogneiss with a minor amphibolite-pelite supracrustal component. The MBG appears to extend to the west, across the Black Bay Fault, into the high grade and intensely deformed Black Bay Domain (Ashton et al., 2001a). Sedimentary rocks of the Paleoproterozoic Martin and Athabasca Basins unconformably overlie the MBG in the southern and central portions of the study area.

The MBG is a metamorphosed and moderately to highly deformed supracrustal package that is comprised primarily of quartzite, basalt, psammite, and pelite, with minor amounts of conglomerate, banded iron formation, and carbonate. These supracrustal rocks rest unconformably on ~3.0 Ga granitic basement and are intruded by gabbro, komatiitic ultramafic rock and at least three suites of granite. The least deformed of these granite suites are the ca. 1.95 and 2.3 Ga granites that intrude rocks on the north shore of Lake Athabasca (Persons, 1983; Bell and Bikerman, 1985; O'Hanley et al., 1994).

The MBG has been variably metamorphosed from lowermost amphibolite to granulite facies (Ashton and Card, 1998; Hartlaub and Ashton, 1998; Ashton et al., 2000). South of Beaverlodge Lake (Fig. 2-2), pelites locally contain the assemblage garnet-biotite-staurolite-quartz-muscovite (520-550° C and 2.5-12 kbars; Pattison, 2001). These low-grade pelitic rocks grade into garnet-sillimanite-biotite migmatites (>600°C, 3-6.5 kbars; Pattison, 2001) along the north, east, and western margins of the study area (Fig. 2-2).

Rocks within the study area have been affected by at least five episodes of deformation. Tight to isoclinal F_1 folds transposed bedding and formed a moderate to strong S_1 fabric that is defined by schistosity and gneissic layering. D_2 is defined by tight to close F_2 folds that locally exhibit an axial planar S_2 fabric. South-southwest-plunging, open, upright F_3 folds are common. Localized cataclasis and shearing is also attributed to the third generation of deformation. D_4 is interpreted to have formed the large fold which has its axial trace passing through Lodge Bay (Ashton et al., 2001a) (Fig. 2-2).

Based on lithological similarities to the Paleoproterozoic Hurwitz Group, which lies to the northeast in the central Hearne Province (Fig. 2-1a), Sibbald and Lewry (1980) interpreted the MBG to be Paleoproterozoic, an interpretation supported by Pb-Pb evaporation dates ranging between 2430 and 2380 Ma for detrital zircons from a MBG quartzite (O'Hanley et al., 1994). We propose, however, that these Pb-Pb dates result from Paleoproterozoic metamorphic overprinting of Archean detrital ages.

3. Basement Complex

The basement complex comprises at least three granitoid inliers: the 3072 ±41 Ma (Persons, 1983) Lodge Bay Granite (Fig. 2-2); the 3014 ±10 Ma (Persons, 1983) Elliot Bay Granite; and the Cornwall Bay Granite.

3.1 The Lodge Bay and Elliot Bay Granites

The Lodge Bay Granite is grey to white, medium to coarse grained and contains a weak S_1 foliation that is locally overprinted and transposed into D_3 mylonite zones. Where weakly strained, it is composed of 40-60% K-feldspar, 20-25% quartz, 15% plagioclase and up to 10% biotite. More highly deformed equivalents contain coarse K-feldspar in a fine-grained matrix of quartz, plagioclase, K-feldspar, muscovite and chlorite, with millimeter-scale quartz veining. The granite is cut by gabbroic sheets and dykes, which, together, comprise 15-20% of the exposed pluton.

3.2 The Cornwall Bay Granite

The Cornwall Bay Granite is a strongly foliated to mylonitic body whose relationship to the MBG has been obscured by deformation and younger magmatism. The mineral composition of this rock is nearly identical to that of the Lodge Bay Granite, and it is cut by a similar suite of deformed gabbroic dykes. Our interpretation of the Cornwall

Bay Granite as part of the Basement Complex is strengthened by the structural symmetry on both limbs of the large F_4 fold centered on Lodge Bay and by the mantling of the granite by the MBG quartzite (Fig. 2-2).

4. Murmac Bay Group

The MBG has been examined in detail by numerous authors (Tremblay, 1972; Sibbald and Lewry, 1980; Macdonald et al., 1982; Sibbald, 1982, 1984; Sibbald et al., 1983), but recent 1:20,000 scale mapping (Fig. 2-2) (Hartlaub and Ashton, 1998; Hartlaub, 1999; Ashton et al., 2000) in the relatively low-grade basal portion of the MBG that directly overlies the basement complex forms the basis of a revised stratigraphy (Fig. 2-3). The column is composite in construction with the basal relationships derived from the area around Elliot and Lodge bays. A detailed map of a basal section of the MBG and its underlying basement is presented in figure 4.

The Murmac Bay Group comprises a stratigraphically thin, basal sequence and a thicker upper sequence. A polymictic conglomerate marks the unconformity between basal MBG quartzites and the granitic basement complex in at least one location (Fig. 2-2, 2-4) (Persons, 1983; Ashton et al., 2001a). The basal quartzite includes coarse sands (grits) and oligomictic quartz-pebble conglomerate. Quartzite is interlayered with basalt and injected by gabbroic and komatiitic sheets. Marble and calc-silicate rocks make up a minor component of the lower sequence and were not observed in the upper sequence. Oxide-and silicate-facies iron formation are most common within the quartzite-bearing lower sequence and tend to be located along strike from, or at the contact with, basalt.

Above the quartzite-bearing sequence lies a much thicker succession of pelitic and psammopelitic rocks. Some mafic volcanic rock is interlayered with this upper sequence; however, the proportion of volcanic material is much less than in the basal sequence.

4.1 Polymictic conglomerate

The basal polymictic conglomerate (Fig. 2-5a) rests directly upon the Elliot Bay Granite and grades into the overlying quartzite. The conglomerate is up to 5 meters thick and is sporadically exposed along strike for more than 1 km (Fig. 2-4; Ashton et al., 2001a). It consists of abundant rounded granitoid cobbles, highly flattened amphibolite pebbles and cobbles, cherty pebbles, fuchsitic quartzite cobbles, and quartz pebbles in a foliated sandy matrix and varies from clast to matrix supported. The foliation in the conglomerate matrix is parallel to the foliation in the basement complex and in the overlying quartzite. Some of the granitoid clasts contain quartz veining that is oblique to the matrix foliation in the conglomerate.

4.2 Quartzite

Although polymictic conglomerate is locally found at the base of the MBG, the basal unit consists predominantly of quartzite that is in direct contact with the basement complex. The contact varies from sheared to locally weakly deformed. White to pale yellow quartzite consists of >90% quartz and locally contains minor muscovite or diopside. Rare fuchsitic muscovite gives the quartzite a bright green colour and likely reflects a chromite-bearing detritus source (e.g. Bleeker et al., 1999). The quartzite tends towards massive except where heavy minerals or muscovite define bedding or foliation planes, respectively. This unit is locally less than 5 m thick, but is > 500 m

thick along the western shore of Lodge Bay (Fig. 2-2). The variability of thickness in the unit is likely a stratigraphic feature, but structural thickening has affected some areas. Centimeter-scale planar crossbedding (Fig. 2-5b), meter-scale trough crossbedding (Fig. 2-5c), ripple marks, and scour channels are locally preserved, but are generally deformed. Beds of pebbly quartzite with well-rounded quartz pebbles are also quite rare. Based on the presence of clasts and the observed sedimentary structures, Harper (1983) suggested that at least some of the quartzites were deposited in a high-energy fluvial or shoreface environment. The high maturity of quartzite without interlayered shale, combined with large-scale trough crossbedding, appears to be consistent with a shallow marine shoreface environment. Unfortunately, the deformed and sporadic nature of sedimentary structures precludes an unequivocal determination of depositional paleoenviroment.

4.3 Oligomictic quartz-pebble conglomerate

A 1-7 m thick intraformational unit of clast-to matrix-supported oligomictic quartz-pebble conglomerate occurs within the quartzite, 50 to 100 metres above the basal unconformity (Figs. 2-3, 2-4 and 2-5d). This unit can be traced for more than 10 kilometers along strike. The presence of clastic textures within clasts and rare laminated quartz clasts suggests that lithified quartz arenite, rather than vein quartz, was the primary source of these pebbles. Clasts range from sub-rounded to highly angular and are on average 1-2 cm in diameter, although some of the highly angular clasts reach 10 cm in their longest dimension. The coarse size and angular nature of these clasts is consistent with localized uplift and faulting of first-cycle quartzite during the deposition of a second-cycle quartzite. This quartzite pebble conglomerate could also represent a

storm deposit or the diagenetic alteration of an originally polymictic conglomerate (Cox et al., 2002).

4.4 Marble and intraformational dolostone

Marble is exposed both as massive layers up to tens of metres thick and as rare isolated pods in quartzite and psammite. Iron formation is interlayered with carbonate on a centimeter-scale at Fish Hook Bay on Lake Athabasca (Fig. 2-2). Marble is composed primarily of dolomite with minor diopside and tremolite. Some quartzite contains variably boudinaged layers of pegmatitic diopside, which may reflect metamorphic reaction between dolomite and quartz. This is supported by the presence of a monomineralic reaction rim of pegmatitic diopside at the contact between marble and quartzite (Fig. 2-5e). The local interlayering of iron formation and marble may indicate that these carbonate rocks represent exhalation deposits related to volcanism.

4.5 Iron Formation

Banded iron formation occurs both at the upper quartzite contact and interlayered with amphibolite higher up in the sequence. Oxide-facies iron formation consists of thin, centimetre-scale alternating quartz and magnetite-hematite-rich layers. Silicate-facies iron formation and related garnetiferous pelite is generally composed of 20 to 50 percent garnet with variable amounts of biotite, amphibole and tourmaline and is locally found in contact with pelitic rocks. The largest unit of iron formation occurs along strike from a thick package of amphibolite exposed northeast of Cornwall Bay. It consists of two ~15 m thick layers that are interbedded with dolomitic marble along a strike length of 1300 m (Harper, 1983). Because of the direct relationship between iron formation, amphibolite and, locally, marble, we interpret the majority of iron formation

in the area to be exhalitive. The silicate-facies iron formation and garnetiferous pelite may represent a distal facies of volcanism where iron deposition was overwhelmed by the input of mud.

4.6 Amphibolite (Basalt)

Green to black amphibolites are fine to medium grained and are generally well-to moderately-layered with rare massive occurrences. They are primarily composed of hornblende and plagioclase with sporadic concentrations of iron sulfide. Pillow-like features are evident in several locations, but their mode of formation is equivocal. Amygdules, cooling cracks, and possible primary flow contacts are all locally present. Therefore, these rocks are interpreted as extrusive. The amphibolites generally lie stratigraphically above or, rarely, are interlayered with quartzite of the basal sequence; however, rare thin layered mafic units within the upper sequence may also be volcanic in origin. The contact between quartzite and basalt is generally marked by a thin unit of siltstone to ferruginous quartzite (e.g. Fig. 2-4), which grades locally into (exhalitive?) iron formation and dolostone. The nature of this contact is consistent with volcanism impinging on an active depositional environment and supports our interpretation that there is a conformable relationship between amphibolite and quartzite.

An unusual, well-layered, fine-to medium-grained, 1-2m thick biotite-cummingtonite schist is interlayered with amphibolite at several locations in the study area. Trace amounts of sulfides and garnet are locally present in this unit, as are layers and pods of carbonate. The sulfide-bearing nature and interlayering of this unit with amphibolite is consistent with an interpretation of this unit as intermediate volcanic or volcaniclastic rock. Alternatively, this schist could represent highly altered mafic volcanic rock.

4.7 Psammite

Aluminous psammitic rocks have a maximum thickness of 10 m and are interlayered with both quartzite and amphibolite. The aluminous psammite is well layered and contains muscovite ± biotite and, locally, abundant variably retrogressed sillimanite faserkiesel.

Above the basal sequence of the MBG lies a voluminous component of calcic quartzofeldspathic rocks that have a weak to moderate compositional layering defined by variations in biotite and hornblende content. At high metamorphic grades these rocks are migmatitic (Fig. 2-5f) and locally contain trace amounts of garnet. They are interpreted as meta-sandstones that may contain a minor volcanogenic component.

4.8 Pelite to psammopelite

These quartzofeldspathic rocks are well layered, fine to medium grained and, dependent on metamorphic grade, contain varying proportions of muscovite, biotite and garnet that together comprise 15 to 35 percent of the rock. Sillimanite or andalusite locally comprises up to 15% of the rock, whereas trace to several percent graphite is common. Psammopelitic rocks with visible rock fragments (i.e. lithic-greywacke) were identified in several locations. Thin discontinuous layers of pelitic to psammopelitic rocks are locally interlayered with rocks of the basal sequence at the contact between amphibolite and quartzite. A large proportion of the eastern and central Nevins Lake Block comprises migmatitic to diatexitic varieties of this unit (Ashton and Card, 1998; Hartlaub and Ashton, 1998).

5. Intrusive Rocks

5.1 Ultramafic Rock

Ultramafic rocks in the study area contain only trace amounts of relict olivine and pyroxene as the rocks have been both hydrated and metamorphosed. Many weather a distinctive steel blue where serpentine veining is extensive. In addition to serpentine, talc, tremolite, chlorite, carbonate and phlogopite comprise the alteration minerals in these rocks. Schwann (1985) reported relict primary cumulate textures and noted that carbonate fills veins and replaces serpentine mesh-textured grains. Hematite and magnetite are ubiquitous and comprise trace to several percent of the rock. In some locations, zones of acicular amphibole alteration were noted (Fig. 2-6a). A geochemical study of the Nicholson Bay ultramafic body (Fig. 2-2), which is emplaced within quartzite and carbonate, indicates that it has an average komatiitic chemical composition that is highlighted by 47 wt % SiO_2, 0.15 wt % total alkalis, 34.63 wt % MgO and 0.24 wt % TiO_2 (Schwann, 1985). The absence of primary layering and emplacement within supracrustal rocks leads us to interpret the Nicholson Bay ultramafic body as a shallow sill. Other exposures of ultramafic rock are less definitive and represent either shallow intrusions or extrusive rocks.

5.2 Gabbro

Abundant coarse-grained, black, variably foliated gabbro dykes and sills that are up to 200 m thick cut the basement complex and overlying rocks of the MBG (Fig. 2-6b). Gabbro is composed of plagioclase and hornblende with minor amounts of clinopyroxene. The gabbro dykes are most abundant in the basement complex and in the basal quartzite, but similar gabbroic rocks are locally found injecting all units of the MBG. However, abundant coarse-grained gabbro dykes are not found cross-cutting the

younger granitic rocks, and thus we interpret these dykes and sills to represent feeders to the MBG volcanism.

5.3 Donaldson Lake Granite to Tonalite

A >25 km^2 heterogeneous zone of mixed supracrustal rocks and injected granite sheets is well exposed in the area around Donaldson Lake, 5 km north of Beaverlodge Lake (Fig. 2-1b). A 2179 ± 10 Ma age was derived for this unit by Tremblay et al. (1981) based on three non-abraded multigrain zircon analyses. This heterogeneous zone of mixed granite and supracrustal rock was originally interpreted as a metasediment and termed the Donaldson Lake Gneiss by Tremblay (1972), but the improved exposure afforded by a recent forest fire confirms the dominantly igneous component. The granitoid component, which makes up >60% of this mixed zone, is pink to white, migmatitic to moderately foliated and ranges from tonalitic to granitic in composition. Thin, 5-20 m wide, zones of layered amphibolite and variably assimilated quartzite and pelite (Fig. 2-6c) characterize the unit and result in local concentrations of hornblende or sillimanite ± andalusite in addition to 10% biotite.

5.4 Dead Man Granite

The Dead Man Granite intrudes pelitic rocks of the MBG ~ 20 km east of the exposed basement complex (Fig. 2-1b) and has an exposed extent of ~5 km^2. It has been affected by granulite-facies metamorphism and by all phases of deformation (D_{1-4}). It is coarse grained, weathers deep orange to red, and is composed of 35% K-feldspar, 20% plagioclase, 20% quartz and 20-25% combined hornblende, biotite, and clinopyroxene ± orthopyroxene (Fig. 6d). Migmatitic garnet-biotite enclaves that occur within the margin of the granite are interpreted as pelitic xenoliths.

5.5 K-feldspar megacrystic granite

The K-feldspar megacrystic granites are coarse grained, moderately foliated and contain 5 to 20 percent biotite ± hornblende and K-feldspar megacrysts that are up to 3 cm in length. These granites cut the MBG and have yielded U-Pb zircon and Rb-Sr ages of ca. 2.0-2.3 Ga (Persons, 1983; Bell and Bikerman, 1985; O'Hanley et al., 1994). Rare migmatitic psammitic to psammopelitic xenoliths near the margins imply a phase of metamorphism that was synchronous, or prior, to granite emplacement.

6. Geochemistry

Fourteen samples of amphibolite were collected for geochemistry from the area south of the Lodge Bay Granite near Elliot Bay on Lake Athabasca (Table 2-1). These samples have all been metamorphosed at low or middle amphibolite facies and were collected to help constrain the tectonic environment of the Murmac Bay Group. All but one of the samples plot as tholeiitic basalt (Fig. 2-7). The near-identical trace element patterns for MBG basalts and gabbro dykes and sills (Fig. 2-8) support our interpretation that the gabbro dykes found cutting the Basement Complex and the overlying quartzite represent feeders to MBG basalts. N-MORB normalized REE patterns for the fourteen MBG basalt and ten MBG gabbro samples are almost identical to the patterns of the North Mountain Basalt in the Early Jurassic Bay of Fundy Rift Basin (Papezik et al., 1988). A generally negative slope resulting from LREE enrichment flattens into a MORB-like HREE trend with a significant negative Nb anomaly. A slight negative Ti anomaly is also apparent in the MBG and North Mountain basalts. LREE enrichment and negative Nb, Zr and Ti anomalies are considered to be a common feature of some continental tholeiites (Pin and Marini,

1993). Negative Nb anomalies in continental tholeiites are suggested to have formed by crustal contamination either during magma ascent or at source (Dupuy and Dostal, 1984; Pin and Marini, 1992), or to have formed by melting of enriched lithospheric mantle (Puffer, 2001). The lack of significant negative Nb and Ti anomalies in Ethiopian Rift basalts (Fig. 8) is consistent with the interpretation by Stewart and Rogers (1996) that these rocks have not seen significant crustal contamination. An enriched lithospheric mantle source for MBG basalt is possible based on evidence in Cousens et al. (2001) for an enriched lithospheric mantle resevoir beneath the Rae Province which had been created by metasomatic processes prior to 2.8 Ga.

7. Geochronology

To improve the age constraints on the Murmac Bay Group and its basement, six samples were collected for geochronological study. A sample of the Lodge Bay Granite (S-1, Fig. 2-2) was taken to confirm the ca. 3.0 Ga age for the basement complex. The Cornwall Granite (S-2, Fig. 2-2) was sampled to test our interpretation of this unit as part of the Basement Complex. The Donaldson Lake and Dead Man Granites (Fig. 2-1b), which intrude the MBG, were studied to establish a minimum age constraint on the MBG. Detrital zircons were separated from samples of quartzite (S-3, Fig. 2-2) and aluminous psammite (S-4, Fig. 2-2) to constrain the maximum age of MBG deposition, and to provide some information on the source of MBG detritus.

7.1 Analytical methods

Uranium and lead were isolated using the anion exchange chromatography method developed by Krogh (1973). Estimated analytical blanks for the procedure were 2 pg for Pb and 0.5 pg for U. The U and Pb were loaded together onto a Re filament following

the Si-gel technique of Cameron *et al.* (1969). Isotopic ratios were measured in single collector mode on a VG354 mass spectrometer. Measurements were taken using either a Faraday cup or Daly photomultiplier detector, depending on signal strength. The 1σ errors reported in Table 2-2 were calculated using an in-house program that numerically propagates all known sources of uncertainty. Regression calculations and age uncertainties were determined using the program Isoplot (Ludwig, 1998). Details of U-Pb procedures are outlined in Heaman et al. (2002).

7.2 Results

7.2.1 Lodge Bay Granite

The Lodge Bay Granite zircon population is dominated by light pink, clear to cloudy, irregular grain fragments that are 100 to 300 μm in length. Initial analyses consisted of non-abraded multi-grain (No. 1) and single grain (No. 2) selections from this population. Analyses Nos. 3-6 comprise single abraded pink grains. A summary of all U-Pb data is presented in Table 2-2. The abraded grains are generally much less discordant than the non-abraded grains, but the most discordant grain was also abraded. This highly discordant grain has the lowest U and Pb concentrations of all the analyses. The upper intercept discordia age of 3060 ±40 Ma based on all 6 analyses is considered the crystallization age for this sample (Fig. 2-9) and is consistent with the 3072 ±41 Ma U-Pb date previously obtained by Persons (1983). The lower intercept of the discordia line at 186 ± 93 Ma may be geologically meaningless or may represent a Jurassic hydrothermal event.

7.2.2 Cornwall Granite

The zircon population of the Cornwall Granite is homogeneous and consists of cloudy prismatic grains with a length to width ratio of 2 to 1. Analyses included one non-abraded cloudy grain (No. 3) and one abraded grain of similar appearance (No. 2). A single grain that was abraded down to its colourless transparent core was also analyzed (No. 1). All three analyses have moderate U concentrations and are co-linear, defining a chord with an upper intercept of 2999 ± 7 Ma (Fig. 2-10), which is interpreted as the crystallization age. The cloudiness of the zircon population may be attributable to a Proterozoic lead-loss event that occurred at 861 ± 18 Ma, the lower intercept of the discordia line.

7.2.3 Donaldson Lake Granite

The sample of Donaldson Lake Granite that was collected did not contain any visible supracrustal xenoliths. The majority of zircons in the sample are prismatic with cloudy cores and transparent, colourless overgrowths. Analyses Nos. 1 and 2 were obtained from single grains that were abraded to analyze their transparent colourless cores. The overgrowth on grain No. 1 was completely removed by abrasion, whereas the core of grain No. 2 still had a visible overgrowth after abrasion. Analysis No. 3 consisted of a single grain from the dominant population that was transparent, colourless and did not have a visible overgrowth. Analysis No. 5 consisted of a cracked, slightly cloudy prismatic grain that was not abraded.

Analyses 1-3 and 5 constrain a chord with an upper intercept of 2634 ± 55 Ma and a lower intercept of 1793 ± 53 Ma (Fig. 2-11). The high U content and low Th/U ratio in analyses No. 2 and No. 5 are consistent with our interpretation that these two grains contain a metamorphic component that grew at ~1.8 Ga during regional orogenesis.

Analysis No. 4 consisted of a single transparent ovoid grain that was not abraded. This rounded nature of this grain could indicate that it is resorbed and represents a xenocrystic component within the Donaldson Lake Granite. Grain No. 4 has an upper intercept age of 3371 Ma assuming the lower intercept of 1800 Ma determined from the chord defining the other analyses in this sample.

We interpret the 2634 Ma upper intercept date for the sample to represent the crystallization age of this granite. The 1.8 Ga age may represent deformational effects related to 1.8 Ga closure of the Trans Hudson Orogen (Fig. 2-1a; Ashton et al., 2001b and references therein).

7.2.4 Dead Man Granite

The Dead Man Granite contains a dominant population of slightly resorbed prismatic grains and minor populations of transparent colourless prisms and fragments. All analyses consist of abraded single grains from the main population, except for Nos. 3 and 5 (Fig. 2-12). Number 3 was composed of 3 clear colourless prisms, whereas No. 5 comprised 3 colourless fragments. Neither of the multi-grain populations was abraded. The clear colourless nature of the grains in analysis No. 3, combined with its lower U and Pb concentrations (111 ppm U, 54 ppm Pb) may indicate a younger (2.3 Ga?) metamorphic component. For this reason analysis No. 3 was not used in our age calculation. The 4 least discordant analyses (Nos. 2,4,5, and 6) plot on a chord that has an upper intercept of 2617 ± 80 Ma and a poorly constrained lower intercept of 1704 ± 530 Ma (Fig. 2-12). If, however, we place the analyses we used from the Donaldson Lake and Dead Man Granites on the same plot, they are colinear (MSWD = 2.8) and constrain a chord with an upper intercept of 2631 ± 12 Ma and a lower intercept of 1791

± 21. We interpret the upper intercept of this chord to be the best estimate for the crystallization age of both granites, and the lower intercept as a regional deformational and/or metamorphic event. The relatively low metamorphic grade of country rocks surrounding the Cornwall Bay and Lodge Bay granites may explain the absence of a 1.8 Ga overprint in these granitoids.

7.2.5 Fookes Lake Quartzite

A green fuchsitic quartzite was sampled adjacent to Fookes Lake in the northern part of the study area (Fig. 2-2). This sample site was chosen in an attempt to avoid any isotopic disturbances that may be related to the Athabasca Group unconformity in the southern portion of the map area. Detrital zircons from the Fookes Lake quartzite are clear, moderately to well rounded and range from colourless to slightly brown. They range from 50 to >200 μm in length and have irregular ovoid shapes that are interpreted to have formed during sediment transport. Scanning electron images of several dozen grains indicate that, although some lack any internal structure, the majority contain faint-to well-developed oscillatory zoning. Zircon overgrowths were observed in a few grains, but these overgrowths have been abraded at the edges and appear to have formed prior to sediment transport. Based on fourteen single zircons it is apparent that the majority of detritus is >3.5 Ga (Table 2-2, Fig. 2-13). Similar to the Dead Man and Donaldson Lake granites, the detrital zircons in this sample show the affects of a strong ca. 1800 Ma lead loss event. It also appears that the grains were affected by a younger lead loss event, possibly similar to the event(s) affecting the basement complex granites. By anchoring each analysis to a lower intercept of 1800 Ma, the upper intercept dates are interpreted to be the maximum ages for each grain (Table 2-2). The $^{207}Pb/^{206}$ Pb

model age, which assumes lead loss at present (T = 0), is considered the minimum age for each grain. The youngest minimum age for any of these grains is 2812 Ma (analysis No. 3) on a slightly blocky clear grain with a few inclusions. Since this grain is 18.63% discordant, the grain could be as old as 3357 Ma. The oldest grain (No. 11) was cloudy, 12.9% discordant, and has a minimum age of 3749 Ma. The oldest grain with less than 5% discordance (No. 4) was clear and colourless, and has a minimum age of 3727 Ma and a probable maximum age of 3767 Ma.

7.2.6 Dunbar Bay Psammite

The Dunbar Bay Psammite is a muscovite-sillimanite faserkiesel bearing unit that is interlayered with amphibolite and is intruded by gabbro. The psammite contains a mixed population of detrital zircons including large yellow oval grains, clear, colourless prismatic grains and clear to cloudy, colourless oval grains. Six grains were analyzed from this suite (Table 2). Three of the grains (Nos. 1, 5 and 6) were clear, colourless, slightly rounded prismatic grains that all have $^{207}Pb/^{206}$ Pb minimum ages of >3.5 Ga. An age calculation through the two least discordant of these analyses (Nos. 1 and 6) has an upper intercept of 3625 ± 16 Ma and a lower intercept of 1822 ± 180 Ma (Fig. 2-14). The lower intercept of this calculation is additional evidence for ca. 1.8 Ga lead loss in the sample. Analysis No. 9 was a large yellow grain that has a $^{207}Pb/^{206}$ Pb model age of ca. 3.0 Ga, consistent with its derivation from the exposed basement complex. The youngest grain in the sample (No. 2) is a clear colourless oval to slightly blocky grain that has a minimum age of 2678 Ma and a maximum age, assuming 1800 Ma lead loss, of 2773 Ma. This 2773 Ma age is interpreted to be the maximum age for deposition of this psammite. By plotting the least discordant >3.5 Ga zircon data from the psammite

with detrital zircon data from the quartzite sample, it is apparent that both samples have a similar provenance (Fig. 2-15). An age calculation based on analyses Nos. 1 and 2 from the psammite and Nos. 7 and 13 from the quartzite has an upper intercept 3619 ±47 and a lower intercept of 1789 ±710 Ma. We interpret the upper intercept of this line to identify a ca. 3.62 Ga magmatic event in the source terrain to the MBG sediments.

8. Discussion

8.1 Age of the MBG

The 3060 ± 40 Ma and 2999 ± 7 Ma ages for the Lodge Bay and Cornwall Bay granites, respectively, establish a 3.0 Ga maximum age for the MBG. McNicoll et al. (2000) report similar ages from the basement complex in the adjacent Taltson Magmatic Zone, including deformed 3076 ± 5 Ma tonalite gneiss and 3186 +17/-13 Ma mylonitic biotite-hornblende granite gneiss. Farther north in the Rae Province, 3129 +13/-10 Ma tonalite gneiss has been reported (Henderson and Theriault, 1994) and 2.9-3.0 Ga detrital zircons occur in the Woodburn Lake Group (Davis and Zaleski, 1998). The presence of ca. 3.62 and >3.75 Ga detritus in MBG sedimentary rocks indicates that an extremely old component of the Rae Province was exposed at the time of sediment deposition. There are currently no known rocks of this age exposed in Rae Province, but previous reconnaissance Nd studies along the westernmost portion of the Rae Province suggest that ancient crust may exist in this area (Theriault, 1992; Theriault *et al.*, 1994). The dominance of old zircons in the MBG may also indicate that some ancient crust was a proximal source.

The youngest detrital zircon from the psammite, which we interpret to lie stratigraphically above the basal quartzite, provides the best maximum age constraint

for the MBG. This 3.95% discordant zircon has a 2773 Ma upper intercept age, assuming 1800 Ma lead loss. The lower age constraint for the MBG is the 2.63 Ga age of the crosscutting Dead Man and Donaldson Lake Granites. These granites are interpreted as part of a 2.58-2.64 Ga granite suite that is exposed throughout the Rae Province (Ashton, 1988; LeCheminant and Roddick, 1991; Frisch and Parrish, 1992; Roddick et al., 1992).

Together, the above age constraints indicate that the MBG was deposited between 2.77 and 2.63 Ga rather than during the Proterozoic as previously suggested (Sibbald and Lewry, 1980; O'Hanley et al., 1994). The highly discordant nature of all non-abraded and some abraded zircons in our study leads us to believe that the youngest Pb-Pb detrital zircon ages reported by O'Hanley et al. (1994) were affected by episodic lead loss and do not require a Proterozoic detritus source.

8.2 Tectonic setting

The presence of continental sedimentary rocks cut by mafic dykes and overlain by basalt, such as is found in the MBG, is typical of many modern rift sequences (Eldholm et al., 1995). The absence of cherts, water-lain tuffs, and widespread pillowed volcanics are all consistent with a subaerial environment for volcanism. An ophiolite model for MBG mafic volcanic rocks is not supported for the following reasons: 1) there are no sheeted dykes or melange, 2) the mafic volcanics and basement gabbroic dykes and sills have similar geochemistry and 3) there is no evidence for a tectonized contact between basalt and underlying quartzite. The thick sequence of pelitic rocks distal to the basement complex may indicate deepening of the sedimentary basin due to rifting.

We interpret the Murmac Bay Group as a late Archean succession that was deposited in an ensialic rift basin. This interpretation is consistent with the geochemistry of MBG basalts and is similar to those made for other Archean sequences characterized by quartzite and komatiite/mafic volcanic rock.

9. Regional correlation

The Murmac Bay Group has lithological and geochronological similarities to the Woodburn Lake, Prince Albert and Mary River groups that are exposed in the northern portion of the Rae Province (Fig. 2-1a). Regional correlation between the northern belts has been previously suggested by virtually all previous workers (Jackson and Taylor, 1972; Jackson and Morgan, 1978; Ashton, 1988; Schau and Ashton, 1988; Zaleski et al., 2000a).

The Woodburn Lake Group (Ashton, 1981) comprises locally fuchsitic quartzite, komatiite, wacke and basalt (Ashton, 1988, Zaleski et al., 1999; 2000b). Felsic volcanic rocks and banded iron formation are locally present, as is minor polymictic and oligomictic conglomerate (Ashton, 1988, Zaleski et al., 1999; 2000b). Tholeiitic pillow basalt from this greenstone belt appears to rest unconformably upon 2.87 Ga basement granodiorite (Zaleski et al., 2001), which in turn intrudes older gneisses. Volcanism in the Woodburn Lake Group appears to have been diachronous, with an early ca. 2.71-2.74 Ga bimodal mafic/ultramafic-felsic cycle and a later ca. 2.64 Ga cycle dominated by felsic volcanic rock (Davis and Zaleski, 1998; Zaleski et al., 2001). The majority of quartzite in the Woodburn Lake Group is considered to be broadly coeval with this ca. 2.64 Ga volcanic event (Zaleski et al., 2001). Based on the presence of quartzite clasts in an oligomictic quartz-pebble conglomerate, Donaldson and de Kemp (1998)

suggested that the Woodburn Lake Group includes at least two major units of quartzite. An unconformity marked by polymictic conglomerate locally separates the younger quartzites from the underlying bimodal volcanic suite (Zaleski et al., 1999). These quartzites are interpreted to have developed in a fluvial and/or shallow marine environment (Donaldson and de Kemp, 1998). Numerous detrital zircons from the Woodburn Lake quartzite have ages between ca. 2.9-3.0 Ga (Ashton 1988, Davis and Zaleski, 1998) and a small population has a ca. 3.7-3.8 Ga age (Eva Zaleski, pers. com., 2001).

The Prince Albert Group (Heywood, 1967) is composed of quartzite, ultramafic to felsic volcanic rock, pelite, psammite and banded iron formation (Schau, 1982, 1997; Sandeman et al., 2001; Skulski et al., 2002). An unconformity between the Prince Albert Group and basement gneiss was reported by Schau (1974). Frisch (1982) reported ca. 2.92 Ga basement to the Prince Albert Group. A ca. 2.73 Ga felsic tuff (Skulski et al., 2002) from the Prince Albert Group indicates that volcanism was contemporaneous with that in the Woodburn Lake Group, and a crosscutting 2.72 Ga tonalite (Skulski et al., 2002) implies a plutonic component to the suite (Sandeman et al., 2001). A diversity of detrital zircon ages have been obtained from Prince Alberta Group quartzites, including ca. 2.72 Ga, ca. 2.86, and at least one that is ca. 3.7 Ga (Tom Skulski, pers. com. 2002).

The Mary River Group (Jackson, 1966) and the correlative Isortoq and Eqe greenstone belts (Morgan, 1982), central Baffin Island (Fig. 1a), comprise locally pillowed mafic and intermediate volcanic flows, felsic volcanic and volcaniclastic rock, banded iron formation, pelite and quartzite (Jackson et al., 1990; Scammell and

Bethune, 1995; Bethune and Scammell, 1997). Ultramafic volcanic rock may also be present (Jackson, 2000). A ca. 2.85 Ga trondhjemite-tonalite makes up one part of an unconformably underlying basement complex (Jackson et al., 1990). At one location the unconformity is angular in nature (Scammell and Bethune, 1995), whereas its presence is suspected at other locations where coarse conglomerates occur in the succession (Jackson et al., 1990). Volcanism in the Mary River Group spans a period from 2730 to 2715 Ma (Jackson et al., 1990; Bethune and Scammell, 1997) and is synchronous with a suite of ca. 2714-2726 Ma quartz monzodiorite to granite plutons (Bethune and Scammell, 1997).

10. Conclusions

There is mounting lithological and geochronological evidence for correlation of the Murmac Bay, Woodburn Lake, Prince Albert and Mary River Groups. All four of these packages contain significant proportions of quartzite and mafic volcanic rock/komatiite, as well as minor banded-iron formation. Felsic and related mafic to ultramafic volcanism appears to have been nearly synchronous at ca. 2.74-2.71 Ga in the three northerly belts and the ca. 2.77 to 2.63 Ga age constraints for the MBG are consistent with coeval deposition. At least three of the four supracrustal successions lie unconformably on ca. 3.0-2.85 Ga sialic basement. The majority of detrital zircon ages from a quartzite in the Woodburn Lake Group mirror the ca. 3.0 Ga basement ages whereas the ca. 2.86 Ga detrital zircon population of the Prince Albert Group is similar in age to the younger component of known basement. In addition, the Murmac Bay, Woodburn Lake, and Prince Albert groups all contain a component of ca. 3.7 Ga detritus, which seems unlikely if each developed in isolation. Regional ca. 2.64-2.58 Ga

granite plutons, of unknown tectonic affinity, intrude all four of the supracrustal packages.

The Woodburn Lake, Prince Albert, and Mary River groups have all been interpreted to have formed via rifting (Schau, 1982; Ashton 1988; Schau and Ashton, 1988; Zaleski et al., 2000a). The linear nature of this supracrustal belt appears to be broadly consistent with a rift geometry. Addition of the Murmac Bay Group to these three northern packages extends the belt, discontinuously, to a total length of at least 2000 km. Detailed geochronology may determine if extension occurred in one pulse, or if it was diachronous.

The presence of an Archean rift that is over 2000 km in length implies that a stable craton of that size existed prior to ca. 2.7 Ga. Schau and Ashton (1988) named the large ensialic core of the Rae Province, Nunavutia. This term is especially appropriate since the craton comprises a large portion of the Canadian Territory that was recently named Nunavut. Recognition of the total extent and nature of Nunavutia, including the possible presence of additional Archean supracrustal belts between the MBG and Woodburn Lake Group, will require further mapping and isotopic studies, similar to those defining the Central Slave Basement Complex (Bleeker et al., 1999) of the Slave Craton. Although Stott (1997) suggested that the Superior Province is the largest fragment of Archean lithosphere, Nunavutia may represent the largest block of coherent pre-2.7 Ga continental crust on Earth. Parts of this craton were characterized by Paleo- to Mesoarchean magmatic events at ca. 3.0, ca. 3.62 and >3.7 Ga.

References

Armstrong, R.L., 1981. Radiogenic isotopes: the case for crustal recycling on a near-steady-state no continental-growth Earth. Phil. Trans. R. Soc. Lond. A 301, 443-472.

Armstrong, R.L., 1991. The persistent myth of crustal growth. Aust. J. Earth Sci. 38, 613-630.

Arndt, N.T., 1999. Why was flood volcanism on submerged continental platforms so common in the Precambrian? Precambrian Res. 97, 155-164.

Ashton, K.E., 1981. Preliminary Report On Geological Studies of the "Woodburn Lake Group" Northwest of Tehek Lake, District of Keewatin. Geol. Surv. Can., Pap. 81-01A, 269-274.

Ashton, K.E., 1988. Precambrian geology of the southeastern Amer Lake area (66H/1), near Baker Lake, N.W.T.. Ph.D. thesis, Queens University, Canada.

Ashton, K.E., Card, C.D., 1998. Rae Northeast: A Reconnaissance of the Rae Province Northeast of Lake Athabasca. Sask. Geol. Surv. Misc. Rep. 98-4, 3-16.

Ashton, K.E., Kraus, J., Hartlaub, R.P., Morelli, R., 2000. Uranium City revisited: A new look at the rocks of the Beaverlodge Mining Camp. Sask. Geol. Surv., Misc. Rep. 2000-4.2, 3-15.

Ashton, K.E., Boivin, D., Heggie, G., 2001a. Geology of the Southern Black Bay Belt, west of Uranium City, Rae Province. Sask. Geol. Surv., Misc. Rep. 2001-4.2. 50-63.

Ashton, K.E., Hartlaub, R.P., Card, C.D., Morelli, R., 2001b. Paleoproterozoic history of the Rae Province in Northern Saskatchewan: The Thelon-Taltson/Trans-Hudson Vise and Beyond. GAC-MAC Abstract Volume 27, pp. 4.

Aspler, L.B., Chiarenzelli, J.R., 1996. Stratigraphy, sedimentology and physical volcanology of the Henik Group, central Ennadai-Rankin greenstone belt, Northwest Territories, Canada: late Archean paleogeography of the Hearne Province and tectonic implications. Precambrian Res. 77, 59-89.

Aspler, L.B., Chiarenzelli, J.R., 1997. Initiation of ~2.45-2.1 Ga intracratonic basin sedimentation of the Hurwitz Group, Keewatin Hinterland, Northwest Territories, Canada. Precambrian Res. 81, 265-297.

Bateman, R., Costa, S., Swe, T., Lambert, D., 2001. Archaean mafic magmatism in the Kalgoorlie area of the Yilgarn Craton, Western Australia: a geochemical and Nd isotopic study of the petrogenetic and tectonic evolution of a greenstone belt. Prec. Res. 108, 75-112.

Bell, K. and Bikerman, M., 1985. Saskatchewan Shield geochronology project: Rb-Sr studies, 1985. Sask. Geol. Surv., Misc. Rep. 85-4, 59.

Bethune, K.M., Scammell, R.J., 1997. Legend and Descriptive notes, Koch Island area, District of Franklin, Northwest Territories, (part of NTS 37C). Geol. Surv. Can., Open File 3391, sheet 4 of 4.

Bickle, M.J., Martin, A., Nisbet, E.G., 1975. Basaltic and peridotitic komatiites, stromatolites and a basal unconformity in the Belingwe Greenstone Belt, Rhodesia: Earth Planet. Sci. Lett. 27, 155-162.

Bickle, M.J., Nisbet, E.G., Martin, A., 1994. Archean greenstone belts are not oceanic crust. J. Geology 102, 121-138.

Blake, T.S., 2001. Cyclic continental mafic tuff and flood basalt volcanism in the late Archaean Nullagine and Mount Jope Supersequences in the eastern Pilbara, Western Australia. Prec. Res. 107, 139-177.

Bleeker, W., Ketchum, J.W.F., Jackson, V.A., Villeneuve, M.E., 1999. The Central Slave Basement Complex, Part 1: its structural topology and autochthonous cover. Can. J. Earth Sci. 36, 1083-1109.

Bleeker, W., Ketchum, J., Tomlinson, K., Thuston, K.S., Stern, R., Davis, D., 2000. Archean quartzite-banded iron formation-komatiite sequences: Indicators of rifting of MesoArchean supercratons. Geocanada 2000 abstract volume, Geol. Assoc. Can.

Blenkinsop, T.G., Fedo, C.M., Bilke, M.J., Erikson, K.A., Marin, A., Nisbet, E.G., Wilson, J.F., 1993. Ensialic origin for the Ngezi Group, Belingwe greenstone belt, Zimbabwe. Geology 21, 1135-1138.

Cameron, E.M., Smith, D.E., Walker, R.L., 1969. Mass spectrometry of nanogram sized samples of lead. Anal. Chem. 41, 525-526.

Card, C.D., Bethune, K.M., 1999. The Oldman-Bulyea Shear Zone: Studies across the Nevins Lake Block-Train Lake Domain boundary in the Rubus-Bulyea lakes and Oldman Lake areas. Sask. Geol. Surv., Misc. Rep. 99-4.2, 27-37.

Card, K.D., 1990. A review of the Superior Province of the Canadian Shield, a product of Archean accretion: Precambrian Res., 48, 99-156.

Chauvel, C., Dupre, B., Arndt, N.T., Hofmann, A.W., 1993. Pb and Nd isotopic correlation in Belingwe komatiites and basalts. In: Bickle, M.J., Nisbet, E.G. (Eds.), The Geology of the Belingwe Greenstone Belt, Zimbabwe: A study of the Archean continental crust: Geol. Soc. Zimbabwe, Special Publication 2, pp. 167-174.

Condie, K.C., 1990. Growth and accretion of continental crust: Inferences based on Laurentia. Chem. Geol. 83, 183-194.

Cousens, B.L., Aspler, L.B., Chiarenzelli, J.R., Donaldson, J.A., Sandeman, H., Peterson, T.D., LeCheminant, A.N., 2001. Enriched Archean lithospheric mantle beneath Western Churchill Province tapped during Paleoproterozoic orogenesis. Geology 29, 827-830.

Cox, R., Gutmann, E.D., Hines, P.G., 2002. Diagenetic origin for quartz-pebble conglomerates. Geology 30, 323-326.

Davis, W.J., Zaleski, E., 1998. Geochronological investigations of the Woodburn Lake Group, western Churchill Province, Northwest Territories: preliminary results. Geol. Surv. Can., Current Res. 1998-F, 89-97.

de Ronde, C.E.J., de Wit, M.J., 1994. Tectonic history of the Barberton greenstone belt, South Africa: 490 million years of Archean crustal evolution. Tectonics 13, 983-1005.

de Wit, M.J., Roering, C., Hart, R.J., Armstrong, A., de Ronde, C.E.J., Green, R.W.E., Tredoux, M., Peberdy, E., Hart, R.A., 1992. Formation of an Archaean continent. Nature 357, 553-562.

Donaldson, J.A., de Kemp, E., 1998. Archaean quartz arenites in the Canadian Shield: examples from the Superior and Churchill Provinces. Sediment. Geol. 120, 153-176.

Drury, S.A., 1978. Were Archaean continental geothermal gradients much steeper than today?. Nature 274, 720-721.

Dunning, G.R., Barr, S.M., Giles, P.S., McGregor, D.C., Pe-Piper, G., Piper, D.J.W., 2002. Chronology of Devonian to early Carboniferous rifting and igneous activity in southern Magdalen Basin based on U-Pb (zircon) dating. Can. J. Earth Sci. 39, 1219-1237.

Dupuy, C., Dostal, J., 1984. Trace element geochemistry of some continental tholeiites. Earth Planet. Sci. Lett. 67, 61-69.

Eldholm, O., Skogseid, J., Planke, S., Gladczenko, T.P., 1995. Volcanic margin concepts. In: Banda, E., Torné, M., Talwani, M. (Eds.), Rifted ocean-continent boundaries. Kluwer Academic Publishers, Dordrecht, pp.1-16.

Frisch, T., 1982. Precambrian Geology of the Prince Albert Hills, western Melville Peninsula, Northwest Territories. Geol. Surv. Can., Bulletin 346.

Frisch, T., Parrish, R.R., 1992. U-Pb zircon ages from the Chantrey Inlet area, Northern District of Keewatin, Northwest Territories. Geol. Surv. Can., Pap. 91-2, 35-41.

Green, M., Sylvester, P.J., Buick, R., 2000. Growth and Recycling of early Archaean continental crust: geochemical evidence from the Coonterunah and Warawoona Groups, Pilbara Craton, Australia. Tectonophysics 322, 69-88.

Hargraves, R.B., 1986. Faster spreading or greater ridge length in the Archean? Geology 14, 750-752.

Harper, C.T., 1983. Iron ores of northern Saskatchewan. Sask. Energy Mines, Regina, Canada.

Hartlaub, R.P., 1999. New insights into the geology of the Murmac Bay Group, Rae Province, Northwest Saskatchewan. Sask. Geol. Survey, Misc. Rep. 99-4.2, 17-26.

Hartlaub, R.P., Ashton, K.E., 1998. Geological investigations of the Murmac Bay Group, Lake Athabasca north shore transect. Sask. Geol. Surv., Misc. Rep. 98-4, 17-28.

Heaman, L.M., Erdmer, P., Own, J.V., 2002. U-Pb geochronologic constraints on the crustal evolution of the Long Range Inlier, Newfoundland. Can. J. Earth Sci. 39, 845-864.

Henderson, J.B., 1981. Archean basin evolution in the Slave Province, Canada. In: Kroner, A. (Ed.), Precambrian Plate Tectonics. Elselvier, Amsterdam, pp. 213-235.

Henderson, J.B., Thériault, R.J., 1994. U-Pb zircon evidence for circa 3.1 Ga crust south of the McDonald Fault, northwestern Canadian Shield, Northwest Territories. Geol. Surv. Can., Current Res. 1994-F, 43-47.

Heywood, W.W., 1967. Geological notes, northeastern District of Keewatin and southern Melville Peninsula, District of Franklin, Northwest Territories (Parts of 46, 47, 56, 57). Geol. Surv. Can., Pap. 66-40.

Hoffman, P.F., 1988. United plates of America: the birth of a craton. Early Proterozoic assembly and growth of Laurentia. Annual Review Earth Planet. Sci. Lett. 60, 543-603.

Hoffman, P.F., 1990. Subdivision of the Churchill Province and extent of the Trans-Hudson Orogen. In. Lewry, J.F., Stauffer, M.R. (Eds.), The early Proterozoic Trans-Hudson Orogen of North America. Geol. Assoc. Can., Spec. Pap. 37, pp. 15-39.

Hofmann, A.W., 1988. Chemical differentiation of the Earth: The relationship between mantle, continental crust, and oceanic crust. Earth Planet. Sci. Lett. 90, 297-314.

Hunter, M.A., Bickle, M.J., Nisbet, E.G., Martin, A., Chapman, H.J., 1998. Continental extension setting for the Archean Belingwe Greenstone Belt, Zimbabwe, Geology 26, 883-886.

Jackson, G.D., 1966. Geology and Mineral possibilities of the Mary River region, northern Baffin Island. Can. Mining J. 87, 57-61.

Jackson, G.D., 2000. Geology of the Clyde-Cockburn Land map area, north-central Baffin Island, Nunavut. Geol. Surv. Can., Memoir 440.

Jackson, G.D., Taylor, F.C., 1972. Correlation of major Aphebian rock units in the Canadian Shield. Can. J. Earth Sci. 9, 1650-1669.

Jackson, G.D., Morgan, W.C., 1978. Precambrian metamorphism on Baffin and Bylot Islands. In: Fraser, J.A., Heywood, W.W. (Eds.), Metamorphism in the Canadian Shield. Geol. Surv. Can., Paper 78-10, 249-267.

Jackson, G.D., Hunt, P.A., Loveridge, W.D., Parrish, R.R., 1990. Reconnaissance geochronology of Baffin Island, N.W.T.. Geol. Surv. Can., Pap. 89-2, 123-148.

Jackson, S.L., Fyon, J.A., Corfu, F., 1994. Review of Archean supracrustal assemblages of the southern Abitibi greenstone belt in Ontario, Canada: Products of microplate interaction within a large-scale plate-tectonic setting. Precambrian Res. 65, 183-205.

Jensen, L.S., 1976. A new cation plot for classifying subalkalic volcanic rocks. Ontario Div. Mines, Misc Pap. 66.

Krogh, T.E., 1973. A low contamination method for hydrothermal decomposition of zircon and extraction of U and Pb for isotopic age determinations. Geochim. Cosmochim. Acta 37, 485-494.

Krogh, T.E., 1982. Improved accuracy of U-Pb zircon ages by the creation of more concordant systems using an air abrasion technique. Geochim. Cosmochim. Acta 46, 637-649.

Kusky T.M., 1989. Accretion of the Archean Slave Province. Geology 17, 63-67.

Kusky, T.M., Kidd, W.S.F., 1992. Remnants of an Archean oceanic plateau, Belingwe Greenstone Belt, Zimbabwe. Geology 20, 43-46.

Kusky, T.M., Hudleston, P.J., 1999. Growth and Demise of an Archean carbonate platform, Steep Rock Lake, Ontario Canada. Can. J. Earth Sci. 36, 1-20.

Kusky, T.M., Kidd, W.S.F., 1999. Continental extensional setting for the Archean Belingwe greenstone belt-discussion of paper by M.A. Hunter, M.J. Bickle, E.G. Nisbet, A. Martin, H.J. Chapman. Geology 27, 861.

LeCheminant, A.N., Roddick, J.C., 1991. U-Pb zircon evidence for widespread 2.6 Ga felsic magmatism in the central District of Keewatin, NWT. Geol. Surv. Can., Paper 90-2, 91-99.

Ludwig, K.R., 1998. Isoplot/Ex, a geochronological toolkit for microsoft excel, Version 2.22. Berkely, California, Berkely Geochronology Center Special Publication 1.

MacDonald, L.A., Barr, S.M., White, C.E., Ketchum, W.F., 2002. Petrology, age, and tectonic setting of the White Rock Formation, Meguma terrane, Nova Scotia: evidence for Silurian continental rifting. Can. J. Earth Sci. 39, 259-277.

Macdonald, R., Thomas, M., Lee, N., 1982. Geology of the Hill Lake area (NTS 74N, CSMA photomap sheet 6500-65900). Sask. Geol. Surv., Misc. Rep. 82-4, 8-11.

McLennan, S.M., Taylor, S.R., 1983. Continental freeboard, sedimentation-rates and growth of the continental crust. Nature 306, 169-172.

McNicoll, V.J., Thériault, R.J., McDonough, M.R., 2000. Taltson basement gneisses: U-Pb and Nd isotopic constraints on the basement to the Taltson magmatic zone, Northeastern Alberta, Can. J. Earth Sci. 37, 1575-1596.

Morgan, W.C., 1982. Geology, Koch Island, District of Franklin, Northwest Territories. Geol. Surv. Can., Map 1535A.

Nisbet, E.G., Martin, A., Bickle, M.J., Orpen, J.L., 1993. The Ngezi Group: komatiites, basalts and stromatolites on continental crust. In: Bickle, M.J., Nisbet, E.G. (Eds.), The Belingwe Greenstone Belt Zimbabwe: A study of Archean continental crust. Geol. Soc. Zimbabwe Spec. Pub., Rotterdam, Balkema.

O'Hanley, D.S., Kyser, K.T., Sibbald, T.I.I., 1994. The age and origin of the North Shore Plutons in the Rae Province, Goldfields area, Saskatchewan. Can. J. Earth Sci. 31, 1397-1406.

Papezik, V.S., Greenough, J., Colwell, J.A., Mallinson, T.J., 1988. North Mountain basalt from Digby, Nova Scotia: models for a fissure eruption from stratigraphy and petrochemistry. Can. J. Earth Sci. 25, 74-83.

Pattison, D.R.M., 2001. Instability of Al2SiO5 "triple-point" assemblages in muscovite+biotite+quartz-bearing metapelites, with implications. American Mineralogist 86, 1414-1422.

Percival, J.A., Bailes, A.H., Corkery, M.T., Dubé, B., Harris, J.R., McNicoll, V., Panagapko, D., Parker, J.R., Rogers, N., Sanborn-Barrie, M., Skulski, T., Stone, D., Stott, G.M., Tomlinson, K.Y., Whalen, J.B., Young, M.D., 2000. Western Superior NATMAP: an integrated view of Archean crustal evolution. Man. Geol. Surv., Report of Activities 2000, 108-116.

Persons, S.S., 1988. U-Pb geochronology of Precambrian rocks in the Beaverlodge area, Northwestern Saskatchewan. M.Sc. Thesis, University of Kansas.

Pin, C., Marini, F., 1993. Early Ordovician continental break-up in Variscan Europe: Nd-Sr isotope and trace element evidence from bimodal igneous associations of the Southern Massif Central, France. Lithos 29, 177-196.

Puffer, J.H., 2001. Contrasting high field strength element contents of continental flood basalts from plume versus reactivated-arc sources. Geology 29, 675-678.

Roddick, J.C., Henderson, J.R., Chapman H.J., 1992. U-Pb ages from the Archean Whitehills-Tehek lakes supracrustal belt, Churchill Province, District of Keewatin, Northwest Territories. Geol. Surv. Can., Pap. 92-2, 31-40.

Sandeman, H.A., Brown, J., Studnicki-Gizbert, C., MacHattie, T., Hyde, D., Johnstone, S., Greiner, E., Plaza, D., 2001. Bedrock mapping in the Committee Bay Belt, Laughland Lake area, central mainland, Nunavut. Geol. Surv. Can., Current Res., 2001-C12.

Scammell, R.J., Bethune, K.M., 1995. Archean and Proterozoic lithology, structure, and metamorphism in the vicinity of Eqe Bay, Baffin Island, Northwest Territories. Geol. Surv. Can, Current Res. 1995-C, 53-66.

Schau, M., 1974. Volcanic rocks of the Prince Albert Group. Geol. Surv. Can., Paper 1974-1A, 187-188.

Schau, M., 1982. Geology of the Prince Albert Group in parts of Walker Lake and Laughland Lake map areas, District of Keewatin. Geol. Surv. Can., Ottawa, Bulletin 337.

Schau, M., 1997. Geology of the Archean Prince Albert Group in the Richards Bay area, northeastern Melville Peninsula, District of Franklin, Northwest Territories. Geol. Surv. Can., Ottawa, Bulletin 385.

Schau, M., Ashton, K.E., 1988. The Archean Prince Albert Group, northeastern Canada: evidence for crustal extension within a >2.9 Ga continent. Abstracts with Programs 20, A50 No. 18961, Geol. Soc. America.

Schwann, P.L., 1985. Geochemistry and Petrology of the Nicholson Bay Ultramafic Complex, Northwestern Saskatchewan. B.Sc. thesis, University of Regina.

Sheth, H.C., 1999. A historical approach to continental flood basalt volcanism: insights into pre-volcanic rifting, sedimentation, and early alkaline magmatism. Earth Planet. Sci. Lett. 168, 19-36.

Sibbald, T.I.I., 1982. Uranium metallogenic studies: Nicholson Bay area. Sask. Geol. Surv., Misc. Rep. 82-4, 43-45.

Sibbald, T.I.I., 1984. Gold metallogenic studies, Goldfields area. Sask. Geol. Surv., Misc. Rep. 84-4, 116-121.

Sibbald, T.I.I., Lewry, J.F., 1980. Uranium metallogenic studies: Lodge Bay area, Lake Athabasca. Sask. Geol. Surv., Misc. Rep. 80-4, 44-48.

Sibbald, T.I.I., Schwann, P.L., Dunn, C.E., 1983. Uranium-gold metallogenic studies: Nicholson Bay Ultramafic Complex. Sask. Geol Surv., Misc. Rep. 83-4, 75-79.

Skulski, T., Sandeman, H.A., Sanborn-Barrie, M., MacHattie, T., Hyde, D., Johnstone, S., Panagapko, D., Byrne, D., 2002. Contrasting crustal domains in the Committee Bay Belt, Walker Lake-Arrowsmith River area, central Nunavut. Geol. Surv. Can., Current Res. 2002-C11.

Srinivasan, R., Ojakangas, R.W., 1986. Sedimentology of quartz-pebble conglomerates and quartzites of the Archean Bababudan Group, Dharwar Craton, South India: evidence for early crustal stability. J. Geol. 94, 199-214.

Stacey, J.S., Kramers, J.D., 1975. Approximation of terrestrial lead isotope evolution by a two-stage model. Earth Planet. Sci. Lett. 26, 207-221.

Stewart, K., Rogers, N., 1996. Mantle plume and lithosphere contributions to basalts from southern Ethiopia. Earth Planet. Sci. Lett. 139, 195-211.

Stott, G.M., 1997. The Superior Province, Canada. In: De Witt M.J., Ashwall, M.D. (Eds.), Greenstone belts. Clarendon, Oxford, pp. 480-507.

Swager, C.P., 1997. Tectono-stratigraphy of late Archaean greensone terranes in the southern Eastern Goldfields, Western Australia. Precambrian Res. 83, 11-42.
Theriault, R.J., 1992. Nd isotopic evolution of the Taltson Magmatic Zone, Northwest Territories, Canada: insights into Early Proterozoic accretion along the western margin of the Churchill Province. J. Geology 100, 465-475.

Thériault, R.J., Henderson, J.B., Roscoe, S.M., 1994. Nd isotopic evidence for early to mid-Archean crust from high grade gneisses in the Queen Maud Block and south of the McDonald Fault, western Churchill Province, Northwest Territories. Radiogenic age and isotopic studies: report 8, Geol. Surv. Can., 1994-F, 37-42.

Thurston, P.C., Chivers, K.M., 1990. Secular variation in greenstone sequence development emphasizing Superior Province, Canada. Precambrian Res. 46, 21-58.

Thurston P.C., Kozhevnikov, V.N., 2000. An Archean quartz arenite-andesite association in the eastern Baltic Shield, Russia: implications for assemblage types and shield history. Precambrian Res. 101, 313-340.

Thurston, P.C., Ayres, L.D., Edwards, G.R., Gelinas, L., Ludden, J.N., Verpaelst, P., 1985. Archean bimodal volcanism. In: Ayres, L.D., Thurston, P.C., Card, K.D., Weber, W. (Eds.), Evolution of Archean Supracrustal Sequences. Geol. Assoc. Can., Special Paper 28. pp. 7-21.

Tomlinson K.Y., Hughes, D.J., Thurston P.C., Hall R.P., 1999. Plume magmatism and crustal growth at 2.9 to 3.0 Ga in the Steep Rock and Lumby Lake area, western Superior Province. Lithos 46, 103-136.

Tremblay, L.P., 1972. Geology of the Beaverlodge Mining Area, Saskatchewan. Memoir 367, Geol. Surv. Can., Ottawa.

Tremblay, L.P., Loveridge, W.D., Sullivan, R.W., 1981. U-Pb ages of zircons from the Foot Bay Gneiss and the Donaldson Lake Gneiss, Beaverlodge Area, Northern Saskatchewan. Geol. Surv. Can., Current Res. 1981-1C, 123-126.

Wheeler, J.O., Hoffman, P.F., Card, C.K., Davidson, A., Sanford, B.V., Okulitch, A.V., Roest, W.R., 1996. Geological Map of Canada. Geol. Surv. Can., scale 1:5,000,000.

Wilks, M.E., Nisbet, E.G., 1988. Stratigraphy of the Steep Rock Group, northwestern Ontario: a major Archean unconformity and Archean stromatolites. Can. J. Earth Sci. 25, 370-391.

Zaleski, E., L'Heureux, R., Duke, N., Wilkinson, L., Davis, W.J., 1999. Komatiitic and volcanic rocks overlain by quartzite, Woodburn Lake group, Meadowbank River area, western Churchill Province, Northwest Territories (Nunavut). Geol. Surv. Can., Current Res. 1999-C, 9-18.

Zaleski, E., Davis, W.J., Pehrson, S.J., Duke, N.A., L'Heureux, R., Greiner, E., 2000a. Archean continental rifting recorded by orthoquartzite and bimodal komatiitic-felsic magmatism in the Woodburn Lake Group, Western Churchill Province, Nunavut. Geocanada 2000 abstract volume, Geol. Assoc. Can.

Zaleski, E., Pehrsson, S., Duke, N., Davis, W.J., L'Heureux, R., Greiner, E., Kerswill, J.A., 2000b. Quartzite sequences and their relationships, Woodburn Lake Group, western Churchill Province, Nunavut. Geol. Surv. Can., Current Res. 2000-C7.

Zaleski E., Davis, W.J., Sandeman, H.A., 2001. Continental extension, mantle magmas & basement/cover relationships. 4th International Archean Symposium 2001, Extended Abstracts. AGSO – Geoscience Australia, Record 2001/37, pp. 374-376.

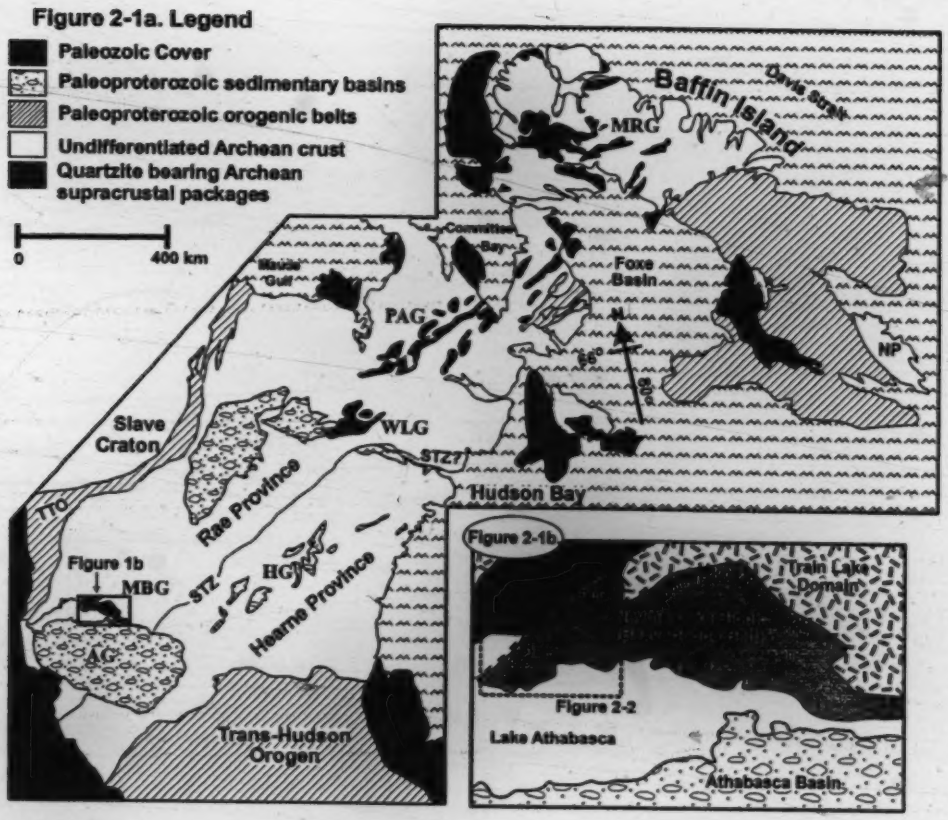

Figure 2-1a. General geology of the Rae Province and bounding tectonic entities. Quartzite-bearing greenstone sequences are highlighted in black (Modified after Jackson et al., 1990; Wheeler et al., 1996; Aspler and Chiarenzelli, 1997; Scott, 1999; and Skulski et al. 2002). The study area (Fig. 2-2) is highlighted on the north shore of Lake Athabasca. AG, Athabasca Group; HG, Hurwitz Group; MBG, Murmac Bay Group; MRG, Mary River Group; NP, Nain Province; PAG, Prince Albert Group; STZ, Snowbird Tectonic Zone; TTO, Taltson-Thelon orogenic belt; WLG, Woodburn Lake Group.
Figure 2-1b. Sketch map showing the major geological subdivisions of the study area. DLG, Donaldson Lake Granite; DMG, Dead Man Granite.

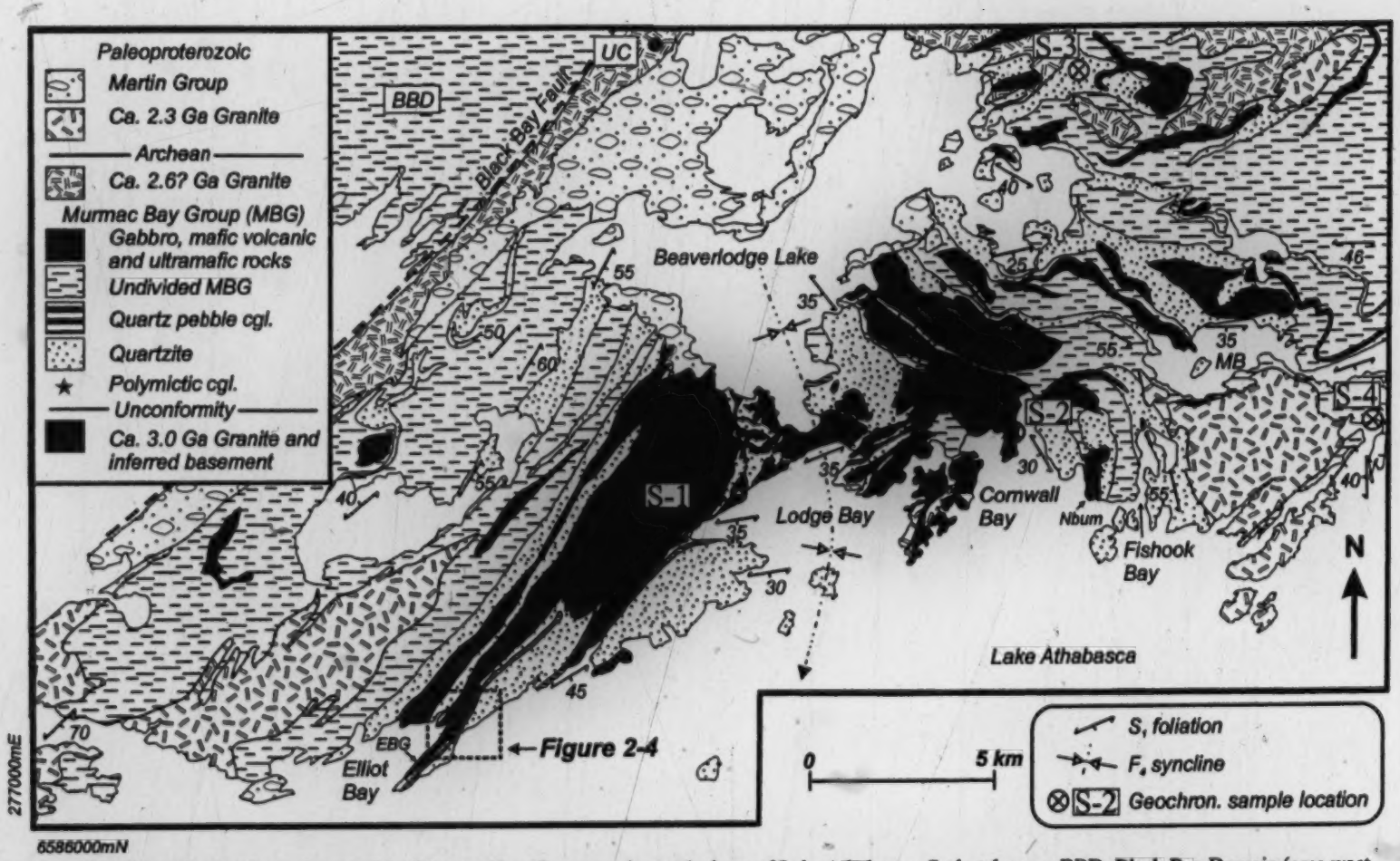

Figure 2-2. Simplified geological map of the Murmac Bay Group on the north shore of Lake Athabasca, Saskatchewan. BBD, Black Bay Domain (area west of the Black Bay Fault); CBG, Cornwall Bay Granite; EBG, Elliot Bay Granite; LBG, Lodge Bay Granite; MB, Macintosh Bay; Nbum, Nicholson Bay ultramafic body; UC, Uranium City. Geochronology sample sites are: the Lodge Bay Granite (S-1), the Cornwall Bay Granite (S-2), the Fookes Lake Quartzite (S-3) and the Dunbar Bay Psammite (S-4).

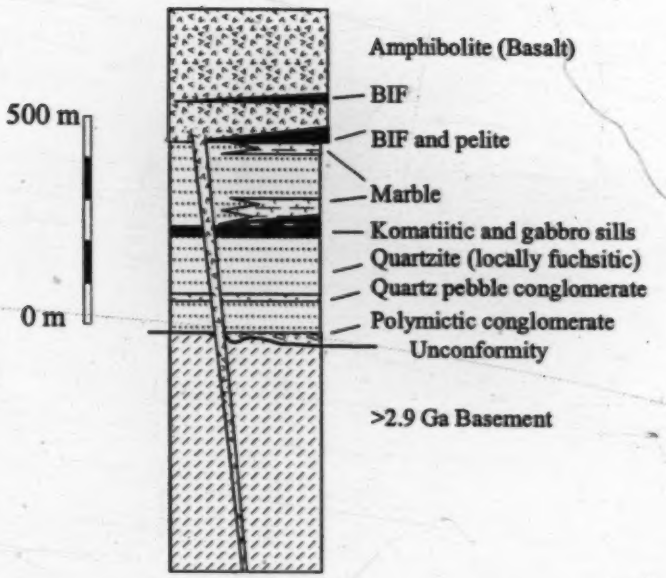

Figure 2-3. Simplified stratigraphy of the lower Murmac Bay Group.

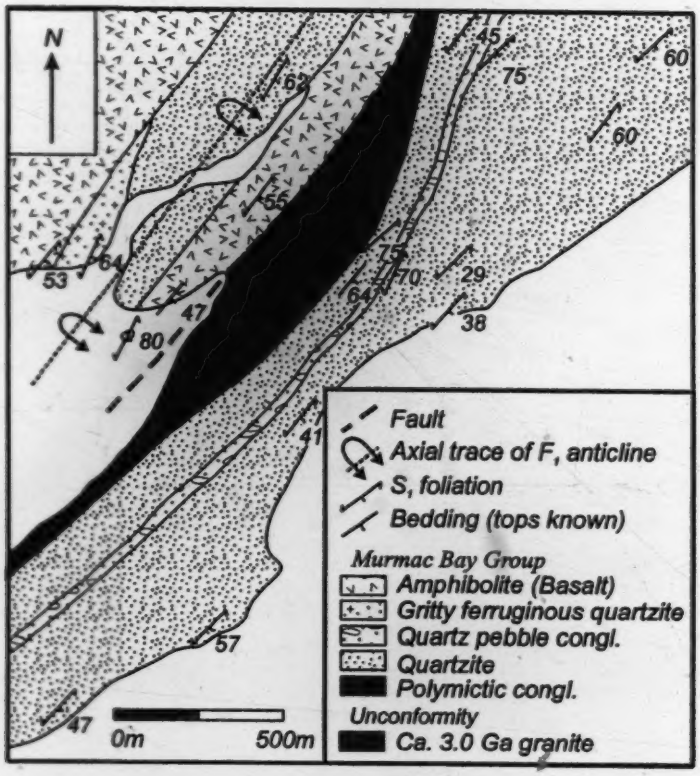

Figure 2-4. Geological map of the Elliot Bay Granite (EBG) and the unconformably overlying Murmac Bay Group.

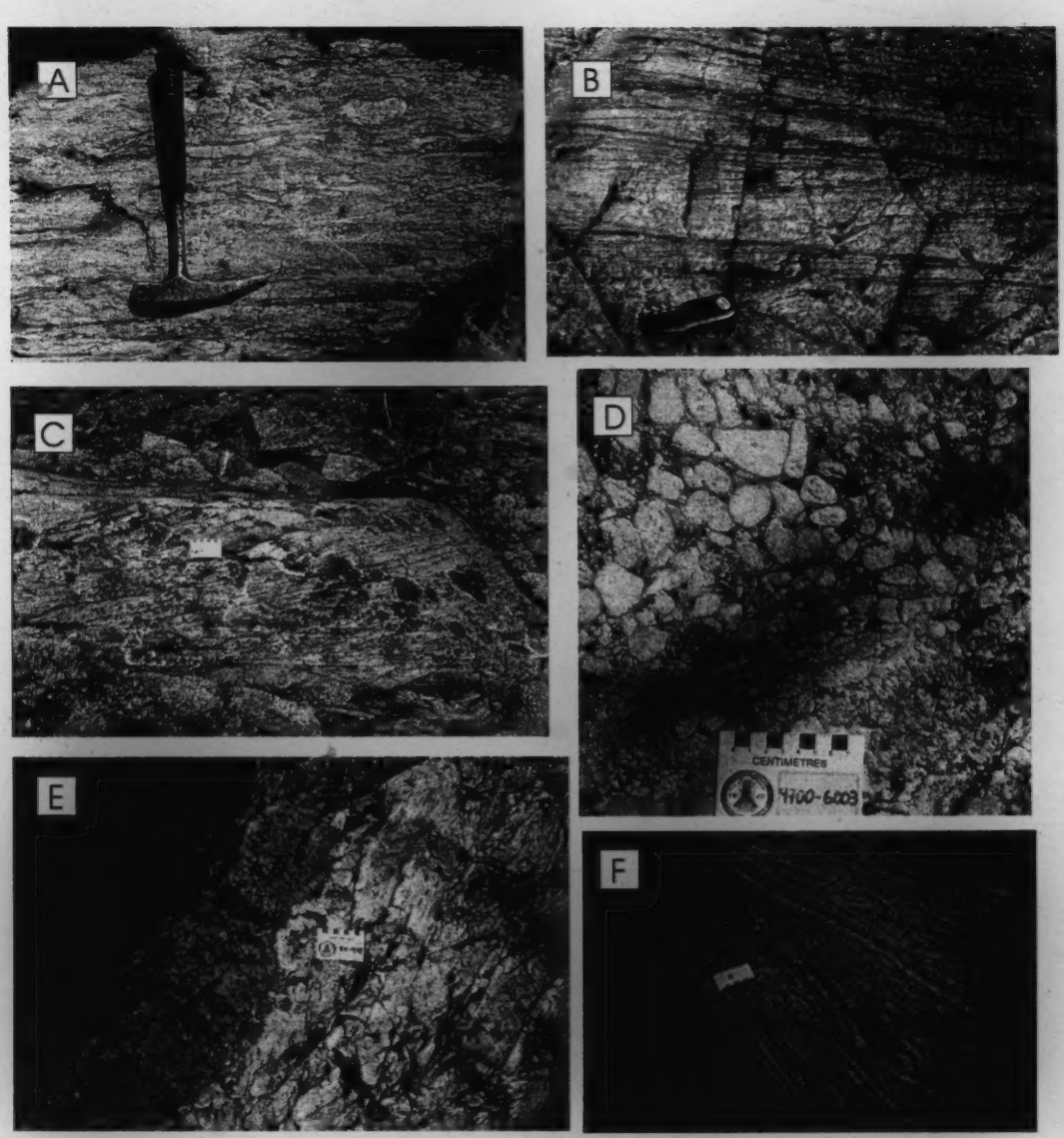

Figure 2-5. A) Polymictic conglomerate at the unconformity between the Lodge Bay Granite and quartzite near Elliot Bay. Note the rounded granitoid clast in upper right. B) Deformed planar crossbedding in a quartzite from Macintosh Bay, Lake Athabasca. C) Large-scale trough crossbedding in a clean white quartzite exposed 1 km northwest of Lodge Bay. D) Oligomictic quartzite-pebble clast-supported conglomerate containing both rounded and angular clasts. This conglomerate is well exposed on the south shore of Beaverlodge Lake. E) Pegmatitic diopside calc-silicate (central band) between brown marble (upper left) and white quartzite (bottom right) exposed on Lake Athabasca. Primary layering is evident in the marble. F) Disrupted amphibolite layer (mafic dyke) within migmatitic quartzofeldspathic rocks that are interpreted to be psammite. This unit is exposed 15 km east of the Cornwall Bay Granite where rocks have reached upper amphibolite-facies.

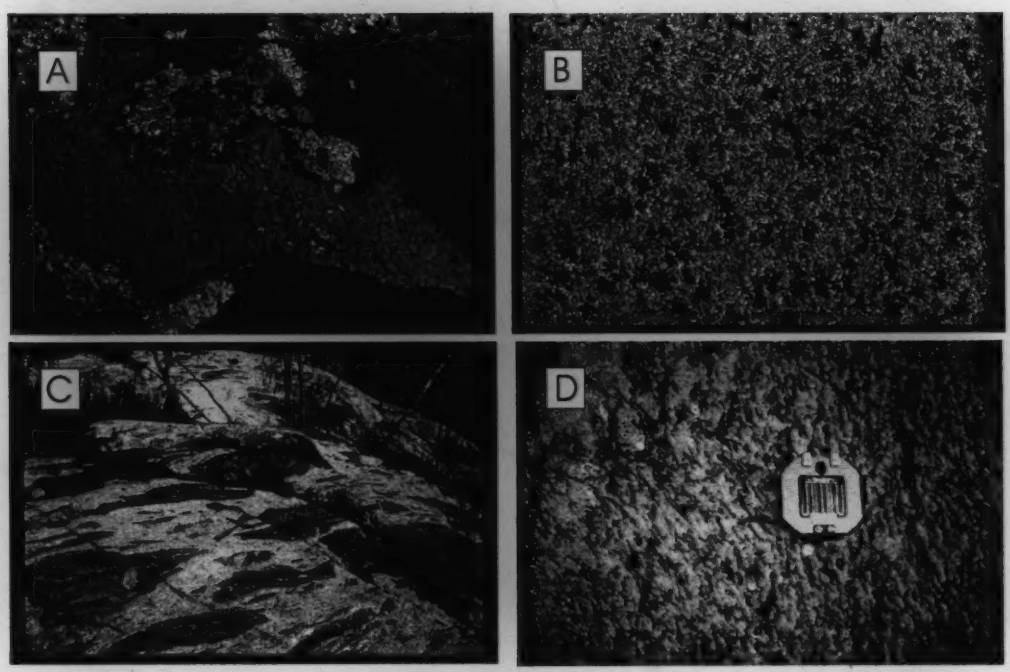

Figure 2-6. A) Close up of metamorphosed ultramafic rock from the margin of the Nicholson Bay ultramafic body (field of view is ~ 30 cm). B) Close up of hornblende porhyroblasts in a gabbro from Lodge Bay (field of view is ~ 20 cm). C) Forest fire exposure of the Donaldson Lake Granite. Numerous large amphibolite xenoliths are apparent (hammer for scale). D) Close-up of the upper-amphibolite to granulite-facies Dead Man Granite (Brunton compass for scale).

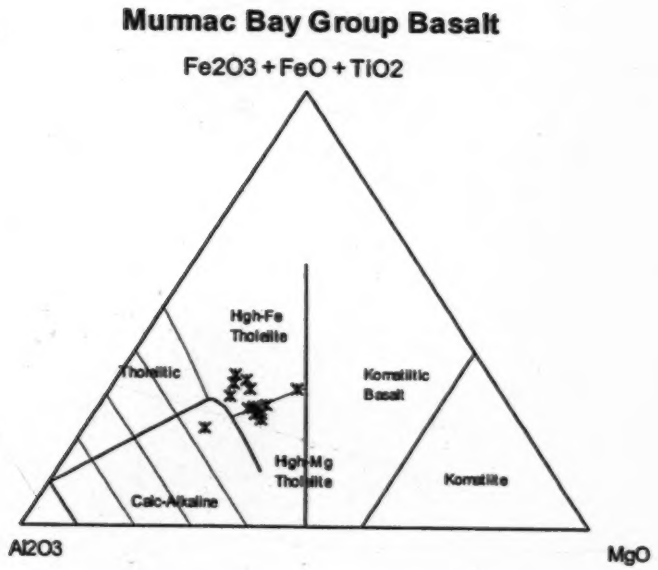

Figure 2-7. Plot of MBG basalts (n=14) on the basalt discrimination diagram of Jensen (1976). Most of the MBG samples cluster together in the high-Fe to high-Mg tholeiite field.

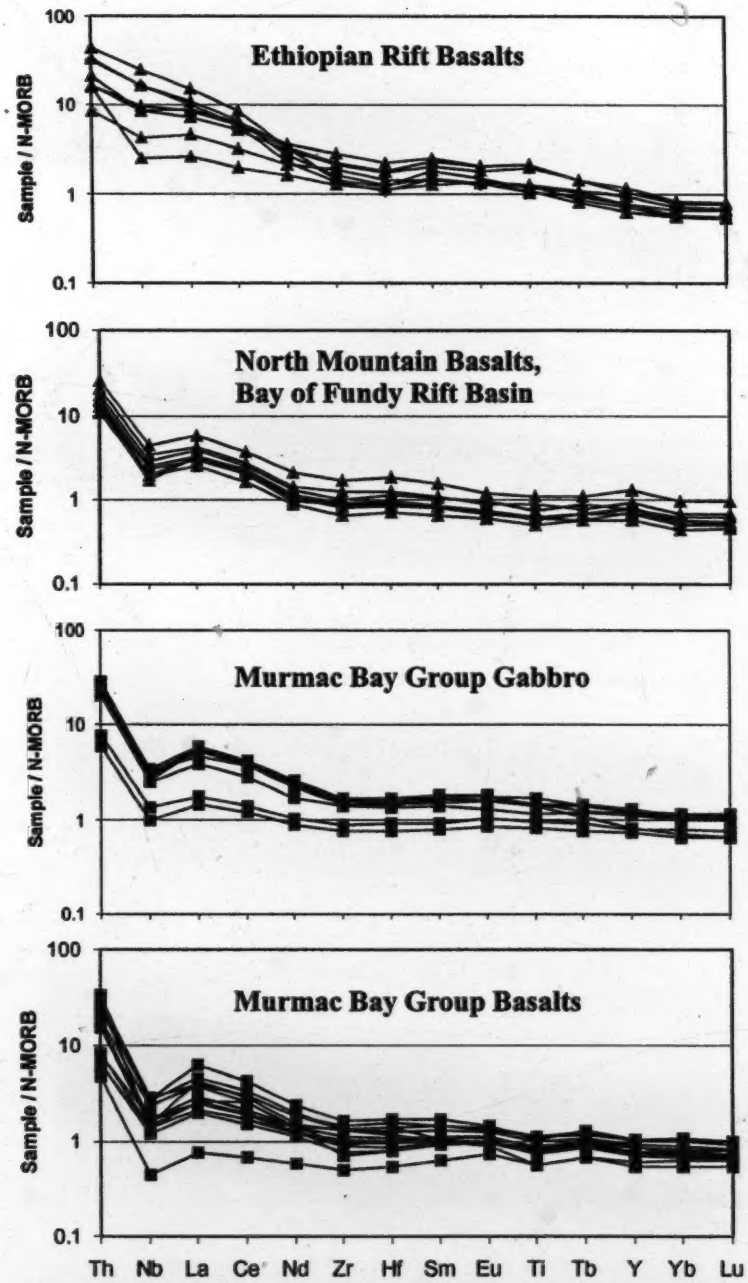

Figure 2-8. N-MORB (Hofmann, 1988) normalized plots of selected trace elements for basalts (n=14) and gabbros (n=10) from the MBG as well as basalts from two known continental rift settings. Data for Ethiopian rift basalts (n=8) comes from Stewart and Rogers (1996), whereas data for North Mountain basalts (n=10) of the Bay of Fundy (Atlantic) Rift is taken from from Papezik et al. (1988).

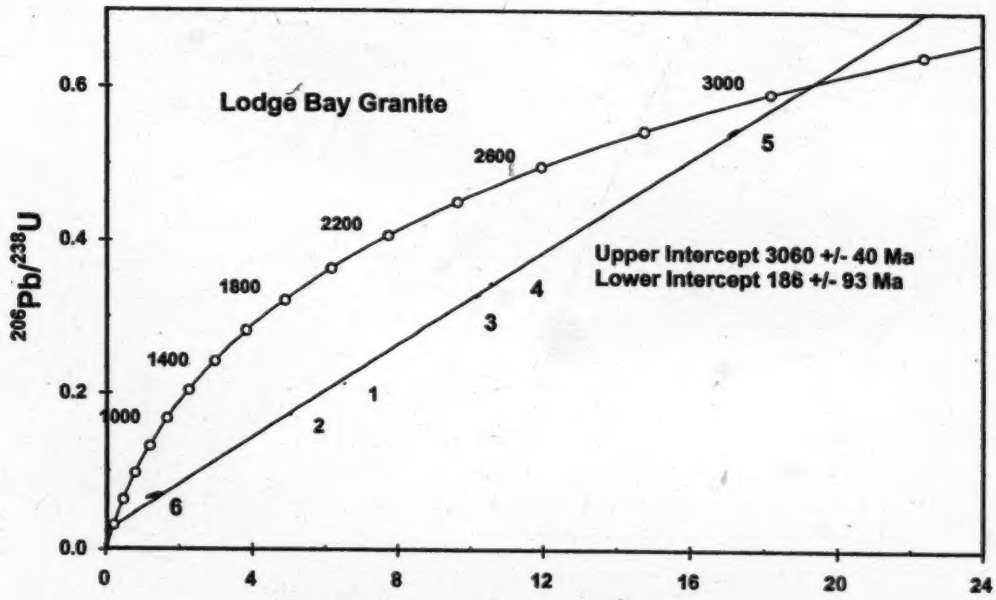

Figure 2-9. Concordia diagram for the Lodge Bay Granite.

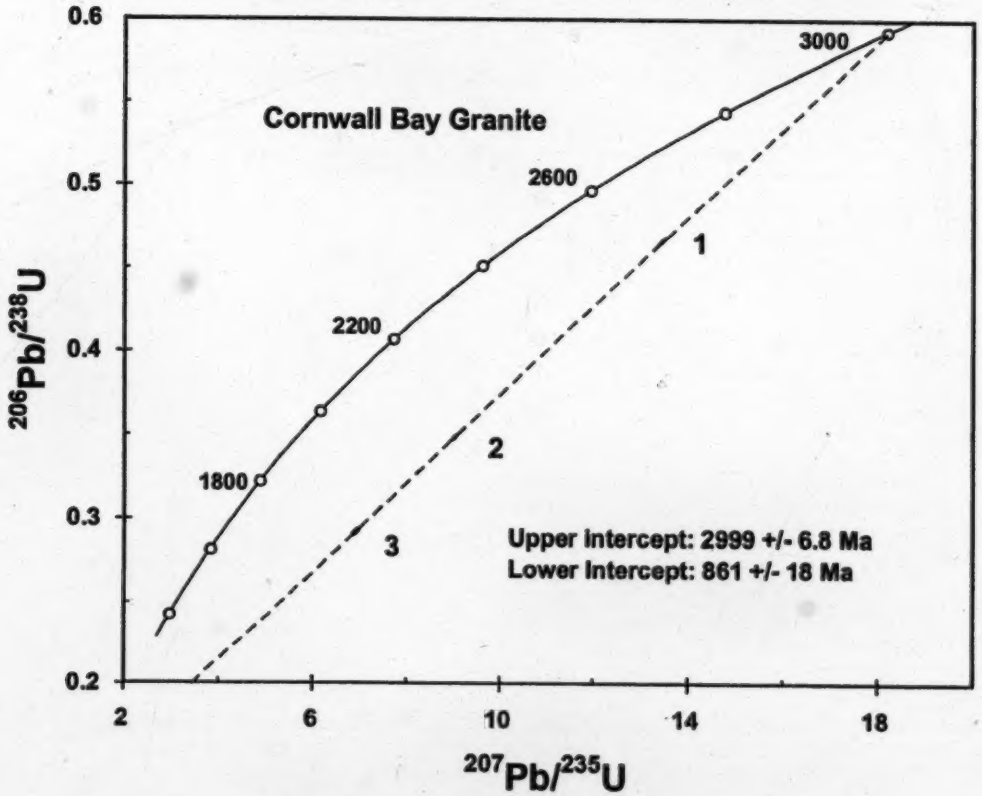

Figure 2-10. Concordia diagram for the Cornwall Bay Granite.

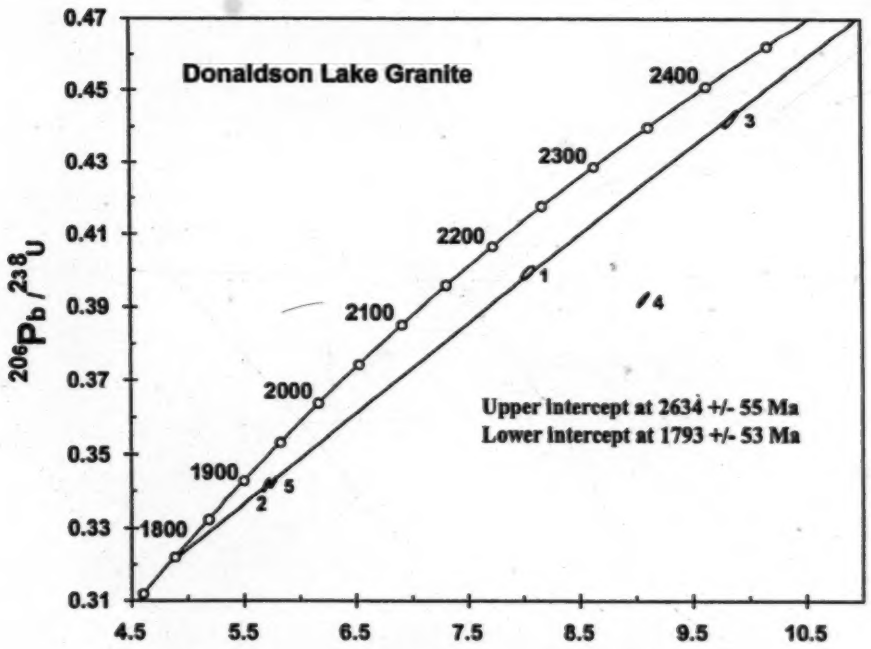

Figure 2-11. Concordia diagram for the Donaldson Lake Granite.

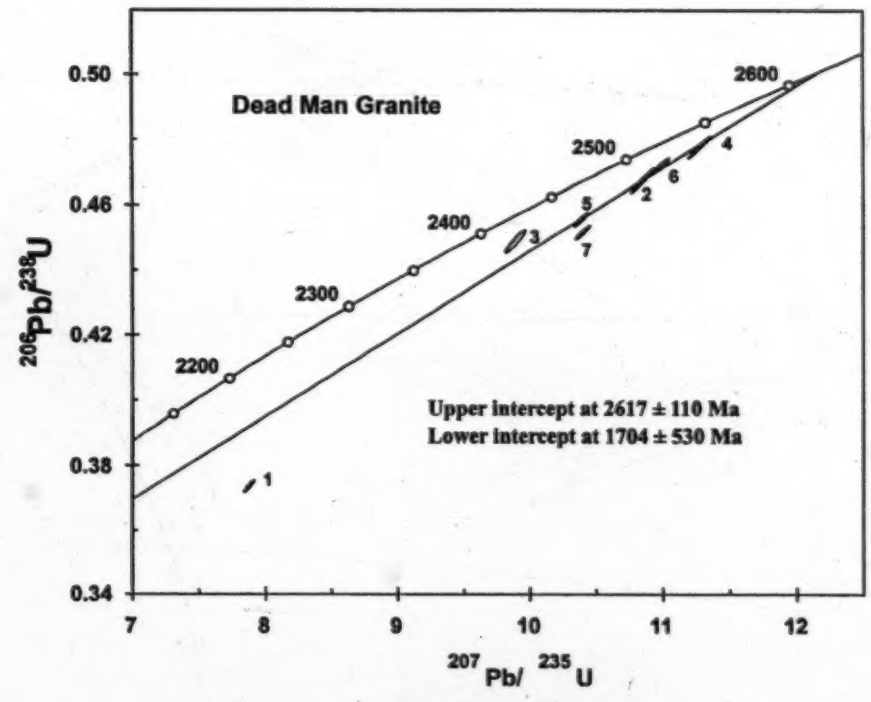

Figure 2-12. Concordia diagram for the Dead Man Granite.

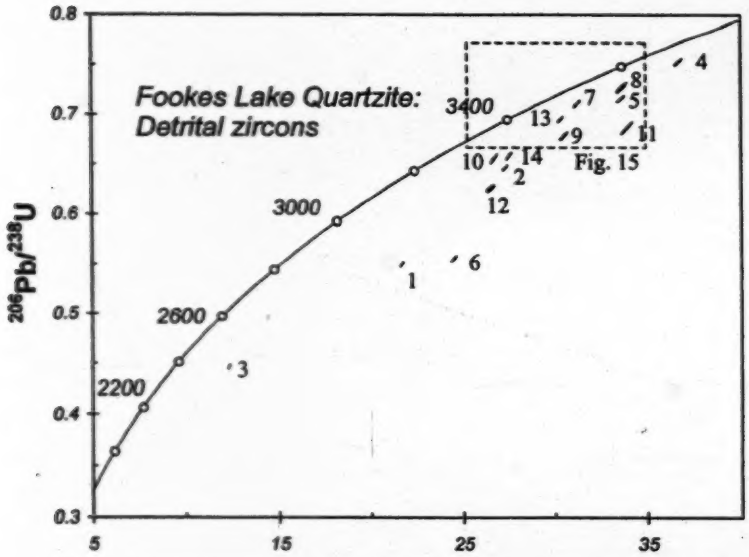

Figure 2-13. Concordia diagram for the Fookes Lake Quartzite.

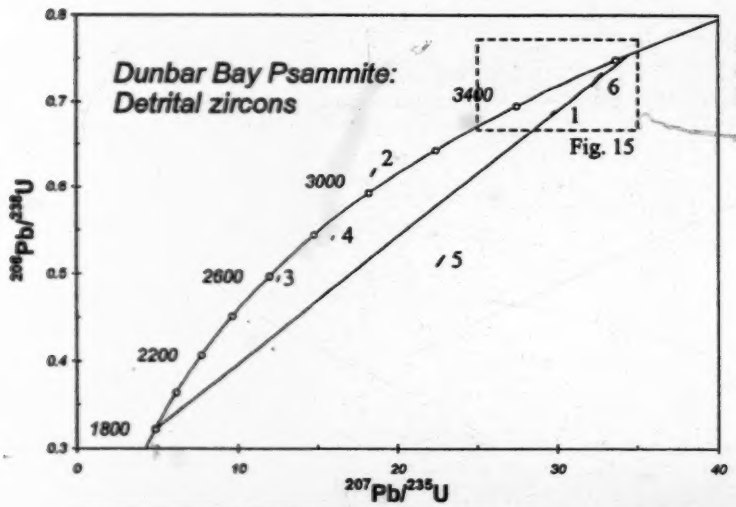

Figure 2-14. Concordia diagram for the Dunbar Bay Psammite.

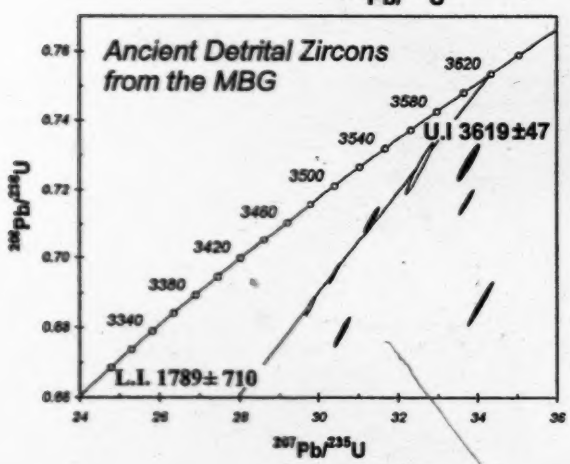

Figure 2-15. Concordia diagram of Ancient detritus from the Fookes Lake Quartzite and the Dunbar Bay Psammite. Open and filled ellipses represent analyses from the Dunbar Bay Psammite and the Fookes Lake Quartzite, respectively.

Table 2-1. Geochemical results for Murmac Bay Group basalts and gabbros

Sample No.	4700-0020	4700-0023	4700-0024	4700-0031	4700-0187	4700-0313B	4700-1049	4700-4307	4700-4341A	4700-4341B
Rock Type	B	B	B	B	B	B	B	B	B	B
SiO2	49.92	52.60	48.37	52.59	50.95	51.60	47.87	49.42	49.92	51.55
TiO2	1.79	1.68	1.27	1.76	0.886	1.60	1.35	0.90	1.29	1.23
Al2O3	14.4	13.8	14.4	13.0	18.5	13.5	12.8	15.6	14.9	14.2
Fe2O3*	14.3	13.44	13.4	13.86	10.53	14.68	16.39	12.13	11.67	11.52
MnO	0.141	0.181	0.191	0.199	0.203	0.218	0.170	0.236	0.161	0.158
MgO	6.36	4.95	7.79	4.68	5.41	5.62	9.27	8.14	7.30	7.35
CaO	6.22	8.99	10.24	8.82	5.88	9.57	8.81	8.18	6.16	8.11
Na2O	2.70	1.85	2.03	2.37	3.46	2.60	1.87	2.16	3.92	4.10
K2O	1.34	0.890	0.850	0.690	1.38	0.520	1.25	1.49	1.81	0.720
P2O5	0.210	0.220	0.140	0.200	0.170	0.180	0.100	0.070	1.420	0.130
L.o.i	2.42	1.13	1.55	1.86	2.80	0.37	1.06	1.95	1.50	1.05
Total	99.74	99.74	100.25	100.05	100.16	100.44	100.99	100.22	100.05	100.13
Cr	38.5	57.6	234.7	65.2	91.1	36.1	221	252	245	236
Ni	38.2	41.8	69.4	33.8	48.9	32.3	199	128	78.8	100
Co	41.0	38.8	44.8	32.3	27.7	40.3	79.0	46.6	38.1	36.1
Sc	40.0	38.0	43.0	37.0	27.0	39.0	42.0	43.0	43.0	42.0
V	351	328	307	322	153	331	445	275	305	279
Zn	105	102	89.1	100	158	104	109	94.8	70.7	63.4
Rb	31.6	11.2	16.9	7.63	41.2	7.47	9.70	40.1	47.5	14.8
Cs	0.415	0.130	0.166	0.101	0.718	0.183	0.100	1.721	1.643	0.218
Ba	1012	234	203	182	516	204	57	242	392	162
Sr	190	169	197	284	103	235	93.9	122	150	180
Ga	21.3	20.7	17.1	18.1	19.8	19.2	18.0	15.5	18.3	16.5
Ge	1.43	1.31	1.38	1.40	1.16	1.29	1.80	1.17	1.55	1.41
Ta	0.786	0.718	0.388	0.720	0.443	0.563	0.290	0.172	0.460	0.434
Nb	10.4	10.1	4.96	9.59	5.28	8.24	4.90	1.53	5.81	5.11
Hf	4.68	4.98	2.54	4.11	3.45	3.76	2.30	1.59	2.94	2.81
Zr	154	169	90.4	137	134	141	73.0	51.5	107	98.6
Y	36.5	36.4	27.0	36.4	19.0	33.3	27.0	21.2	27.4	26.7
Th	5.89	4.93	1.55	4.37	5.22	3.58	1.20	0.92	2.91	2.85
U	1.28	0.805	0.310	0.948	1.19	0.625	0.360	0.339	0.739	0.651
La	15.6	24.3	8.52	18.2	16.5	16.1	10.3	2.89	9.57	10.2
Ce	36.4	52.3	20.1	40.4	35.3	36.5	31.3	7.90	23.0	23.8
Pr	4.62	6.39	2.78	5.07	4.21	4.73	3.32	1.23	3.04	3.07
Nd	20.3	27.0	13.2	22.1	16.9	20.6	15.1	6.38	13.6	13.9
Sm	5.42	6.37	3.53	5.51	3.71	4.93	4.07	2.28	3.65	3.67
Eu	1.87	1.93	1.25	1.73	1.16	1.66	1.29	0.97	1.30	1.29
Gd	5.75	6.27	4.07	5.56	3.45	5.18	4.42	2.86	4.26	4.15
Tb	1.11	1.15	0.761	1.04	0.601	0.938	0.810	0.590	0.826	0.798
Dy	7.53	7.44	4.81	6.73	3.60	6.13	4.93	4.06	5.10	4.89
Ho	1.55	1.52	1.01	1.40	0.735	1.28	1.00	0.858	1.08	1.03
Er	4.54	4.49	3.07	4.07	2.18	3.80	2.90	2.60	3.26	3.14
Tm	0.658	0.653	0.454	0.613	0.318	0.536	0.416	0.393	0.475	0.454
Yb	4.11	4.05	2.83	3.87	2.05	3.41	2.68	2.42	2.98	2.86
Lu	0.587	0.575	0.398	0.545	0.315	0.478	0.428	0.360	0.431	0.403

Note: Major elements in wt%; Trace elements in ppm; bd: below detection limits; B: basalt; Gb: gabbro

Table 2-1. Geochemical results for Murmac Bay Group basalts and gabbros (continued)

Sample No.	4700-4344A	4700-4344B	4700-4537	4700-4568	4700-0320	4700-0324	4700-0416B	4700-2057	4700-2280	4700-4343
Rock Type	B	B	B	B	Gb	Gb	Gb	Gb	Gb	Gb
SiO2	48.22	51.45	49.84	55.99	49.87	43.28	49.95	51.61	51.16	51.52
TiO2	1.18	1.412	1.39	1.30	2.22	2.32	2.30	1.55	1.32	1.88
Al2O3	14.4	14.3	14.8	13.9	14.19	16.26	15.82	13.39	13.73	13.04
Fe2O3*	12.35	12.14	11.92	12.01	14.02	13.87	14.45	14.03	14.04	16.36
MnO	0.208	0.181	0.181	0.138	0.155	0.377	0.215	0.188	0.167	0.194
MgO	7.03	6.71	6.68	5.01	6.43	5.17	4.54	7.37	6.88	5.35
CaO	11.28	9.60	9.28	5.43	6.70	11.27	5.83	7.89	8.56	6.61
Na2O	1.62	2.39	3.69	3.12	3.74	1.02	3.77	1.72	1.91	2.71
K2O	1.68	0.850	0.730	1.04	0.70	1.74	1.51	0.52	0.87	1.05
P2O5	0.120	0.150	0.160	0.160	0.31	0.42	0.43	0.13	0.12	0.20
L.o.i	1.95	1.05	1.74	2.00	1.86	2.62	1.65	2.04	1.73	1.26
Total	100.04	100.23	100.38	100.11	100.18	98.34	100.46	100.44	100.47	100.16
Cr	258	119	161	bd	52.3	276	123	99.0	23.5	bd
Ni	71.4	66.4	58.6	24.9	39.3	47.1	bd	64.4	55.1	bd
Co	38.4	33.5	41.5	32.5	55.2	68.3	39.9	54.1	58.6	58.9
Sc	43.0	45.0	45.0	34.0	28.0	46.0	44.0	49.0	49.0	42.0
V	285	306	307	253	266	280	248	408	373	400
Zn	72.9	85.6	90.5	96.7	78.6	175	144	92.5	90.8	104
Rb	29.0	15.6	13.2	23.1	12.8	71.4	37.8	10.7	20.6	28.5
Cs	0.430	0.232	0.228	0.333	0.144	0.929	1.86	0.536	0.557	1.97
Ba	154	305	117	480	230	678	673	362	74.0	272
Sr	260	147	195	303	268	275	221	116	143	178
Ga	16.2	17.7	18.9	20.8	24.5	26.0	19.6	19.8	20.5	22.0
Ge	1.34	1.37	1.55	1.09	1.43	1.81	1.45	1.61	1.60	1.75
Ta	0.366	0.498	0.451	0.639	0.729	0.814	0.879	0.350	0.263	0.647
Nb	4.23	6.04	6.09	8.32	11.4	10.5	11.8	4.81	3.47	8.92
Hf	2.31	3.18	2.97	4.11	4.26	4.56	5.00	2.75	2.24	3.94
Zr	79.9	115	96.0	139	152	163	178	93	79	147
Y	24.9	26.8	30.1	30.1	28.9	46.1	45.4	28.6	26.0	39.3
Th	1.23	3.10	1.50	6.34	5.33	4.86	4.65	1.42	1.12	3.80
U	0.253	0.746	0.460	1.55	0.643	1.55	1.72	0.278	0.198	1.08
La	7.81	11.3	9.66	14.7	17.9	21.8	22.7	6.77	5.64	14.7
Ce	18.4	26.2	23.1	31.3	44.0	48.5	50.3	16.9	14.1	33.4
Pr	2.58	3.43	3.27	3.84	5.77	6.37	6.49	2.37	2.01	4.26
Nd	12.2	15.5	15.5	15.6	24.9	27.9	29.2	11.7	9.75	19.4
Sm	3.39	4.10	4.08	3.78	5.59	6.74	6.88	3.48	2.94	5.17
Eu	1.25	1.44	1.49	1.32	2.08	2.35	2.42	1.35	1.11	1.75
Gd	3.84	4.46	4.63	4.44	5.37	7.12	7.23	4.22	3.55	5.77
Tb	0.745	0.873	0.896	0.854	0.95	1.27	1.25	0.79	0.67	1.04
Dy	4.64	5.47	5.54	5.38	5.60	7.95	7.89	5.20	4.54	7.03
Ho	0.975	1.14	1.17	1.14	1.13	1.65	1.66	1.08	0.96	1.46
Er	2.98	3.42	3.55	3.40	3.14	4.81	4.98	3.29	2.86	4.40
Tm	0.431	0.513	0.519	0.488	0.428	0.700	0.705	0.487	0.405	0.646
Yb	2.61	3.18	3.20	3.10	2.68	4.27	4.42	3.07	2.56	3.87
Lu	0.384	0.457	0.467	0.465	0.385	0.628	0.676	0.446	0.382	0.572

Note: Major elements in wt%; Trace elements in ppm; bd: below detection limits; B: basalt; Gb: gabbro

Table 2-1. Geochemical results for Murmac Bay Group basalts and gabbros (continued)

Sample No.	4700-6147	4700-6147/R	4700-6148	4700-0416A
Rock Type	Gb	Gb	Gb	Gb
SiO2	49.51	49.40	46.63	48.88
TiO2	2.38	2.37	2.35	2.69
Al2O3	14.31	14.31	15.26	14.61
Fe2O3*	15.10	15.09	16.69	16.03
MnO	0.235	0.234	0.250	0.251
MgO	5.85	5.87	5.96	5.46
CaO	6.72	6.72	8.27	6.38
Na2O	2.97	2.95	2.90	3.56
K2O	1.59	1.57	0.71	0.89
P2O5	0.40	0.39	0.39	0.41
L.o.i	1.49	1.49	0.99	1.26
Total	100.54	100.37	100.41	100.43
Cr	198	212	228	137
Ni	bd	21.2	40.7	bd
Co	45.7	48.7	58.6	46.4
Sc	49.0	48.0	47.0	48.0
V	312	324	287	327
Zn	114	130	186	129
Rb	37.5	40.8	15.6	20.9
Cs	0.434	0.470	0.527	0.300
Ba	503	502	222	400
Sr	214	212	203	257
Ga	23.5	23.8	23.9	24.4
Ge	1.65	1.85	1.85	1.66
Ta	0.747	0.762	0.852	0.845
Nb	9.11	9.83	10.3	11.2
Hf	4.34	4.20	4.12	4.62
Zr	161	153	150	170
Y	40.5	41.4	41.1	43.2
Th	4.07	4.00	3.91	4.44
U	1.22	1.21	1.20	1.38
La	21.1	22.1	20.0	20.9
Ce	45.8	47.5	44.4	47.3
Pr	5.77	6.07	5.87	6.19
Nd	25.7	26.5	25.7	27.9
Sm	6.14	6.26	6.31	6.71
Eu	2.18	2.16	2.11	2.34
Gd	6.45	6.88	6.62	7.16
Tb	1.12	1.12	1.10	1.24
Dy	7.22	7.21	7.10	7.94
Ho	1.51	1.54	1.49	1.66
Er	4.43	4.52	4.35	4.81
Tm	0.661	0.655	0.633	0.711
Yb	4.06	4.11	3.97	4.44
Lu	0.592	0.613	0.584	0.635

Note: Major elements in wt%; Trace elements in ppm; bd: below detection limits; B: basalt; Gb: gabbro

Table 2-2. U-Pb results

	Sample Description[a]	Weight (mg)	Concentrations (ppm) U	Th[b] model	Pb rad.	Th/U ratio	Pb (pg)[c]	Isotopic Ratios[d] $^{208}Pb/^{204}Pb$	$^{206}Pb/^{238}U$	$^{207}Pb/^{235}U$	$^{207}Pb/^{206}Pb$	Apparent Ages (Ma) $^{206}Pb/^{238}U$	$^{207}Pb/^{235}U$	$^{207}Pb/^{206}Pb$	PD[e]
Lodge Bay Granite															
1	Zr (5)	0.023	98	29	26	0.293	58	542	0.2135±4	6.531±15	0.2219±3	1247	2050	2994±2	63.89
2	Zr (1)	0.003	155	48	35	0.306	22	253	0.1737±4	5.051±18	0.2109±5	1032	1827	2912±4	69.59
3	Zr, abr, (1)	0.003	59	30	25	0.503	24	189	0.3282±17	10.19±6	0.2252±6	1830	2452	3019±5	45.04
4	Zr, abr, (1)	0.002	461	321	212	0.697	47	393	0.3448±7	10.54±3	0.2218±3	1910	2484	2994±2	41.66
5	Zr, abr, (1)	0.002	46	47	33	1.02	18	173	0.5449±30	17.21±12	0.2291±7	2804	2947	3046±5	9.77
6	Zr, abr, (1)	0.002	19	6	2	0.323	15	25	0.0688±30	1.307±160	0.1378±125	429	849	2200±100	83.08
Cornwall Bay Granite															
1	Zr, abr (1)	0.001	260	107	139	0.411	13	680	0.4662±11	13.45±4	0.2092±2	2467	2711	2899±2	17.90
2	Zr, abr (1)	0.001	375	136	147	0.362	11	456	0.3487±8	9.047±28	0.1882±3	1928	2343	2726±3	33.76
3	Zr (1)	0.001	224	109	79	0.485	14	215	0.2921±10	6.920±37	0.1718±6	1652	2101	2575±6	40.52
Dead Man Granite															
1	Zr, abr (1)	0.008	679	238	274	0.350	7	16315	0.3737±7	7.878±16	0.1529±1	2047	2217	2379±1	16.28
2	Zr, abr (1)	0.011	383	191	202	0.499	4	33572	0.4674±15	10.85±4	0.1684±1	2472	2510	2542±1	3.30
3	Zr (3)	0.011	111	41	54	0.366	6	5546	0.4488±14	9.892±31	0.1599±2	2390	2425	2454±2	3.15
4	Zr,abr (1)	0.008	619	305	334	0.493	15	10153	0.4775±13	11.27±3	0.1712±1	2517	2546	2570±1	2.50
5	Zr (3)	0.02	224	67	110	0.301	14	9177	0.4555±9	10.39±2	0.1654±1	2420	2470	2512±1	4.40
6	Zr, abr (1)	0.006	533	304	288	0.571	26	3595	0.4722±9	11.00±2	0.1689±1	2493	2522	2547±1	2.55
7	Zr, abr (1)	0.008	540	217	269	0.401	11	10744	0.4515±8	10.40±2	0.1671±1	2402	2471	2529±1	5.99
Donaldson Lake Granite															
1	Zr, abr (1)	0.003	146	35	61	0.242	38	341	0.3993±8	8.040±22	0.1460±3	2166	2235	2300±3	6.85
2	Zr, abr (1)	0.003	1097	68	367	0.062	13	4925	0.3416±8	5.696±13	0.1209±1	1895	1931	1970±2	4.38
3	Zr (1)	0.013	18	13	10	0.704	10	687	0.4424±10	9.849±26	0.1615±2	2361	2420	2471±2	5.30
4	Zr (1)	0.002	163	46	69	0.281	7	1362	0.3922±8	9.069±21	0.1677±1	2133	2345	2535±1	18.60
5	Zr (1)	0.004	941	57	316	0.061	70	1056	0.3424±6	5.761±12	0.1220±1	1898	1941	1986±2	5.10

Table 2-2. U-Pb results

	Sample Description	Weight (mg)	Concentrations (ppm) U	Th[b] model	Pb rad.	Th/U ratio	Pb (pg)[c]	Isotopic Ratios[d] $^{208}Pb/^{204}Pb$	$^{206}Pb/^{238}U$	$^{207}Pb/^{235}U$	Apparent Ages (Ma) $^{207}Pb/^{206}Pb$	$^{206}Pb/^{238}U$	$^{207}Pb/^{235}U$	$^{207}Pb/^{206}Pb$	PD[e]	age[f]
Fookes Lake Quartzite																
1	Zr, (1)	0.003	225	75	147	0.332	29	914	0.5492±10	21.66±4	0.2860±1	2823	3169	3396±1	20.82	3761
2	Zr, abr (1)	0.004	403	204	324	0.506	9	7084	0.6464±11	27.36±5	0.3070±2	3214	3396	3506±1	10.55	3646
3	Zr, (1)	0.001	737	242	365	0.328	13	2112	0.4451±8	12.17±2	0.1983±1	2373	2617	2812±1	18.63	3357
4	Zr, abr (1)	0.002	202	119	199	0.587	12	1878	0.7536±14	36.87±8	0.3548±2	3620	3690	3727±1	3.74	3767
5	Zr, abr (1)	0.002	230	148	215	0.644	12	1505	0.7163±14	33.72±8	0.3414	3482	3602	3669±1	6.57	3743
6	Zr, (1)	0.003	134	66	93	0.491	9	1408	0.5548±11	24.52±6	0.3206±2	2845	3290	3573±1	25.09	3996
7	Zr, abr (1)	0.002	160	87	143	0.544	14	972	0.7112±14	31.33±7	0.3195±2	3463	3530	3568±1	3.79	3611
8	Zr, abr (1)	0.001	132	81	124	0.615	12	536	0.7277±21	33.76±11	0.3366±4	3525	3603	3647±2	4.36	3695
9	Zr, abr (1)	0.002	84	50	73	0.595	5	1441	0.6787±17	30.60±8	0.3270±2	3339	3506	3603±1	9.37	3718
10	Zr, abr (1)	0.003	381	92	295	0.241	10	4766	0.6584±13	27.58±6	0.3038±2	3261	3404	3490±1	8.34	3598
11	Zr, abr (1)	0.004	235	88	203	0.375	6	6343	0.6868±26	34.06±13	0.3597±2	3370	3612	3749±1	19.92	3902
12	Zr, abr (1)	0.002	188	59	141	0.315	25	503	0.6260±14	26.56±8	0.3077±5	3134	3367	3509±3	13.48	3621
13	Zr, abr (1)	0.003	97	42	83	0.434	6	1860	0.6954±12	30.40±6	0.3171±1	3403	3500	3556±1	5.52	3699
14	Zr, abr (1)	0.001	86	24	67	0.283	3	1786	0.6557±18	26.76±8	0.2960±2	3251	3375	3450±1	7.34	3546
Dunbar Bay Psammite																
1	Zr, abr (1)	0.001	445	301	394	0.677	11	1522	0.6862±12	29.79±5	0.3149±2	3368	3480	3545±1	6.41	3623
2	Zr, abr (1)	0.001	195	137	145	0.701	9	630	0.6174±17	18.51±6	0.2174±3	3100	3017	2962±2	-5.86	n.a.
3	Zr, abr (1)	0.001	213	116	122	0.544	3	1553	0.4949±11	12.48±3	0.1829±2	2592	2641	2679±2	3.95	2773
4	Zr, abr (1)	0.001	420	88	249	0.211	5	3948	0.5409±8	15.97±3	0.2142±1	2787	2875	2937	6.28	3058
5	Zr, abr (1)	0.001	139	44	86.96	0.317	4	704	0.5152±23	22.70±11	0.3195±4	2679	3214	3567	30.29	4148
6	Zr, abr (1)	0.001	121	91	116	0.751	3	1298	0.7259±30	32.53±14	0.3250±3	3518	3567	3594	2.73	3624

Note: [a] Abreviations: Zr, zircon; abr, air abraded following the techniques of Krogh (1982). The number in parentheses identifies the number of grains or grain fragments analyzed. [b] Model Th concentration calculated from $^{208}Pb/^{206}Pb$ ratio and $^{207}Pb/^{206}Pb$ age. [c] Total common lead in analysis. [d] Isotopic ratios corrected for 2.0 pg Pb and 0.5 pg U in blanks, fractionation, and initial common Pb (Stacey and Kramers, 1975). Uncertainties are reported at 1σ. e PD refers to the percent discordance along a chord to the origin. [f] Upper intercept ages for grains with a fixed lower intercept of 1800 Ma.

Chapter 3: Ca. 2.3 Ga magmatism in the western Canadian Shield: remnants of an important period of Laurentian accretion

This chapter is in preparation for submission to Canadian Journal of Earth Science. Co-authors are T. Chacko[a], L.M. Heaman[a], and K.E. Ashton[b].
[a]Department of Earth and Atmospheric Sciences, 1-26 Earth Sciences Building, University of Alberta, Edmonton, Alta., Canada, T6G 2E3
[b]Saskatchewan Geological Survey, 2101 Scarth St., Regina, Sask., Canada, S4P 3V7

Introduction

The amalgamation of Laurentia is generally accepted as having occurred during the Hudsonian Orogeny (Stockwell, 1982) between 2.0 and 1.6 Ga (Hoffman, 1988). The Archean Churchill Province, which cores Laurentia (Fig. 3-1, 3-2), was welded to the Slave Province along the ca. 2.0-1.9 Ga Taltson and Thelon magmatic zone (TTMZ) (Hoffman, 1988, 1989). The TTMZ has been interpreted to represent a post-collisional S-type intracontinental batholith superimposed on a pre-collisional I-type continental magmatic arc (Hoffman, 1989; McDonough et al., 2000). A recent geochemical and isotope study of TTMZ plutonic rocks argues that there is no evidence for a 2.0-1.9 Ga pre-collisional arc and that the TTMZ is entirely related to intracontinental deformation and magmatism (Chacko et al., 2000; De et al., 2000). If the TTMZ formed in response to intraplate deformation at 2.0-1.9 Ga, an important question arises as to when the Slave craton and Buffalo Head terrain were initially welded to the Churchill craton.

Stockwell (1982) highlighted a number of 2.3-2.4 Ga ages in the Churchill craton and grouped these as the ill-defined Blezardian Orogeny. On the basis of crystallization ages of granitoids, Hoffman (1989) also alluded to the possibility of eastward directed subduction along the western margin of the Churchill craton prior to the formation of the TTMZ. Aspler and Chiarenzelli (1998) have argued, however, that

earliest Paleoproterozoic ages in Laurentia do not define a linear orogenic belt and are not restricted to a relatively short time interval. They interpreted widespread 2.5-2.0 Ga magmatic, metamorphic, detrital and xenocystic U-Pb zircon ages from Laurentia to record the breakup of a Neoarchean supercontinent. Similarly, tectonic models proposed by McNicoll et al. (2000) and Ross et al. (2002) interpret 2.4-2.3 Ga magmatic rocks in the Buffalo Head terrane and the Taltson Magmatic Zone to be related to rifting of the Buffalo Head Terrane from the Churchill craton. The later amalgamation of these crustal blocks was suggested to occur after 2.0 Ga.

Although the idea of > 2.1 Ga orogenesis along the western margin of the Churchill craton has been repeatedly cited (e.g. Ross et al., 1991; Bostock and van Breeman, 1994), a tectonic model that adequately accounts for the igneous and metamorphic history of this region has not been fully developed. In this work I present new U-Pb zircon constraints on ca. 2.3 Ga granites from the western boundary of the Churchill craton. I also examine the geochemical and isotopic characteristics of these granites to determine their potential tectonic setting. The new data, combined with previously published research on 2.4-2.26 Ga igneous and metamorphic rocks from the western margin of the Churchill craton, suggest that this time period was characterized by orogenesis rather than by rifting. Following Stockwell (1982), I refer to this tectono-magmatic episode as the Blezardian Orogeny.

Local Geology, Field Relationships and Petrology

Along the north shore of Lake Athabasca, near Uranium City, Saskatchewan, Proterozoic granitoid rocks that intrude Archean supracrustal rocks are abundant (Fig. 3-3). These Proterozoic granitoids were grouped together as the "North Shore Plutons"

(O'Hanley et al., 1994), even though Persons (1988) divided them into a younger ca. 1.9-2.0 Ga suite related to the TTMZ and one or more suite(s) of older Paleoproterozoic granitoids with an unknown tectonic affinity. I refer exclusively, therefore, to the North Shore Plutons as the older Paleoproterozoic suite of granites. Re-mapping of this region has enabled us to identify that the North Shore Pluton suite includes both granitic and gabbroic-to-dioritic members. The granitic component locally contains migmatized supracrustal xenoliths and has been affected by at least 3 deformational events and amphibolite facies metamorphic conditions.

All granitic samples were examined in thin-section. Si, Na, Ca and K element maps were produced on a JEOL8900 electron microprobe to aid determination of modal mineralogy for several samples. Most of the North Shore Plutons are coarse-grained moderately foliated K-feldspar megacrystic monzogranite containing 0 to 15 percent biotite. Hornblende is locally abundant (5-10%), but has largely been replaced with chlorite. The largest of these plutons are the Gunnar, Macintosh Bay, Athona Mine and Cameron Island monzogranites (Fig. 3-3). At least two phases of co-magmatic quartz- and quartz-feldspar-phyric porphyries to the Gunnar granite have been identified. The Macintosh Bay granite is medium-grained and lacks a K-feldspar megacryst component along its intrusive margins. The Yahyah Lake leuco-monzogranite is slightly more felsic than the other granites containing <5% biotite with trace muscovite and hematite. This granite is coarse grained and moderately foliated but local strain gradients are apparent where metre-scale shear zones cut through the granite. A clear intrusive relationship has not been identified between this granite and the surrounding Archean supracrustals. The Hayter Bay gneissic monzogranite is a moderately strained, medium

grained to pegmatitic monzogranite that contains 5-10% biotite, 2-3% hornblende and trace magnetite. This granite is of special interest because it contains abundant amphibolite xenoliths and sills of this granite form an injection leucosome into surrounding supracrustal migmatites.

Although the majority of the North Shore Plutons are granitic, a single fine-grained mylonitic tonalite (the Geebee Lake Tonalite) that occurs as a one-metre-thick felsic sheet exposed within a thick package of amphibolite. This unit consists of highly strained plagioclase and quartz with 5-10% biotite.

U-Pb geochronology

Five felsic intrusions representative of the North Shore Plutons were sampled for U-Pb geochronology (Fig. 3-3) in order to place better constraints on crystallization ages. The U-Pb geochronology techniques used in this study are outlined in chapter 4. Regression calculations and age uncertainties were determined using Isoplot version 3.0 (Ludwig, 2003). All quoted errors (Table 3-1) are 2 sigma.

a) Macintosh Bay monzogranite (RH98-22)

The Macintosh Bay monzogranite contains brown, cloudy prismatic zircon grains and fragments (Fig. 3-4a). The most transparent grains were selected in order to reduce the discordance of analyses. Most grains were abraded (e.g. Krogh, 1982) down to spheres prior to analysis. All 6 zircon analyses have similar grain composition (574-273 ppm U, 175-69 ppm Pb, and 0.62-0.44 Th/U), consistent with a single period of igneous crystallization. Five of the analyses define a chord with an upper intercept crystallization age of 2326 ± 15 Ma (Fig. 3-5; Table 3-1) and MSWD of 9.6. This result is close to the previously determined age of 2356 ± 14 Ma (Persons, 1988) for this

granite. The difference in ages may be related to the highly discordant nature (>10%) of the multi-grain analyses of Persons (1988). The analysis of grain no. 4 was not used in our calculation as it plotted above concordia.

b) The Gunnar monzogranite (RH00-03)

The zircon population of the Gunnar monzogranite is dominated by colourless, clear to cloudy prismatic crystals that have a 2:1 length-to-width ratio (Fig. 3-4b). All analyses are from the main population except for a single, yellow prismatic grain (No. 1). All 5 analyses from the main zircon population have U-Th-Pb compositions (Table 3-1) that are identical to the range from the Macintosh Bay Granite. The yellow prismatic grain (No. 1) had, however, much lower U (49 ppm) and Pb (21 ppm) concentrations. A discordia line defined by the three most concordant analysis of the dominant population (Nos. 2, 5 and 6) has an upper intercept age of 2321 ± 3 Ma (MSWD = 1.6), which I interpret to be the crystallization age of this granite. Analysis no. 1 was not used in the age calculation since it has a significantly larger error than the other analyses. A U-Pb zircon age (2214 ± 34 Ma) previously determined for this granite (Persons, 1988) was based on a non-linear array of 4 analyses.

c) The Geebee Lake tonalite (RH99-576)

The Geebee Lake tonalite contains abundant clear to slightly cloudy prismatic zircons that have a 4:1 length-to-width ratio (Fig. 3-4c). All analyzed grains have similar U contents (436-524 ppm), Pb contents (184-243 ppm), and Th/U ratios (0.60-0.96). A chord defined by four single grain analyses (nos. 1-4) has an upper intercept crystallization age of 2320 ± 44 Ma (Fig. 3-6) and an MSWD of 9.1. An analysis that comprised five prisms (No. 5) was not used in the age calculation due to potential

mixing of a metamorphic component. The fact that the two abraded grains (nos. 1 + 2) are also the most concordant indicates that air abrasion was of critical importance for attaining a robust age for this sample.

d) The Yahyah Lake granite (RH99-518)

The sample of Yahyah Lake granite was collected from a moderately sheared rock located near the margin of the granite (Fig. 3-3). The zircon separate consists of prismatic cloudy grains that have a 2:1 length-to-width ratio (Fig. 3-4d). The range in zircon U concentrations (464-1406 ppm) is slightly higher than in the previous samples, but the Th/U ratio is fairly consistent (0.40-0.75). Four single zircon grain U-Pb analyses (Nos. 2-5) define a discordia line for the Yahyah Lake granite (Fig. 3-6). The reversely discordant analysis (No. 1) was not used in the age calculation. I consider the 2287 ± 14 Ma upper intercept age (MSWD = 2.4) to be the crystallization age for this granite.

e) The Hayter Bay monzogranite (RH98-360)

The Hayter Bay monzogranite contains numerous transparent, to slightly cloudy, colourless, elongate prismatic zircons (Fig. 3-4e). The Th/U ratio of the three zircon analyses is nearly identical (1.03-1.05) and is consistent with a single period of zircon growth. Two concordant and one slightly discordant single grain analyses define a **2297 ± 10** Ma age (MSWD = 1.3). I interpret this age to be the time of crystallization for this unit (Fig. 3-6).

Geochemistry

Although there are several models for the tectonic setting of ca. 2.3 Ga magmatism in western Laurentia (e.g. Hoffman, 1989; Aspler and Chiarenzelli, 1998)

there are currently no published geochemical analyses for igneous rocks with well defined ca. 2.3 Ga ages. A representative suite (n=16) of samples was selected from across the study area in order to begin placing geochemical constraints on the tectonic setting of this magmatic event. Whole-rock geochemistry was completed at Activation Laboratories, Ontario, Canada. The North Shore Plutons are high-K, calc-alkaline, and have SiO_2 contents ranging from 67.5 to 77.5% with the majority (n=12) greater than 73% (Table 3-1). Harker diagrams (Figure 3-7) display the usual granitic trends of decreasing TiO_2, FeO_2, Al_2O_3, MnO, and MgO with increasing silica. For comparison, I have included analyses from gneissic rocks from the basement to the exposed Taltson Magmatic Zone in northeastern Alberta (Goff et al. 1986), the majority of which are ca. 2.3 Ga in age (McNicoll et al., 2000). The geochemical trends of the North Shore Plutons are co-linear with the data reported in the present study.

A plot of chondrite normalized rare-earth elements (REE) from average (SiO_2 70-76%) 2.3 Ga North Shore Plutons displays LREE enrichment and a flat pattern of HREE's (Figure 3-8). A large negative Eu anomaly is present, a common feature of crustally derived granites (Taylor and McLennan, 1995) Eu anomalies are typically produced by either crystal fractionation involving the removal of plagioclase or melting at low-to moderate-pressures (upper- to mid-crustal conditions) at which plagioclase would remain in the residue (Drake, 1975; Moller and Muecke, 1984; Taylor and McLennan, 1995). The second interpretation is consistent with the flat HREE pattern which indicates that garnet was not left in the residue during melt production. The average REE composition for the Cassiar Batholith (70-76% SiO_2) from the Cordilleran interior is plotted for comparison. This batholith, which is interpreted to have formed

via intracontinental collision (Driver et al., 2000), has a similar REE pattern to the North Shore Plutons but with a smaller Eu anomaly and with a moderate depletion in the HREE's.

A comparison of selected MORB normalized major and trace elements from the North Shore Plutons, and from granitoids of known tectonic environments are displayed in Figure 3.9. Although the North Shore Plutons, Cassiar Batholith, Volcanic Arc Granite of Chile, and Lachland fold belt (A-type) granites have similar patterns, both the Lachlan (A-type) granites and Oslo within-plate-granites (WPG's) are preferentially enriched in Nb, Zr, Hf and Yb. These differences in trace element characteristics are best illustrated on a Nb vs Y discrimination diagram (Figure 3-10). Most of the samples from this study and those from the basement to the Taltson Magmatic Zone Basement (Goff et al., 1986) plot within the volcanic-arc granite and syn-collisional granite field, although some samples straddle the boundary or lie within WPG field. The general composition of these samples, as shown in Figure 3-8, is similar to average I and S type granites but inconsistent with an anorogenic setting (A-type granite). The Rb vs Y+Nb discrimination diagram (Figure 3-11) also suggests that ca. 2.3 Ga magmatism does not appear to be anorogenic, although Rb may be more mobile than the REE's,.

Nd isotope compositions

In order to constrain the source material for the North Shore Plutons better, three samples were analyzed for their Nd isotopic composition. Sm-Nd isotope geochemistry is ideal for identifying the characteristics of granite source material because the system has a long half-life and is extremely resistant to resetting (Barovich and Patchett, 1992).

Samples were processed and analyzed at the Radiogenic Isotope Facility at the University of Alberta. Analytical procedures are detailed in chapter 5.

The North Shore Plutons have Nd depleted mantle model ages (T_{DM})(after Goldstein et al. 1984) that are considerably older (2.87-3.05 Ga) than their ca. 2.3 Ga crystallization ages (Table 3-3). All three samples have negative initial ϵNd values, but there is a fairly wide spread (-1.5 to -6.7). The numerous xenoliths and injected nature of the Hayter Bay Monzogranite is consistent with its highly radiogenic Nd signature (-6.7 ϵNdt, 3.05 Ga T_{DM}). The Macintosh Bay Granite (-1.5 ϵNdt), alternatively, may have had a larger contribution from juvenile sources.

DISCUSSION

Coincidence of ca. 2.3 Ga magmatism and metamorphism in western Laurentia

Churchill craton

Although Stockwell (1982) did not present a tectonic model when he coined the term Blezardian Orogeny, he was the first to point out that clusters of K-Ar ages in the Chrurchill Province averaged 2396 Ma for hornblende and 2365 Ma for biotite. A rock within ~60 km of the study area, yielded a ca. 2.25 Ga Rb-Sr age (Baadsgaard and Godfrey, 1966) and a 2315 ± 60 Ma Rb-Sr isochron age for a garnetiferous felsic gneiss was interpreted to represent Paleoproterozoic metamorphism (Bell and Blenkinsop, 1984). On Boothia Peninsula (# 21, Fig. 3-2a), a granodiorite gneiss with a U-Pb zircon 2776+67/-56 Ma upper intercept crystallization age and 2199±68 Ma lower intercept metamorphic age was reported (Frisch and Hunt, 1993). By re-calculating the discordia line of this unit using only the single grain analyses reported, an upper intercept age of

2830 ± 22 Ma is obtained, consistent with known 2.85-2.87 Ga basement granitoid ages from the Rae Province (e.g. Jackson et al., 1990), and a lower intercept age of 2285 ± 20 Ma, consistent with local ca. 2.3 Ga magmatism, is produced. At the northwestern tip of Baffin Island (Fig. 3-2a), Jackson et al. (1990) report a 2321 ± 76 Ma Rb-Sr whole-rock isochron defined by 10 analyses from granitoid augen gneiss, metavolcanic rock, and a granitoid dyke. This age was interpreted to represent either the emplacement time of these units or, more likely, metamorphic resetting (Jackson et al. 1990). Based on a 2274 ± 102 Ma Rb-Sr age for upper amphibolite to granulite facies supracrustal rocks, and ca. 2.2-2.3 Ga U-Pb SHRIMP ages for metamorphic zircon, Crocker et al. (1993) suggested that significant 2.3-2.2 Ga thermotectonism occurred in the western Churchill craton south of the Athabasca Group (Fig. 3-2a). In the northwestern Churchill craton, in-situ ca. 2.35 Ga chemical ages for elongate monazite inclusions in garnet record the timing of D_1 deformation and M_1 lower-to upper-amphibolite facies metamorphism (Berman et al., 2003). Within our study area, ca 2.3 Ga metamorphic monazite and zircon growth record the timing of middle to upper amphibolite facies metamorphism (M_1) and coeval deformation (D_1) (Chapter 4).

Slave craton

The extent of ca. 2.3 Ga deformation in the Slave craton is difficult to constrain due to the strong 2.0-1.9 Ga metamorphic overprinting of the TTMZ, as well as due to the inherent similarities between Churchill and Slave crust that make the exact location of the paleomargin difficult to ascertain. Biotite in the core of a tonalite from the northern Slave craton records 2276±12 Ma conventional and 2310 ± 8 Ma laser $^{40}Ar/^{39}Ar$ ages (Relf et al., 1999). The edge of this pluton, as well as other smaller

plutons in the area, recorded ca. 1.9-2.0 Ga ages. The same study reported an integrated 2278 ± 11 Ma $^{40}Ar/^{39}Ar$ hornblende age from mafic gneiss and a 2337 ± 8 Ma age for muscovite from the Tokhokatak shear zone in the eastern Slave craton. The ca. 2185 and 2354 ± 212 Ma lower intercepts on two U-Pb discordia lines from the southeastern Slave Province (Bleeker at al., 1999) could also represent a ca. 2.3 Ga disturbance.

2.4-2.26 Ga – Arc and collisional magmatism in western Laurentia

Unlike anorogenic igneous suites, which are typically bimodal and may contain significant amounts of quartz syenite, alkali-feldspar granite, and other alkaline rocks (Pitcher, 1997), the 2.40-2.26 Ga magmatic rocks of the western Churchill craton contain a complete spectrum of rock types from felsic to mafic (Fig. 3-2 inset). Alkaline rocks have not been identified. Aspler and Chiarenzelli (1998) proposed that igneous rocks of this age in the Churchill craton are not distributed in linear belts but are, instead, widely dispersed across Laurentia. Their conclusion was based on the wide geographic distribution of U-Pb zircon ages from both igneous and clastic sedimentary rocks, which they interpreted as evidence for a regional anorogenic mantle upwelling. However, an examination of U-Pb zircon ages from solely igneous rocks in western Laurentia (Fig. 3-2) reveals that these rocks are in fact preferentially distributed along the western margin of the Churchill craton, consistent with an orogenic model. This ca. 2.3 Ga magmatism extends into the buried terranes of the Alberta basment and indicates that the Buffalo Head terrane was a component of the Churchill craton by 2.3 Ga.

The majority of magmatic rocks, including those from this study, appear to have been emplaced between about 2340-2320 Ma (Fig. 3-2 inset), synchronous with

widespread ca. 2.3 Ga metamorphism and deformation. The coincidence of ca. 2.3 Ga high-grade metamorphism, deformation and granite magmatism lead me to suggest that orgenesis is related to the collision of terranes along the western margin of the Churchill craton, possibly coeval with east-dipping subduction (Fig. 3-12). The presence of ca. 2.3 Ga $^{40}Ar/^{39}Ar$ ages in the Slave craton is consistent with its accretion at this time. The widespread ca. 2.3 Ga metamorphism in the Churchill craton may indicate that crustal thickening was focused on this plate. The petrology, whole-rock geochemistry and Nd isotope signature of the North Shore Plutons are consistent with a collisional setting. Far field effects of collision along the western margin of the Laurentia may include Blezardian magmatism, metamorphism and NW-SE compression (Riller et al., 1999) and ca. 2.3 Ga re-activation of the Kapuskasing Uplift (Hanes et al., 1994; Percival and Peterman, 1994) in the Superior Province.

Global analogies to ca. 2.3 Ga magmatism in Laurentia:

A modern analogy for ca. 2.3 Ga magmatism in Laurentia might be the Cordilleran Interior granitoids (e.g. Driver et al., 2000) which, like the North Shore Plutons, are several hundered kilometers inboard from a major plate boundary. If this analogy is correct, ca. 2.3 Ga granites closer to the western Churchill craton margin might have a subduction signature highlighted by lower K contents, arc geochemistry, and juvenile Nd isotopic compositions, similar to the Cordilleran Coast Plutonic Complex (e.g. Freidman et al., 1995). It is interesting to note that the ca. 2.3 Ga magmatic rocks from southwest of the study area (Nos. 1-7, Figure 3-2a) predominantly have lower K-contents (diorite-tonalite-granodiorite) than granitoids in the study area,

and more primitive isotopic compositions (ϵNdT -1.3 to + 0.9 (n=3), Villeneuve et al., 1993). In addition, basement to the Taltson Magmatic Zone contains a complete suite of mafic to felsic rocks (Figure 3-7)

A Neoproterozoic analogy for ca. 2.3 Ga orogenesis in Laurentia is the Pan-African orogeny. Collision of terranes in the Pan-African orogeny commenced at ~750 Ma but continued until 580 Ma (Liégeois, et al. 1994). Both the Pan-African (Liégeois, et al. 1998) and Blezardian orogenies had voluminous post-collisional high-K calc-alkaline magmatism that is coeval with regional metamorphism. Post-orogenic mafic magmatism was also present in the Pan-African orogeny (Cottin et al., 1998; Ait-Djafer et al., 2003). In the Uranium City area, mixing of undated gabbro and granite may indicate that post-orogenic mafic magmatism also occurred. Finally, both the Pan-African (Liégeois, et al. 1998) and the North Shore Plutons have Nd isotope characteristics that suggest mixing of juvenile and older crustal material.

Foredeep deposition and post-orogenic extension – 2.3-2.1 Ga

The Noomut Formation, which is at the 2.45-2.1 Ga base of the Hurwitz Group (Fig. 3-2), is composed entirely of sandstone and conglomerate and interpreted to be initiated at ca. 2.3 Ga in a fluvial setting (Aspler et al., 2001 and refs. therein). The relative timing and fluvial nature of this formation lead me to suggest that the Noomut Formation, and other 2.3-2.1 Ga sedimentary basins in the Churchill Province, initiated as a foredeep to the Blezardian Orogenic belt.

Although I do not dispute the occurrence of 2.45-2.1 Ga continental extension in Laurentia (Aspler and Chiarenzelli, 1998; Aspler et al., 2001, 2002), some of this

extension, including the 2.19- to 2.02 Ga alkaline-peralkaline intrusive complexes in the Slave Province (Cavell and Baadsgaard, 1986) and the 2.13-2.09 Ga Rutledge River Basin on the western margin of the Rae Province (Bostock and van Breeman, 1994), may be post-orogenic rather than anorogenic. This would be similar to the evolution of magmatism from syn-collisional, to post-collisional, to typical anorogenic in the Pan-African Orogen (Liégeois, et al. 1998).

2.1-1.9 Ga Reactivation of the western Churchill margin

De et al. (2000) and Chacko et al. (2000) demonstrated that the petrology and isotope geochemistry of 2.0-1.93 Ga magmatic rocks of the TTMZ are not consistent with arc magmatism, and could be best explained as a result of crustal thickening in a continental interior. One of the compelling arguments against an arc model at 2.0-1.9 Ga is the lack of mafic and intermediate intrusive rocks that could represent a mantle component to this magmatism. In contrast, mafic to intermediate rocks are well represented in the 2.3 Ga magmatic suite (Fig. 3-2 inset). Any post-Blezardian extension could have thermally softened the suture zone, enabling significant horizontal shortening and crustal thickening (Thompson et al., 2001) during later orogenesis. I suggest that 2.0-1.9 Ga TTMZ magmatism represents reactivation of the 2.3 Ga suture. This reactivation may have been initiated by the ca. 2.1 Ga rifting of the Superior from the Churchill craton that formed the Manikewan Ocean (Ansdell et al., 2000). Collision of terranes that are imaged in the subsurface to the west of the Buffalo Head terrane (Ross et al., 1991) may also have had a significant influence at this time, the details of which remain to be established.

CONCLUSIONS

The western margin of the Churchill craton has been overprinted by several episodes of Paleoproterozoic magmatism. Although the 2.0-1.9 Ga Taltson and Thelon Magmatic zones are most obvious, relicts of an older ca. 2.3 Ga magmatic belt have also been identified. In the Uranium City area on the north shore of Lake Athabasca, ca. 2.3 Ga granites have geochemical and Nd isotopic signatures suggestive of crustal derivation. This crustally-derived magmatism is likely related to continental thickening which occurred as a result of collision of terranes along the western margin of the Churchill craton. This orogenic model links 2.3 Ga magmatism, metamorphism and deformation in western Laurentia together (Fig. 3-12) and provides a better fit to the currently available data than does an anorogenic model. The 2.4-2.1 Ga period of Earth's history has been considered notable for its apparent tectonic quiescence (e.g. Plumb and James, 1986). The Blezardian Orogeny appears to represent a tectonic squall in this interval of global tectonic calm.

REFERENCES

Ait-Djafer, S., Ouzegane, K., Paul-Liegeois, J., and Kienast, J.R. 2003. An example of post-collisional mafic magmatism: the gabbro-anorthosite layered complex from the Tin Zebane area (western Hoggar, Algeria). Journal of African Earth Sciences, **37**: 313-330.

Ansdell, K.M., MacNeil, A., Delaney, G.D., and Hamilton, M.A., 2000, Rifting and development of the Hearne craton passive margin: Age constraint from the Cook Lake area, Wollaston Domain, Trans-Hudson Orogen, Saskatchewan: Geocanda 2000, Calgary, Alberta, abstracts CD.

Ashton, K.E., Kraus, J., Hartlaub, R.P., and Morelli, R., 2000, Uranium City revisited: A new look at the rocks of the Beaverlodge Mining Camp: Saskatchewan Geological Survey Miscellaneous Report 2000-4.2, p. 3-15.

Aspler, L.B., and Chiarenzelli, J.R., 1998, Two Neoarchean supercontinents? Evidence from the Paleoproterozoic: Sedimentary Geology, v. 120, p. 75-104.

Aspler, L.B., Chiarenzelli, J.R., Cousens, B.L., McNicoll, V.J. and Davis, W.J. 2001. Paleoproterozoic intracratonic basin processes, from breakup of Kenoraland to Assembly of Laurentia: Hurwitz Basin, Nunavut, Canada. Sedimentary Geology, **141-142**: 287-318.

Aspler, L.B., Cousens, B.L., and Chiarenzelli, J.R. 2002. Griffin gabbro sills (2.11 Ga), Hurwitz Basin, Nunavut, Canada: long-distance lateral transport of magmas in western Churchill Province crust. Precambrian Research, **117**: 269-294.

Barovich, K.M., and Patchett, P.J. 1992. Behavior of Isotopic Systematics During Deformation and Metamorphism - a Hf, Nd and Sr Isotopic Study of Mylonitized Granite. Contributions to Mineralogy and Petrology, **109**: 386-393.

Berman, R.G., Carson, C., Sanborn-Barrie, M., Skulski, T., Stern, R., and Rayner, N., 2003, New constraints on polymetamorphism in the Committee Bay belt, Rae domain, with implications for the tectonometamorphic history of the Western Churchill province: GAC-MAC-SEG joint annual conference, Vancouver, conference CD.

Bostock, H.H., and Loveridge, W.D. 1988, Geochronology of the Talston Magmatic zone and its eastern cratonic margin, District of Mackenzie: Geological Survey of Canada Paper 88-2, p. 59-65.

Bostock, H.H., and van Breemen, O., 1994, Ages of detrital zircons and monazites from a pre-Taltson magmatic zone basin at the western margin of the Rae Province: Canadian Journal of Earth Science, v. 31, p. 1352-1364.

Bostock, H.H., van Breemen, O., and Loveridge, W.D., 1991, Further geochronology of plutonic rocks in northern Taltson Magmatic Zone, District of Mackenzie, N.W.T.: Geological Survey of Canada Paper 90-2, p. 67-78.

Cavell, P.A., and Baadsgaard, H. 1986. Geochronology of the Big Spruce Lake Alkaline Intrusion. Canadian Journal of Earth Sciences, **23**: 1-10.

Chacko, T., De, S.K., Creaser, R.A., and Muehlenbachs, K., 2000, Tectonic setting of the Taltson magmatic zone at 1.9-2.0 Ga: a granitoid based perspective, Canadian Journal of Earth Sciences, v. 37, p. 1597-1609.

Cottin, J.Y., Lorand, J.P., Agrinier, P., Bodinier, J.L., and Liegeois, J.P. 1998. Isotopic (O, Sr, Nd) and trace element geochemistry of the Laouni layered intrusions (Pan-African belt, Hoggar, Algeria): evidence for post-collisional continental tholeiitic magmas variably contaminated by continental crust. Lithos, **45**: 197-222.

Crocker, C.H., Collerson, K.D., Lewry, J.F., and Bickford, M.E., 1993, Sm-Nd, U-Pb, and Rb-Sr geochronology and lithostructural relationships in the southwestern Rae province: constraints on crustal assembly in the western Canadian Shield: Precambrian Research, v. 61, p. 27-50.

De, S.K., Chacko, T., Creaser, R., and Muehlenbachs, K., 2000, Geochemical and Nd-Pb-O isotope systematics of granites from the Taltson Magmatic Zone, NE Alberta: implications for early Proterozoic tectonics in western Laurentia: Precambrian Research, v. 102, p. 221-249.

Friedman, R.M., Mahoney, J.B., and Cui, Y. 1995. Magmatic evolution of the southern Coast Belt: Constraints from Nd-Sr isotopic systematics and geochronology of the southern Coast Plutonic Complex. Canadian Journal of Earth Sciences, 32: 1681-1698.

Frisch, T., and Hunt, P., 1993, Reconnaissance U-Pb geochronology of the crystalline core of the Boothia Uplift, District of Franklin, Northwest Territories: Geological Survey of Canada, Paper 93-2, p. 3-22.

Goff, S.P., Godfrey, J.D., and Holland, J.G., 1986, Petrology and geochemistry of the Canadian Shield of northeastern Alberta: Alberta Research Council Bulletin 51, 60p.

Goldstein, S.L., Onions, R.K., and Hamilton, P.J., 1984. A Sm-Nd Isotopic Study of Atmospheric Dusts and Particulates from Major River Systems: Earth and Planetary Science Letters, v. 70, p. 221-236.

Hanmer, S., Bowring, S., Vanbreemen, O., and Parrish, R., 1992, Great Slave Lake Shear Zone, Nw Canada - Mylonitic Record of Early Proterozoic Continental Convergence, Collision and Indentation: Journal of Structural Geology, v. 14, p. 757-773.

Heaman, L.M., Erdmer, P., and Own, J.V., 2002, U-Pb geochronologic constraints on the crustal evolution of the Long Range Inlier, Newfoundland: Canadian Journal of Earth Sciences, v. 39, p. 845-864.

Hoffman, P.F., 1988, United Plates of America, the Birth of a Craton - Early Proterozoic Assembly and Growth of Laurentia: Annual Review of Earth and Planetary Sciences, v. 16, p. 543-603.

Hoffman, P.E., 1989, Precambrian Geology and tectonic history of North America, *in* Bally, A.W., and Palmer, A.R., eds., The Geology of North America – An Overview: Boulder, Colorado, Geological Society of America, p. 447-512.

Jackson, G.D., Hunt, P.A., Loveridge, W.D., and Parrish, R.R., 1990, Reconnaissance geochronology of Baffin Island, N.W.T.: Geological Survey of Canada Paper 89-2, p. 123-148.

Krogh, T.E., 1982, Improved accuracy of U-Pb zircon ages by the creation of more concordant systems using an air abrasion technique: Geochimica et Cosmochimica Acta, v. 46, p. 637-649.

Landenberger, B. and Collins, W.J. 1996. Derivation of A-type granites from a dehydrated charnockitic lower crust: evidence from the Chaelundi complex, Eastern Australia. Journal of Petrology, **37**: 145-170.

Liegeois, J.P., Black, R., Navez, J., and Latouche, L. 1994. Early and Late Pan-African Orogenies in the Air Assembly of Terranes (Tuareg Shield, Niger). Precambrian Research, **67**: 59-88.

Liegeois, J.P., Navez, J., Hertogen, J., and Black, R. 1998. Contrasting origin of post-collisional high-K calc-alkaline and shoshonitic versus alkaline and peralkaline granitoids. The use of sliding normalization. Lithos, **45**: 1-28.

Ludwig, K.R., 2003. Isoplot/Ex, a geochronological toolkit for microsoft excel, Version 3.0. Berkely, California, Berkely Geochronology Center Special Publication 4.

McDonough, M.R., McNicoll, V.J., Schetselaar, E.M., and Grover, T.W., 2000, Geochronological and kinematic constraints on crustal shortening and escape in a two-sided oblique-slip collisional and magmatic orogen, Paleoproterozoic Taltson magmatic zone, northeastern Alberta: Canadian Journal of Earth Sciences, v. 37, p. 1549-1573.

McNicoll, V.J., Thériault, R.J., and McDonough, M.R., 2000, Taltson Basement gneisses: U-Pb and Nd isotopic constraints on the basement to the Taltson magmatic zone, Northeastern Alberta: Canadian Journal of Earth Sciences, v. 37, p. 1575-1596.

Moller, P., and Muecke, G.K. 1984. Significance of Europium Anomalies in Silicate Melts and Crystal-Melt Equilibria - a Re-Evaluation. Contributions to Mineralogy and Petrology, **87**: 242-250.

O'Hanley, D.S., Kyser, K.T., and Sibbald, T.I.I. 1994. The age and origin of the North Shore Plutons in the Rae Province, Goldfields area, Saskatchewan. Canadian Journal of Earth Sciences, **31**: 1397-1406.

Patchett, P.J., and Arndt, N.T., 1986, Nd Isotopes and Tectonics of 1.9-1.7 Ga Crustal Genesis: Earth and Planetary Science Letters, v. 78, p. 329-338.

Pearce, J.A., and Cann, J.R., 1983, Role of the sub-continental lithosphere in magma genesis at active continental margins, *in* Hawkesworth, C.J., and Norry, M.J., eds., Continental basalts and mantle xenoliths: Cheshire, United Kingdom, Shiva Publishing Limited, p. 230-249.

Pearce, J.A., Harris, N.B.W., and Tindle, A.G., 1984, Trace element discrimination diagrams for the tectonic interpretation of granitic rocks: Journal of Petrology, v. 25, p. 956-983.

Persons, S.S., 1988, U-Pb geochronology of Precambrian rocks in the Beaverlodge area, Northwestern Saskatchewan [M.Sc. Thesis]: Lawrence, University of Kansas, 68p.

Pitcher, W.S., 1997, The nature and origin of granite: London, Chapman and Hall, 387 p.

Plumb, K.A., and James, H.L., 1986, Subdivision of Precambrian Time - Recommendations and Suggestions by the Subcommission on Precambrian Stratigraphy: Precambrian Research, v. 32, p. 65-96.

Relf, C., Sandeman, H.A., and Villeneuve, M.E., 1999, Tectonic and thermal history of the Anialik River area, northwestern Slave Province, Canada: Canadian Journal of Earth Science, v. 36, p. 1207-1226.

Riller, U., Schwerdtner, W.M., Halls, H.C., and Card, K.D., 1999, Transpressive tectonism in the eastern Penokean orogen, Canada. Consequences for Proterozoic crustal kinematics and continental fragmentation: Precambrian Research, v. 93, p. 51-70.

Roddick, J.C., and van Breemen, O., 1994, U-Pb zircon dating: a comparison of ion microprobe and single grain conventional analyses: Geological Survey of Canada Current Research 1994-F, p. 1-9.

Ross, G.M., and Eaton, D.W., 2002, Proterozoic tectonic accretion and growth of western Laurentia: results from Lithoprobe studies in northern Alberta: Canadian Journal of Earth Science, v. 39, p. 313-329.

Ross, G.M., Parrish, R.R., Villeneuve, M.E., and Bowring, S.A., 1991, Geophysics and geochronology of the crystalline basement complex of the Alberta Basin, Western Canada: Canadian Journal of Earth Science, v. 28, p. 512-522.

Stacey, J.S., and Kramers, J.D., 1975, Approximation of terrestrial lead isotope evolution by a two-stage model: Earth and Planetary Science Letters, v. 26, p. 207-221.

Stockwell, C.H., 1982, Proposals for the time classification and correlation of Precambrian rocks and events in Canada and adjacent areas of the Canadian Shield: Geological Survey of Canada Paper 80-19, 135p.

Sun, S.-s., and McDonough, W.F., 1989, Chemical and isotopic systematics of oceanic basalts: implications for mantle compositions and processes, *in* Saunders, A.D., and Norry, M.J., eds., Magmatism in Ocean Basins, Geol. Soc. Spec. Pub. No. 42, p. 313-345.

Taylor, S.R., and McLennan, S.M. 1995. The Geochemical Evolution of the Continental-Crust. Reviews of Geophysics, 33: 241-265.

Thompson, A.B., Schulmann, K., Jezek, J., and Tolar, V., 2001, Thermally softened continental extension zones (arcs and rifts) as precursors to thickened orogenic belts: Tectonophysics, v. 332, p. 115-141.

van Breemen, O. and Bostock H.H., 1994, Age of emplacement of the Thoa metagabbro, western margin of the Rae Province, Northwest Territories: initiation of rifting prior to Taltson magmatism: Geological Survey of Canada Current Research 94-F, p. 61-68.

van Breemen, O., Bostock H.H., and Loveridge, W.D., 1992, Geochronology of granites along the western margin of the northern Taltson magmatic zone and western Rae Province, Northwest Territories: Geological Survey of Canada Paper 91-2, pp. 17-24.

Villeneuve, M.E., Ross, G.M., Thériault, R.J., Miles, W., Parish, R.R., and Broome, J., 1993, Tectonic subdivision and U-Pb geochronology of the crystalline basement of the Alberta Basin,western Canada: Geological Survey of Canada Bulletin 447, 86p.

Whalen, J.B., Currie, K.L., and Chappell, B.W., 1987, A-type granites: geochemical characteristics, discrimination and petrogenesis: Contibutions to Mineralogy and Petrology, v. 95, p. 407-419.

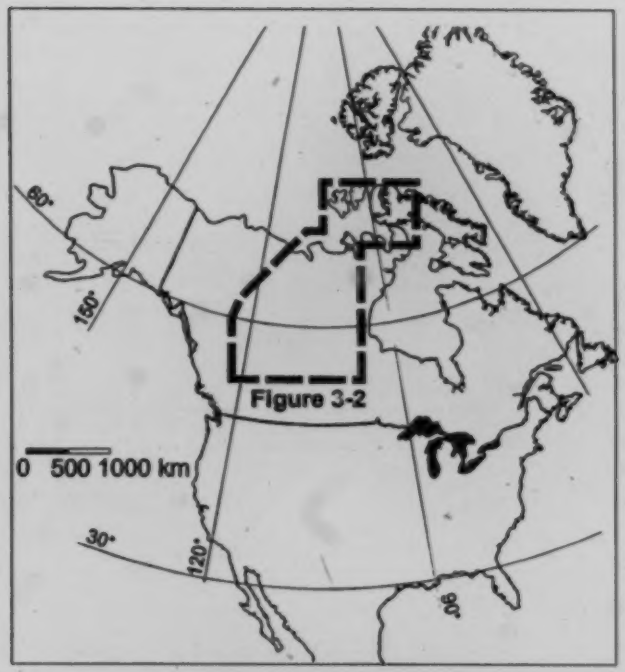

Figure 3-1. Map of North America with the area of figure 3-2 highlighted.

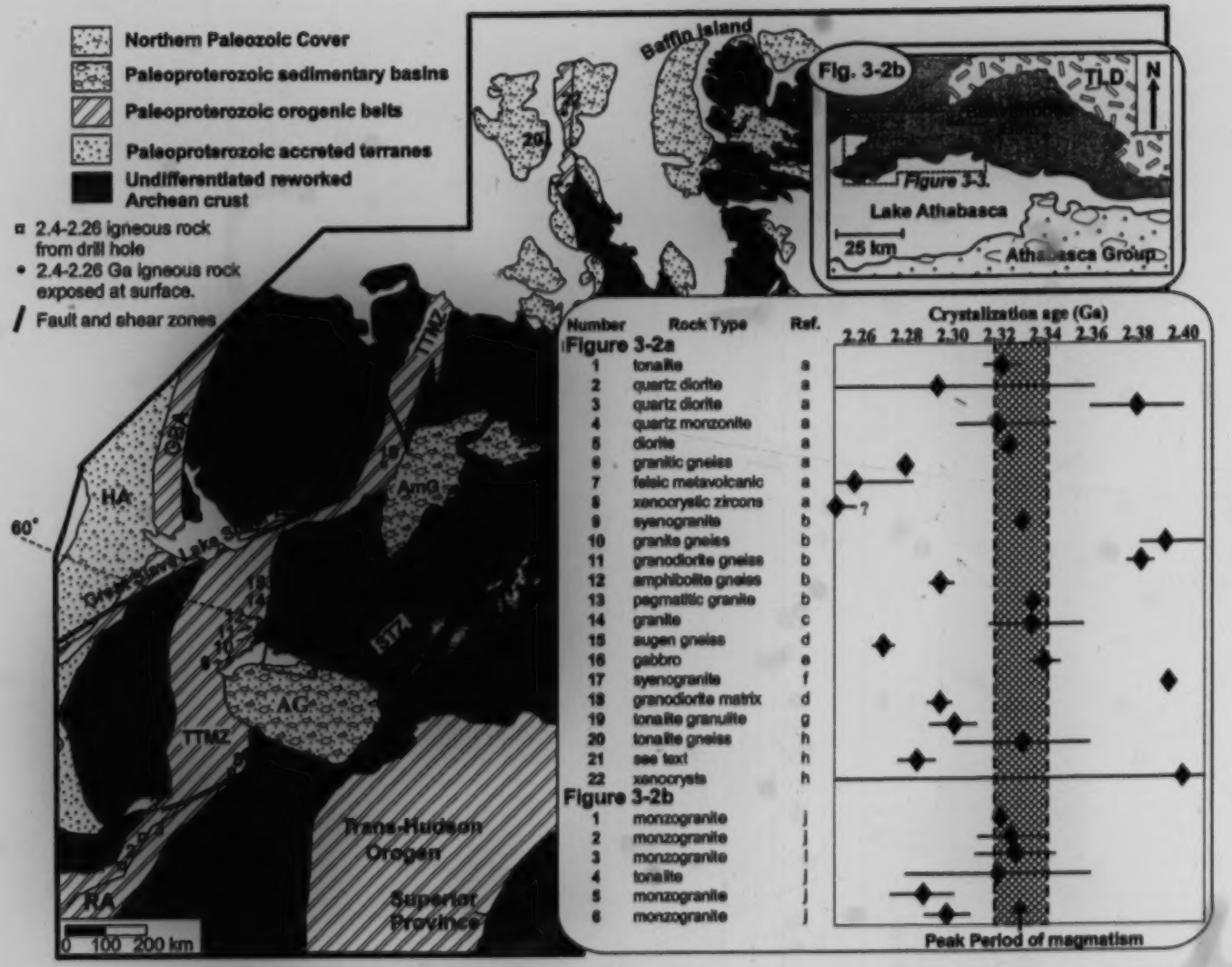
Northern Paleozoic Cover
Paleoproterozoic sedimentary basins
Paleoproterozoic orogenic belts
Paleoproterozoic accreted terranes
Undifferentiated reworked Archean crust
2.4-2.26 igneous rock from drill hole
2.4-2.26 Ga igneous rock exposed at surface.
Fault and shear zones
Baffin Island
Fig. 3-2b
TLD
N
Figure 3-3
Lake Athabasca
25 km
Athabasca Group
60°
HA
GSL
AmG
TTMZ
Great Slave Lake Shear Zone
AG
RA
Trans-Hudson Orogen
Superior Province
0 100 200 km
Number
Rock Type
Ref.
Crystalization age (Ga)
2.26 2.28 2.30 2.32 2.34 2.36 2.38 2.40
Figure 3-2a
1 tonalite a
2 quartz diorite a
3 quartz diorite a
4 quartz monzonite a
5 diorite a
6 granitic gneiss a
7 felsic metavolcanic a
8 xenocrystic zircons a
9 syenogranite b
10 granite gneiss b
11 granodiorite gneiss b
12 amphibolite gneiss b
13 pegmatitic granite b
14 granite c
15 augen gneiss d
16 gabbro e
17 syenogranite f
18 granodiorite matrix d
19 tonalite granulite g
20 tonalite gneiss h
21 see text h
22 xenocrysts h
Figure 3-2b
1 monzogranite j
2 monzogranite j
3 monzogranite j
4 tonalite j
5 monzogranite j
6 monzogranite j
Peak Period of magmatism

Figure 3-2. Geological sketch map of the western Canadian Shield with southern Paleozoic cover removed (modified after Hoffman, 1989; Ross et al., 1991; Aspler and Chiarenzelli, 1998). AG, Athabasca Group; AmG, Amer Group; GBA, Great Bear Arc; HA, Hottah Arc; HG, Hurwitz Group; RA, Rimbey Arc; STZ, Snowbird Tectonic Zone; TTMZ, Taltson-Thelon Magmatic Zone. **Figure 3-2b.** Geological domains of the study region in northwestern Saskatchewan. The area of Figure 3-3 is identified. TLD, Train Lake granite-greenstone domain.

Figure 3-2 table inset presents compilation of 2.26-2.40 Ga igneous rock ages for western Laurentia with striped box indicating probable period of Slave-Churchill collision. The lower intercept age presented for #21 is from a granodiorite gneiss and is based solely on the single zircon grain analyses reported in Frisch and Hunt (1993).

References:

a. Villeneuve et al., 1993.
b. McNicoll et al., 2000.
c. Bostock and Loveridge, 1988.
d. Bostock et al., 1991.
e. van Breemen and Bostock, 1992.
f. van Breemen et al., 1992.
g. Roddick and van Breemen, 1994.
h. Frisch and Hunt, 1993.
i. Persons, 1988.
j. This study.

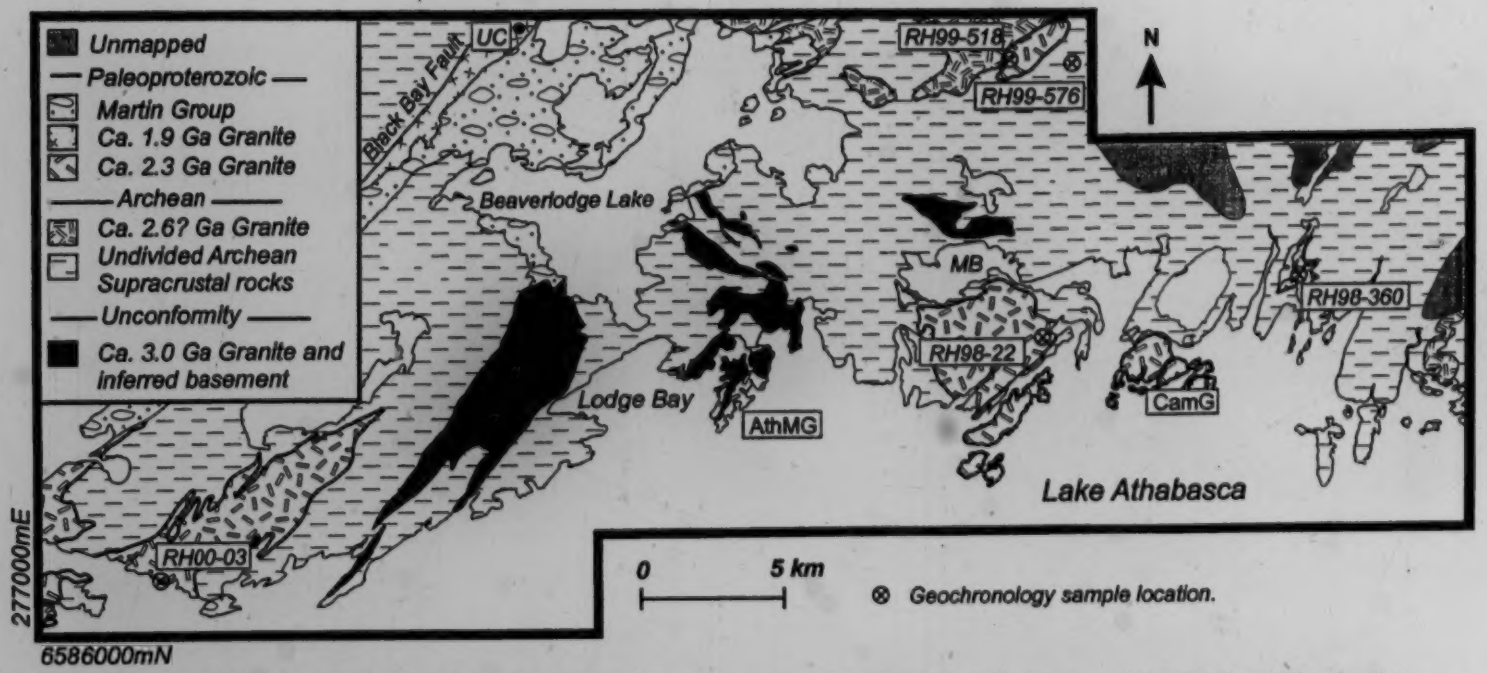

Figure 3-3. Simplified geological map highlighting the North Shore Plutons near Uranium City, Saskatchewan. AthMG, Athona Mine Granite; CamG; Cameron Island Granite; MB, Macintosh Bay; UC, Uranium City. Geochronology sample sites are: The Macintosh Bay Granite (RH98-22), The Gunnar Granite (RH00-03); The Geebee Lake Tonalite (RH99-576), The Yahyah Lake Granite (RH99-518), and The Hayter Bay Granite (RH98-360).

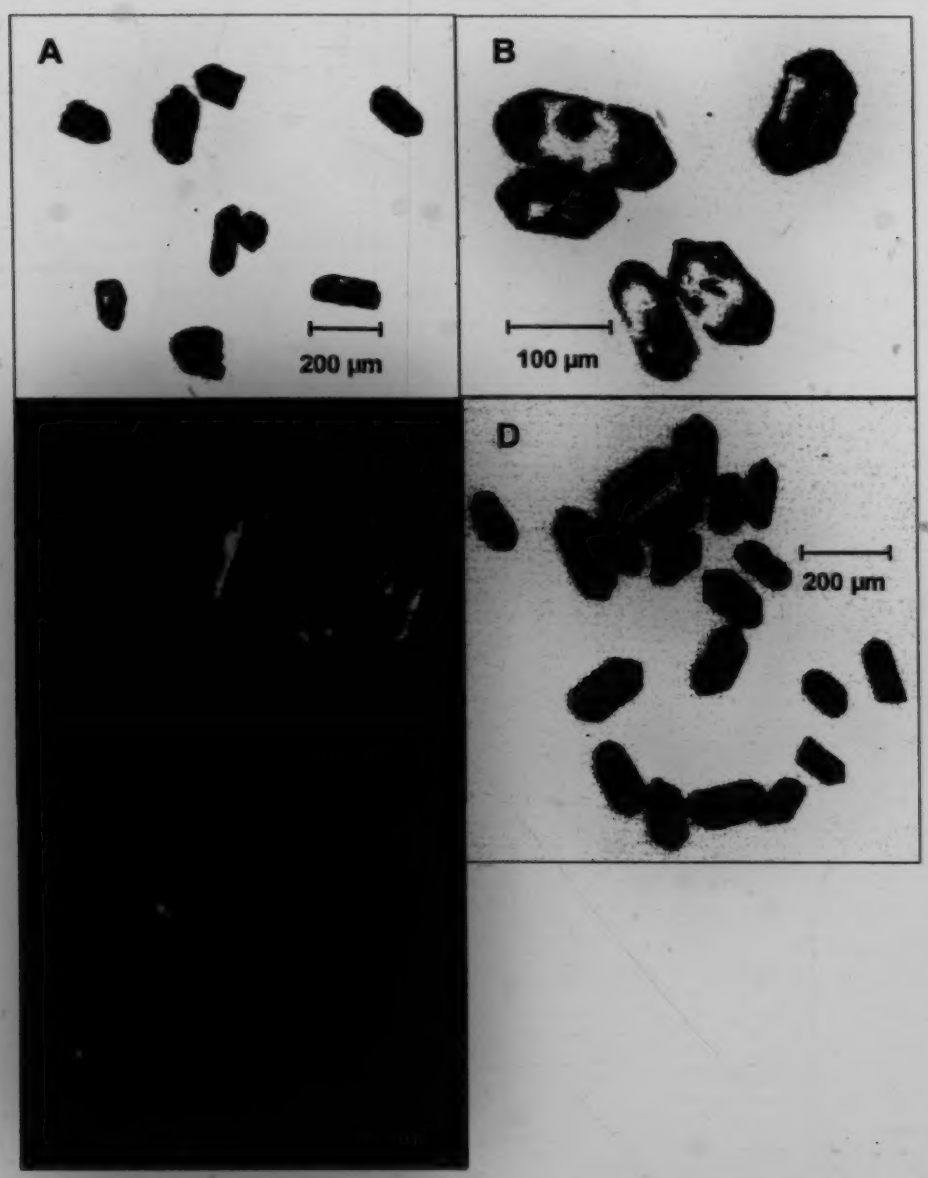

Figure 3-4. Plane light photomicrograph of zircons from the North Shore Plutons; A) Macintosh Bay Granite, B) Gunnar Granite, C) Geebee Lake Tonalite, D)Yahyah Lake Granite, and E) Hayter Bay Granite.

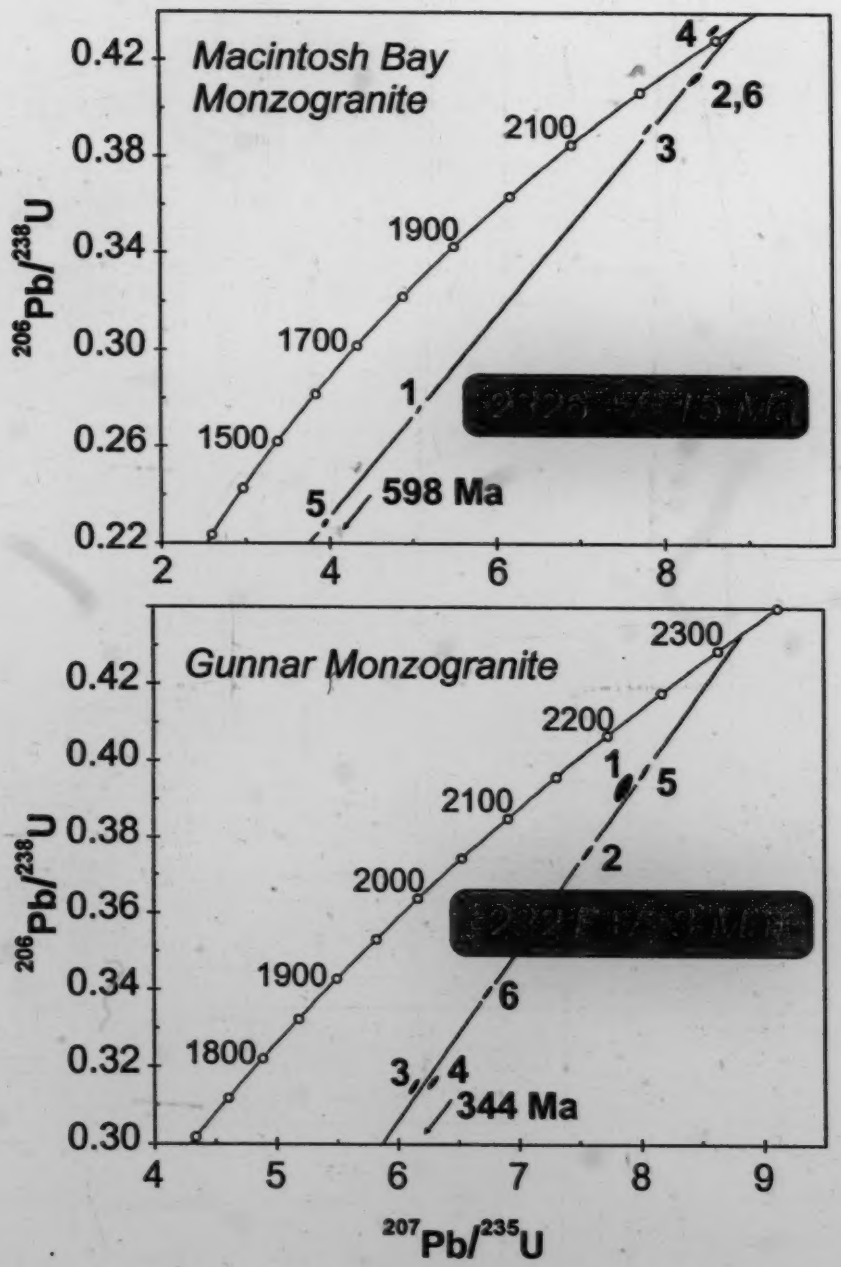

Figure 3-5. Concordia plots for the Gunnar and Macintosh Bay granites.

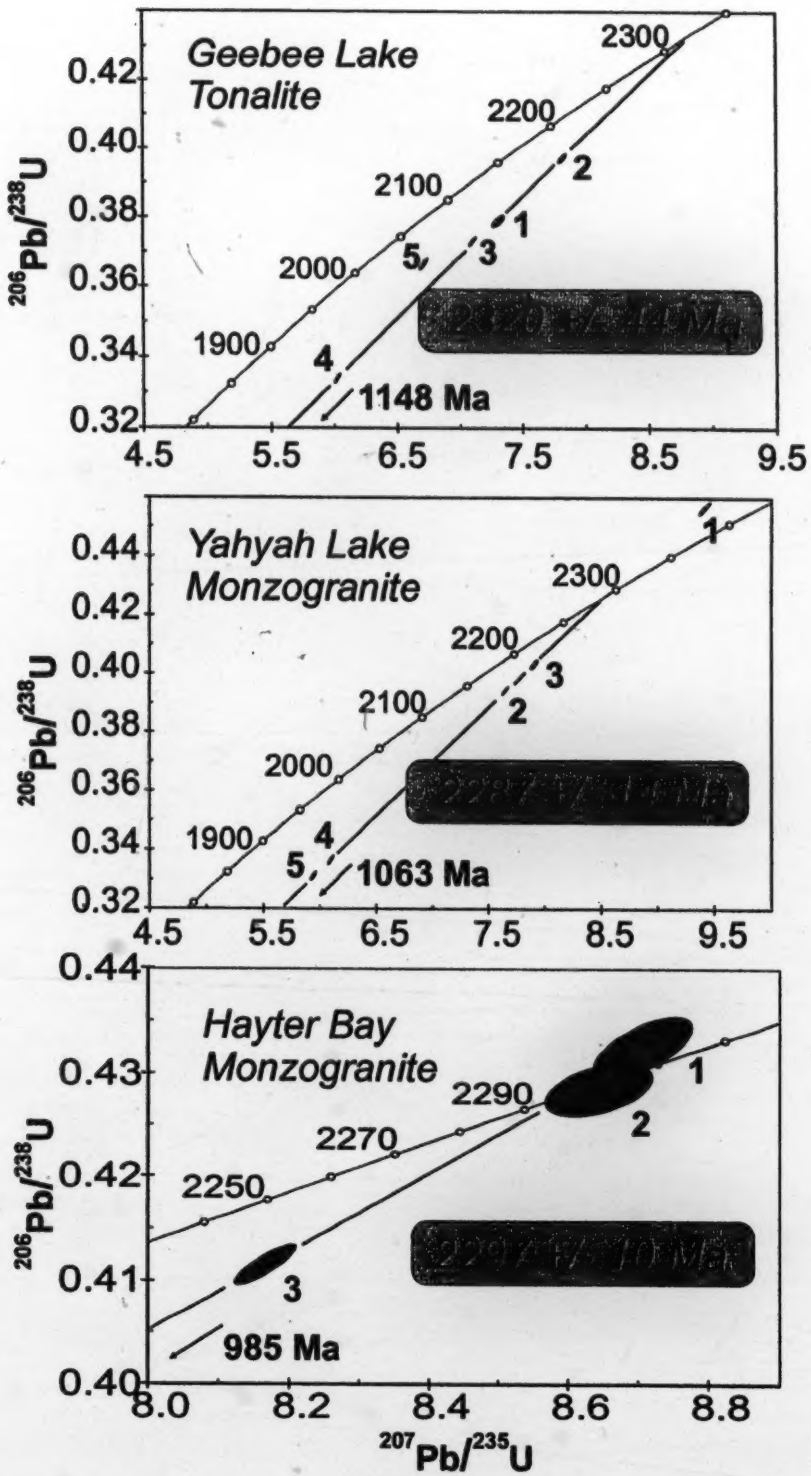

Figure 3-6. Concordia plots for Geebee Lake, Yahyah Lake, and Hayter Bay granites.

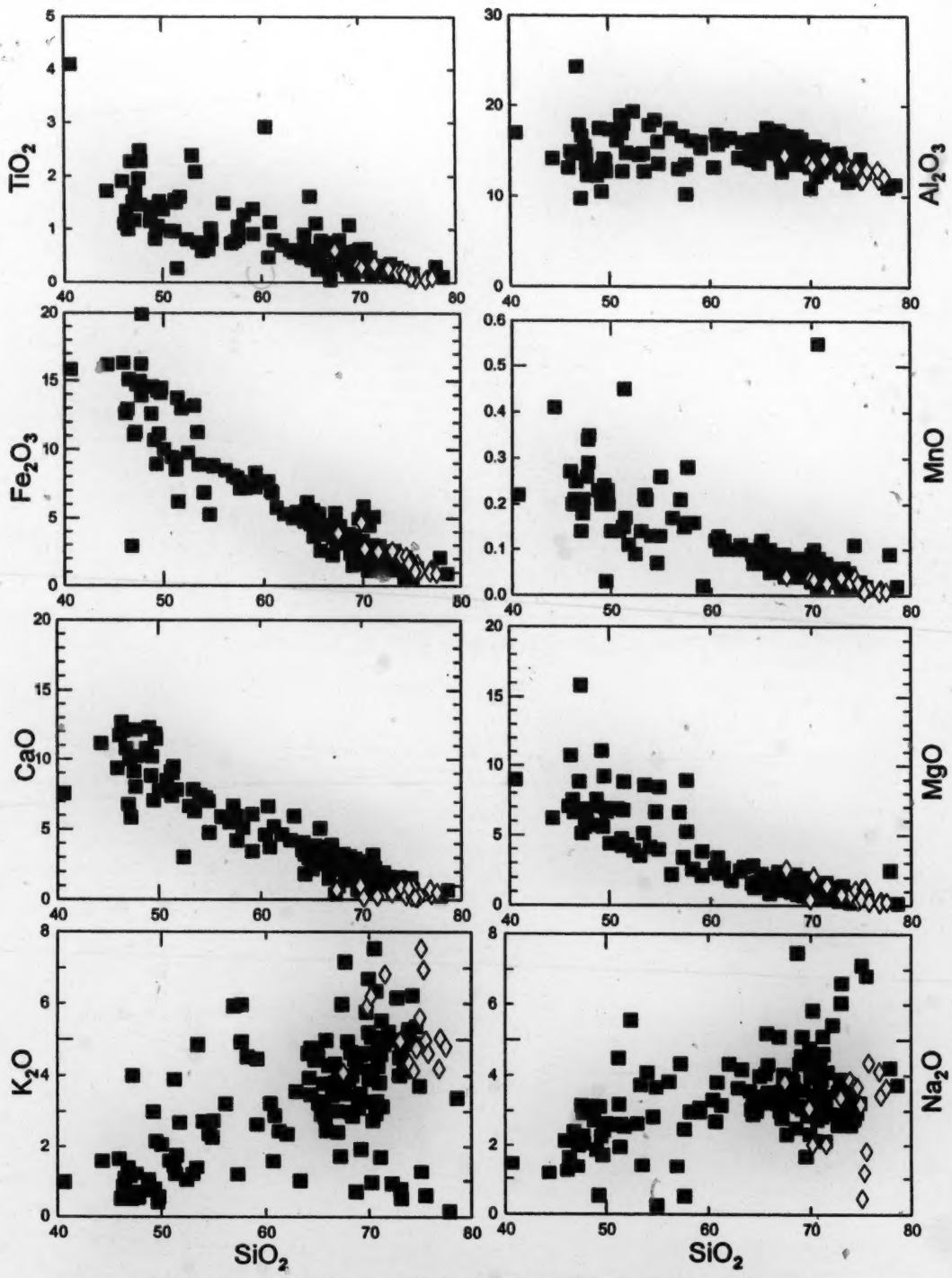

Figure 3-7. Harker variation diagrams displaying the major element oxides in weight percent for the 2.3 Ga North Shore Plutons (Diamonds, n=16), and biotite and hornblende gneiss (Squares, n=143) from basement to the Taltson Magmatic Zone (Goff et al., 1986).

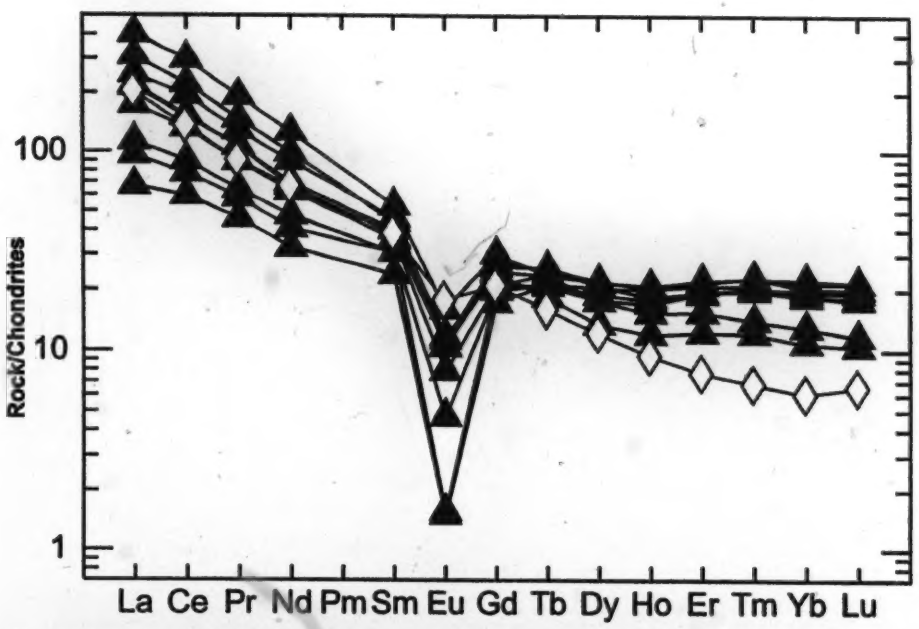

Figure 3-8. Chondrite (Sun and McDonough, 1989) normalized REE plot for the 2.3 Ga North Shore Plutons (closed triangles), excluding porphyritic dykes. An average of the Cassiar Batholith.(open diamonds, Driver et al., 2000) is included for comparison. Plot is restricted to samples with 70% to 76% SiO_2.

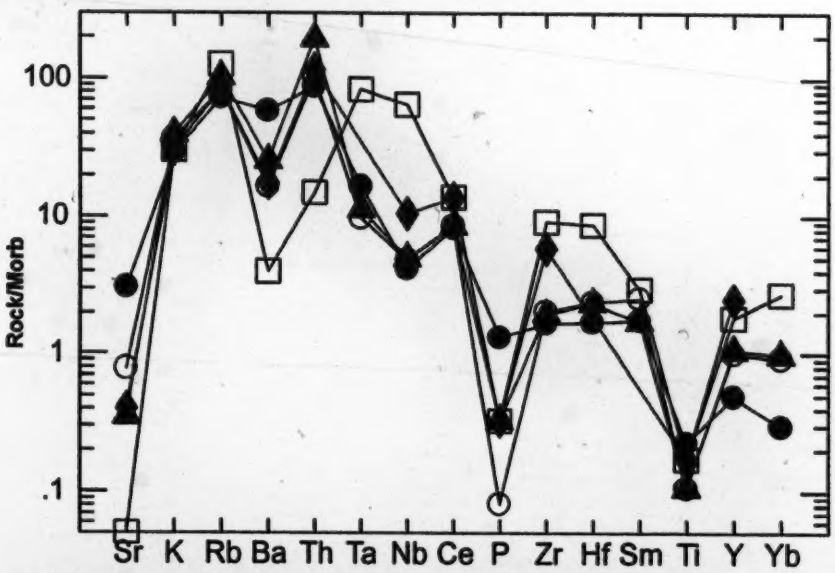

Figure 3-9. MORB normalized (Pearce, 1983) plot for selected trace and major elements from several suites of granites. ▲ Average of North Shore Plutons with 70-76% SiO_2 . ○ Volcanic arc granite from Chile (data from Pearce et al., 1984). □ Within-plate granite from the Oslo Rift (data from Pearce et al., 1984). ♦ Average of anorogenic (A-type) granites from the Lachlan area (Landenberger et al., 1996). ● Average of felsic samples from the Cassiar Batholith (Driver et al., 2000).

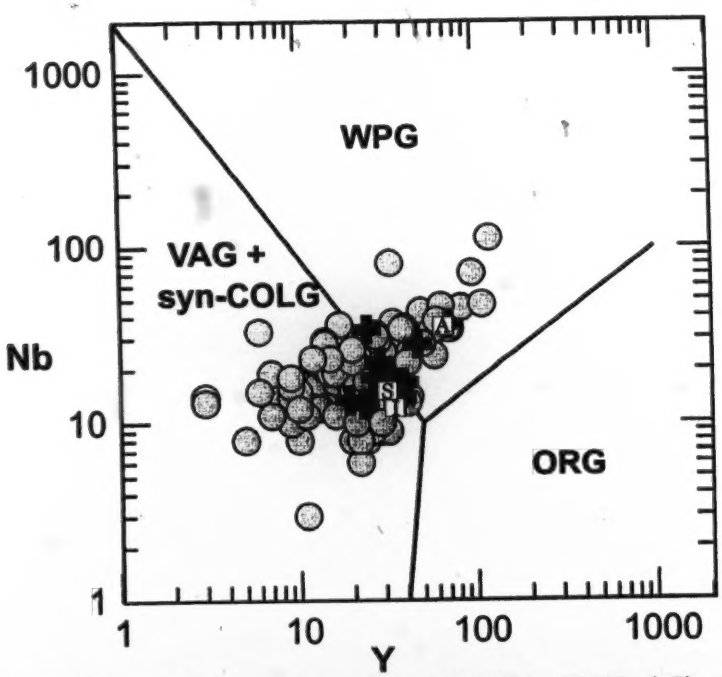

Figure 3-10. Nb vs Y discrimination plot (Pearce et al., 1984) of the North Shore Plutons (plus symbols, n=16). Biotite and hornblende granite gneiss (circles, n=143) from the basement to the TTMZ are also plotted. Also included are boxes that indicate average compositions of A-, I-, and S-type granites (Whalen et al., 1987; Landenberger et al., 1996). VAG, volcanic arc granite; syn-COLG, syn-collisional granite; WPG, within plate granite; ORG, Ocean Ridge Granite.

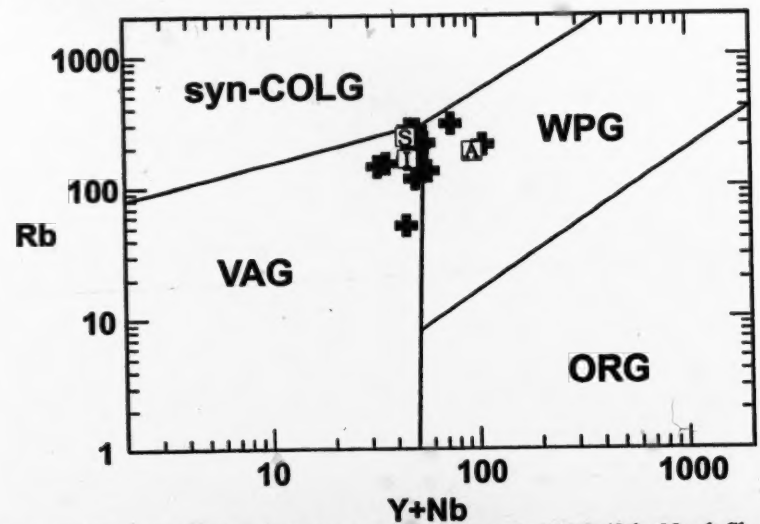

Figure 3-11. Rb vs Y+Nb discrimination plot (Pearce et al., 1984) of the North Shore Plutons (plus symbols, n=16). Also included are the averages for some A-, I-, and S-type granites (Whalen et al. 1987; Landenberger et al., 1996). VAG, volcanic arc granite; syn-COLG, syn-collisional granite; WPG, within plate granite; ORG, Ocean Ridge Granite.

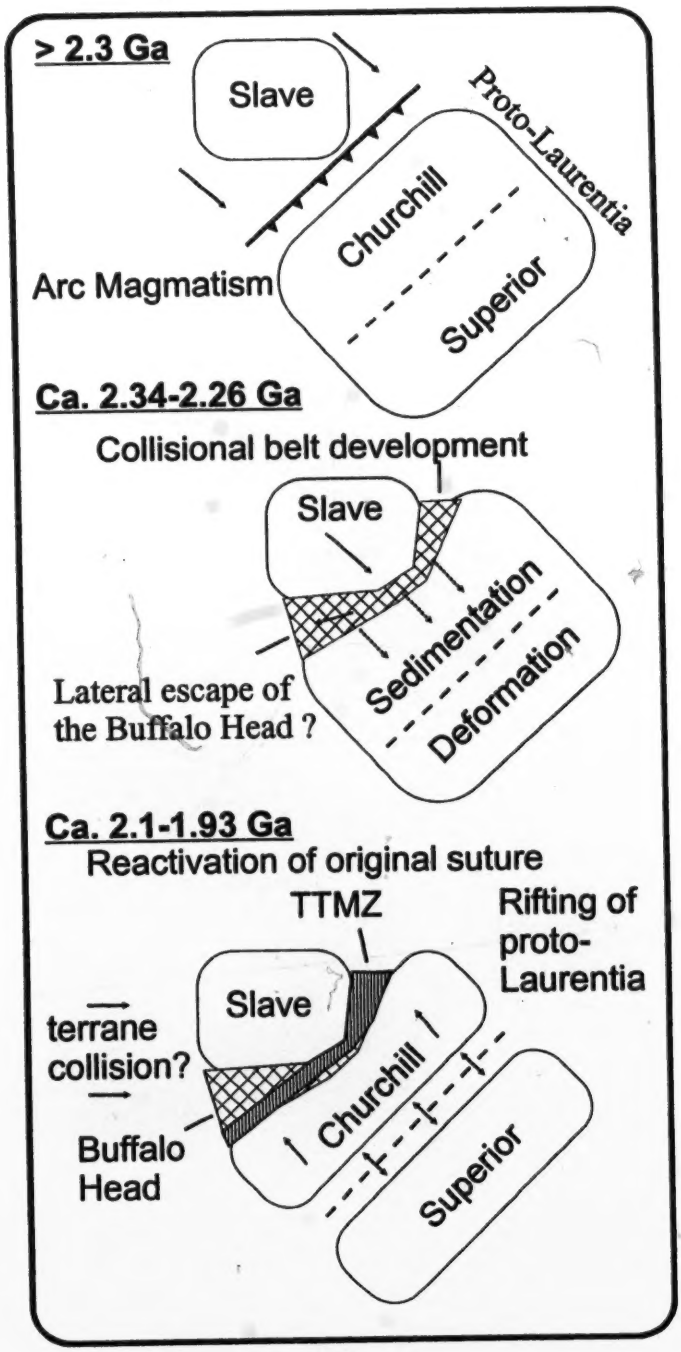

Figure 3-12. Cartoon diagram displaying Paleoproterozoic tectonic history for northwestern Laurentia. Details are discussed in the text. TTMZ Taltson-Thelon Magmatic Zone.

Table 3-1. U-Pb results

	Sample Description[a]	Weight (mg)	Concentrations (ppm) U	Th[b] model	Pb rad.	Th/U ratio	Pb (pg)[c]	Isotopic Ratios[d] $^{206}Pb/^{204}Pb$	$^{206}Pb/^{238}U$	$^{207}Pb/^{235}U$	$^{207}Pb/^{206}Pb$	Apparent Ages (Ma) $^{206}Pb/^{238}U$	$^{207}Pb/^{235}U$	$^{207}Pb/^{206}Pb$	PD[e]
Macintosh Bay Monzogranite (RH98-22)															
1	Zr, abr, (4)	0.004	574	275	175	0.48	12	3608	0.2756±5	5.081±10	0.1337±1	1569	1833	2147	30.26
2	Zr, abr, (1)	0.002	259	114	117	0.44	48	296	0.4132±9	8.391±27	0.1473±3	2229	2274	2314	4.37
3	Zr, abr, (1)	0.001	342	181	150	0.53	9	1380	0.3919±7	7.818±17	0.1447±1	2132	2210	2284	7.82
4	Zr, abr, (1)	0.002	319	198	157	0.62	43	441	0.4331±9	8.601±23	0.1440±2	2320	2297	2276	-2.28
5	Zr, (3)	0.003	273	121	69	0.44	23	551	0.2285±4	3.951±10	0.1254±2	1327	1624	2034	38.41
6	Zr, abr, (1)	0.001	334	208	158	0.62	34	350	0.4122±9	8.367±25	0.1472±3	2225	2272	2314	4.53
Gunnar Monzogranite (RH00-03)															
1	Zr, (1)	0.002	49	23	21	0.46	6	430	0.3934±13	7.866±34	0.1449±4	2138	2215	2286	7.55
2	Zr, (1)	0.002	381	183	159	0.48	6	2501	0.3762±7	7.565±16	0.1458±1	2059	2181	2298	12.14
3	Zr, (1)	0.001	291	150	103	0.51	6	934	0.3151±7	6.134±17	0.1412±2	1766	1995	2242	24.25
4	Zr, abr, (2)	0.002	261	162	95	0.62	16	700	0.3162±6	6.289±15	0.1443±2	1771	2017	2279	25.45
5	Zr,abr, (2)	0.004	339	205	153	0.61	10	3361	0.3974±7	8.029±16	0.1465±1	2157	2234	2306	7.60
6	Zr, (4)	0.003	248	125	94	0.50	7	2660	0.3394±6	6.738±14	0.1440±1	1884	2078	2276	19.83
Geebee Lake Tonalite (RH99-576)															
1	Zr, abr, (1)	0.001	524	502	243	0.96	22	476	0.3787±7	7.299±19	0.1398±2	2070	2149	2225	8.12
2	Zr, abr, (1)	0.001	473	447	229	0.94	17	795	0.3970±6	7.808±14	0.1427±1	2155	2209	2260	5.45
3	Zr, (1)	0.001	508	378	221	0.74	10	1618	0.3729±5	7.094±11	0.1380±1	2043	2123	2202	8.40
4	Zr, (1)	0.002	489	294	184	0.60	4	4111	0.3337±5	6.022±10	0.1309±1	1856	1979	2110	13.82
5	Zr, (5)	0.005	436	310	184	0.71	31	1549	0.3662±6	6.704±13	0.1328±1	2012	2073	2135	6.71
Yahyah Lake Monzogranite (RH99-518)															
1	Zr, abr, (1)	0.003	464	214	232	0.46	11	3175	0.4563±9	9.402±20	0.1495±1	2423	2378	2340	-4.28
2	Zr, abr, (1)	0.002	1027	503	447	0.49	26	2169	0.3941±5	7.640±11	0.1406±1	2142	2190	2235	4.90
3	Zr, (1)	0.002	501	377	237	0.75	24	920	0.4030±6	7.901±13	0.1422±1	2183	2220	2254	3.74
4	Zr, abr, (1)	0.001	1406	563	521	0.40	18	1846	0.3362±6	6.093±11	0.1314±1	1869	1989	2117	13.52
5	Zr, abr, (1)	0.001	857	459	315	0.54	16	1042	0.3308±5	5.941±11	0.1303±1	1842	1967	2101	14.15
Hayter Bay Monzogranite (RH98-360)															
1	Zr, abr, (1)	0.003	93	97	50	1.04	16	405	0.4326±12	8.707±29	0.1460±4	2317	2308	2300	-0.91
2	Zr, abr, (1)	0.001	422	441	226	1.05	35	208	0.4284±11	8.643±31	0.1463±5	2298	2301	2304	0.26
3	Zr, abr, (1)	0.001	314	322	160	1.03	3	1900	0.4114±8	8.164±17	0.1439±1	2221	2249	2278	2.78

Table 3-1. comments

[a] Abreviations: Zr, zircon; abr, air abraded following the techniques of Krogh (1982). The number in parentheses identifies the number of grains or grain fragments analyzed.

[b] Model Th concentration calculated from $^{208}Pb/^{206}Pb$ ratio and $^{207}Pb/^{206}Pb$ age

[c] Total common lead in analysis

[d] Atomic ratios corrected for 2.0 pg Pb and 0.5 pg U in blanks, fractionation, and initial common Pb (Stacey and Kramers, 1975). Uncertainties are reported at 1σ.

[e] PD refers to the percent discordance along a chord to the origin.

Table 3-2: Whole rock geochemistry of 2.3 Ga granitoids.

Sample	Rock Type	SiO2	TiO2	Al2O3	Fe2O3	MnO	MgO	CaO	Na2O	K2O	P2O5
4701 0029	Athona Granite	76.96	0.062	11.85	1.23	0.014	0.31	0.35	3.42	5.03	0.02
RH98-C28	Cameron Island Granite	69.85	0.310	13.94	4.66	0.038	0.39	0.99	3.07	5.92	0.03
RH98-C56	Cameron Island Granite	76.83	0.039	12.99	0.99	0.007	0.13	0.77	4.12	4.20	0.01
RH98-C58	Cameron Island Granite	73.89	0.188	13.34	2.14	0.028	0.77	0.86	3.86	4.35	0.05
4700 0085	Gunnar Granite	74.37	0.204	13.21	2.17	0.039	1.10	0.26	3.71	4.14	0.07
4700 0088	Gunnar Granite	73.01	0.253	13.31	2.56	0.039	0.75	0.46	3.37	4.95	0.07
4700 0132A	Gunnar Granite	67.49	0.600	14.54	3.87	0.041	2.59	0.70	3.81	4.08	0.17
4700 0146	Gunnar Granite	70.20	0.274	13.43	2.70	0.034	2.07	0.14	2.02	6.20	0.08
4700 4060	Gunnar Granite	71.55	0.328	14.19	2.50	0.026	1.39	0.23	2.03	6.82	0.08
4700 0119	Gunnar Granite - Porphyry	75.55	0.105	12.24	1.62	0.017	0.99	0.12	1.83	4.97	0.02
4700 4308	Gunnar Granite - Porphyry	75.10	0.087	11.77	1.68	0.017	1.23	0.86	0.44	7.53	0.03
RH98-22	Mackintosh Bay Granite	74.96	0.182	12.94	1.65	0.013	0.47	0.18	3.17	5.61	0.05
RH98-J09	Mackintosh Bay Granite	75.78	0.055	12.95	1.10	0.015	0.22	0.28	4.36	4.62	0.02
RH98-J32	Mackintosh Bay Granite	75.33	0.084	11.84	1.06	0.007	1.28	0.16	1.19	6.95	0.01
RH98-518	Yahyah Lake Granite	74.64	0.155	13.17	1.67	0.027	0.31	0.84	3.67	4.75	0.04
RH99-517	Yahyah Lake Granite	77.51	0.079	12.20	0.90	0.008	0.22	0.52	3.65	4.80	0.02

Whole rock geochemistry completed at Activation Laboratories, Ontario, Canada.

Table 3-2: Whole rock geochemistry of 2.3 Ga granitoids.

Sample	LOI	TOTAL	Sc	Pb	Sn	Rb	Cs	Ba	Sr	Tl	Ga	Ge	Ta
4701 0029	0.66	99.90	2	54	3	161	0.4	111	15	0.90	17	1.0	1.91
RH98-C28	0.81	100.00	5	33	2	208	2.0	597	49	1.14	30	1.9	1.37
RH98-C56	0.21	100.31	1	18	-1	132	1.0	319	47	0.71	21	1.2	3.24
RH98-C58	0.70	100.16	4	20	3	182	0.8	808	65	1.03	20	0.9	1.98
4700 0085	0.96	100.23	6	23	3	165	0.4	567	55	0.99	19	0.9	2.94
4700 0088	0.57	99.35	6	21	3	273	2.0	685	65	1.44	20	1.0	2.35
4700 0132A	1.86	99.74	10	17	4	51	0.2	1161	63	0.31	20	0.7	2.40
4700 0146	1.55	98.70	7	20	2	143	0.7	840	56	0.72	18	0.7	1.18
4700 4060	1.36	100.50	7	24	3	150	0.5	1133	78	0.80	18	0.7	1.05
4700 0119	1.28	98.72	6	18	3	115	0.7	413	31	0.62	17	0.7	1.62
4700 4308	1.15	99.89	4	27	4	301	5.0	350	33	1.65	22	1.1	2.15
RH98-22	0.45	99.69	4	23	3	224	3.8	400	35	1.36	19	1.1	2.32
RH98-J09	0.35	99.75	2	16	4	210	4.8	34	9	1.14	18	1.1	2.35
RH98-J32	1.21	99.14	2	11	2	210	1.1	127	9	1.09	17	0.9	1.89
RH98-518	0.50	99.77	3	20	4	272	1.1	786	83	1.44	20	1.1	3.64
RH99-517	0.59	100.50	2	16	5	215	0.8	553	50	1.35	16	0.9	3.76

Table 3-2: Whole rock geochemistry of 2.3 Ga granitoids.

Sample	Nb	Hf	Zr	Y	Th	U	La	Ce	Pr	Nd	Sm	Eu	Gd
4701 0029	16.5	3.7	91	29.6	27.0	9.98	23.0	48.4	5.20	18.8	4.01	0.078	3.51
RH98-C28	36.1	15.9	636	70.3	57.2	4.65	270	498	57.7	191	28.3	2.73	20.9
RH98-C56	33.6	6.0	105	24.2	26.5	25.3	3.25	5.74	0.7	2.88	1.61	0.243	2.40
RH98-C58	14.5	5.2	183	36.0	47.1	6.32	51.1	92.6	10.1	32.4	6.14	0.602	5.34
4700 0085	13.6	4.3	146	37.4	35.5	10.2	41.4	80.7	8.45	29.3	5.58	0.614	5.09
4700 0088	14.5	5.4	196	32.0	44.7	9.00	59.4	119	12.2	41.7	7.04	0.658	5.61
4700 0132A	17.9	8.8	327	26.9	34.4	4.01	104	194	20.3	68.9	10.3	1.78	7.55
4700 0146	13.4	6.1	230	19.3	41.7	3.95	73.9	137	14.0	46.2	6.67	0.687	4.93
4700 4060	12.7	7.1	282	23.2	38.9	4.62	95.9	183	18.3	58.9	8.11	0.927	6.19
4700 0119	13.1	4.3	124	36.7	43.7	10.4	18.4	42.9	4.93	18.0	4.17	0.166	4.55
4700 4308	27.7	6.3	157	46.9	43.1	4.80	33.8	84.3	9.28	34.8	7.69	0.051	6.80
RH98-22	17.9	5.6	148	30.3	33.7	7.16	26.8	55.0	6.07	22.2	4.71	0.272	4.08
RH98-J09	16.7	3.8	98	35.8	34.7	6.68	22.8	47.3	5.54	19.0	4.70	0.091	4.29
RH98-J32	16.3	6.6	201	31.9	32.5	5.50	15.8	36.4	4.36	15.2	3.64	0.087	3.55
RH98-518	21.9	5.6	170	28.6	40.6	9.50	52.2	94.1	10.1	31.1	5.44	0.458	4.35
RH99-517	16.8	3.1	82	38.8	21.4	8.63	27.9	52.3	5.73	18.6	4.04	0.294	3.93

Table 3-2: Whole rock geochemistry of 2.3 Ga granitoids.

Sample	Tb	Dy	Ho	Er	Tm	Yb	Lu	Y-mai	Zr-mai	Be-na	V-mai	Sr-mai	Ba-na
4701 0029	0.67	4.33	0.92	2.82	0.470	2.87	0.427	29	82	2	6	16	105
RH98-C28	2.85	14.5	2.65	6.75	0.863	4.06	0.467	65	582	3	6	51	579
RH98-C56	0.73	5.03	1.10	3.58	0.541	3.31	0.452	23	99	3	-5	48	310
RH98-C58	0.96	5.59	1.15	3.47	0.532	3.17	0.461	34	167	2	14	69	810
4700 0085	0.88	5.54	1.17	3.68	0.578	3.79	0.550	37	145	3	15	52	567
4700 0088	0.94	5.31	1.04	3.22	0.504	3.14	0.452	31	191	3	18	62	693
4700 0132A	1.08	5.63	1.03	2.99	0.437	2.78	0.381	26	329	2	34	60	1,150
4700 0146	0.69	3.43	0.68	2.04	0.310	1.84	0.265	16	223	2	22	58	834
4700 4060	0.88	4.48	0.87	2.57	0.359	2.21	0.298	23	271	1	16	74	1,180
4700 0119	0.99	6.50	1.41	4.45	0.678	4.05	0.587	35	126	2	6	30	413
4700 4308	1.28	7.84	1.62	5.01	0.770	4.68	0.658	45	141	2	-5	31	362
RH98-22	0.80	4.81	1.00	3.22	0.523	3.28	0.490	28	149	3	11	35	405
RH98-J09	0.90	5.51	1.18	3.64	0.581	3.48	0.510	34	93	2	-5	11	36
RH98-J32	0.80	5.19	1.13	3.57	0.586	3.67	0.544	30	186	1	-5	11	127
RH98-518	0.78	4.49	0.97	3.16	0.516	3.39	0.513	26	156	4	8	87	767
RH99-517	0.90	5.54	1.24	4.17	0.689	4.20	0.655	35	77	3	5	51	543

Table 3-3: Sm-Nd isotope results for samples of ca. 2.3 Ga granites from the Uranium City area.

Sample	Sample #	Sm ppm	Nd ppm	$^{147}Sm/^{144}Nd_1$	$^{143}Nd/^{144}Nd_1$	uncert.	εNdT_1	$T_{DM\,2}$
Macintosh Bay Monzogranite	RH98-022	4.92	24.61	0.1210	0.511403	0.000006	-1.5	2.87
Hayter Bay Monzogranite	RH98-360	5.24	34.53	0.0918	0.510705	0.000007	-6.7	3.05
Gunnar Monzogranite	RH00-03	10.07	71.87	0.0847	0.510712	0.000009	-4.3	2.88

$_1$, measured values; $_2$, Time of seperation from depleted mantle (Goldstein et al. 1984) in billions of years.

Chapter 4: Paleoproterozoic metamorphism and deformation of the Archean Churchill craton, Canada: New results from the western Beaverlodge Belt, Saskatchewan

A version of this chapter is in preparation for submission to the Journal of Metamorphic Geology. Co-authors are L.M. Heaman[a], T. Chacko[a], and K.E. Ashton[b]
[a]Department of Earth and Atmospheric Sciences, 1-26 Earth Sciences Building, University of Alberta, Edmonton, Alta., Canada, T6G 2E3
[b]Saskatchewan Geological Survey, 2101 Scarth St., Regina, Sask., Canada, S4P 3V7

Introduction

The Rae and Hearne Provinces of the Canadian Shield (Hoffman, 1988; Fig. 4-1) comprise a remote area of reworked Archean crust that has an exposed extent of nearly one million km^2. Together, these two provinces form the core of the Churchill craton (also known as the Western Churchill Province), which was subdivided based on the presence of a major structural break termed the Snowbird tectonic zone (Hoffman, 1988). The Churchill craton underwent Proterozoic metamorphism and deformation that is much more extensive than in the bordering Superior and Slave cratons. This difference is primarily due to its position as hinterland during later orogenies. This paper examines the metamorphic history of an area (~600 km^2) near the southwestern margin of the Churchill craton. This area is ideal for study because it is midway between two of the Churchill craton's bounding Proterozoic belts (Trans Hudson Orogen and Taltson-Thelon Magmatic Zone, Fig 4-1) and adjacent to the Snowbird Tectonic Zone. In addition, the exposed supracrustal rocks in the area are ideal for determining the conditions and timing of metamorphism.

Methodologies aimed at placing age constraints on thermotectonism include dating of igneous rocks that bracket metamorphism and/or deformation, use of

radiogenic systems that may be partially or entirely reset during metamorphism (e.g. Re-Os, U-Pb, K-Ar, Rb-Sr), and dating of metamorphic minerals (e.g. Mezger et al., 1991) such as garnet, hornblende, muscovite, biotite, titanite, zircon, and monazite. Although the last of these methods may be the best for directly dating metamorphism and deformation, the most robust chronology may be derived from a combination of all three methods. This study highlights the strength of combining traditional techniques of mapping and ID-TIMS whole-mineral geochronology with the quickly evolving methods of in-situ EMP and LA-MC-ICPMS dating.

Regional Geology

The Snowbird Tectonic Zone was initially considered to be a Paleoproterozoic suture (Hoffman, 1988, 1989) between the Rae and Hearne Provinces, but it was later argued that it is an Archean intracontinental strike-slip shear zone which may have overprinted an earlier Archean suture (Hanmer et al., 1994; 1995). Ca. 2.6 Ga granulite-facies metamorphism has been recorded within the Snowbird Tectonic Zone (Kopf, 2002). More recent work has revised the timing of this event to ca. 2.55-2.52 Ga (Baldwin et al., 2003). The most recent models for the Snowbird tectonic zone (Sanborn-Barrie et al., 2001; Baldwin et al., 2003) relate it to an Archean structure that was reactivated and rapidly exhumed at 1.9 Ga, coeval with widespread 1.9 Ga metamorphism within and adjacent to the structure (Williams et al., 1999; Sanborn-Barrie et al., 2001; Baldwin et al., 2003). On the east side of the East Athabasca triangle (Fig. 4-1), a block of high-pressure granulites along the Snowbird Tectonic Zone, east-vergent thrusting is interpreted to have occurred at 1830-1810 Ma (Mahan et al., 2003).

The western margin of the Churchill craton has generally been accepted to be marked by the Taltson-Thelon Magmatic Zone (Hoffman, 1988). Ca. 2.0-1.93 Ga magmatism within this belt overprints an earlier magmatic belt that is interpreted to have formed during the ca. 2.3 Ga Blezardian Orogeny (Chapter 3). On the east margin of the Churchill craton, the Trans-Hudson Orogen marks the 1.9-1.8 Ga closure of the Manikewan Ocean that amalgamated the Churchill, Superior, and Sask cratons and intervening oceanic arcs and basins (Hoffman, 1988; Lewry and Collerson, 1990; Ashton et al., 1999).

Local Geology

In the southwestern portion of the Churchill craton, Saskatchewan (Fig. 4-2) an area of Neoarchean supracrustal rocks and 3.0 Ga basement granitoids (Chapter 2) compose an area termed the Beaverlodge Belt. Relatively low- to medium-grade rocks are exposed in the west end of this generally high-grade belt (Ashton and Card, 1998; Hartlaub and Ashton, 1998). The belt is bounded, in part, by a network of major shear zones that have a complicated history of reactivation. Along the northeastern margin of the belt, the 6-8 km thick Oldman-Bulyea shear zone separates granulite-facies rocks of the Beaverlodge Belt from the amphibolite-facies Train Lake Domain (Card, 2001). The present work focuses primarily on the western end of the Beaverlodge Belt (Fig. 4-3) where the transition between medium- and high-grade rocks is exposed. This transition coincides with a series of crustal faults that may roughly mark the eastern edge of the ancient crustal block described in Chapter 5. The high- and medium-grade areas will be described separately because of differences in the conditions and timing of metamorphism and deformation.

Metamorphism and deformation

Medium-grade zone

The eastern margin of the Beaverlodge Belt contains several zones of medium-grade supracrustal rocks that coincide with exposed domes of known and suspected Mesoarchean granite (Chapter 2). These basement granitoids are moderately deformed but are not gneissic or migmatitic. The deformational and metamorphic history of the area is summarized in table 4-1. The earliest phase of deformation recorded in the supracrustal rocks in the medium-grade zone involved isoclinal folding that transposed bedding and developed a moderate to strong axial planar fabric. We interpret this phase of deformation to be equivalent to regional D_2 (Table 4-1). The type of S_2 fabric present is dependent on the grade of coeval metamorphism, but ranges from schistosity to local gneissosity. The ca. 2.3 Ga suite of North Shore Plutons (Chapter 3) have a moderate to strong biotite foliation ($S_{2?}$) which has been folded by south-southwest-plunging, open to tight upright folds (F_3). These folds define the obvious structural grain to much of the study area (Fig. 4-4) and form the regional-scale folding of the Beaverlodge Belt (Fig. 4-2). These folds progressively tighten towards the Black Bay Fault (Fig. 4-2). Cleavage and rodding related to this folding event are well developed in the vicinity of Macintosh Bay (Fig. 4-3). Some psammitic rocks contain an axial planar fabric to these folds, defined by quartz-sillimanite nodules, that cuts the earlier S_2 fabric (Fig. 4-6c,d).

The peak metamorphic assemblages define the S_2 fabrics in the area (e.g. Fig. 4-6a). The assemblage garnet-biotite-staurolite-quartz-muscovite in pelites represents the lowest grade of peak metamorphism in the area and indicates mid-amphibolite conditions of 520-675° C and >4 kbars (Pattison, 2001). The presence of garnet and

staurolite and lack of cordierite are consistent with moderate to high pressures. The prograde breakdown of early muscovite + staurolite + quartz to form andalusite + biotite + H_2O (Fig. 4-7b,c) indicates metamorphic conditions reached 550° C and < 4 kbars (Pattison et al., 1999). Thus, the prograde metamorphic P-T path displayed in the medium-grade pelites would have initial pressures higher than later ones and initial temperatures that may have been lower than later ones, consistent with an orogenic clockwise P-T path. Quartz-sillimanite nodules that overprint S_2 and are axial planar to the open NE-tending folds (Fig. 4-6d) indicate that a second phase of metamorphism occurred coeval with D_3. Overprinting of andalusite by muscovite and sillimanite (Fig. 4-7c) in the lowest-grade pelites indicates that this second phase of metamorphism may have been at a slightly higher temperature or pressure than the first.

Within the eastern zone of medium-grade rocks (Fig. 4-4), muscovite is completely absent from pelites. Although these pelites do not appear to have undergone anatexsis, some samples have the peak mineral assemblage of garnet-biotite-sillimanite-quartz-K-feldspar. This assemblage indicates that peak metamorphism locally surpassed 650° C (Pattison, 2001). Mafic rocks throughout the study area are hornblende-bearing and pyroxene-free, consistent with amphibolite-facies conditions (Spear, 1995).

The ca. 1.82 Ga Martin Basin (Morelli et al., in prep.), which is exposed along the length of the Black Bay Fault (Fig. 4-2) has not been affected by any of the metamorphism or deformation discussed above. This places a lower age limit of 1.82 Ga on these events.

High-grade zone

The earliest metamorphic fabrics (S_1) within the high-grade zones comprise gneissic and lit-par-lit migmatitic layering (Fig. 4-6a). Moderate to strong L_1 stretching and mineral lineations are locally developed. Upper amphibolite facies conditions are recorded to the east of a fault north of the Cameron Island Granite, where 10% in-situ granitic neosome is present. The pelitic rocks surrounding the Dead Man Granite (Fig. 4-3) have undergone the highest degree of partial melting (>25%) and have the peak M_1 assemblage of garnet-biotite-sillimanite-quartz-K-feldspar-melt. Although the peak conditions of metamorphism in the study area do not appear to exceed upper-amphibolite facies, granulite-facies rocks are well developed along the eastern margin of the Beaverlodge Belt (Ashton and Card, 1998). D_2 folds range from tight to isoclinal, and are doubly north-northeast- to south-southwest-plunging with gently east- or west-dipping axial planes. A strong S_1/S_2 intersection lineation is apparent in the rare locations where an S_2 gneissic layering intersects S_1. Crustal conditions during D_2 deformation are likely similar to that during D_1 because there is no retrogression of S_1 mineral assemblages associated with F_2 folds, and local intersection between two sets of migmatite layering (S_1 and S_2) was recorded.

The suite of open to close NE-trending folds (F_3) that are described in the medium-grade zone also deform rocks in the high-grade zone. The fold axis indicated by the pole to the great circle girdle of the $S_{1/2}$ fabrics from the entire region is identical to the measured F_3 fold axes (Fig. 4-5a,b). In addition, the bisecting surface identified in figure 4-6a corresponds to the orientation of F_3 axial planes and S_3 fabrics recorded in figure 4-6c. M_3 melt patches cross-cut the $S_{1/2}$ migmatites and these late anatexic melts have a NE trending S_3 fabric that is defined by the alignment of cordierite (Fig. 4-6e).

This neosome contains the assemblage cordierite-biotite-K-feldspar-melt, indicating high temperature (> 650° C) and moderate to low pressures of M_3 metamorphism. Widespread NE trending S_3 fabrics in eastern diatexites are defined by biotite + cordierite overgrowths on garnet (Fig. 4-6f). Both M_1 garnet and sillimanite are highly resorbed. The decompression reaction of garnet + sillimanite + quartz → cordierite, indicates that pressures had dropped below ~4 kbar (e.g., Pereira and Bea, 1994). The prevalence of low pressure mineral growth associated with F_3 folding indicates that deformation was coeval with regional decompression.

Monazite Chemical Dating

The importance of in-situ methods of geochronology has been well demonstrated in polymetamorphic terrains where crucial textural information is often lost when minerals are separated from the rock for dating (e.g. Crowley and Ghent, 1999; Böhm et al., 2003). Monazite is an important accessory mineral because it commonly grows coevally with garnet during metamorphism (e.g. Foster et al., 2000; Catlos et al., 2002). Although ion microprobe and laser-ablation methods of in-situ dating are now available, only electron microprobe (EMP) dating provides a combination of rapid, inexpensive, reconnaissance-style age determinations for small (<10μm) domains in metamorphic monazite (Suzuki and Adachi, 1991; Montel et al., 1996; Cocherie et al., 1998). Dating of monazite by EMP is possible due to its high levels of Th (generally >3%), lack of common Pb (Parrish, 1990), and rapid accumulation of radiogenic Pb (Montel et al., 1996). In addition, studies indicate that diffusion (Cocherie et al., 1998) or loss (Parrish, 1990) of radiogenic Pb is minimal at

low temperatures. Diffusion of Pb in monazites from the study area is unlikely to have occurred since the Pb closure temperature is estimated to exceed 900° C (Cherniak et al., 2004).

Methodology

Carbon coated thin sections were analyzed with a JEOL 8900 EMP using a beam diameter that was 3-5 μm. Analyses were conducted using an accelerating voltage of 20 kV and beam current of 100 nA. Rare earth element concentrations were determined by standardization with the Smithsonian Microbeam Standards (Jarosewich, 2002). Pb and Si were standardized with a Pb-silicate glass (NBS-K-456). Th was standardized using a synthetic ThO_2. The X-ray lines used were PbMα, UMβ and ThMα.

Individual spot analyses whose weight percent totals were < 98 or > 102% were discarded. Individual spot ages were calculated by iteration using the equation of Suzuki and Adachi (1991). The relative 1σ precision of U, Th, and Pb from representative spot analyses was calculated based on counting statistics following Scott and Love (1983). The 1σ error calculated for these individual spot analyses ranged from 18 to 46 Ma with a mean of 26 Ma. This mean error is considered to represent the minimum analytical error for the majority of spot analyses reported in this work and is similar to errors calculated by Montel et al. (1996). The strength of EMP dating is, however, the ability to obtain large numbers of spot analyses rapidly. Over 400 spots from 5 samples were analyzed (Table 4-2). Data was compiled into histogram format with overlapping probability density plots utilizing Isoplot version 3.0 (Ludwig, 2003) (Fig. 4-8).

Results

Four samples of pelite and one sample of granitic neosome (Fig. 4-4) were chosen to provide a complete transect across the metamorphic gradient of the western Beaverlodge Belt. Backscattered electron images of all complex grains were gathered prior to analysis to aid in selection of points for analysis.

A) Medium-grade zone

Andalusite-biotite schist (4700-6389)

This sample consists of a fine-grained muscovite-biotite-garnet schist that contains large (>1 cm) andalusite porphyroblasts. This sample does not have an S_3 fabric overprinting the dominant S_2 assemblage. Monazite grains are typically small (< 30 μm), do not contain visible zoning, and are located within the groundmass and within the andalusite pophyroblasts. The distribution of monazite ages forms a bell curve with a primary peak of ca. 1950 Ma with some evidence for a slightly older component (Fig. 4-8). This peak age is interpreted to represent the timing of peak metamorphism in this sample.

Fibrolite-biotite schist (RH98-465)

This biotite-quartz-K-feldspar schist contains nodules of fibrolite sillimanite. Monazite grains in this sample are quite small with a mean diameter of < 30 μm. The analyses from this sample form a Gaussian bell curve of monazite ages with a ca. 2.0 Ga peak (Fig. 4-8). This age is considered a good estimate for the peak of metamorphism in this sample.

B) High-grade zone

Migmatitic garnet-sillimanite-biotite pelite (RH98-378)

This sample is a migmatitic garnet-sillimanite-biotite pelite that contains M_3 overgrowths of cordierite and biotite on garnet. In addition to being the highest grade pelite studied, this unit contains some of the largest and most complex monazite crystals. The majority of grains are >60 μm in diameter and have cores with one or more overgrowths that are identifiable on BSE images (Fig. 4-9). These large monazite grains are commonly found encased within the M_1 garnet (Fig. 4-9), and likely crystallized coevally with that garnet (e.g. Foster et al., 2000; Catlos et al., 2002) during the early phase of high-grade metamorphism. The largest peak in monazite ages, and the one that we interpret to represent M_1 metamorphism, is centered at ca. 2.34 Ga. Monazites of this age have distinctively high ThO_2 contents that are commonly above 15 wt%. We interpret the younger ca. 1.9 Ga peak to represent the decompression of the early metamorphic assemblages during M_3. Older 2.4 to 2.55 Ga ages in the core of some grains may represent either a detrital component or evidence for an initial Archean metamorphism of the sediments. The inclusion of early monazites within M_1 garnet may have protected these grains from later dissolution and recrystallization during M_2 and M_3 metamorphism (e.g. Catlos et al., 2002).

Garnet-biotite pelite diatexite (RH98-698)

This sample consists of a migmatitic garnet-biotite pelite which was collected from a location that is close to RH98-378 (Fig. 4-3). The sample contains abundant M_3 cordierite overgrowths on garnet, but unlike RH98-378 has numerous fine-grained 2-3 mm thick shear zones that transect the S_1 fabric. Monazites from this sample are much smaller and have less internal complexity that those from RH98-378. No monazites

within M_1 garnet were located and only a few older core ages were recorded. The bulk of the analyses from this sample produce a peak of monazite ages at ca. 1.9 Ga (Fig. 4-8). We interpret this age peak to represent the timing of M_3 metamorphism.

Quartzofeldspathic migmatite (RH98-542)

Sample RH98-542 is composed primarily of quartz, K-feldspar, and plagioclase with less than 15% biotite, garnet, sillimanite, and cordierite. The $M_{1/2}$ assemblage in this rock is garnet-biotite-sillimanite-melt. This early assemblage is overprinted by later cordierite coeval with a late phase of melting (M_3). A sample of the late phase neosome was collected for ID-TIMS work (next section). Garnet crystals in the sample are highly resorbed and armored in the cordierite overgrowths. Monazites from this sample are up to 100 μm in diameter and display clear cores and overgrowths. The spectrum of ages from this sample indicates that the main monazite growth event occurred at ca. 1.92 Ga (Fig. 4-8). The cores of most grains recorded older ages ranging from ca. 2.55 to ca. 2.3 Ga.

U-Pb ID-TIMS Geochronology

Methodology

Samples were crushed and milled using a jaw crusher and Bico disk mill. The resulting powder was passed across a Wilfley table to obtain a separate of the dense minerals. This separate was passed through a fine 70-mesh sieve to obtain uniformly fine material. Highly magnetic particles were removed by dropping the sample in front of a high-strength magnetic field. A final separate consisting entirely of heavy minerals was ensured by flotation of the sample in the heavy liquid methyl iodide. The heavy mineral separate was then split into magnetic fractions by passing the material across a

Frantz isodynamic separator. With the aid of a binocular microscope, individual fractions of zircon, monazite, and titanite were hand picked from this separate. Some fractions were air abraded (Krogh, 1982) in order to remove zircon overgrowths, near-surface imperfections, and alteration.

All additional work on mineral fractions was performed in an ultraclean U-Pb laboratory at the University of Alberta Radiogenic Isotope Facility. All fractions were cleaned in heated nitric acid and washed repeatedly with H_2O and acetone in order to remove particles that could be adhering to grain surfaces. The cleaned fractions were weighed using a Mettler UTM-2 ultra-microbalance. Zircon and titanite fractions were loaded into pre-cleaned teflon TFE dissolution vessels, whereas monazite was loaded into pre-cleaned teflon PFA screw-top vessels. Zircon and titanite fractions were immersed in a 10:1 mixture of 48% HF:7N HNO_3 and a measured amount of ^{205}Pb-^{235}U tracer solution. Teflon capsules were placed in an oven at 215°C for five days. In order to convert the aliquots to a chloride, the open teflon capsules were placed on a hot-plate until dry. 3N HCl was added and the capsules were returned to the oven for ≥ 8 hours. Monazite fractions were immersed in 6N HCl and the ^{205}Pb-^{235}U tracer solution and placed on a hot plate for more than 3 days. Uranium and Lead were purified from fractions weighing more than 5 μg using the anion exchange chromatography methods described by Heaman et al. (2002). Two drops of H_3PO_4 acid were added to sample aliquots and then dried down in pre-cleaned beakers. Uranium and lead were loaded together onto a Re filament following the Si-gel technique of Cameron *et al.* (1969). Isotopic ratios were measured in single collector mode on a VG354 mass spectrometer using either a Faraday cup or Daly photomultiplier detector, depending on signal

strength. The 1σ errors reported in table 4-3 were calculated using an in-house program that numerically propagates all known sources of uncertainty (e.g. Ludwig, 1979). The composition of common lead in the samples was determined using the model of Stacey and Kramers (1975). Regression calculations and age uncertainties were determined using Isoplot version 3.0 (Ludwig, 2003).

Results from the medium-grade zone

Amphibolite (RH98-521)

Mafic volcanic rocks typically do not contain igneous zircon, but may contain metamorphic zircon (e.g. Fraser et al., 1997). We selected a sample of black medium-grained amphibolite to constrain the timing of metamorphism. This rock is composed of near equal parts of interlocking plagioclase and hornblende. No pyroxene is present. The heavy mineral separate contains a single population of spherical to blocky structureless zircons. The three spherical grains that were analyzed have similar U (119-197 ppm) and Pb (45-82 ppm) contents and Th/U ratios (0.368-0.414) (Table 4-3). All three analyses were concordant, or nearly so, and tightly constrain an upper intercept age of 1905 ± 3 Ma (Fig. 4-10, Table 4-3). This age is considered a good estimate for the timing of peak temperatures of metamorphism in the sample. There is no evidence for a later Proterozoic disturbance to this system.

Meta-volcanic rock (RH98-780)

This sample consists of a tremolite-plagioclase MBG meta-volcanic rock that is interlayered with amphibolite. Zircons from this sample consists entirely of clear, colourless, ovoid zircons with a diameter of 30-60 μm. All three multi-grain analyses from this sample (Table 4-3) have similar U (411-628 ppm) and Pb (134-213 ppm)

contents, and Th/U ratios (0.140-0.177). The 1901 ± 5 Ma upper intercept age for this sample is considered a good constraint on the timing of peak metamorphic temperatures in the sample (Fig. 4-10, Table 4-3).

Meta-basalt (4700-4541)

This sample consists of fine-grained amphibolite from the medium-grade western portion of the Beaverlodge Belt. Titanite in this sample ranges from clear and nearly colourless to slightly cloudy and yellow. The two analyses of yellow titanite have higher uranium values and are less discordant than the analysis of colourless titanite (Table 4-3). The 1911 ± 10 Ma upper intercept age for this sample is considered to represent a significant period of metamorphism that led to the growth of titanite (Fig. 4-11). There is no evidence for later Proterozoic disturbance in this sample.

Results from the high-grade zone

Cordierite-bearing granite neosome (RH98-543)

Sample RH98-543 was taken from a two-meter wide zone of granite neosome that contains large (>1cm) cordierite porphyroblasts that are aligned parallel to the axial plane of an open F_3 fold (Fig. 4-6e). This M_3 neosome crosscuts an earlier M_1 garnet-biotite-sillimanite migmatite layering. This neosome was, therefore, selected to constrain better the timing of both M_1 and M_3 metamorphism. The quartzofeldspathic gneiss (RH98-542) described in the chemical dating section of this paper is the host rock to this granite neosome. The neosome sample is primarily composed of K-feldspar, quartz and cordierite. Trace amounts of garnet, sillimanite and biotite are also present, but these minerals are highly resorbed. Spherical zircon, prismatic zircon, and spherical monazite all occur in this sample. Since zircon with a spherical morphology is

commonly metamorphic (Kroner et al., 2000, Corfu et al., 2003), 15 of these grains were mounted in epoxy and a series of BSE images were produced. These spheroid grains appear to have three predominant zircon growth components. The core of many grains show some form of oscilatory zoning (Fig. 4-12a-d). These cores represent the oldest component of the sample. A structureless overgrowth appears to be the second oldest and the most volumetrically important zircon component. The intergrowth of monazite with this second phase may indicate their coeval crystallization (Fig. 4-12 a,d). The final zircon growth phase consists of prominent ~5 μm wide overgrowths on the grains (Fig. 4-12 a-d).

The 12 analyses from this sample include 4 single monazite grains (Nos. 1-4), 1 prismatic zircon (No. 7), and 7 of spherical zircons. Monazites 1, 2 and 3 are slightly discordant with variable $^{207}Pb/^{206}Pb$ ages between 1906 and 1980 Ma (Table 4-3). These ages are consistent with the chemical monazite dating from this sample that displayed a large age peak at ca. 1920 Ma. The spheroidal zircon grains, on the other hand, appear to be dominated by a component that has an age similar to the 2550-2300 Ma EMP ages from monazite cores in the host rock (Fig. 4-8, RH98-542). These spherical grains have a relatively high U content (819-2207 ppm) and an extremely low Th/U ratio (0.032-0.085) (Table 4-3). This Th/U ratio is an order of magnitude lower than the igneous and detrital zircons in the region (Chapters 2 and 3), and is consistent with a predominantly metamorphic origin for these grains. One possible interpretation is that the structureless core grew during early ca. 2.3 Ga (M_1) metamorphism, whereas the rims formed during ca. 1.9 Ma (M_3) metamorphism.

U-Pb LA-MC-ICP-MS Geochronology

Methodology

In order to test the hypothesis that sample RH98-543 experienced two episodes of metamorphism, additional zircon grains were mounted in epoxy and dated by laser ablation Multicollector Inductively Coupled Plasma Source Mass Spectrometry (LA-MC-ICPMS). LA-MC-ICPMS geochronology enables the dating of individual zones within zircon, an important factor when dealing with complex growth histories (Horstwood et al., 2003). The Nu Plasma MC-ICPMS utilized in this study has three ion multipliers which enabled simultaneous collection of ^{207}Pb, ^{206}Pb and ^{204}Pb. ^{235}U, ^{238}U and ^{203}Tl were determined on Faraday collectors. A New Wave Research 213 nanometer laser unit was employed to ablate selected spots on zircon grains mounted in epoxy. Because the U content (2200-800 ppm) of the spherical zircons in sample RH98-543 was extremely high (Table 4-3), small spot sizes of 20 μm were analyzed in order to reduce the signal strength. One ratio was collected per second, for a total dwell time of 30 seconds at each spot. Measured ratios were corrected for machine drift by bracketing analyses with a known standard. The lower U content (300 ppm) for the in-house 1830 Ma zircon standard required the use of larger (30 μm) laser spot sizes for these grains. This spot size yielded an external reproducibility (2σ) of 2 to 3% for $^{207}Pb/^{206}Pb$ (~ ±35 Ma) and 3-6% for $^{206}Pb/^{238}U$. Due to the poor precision of ^{235}U measurement by MC-ICPMS, reported $^{207}Pb/^{235}U$ ratios (Table 4-4) are calculated from $^{207}Pb/^{206}Pb$ and $^{206}Pb/^{238}U$ values. Individual spot ages (Table 4-4) were calculated with Isoplot version 3.0 (Ludwig, 2003) using a lower intercept of 0 Ma. Additional details

regarding operations of the LA-MC-ICPMS facility at the University of Alberta are given by Simonetti et al. (2004).

Results for the cordierite-bearing granite neosome (RH98-543)

The analyses were primarily restricted to the large cores of grains where little or no lead loss is expected and $^{207}Pb/^{206}Pb$ ages are expected to be robust. Tera-Wasserburg (Tera and Wasserburg, 1972) and age histogram plots of the data (Fig. 4-13) indicate that the majority of zircon in this sample crystallized ca. 2.3 Ga. Mixing of components of different ages may, however, make interpretation of these U-Pb data difficult. All individual analyses were examined for $^{207}Pb/^{206}Pb$ variation during ablation. At spots where variation was significant, ratios that appeared to represent a single growth zone were preferentially selected from the data set (e.g. Fig 4-14). At some of these spots it was possible to calculate two ages based on depth of analysis (Fig. 4-14). Two main types of grains were analyzed; spherical grains 60 to 100 μm in diameter, and prismatic grains that are 100-200 μm in length (Fig. 4-15). The prismatic grains have lower U and Pb contents, similar to that found in the ID-TIMS work (Table 4-3, No. 7), and consistently gave ages of ca. 2.3 Ga (Fig. 4-15, spots 13, 16, 17, and 20). The three main components of the spherical zircons that are described in the ID-TIMS section were identified and analyzed. The inner prismatic cores gave mixed, $\geq$2.4 Ga ages (Fig. 4-15, spots 11, 28, 35; Fig. 4-14, spot 12). Mixed U-Pb ages from the cores of zircon in high-grade metamorphic rocks are consistent with re-setting and partial recrystallization of protolith zircon (Hoskin and Black, 2000). Spots from the massive core (spots 3, 5, 34 and 36), and those that only slightly overlap the prismatic

core yielded relatively stable $^{207}Pb/^{206}Pb$ ratios corresponding to ages in the range of ca. 2.3 Ga (Fig. 4-14, spot 6). This massive zircon is interpreted to be related to high-grade (M_1) metamorphism of the host rock at ca. 2.3 Ga. The source of zirconium for this ca. 2.3 Ga metamorphic zircon growth may be dissolution of the older ocillatory zoned cores that have a probable Archean age. The ca. 2.3 Ga prismatic low-U zircon, on the other hand, likely represents a migmatitic injection into the host rock that is coeval with high-grade metamorphism.

The outer rims of the spherical grains were not specifically targeted because of their relatively small size. Several spots from these rims were analyzed, however, and yielded ca. 1.9 Ga ages (e.g. Fig. 4-14, spot 21 and 22). The ca. 1.9 Ga age for this metamorphic zircon overgrowth is identical to chemical (Fig. 4-8) and ID-TIMS (Fig. 4-11) ages for monazite in this sample. The 1.9 Ga age for these zircon overgrowths likely records the M_3 decompression reaction (Fraser et al., 1997; Degeling et al., 2001) of garnet + sillimanite + quartz → cordierite + zircon.

Discussion

Ca 2.3 Ga plutonism, metamorphism and post-collisional uplift

The complex Proterozoic magmatic, deformational and metamorphic history of the Uranium City area is summarized in table 4-1. The presence of widespread ca. 2.3 Ga metamorphism and plutonism along the western margin of the Churchill craton has been attributed to subduction and collision related to the Blezardian Orogeny (Chapter 3). Ca. 2.3 Ga plutonism related to this orogeny is widespread in the study area. In-situ analysis of monazites by EMP (Fig. 4-8) and zircon by LA-ICP-MS indicates ca. 2.3 Ga metamorphism occurred within the high-grade zone along the eastern margin of the

study area. M_1 metamorphism appears to be coeval with the development of the S_1 fabric present in migmatites in this area. The fact that the 2297 ± 10 Ma Hayter Bay Granite (Chapter 3) appears to grade into an injection migmatite of the surrounding host rocks of the high-grade zone (Fig. 4-3) supports the interpretation that ca. 2.3 Ga is a time of crustal melting. A $\geq$ 2.3 Ga deformational event is confirmed by the presence of xenoliths with a pre-existing S_1 fabric in the ca. 2.3 Ga Gunnar Granite (Fig. 4-6b).

The lack of ca. 2.3 Ga metamorphic mineral ages in the lower-grade portion of the study area may indicate that ca. 2.3 Ga metamorphism was limited to the deeper crust. The presence of fine-grained quartz-phyric dykes related to intrusion of the Gunnar Granite (Chapter 3) confirms that rocks surrounding the Mesoarchean basement must have been near surface at ca. 2.3 Ga. It seems more than coincidental that the lowest grade rocks envelop the only known inliers of Meso- to Paleoarchean basement in the region (Chapter 2, 5). A plausible explanation is that the basement acted as a stable block, around which the younger igneous and supracrustal rocks were deformed. Future detailed structural studies may be required to test the extent and nature of ca. 2.3 Ga metamorphism and deformation and to fully explore the effects of Mesoarchean basement on Paleoproterozoic metamorphism and deformation.

Ca. 2.0-1.93 Ga deformation, metamorphism, and magmatism

The timing of the initial stages of isoclinal folding and related metamorphism (D_2/M_2) within the medium-grade zone is difficult to constrain. The initial phases of deformation and metamorphism are likely coeval with the large numbers of metamorphic monazite chemical dates that extend to 2.0 Ga. Although an older ca. 2.3

Ga deformation and metamorphism of the medium-grade zone is possible, the grade of metamorphism must not have been high enough for U-bearing accessory minerals to grow. Within the high-grade zone, tight-to isoclinal-folding (F_2) also occurred, but these rocks record upper amphibolite-facies crustal conditions at that time. Ca. 2.05 Ga monazite cores were reported by Williams et al. (1999) from granulite-facies rocks in the eastern Beaverlodge Belt. Ca. 2.0-1.9 Ga deformation and metamorphism coincided with crustal melting that produced the 1.98-1.93 Ga granites highlighted in chapter 5. This timing is coeval with the intracontinental collision between the Slave and Churchill cratons to form the Taltson Magmatic Zone (e.g. Chacko et al., 2000).

1.91-1.90 Ga metamorphism, deformation and exhumation

In the medium-grade zone, F_3 folding appears to coincide with peak temperatures and the growth of metamorphic titanite, monazite and zircon. In the high-grade zone, this period of folding was coeval with crustal exhumation. The NE trending biotite-cordierite overgrowth fabric on garnet from this area indicates that retrogression of upper amphibolite- to granulite-facies rocks occurred coeval with the F_3 folding. A model involving ca. 1.9 Ga decompression is supported by the presence of ca. 1.9 Ga metamorphic zircon and monazite in a granitic neosome (RH98-543) that has an S_3 fabric defined by cordierite. In addition, ca. 1.9 Ga rims on ca. 2.05 Ga cores were recorded from monazite in the eastern Beaverlodge Belt (Williams et al., 1999). Deep crustal slices, buried and metamorphosed to upper amphibolite facies at ca. 2.3 Ga, remained deep in the crust until they were uplifted and exposed at 1.9 Ga. This is

consistent with results that indicate that deep crustal slices were exhumed all along the Snowbird tectonic zone at 1.9 Ga (Sanborn-Barrie et al., 2001; Baldwin et al., 2003).

Although magmatism in the Taltson-Thelon Magmatic Zone (McDonough et al., 2000; Chacko et al., 2000) is slightly older than the ca. 1.91-1.90 Ga U-Pb ages for M_3/D_3 recorded herein, the NE trending F_3 folding parallels this major Paleoproterozoic magmatic and deformational zone. In addition, ca. 1920 Ma metamorphic monazite and zircon have been recorded from within the Taltson-Thelon Magmatic Zone (McDonough et al., 2000). The ca. 1.9 Ga timing of D_3/M_3 exhumation in the Beaverlodge Belt is consistent, therefore, with the final phases of intracontinental collision (Hanmer et al., 1992; Chacko et al., 2000) between the Slave, Buffalo Head, and Churchill cratons, although the cause of this intracontinental deformation is debatable.

1.8-1.84 Deformation and metamorphism

The deformation and metamorphism described in this paper have not affected the ca. 1.82 Ga supracrustal rocks of the Martin Basin that unconformably overlie the Murmac Bay Group (Morelli et al., in prep.). This basin has, however, been gently folded and metamorphosed to sub-greenschist facies (Ashton et al., in prep). This last phase of deformation and metamorphism (D_4/M_4) does not, in turn, affect the upper ca. 1.66 Ga part (Rainbird et al., submitted) of the Athabasca Basin. Together, the above constraints indicate that D_4 occurred between ca. 1.66 and 1.82 Ga. Widespread ca. 1.8 Ga partial resetting of the U-Pb isotopic system in Archean zircon (Chapter 2) may be related to this event(s). The timing of D_4/M_4 therefore coincides with 1830-1810 Ma

uplift on the eastern margin of the Athabasca triangle (Mahan et al., 2003) and penultimate stages of the Trans-Hudson Orogen. Although D_4/M_4 may be related to far field effects of the Trans-Hudson Orogen, this time period also may have coincided with accretion (Hoffman, 1989) to the west of the Slave Craton.

Conclusions

The Archean Churchill craton of northern Canada has a complex history of Paleoproterozoic crustal reworking. In-situ EMP chemical dating and LA-MC-ICPMS geochronology identify ca. 2.3 Ga ages for metamorphic monazite and zircon in high-grade rocks. This metamorphic event was not readily apparent from conventional ID-TIMS whole-grain analyses. Local ca. 2.3 Ga metamorphism and deformation is just one component of widespread ca. 2.3 Ga crustal reworking related to the Blezardian Orogeny. Archean supracrustal rocks of the Beaverlodge Belt that directly overlie ca. 3.0 Ga granitoid basement remained in the upper crust throughout their evolution. These supracrustal rocks grade into upper amphibolite-to granulite facies equivalents to the east and north. Reconnaissance-style electron microprobe chemical dating of monazite from the medium-grade rocks indicates that a major metamorphism occurred at ca. 2.0 and 1.9 Ga; a result that is corroborated by ca. 1.9 Ga U-Pb ID-TIMS ages for metamorphic zircon and titanite in mafic rocks. The cause of widespread ca. 1.9 Ga metamorphism and deformation in the southern Churchill craton and along the Snowbird tectonic zone is still debatable, but the timing and orientation of structures is consistent with the final stages of intracontinental collision between the Slave, Buffalo Head, and Churchill cratons.

References

Ashton, K.E., and Card, C.C. 1998. Rae Northeast: A Reconnaissance of the Rae Province Northeast of Lake Athabasca. Saskatchewan Geological Survey Sask. Energy Mines, Misc. Rep. 98-4, pp. 3-16.

Ashton, K.E., Heaman, L.M., Lewry, J.F., Hartlaub, R.P., and Shi, R. 1999. Age and origin of the Jan Lake Complex: a glimpse at the buried Archean craton of the Trans-Hudson Orogen. Canadian Journal of Earth Sciences, **36**: 185-208.

Ashton, K.E., Hartlaub, R.P., and Card, C. in prep. Southeastern Extension of the 1825 Ma Sparrow Diabase, the Age of the Martin Group, and it's Possible Correlation with the Dubawnt Supergroup, Rae Province. Canadian Journal of Earth Sciences

Baldwin, J.A., Bowring, S.A., and Williams, M.L. 2003. Petrological and geochronological constraints on high pressure, high temperature metamorphism in the Snowbird tectonic zone, Canada. Journal of Metamorphic Geology, **21**: 81-98.

Catlos, E.J., Gilley, L.D., and Harrison, T.M. 2002. Interpretation of monazite ages obtained via in situ analysis. Chemical Geology, **188**: 193-215.

Cameron, E.M., Smith, D.E., and Walker, R.L. 1969. Mass spectrometry of nanogram sized samples of lead. Analytical Chemistry, **41**: 525-526.

Card, C.D. 2001. Geology and Tectonic Setting of the Oldman-Bulyea shear zone, northern Saskatchewan, Canada. Unpublished M.Sc. thesis, University of Regina: 188p.

Chacko, T., De, S.K., Creaser, R.A., and Muehlenbachs, K. 2000. Tectonic setting of the Taltson magmatic zone at 1.9-2.0 Ga: a granitoid-based perspective. Canadian Journal of Earth Sciences, **37**: 1597-1609.

Cherniak, D.J., Watson, E.B., Grove, M., and Harrison, T.M. 2004. Pb diffusion in monazite: A combined RBS/SIMS study. Geochimica Et Cosmochimica Acta, **68**: 829-840.

Cocherie, A., Legendre, O., Peucat, J.J., and Kouamelan, A.N. 1998. Geochronology of polygenetic monazites constrained by in situ electron microprobe Th-U total lead determination: Implications for lead behaviour in monazite. Geochimica et Cosmochimica Acta, **62**: 2475-2497.

Corfu, F., Hanchar, J.M., Hoskin, P.W.O., and Kinny, P. 2003. Atlas of zircon textures. *In* Zircon. *Edited by* J.M. Hanchar and P.W.O. Hoskin. The Mineralogical Society of America, Washington, Reviews in mineralogy and geochemistry, 53, pp. 469-500.

Degeling, H., Eggins, S., and Ellis, D.J. 2001. Zr budgets for metamorphic reactions, and the formation of zircon from garnet breakdown. Mineralogical Magazine, **65**: 749-758.

Fraser, G., Ellis, D., and Eggins, S. 1997. Zirconium abundance in granulite-facies minerals, with implications for zircon geochronology in high-grade rocks. Geology, **25**: 607-610.

Foster, G., Kinny, P., Vance, D., Prince, C., and Harris, N. 2000. The significance of monazite U-Th-Pb age data in metamorphic assemblages; a combined study of monazite and garnet chronometry. Earth and Planetary Science Letters, **181**: 327-340.

Hanmer, S., Parrish, R., Williams, M., and Kopf, C. 1994. Striding-Athabasca Mylonite Zone - Complex Archean Deep-Crustal Deformation in the East Athabasca Mylonite Triangle, Northern Saskatchewan. Canadian Journal of Earth Sciences, **31**: 1287-1300.

Hanmer, S., Williams, M., and Kopf, C. 1995. Striding-Athabasca Mylonite Zone - Implications for the Archean and Early Proterozoic Tectonics of the Western Canadian Shield. Canadian Journal of Earth Sciences, **32**: 178-196.

Hartlaub, R.P., and Ashton, K.E. 1998. Geological investigations of the Murmac Bay group, Lake Athabasca north shore transect. Saskatchewan Geological Survey, Sask. Energy Mines, Misc. Rep. 98-4, 17-28.

Heaman, L.M., Erdmer, P., and Owen, J.V. 2002. U-Pb geochronologic constraints on the crustal evolution of the Long Range Inlier, Newfoundland. Canadian Journal of Earth Sciences, **39**: 845-865.

Hoffman, P.F. 1988. United Plates of America, the Birth of a Craton - Early Proterozoic Assembly and Growth of Laurentia. Annual Review of Earth and Planetary Sciences, **16**: 543-603.

Hoffman, P.E. 1989. Precambrian Geology and tectonic history of North America. *In* The Geology of North America - An Overview. *Edited by* A.W. Bally and A.R. Palmer. Geological Society of America, Boulder, Colorado, Decade of North American Geology, Summary Volume A, pp. 447-512.

Horstwood, M.S.A., Foster, G.L., Parrish, R.R., Noble, S.R., and Nowell, G.M. 2003. Common-Pb corrected in situ U-Pb accessory mineral geochronology by LA-MC-ICP-MS. Journal of Analytical Atomic Spectrometry, **18**: 837-846.

Hoskin, P.W.O., and Black, L.P. 2000. Metamorphic zircon formation by solid-state recrystallization of protolith igneous zircon. Journal of Metamorphic Geology, **18**: 423-439.

Jackson, G.D., Hunt, P.A., Loveridge, W.D., Parrish, R.R., 1990. Reconnaissance geochronology of Baffin Island, N.W.T.. Geol. Surv. Can., Pap. 89-2, 123-148.

Jarosewich, E. 2002. Smithsonian Microbeam Standards. Journal of Research of the National Institute of Standards and Technology, **107**: 681-685.

Kopf, C.F. 2002. Archean and early Proterozoic events along the snowbird Tectonic Zone in northern Saskatchewan, Canada. Gondwana Research, **5**: 79-83.

Krogh, T.E. 1982. Improved accuracy of U-Pb zircon ages by the creation of more concordant systems using an air abrasion technique. Geochim. Cosmochim. Acta, **46**: 637-649.

Kroner, A., O'Brien, P.J., Nemchin, A.A., and Pidgeon, R.T. 2000. Zircon ages for high pressure granulites from South Bohemia, Czech Republic, and their connection to Carboniferous high temperature processes. Contributions to Mineralogy and Petrology, **138**: 127-142.

Lewry, J.F. and Collerson, K.D. 1990. The Trans-Hudson Orogen: Extent, subdivision, and problems; *in* Lewry, J.F. and Stauffer M.R. (eds.), The Early Proterozoic Trans-Hudson Orogen of North America. Geological Association of Canada, Spec. Pap. 37, pp. 1-14.

Ludwig, K.R. 1980. Calculation of Uncertainties of U-Pb Isotope Data. Earth and Planetary Science Letters, **46**: 212-220.

Ludwig, K.R., 2003. Isoplot/Ex, a geochronological toolkit for microsoft excel, Version 3.0. Berkely, California, Berkely Geochronology Center Special Publication 4.

Mahan, K.H., Williams, M.L., and Baldwin, J.A. 2003. Contractional uplift of deep crustal rocks along the Legs Lake shear zone, western Churchill Province, Canadian Shield. Canadian Journal of Earth Sciences, **40**: 1085-1110.

McDonough, M.R., McNicoll, V.J., Schetselaar, E.M., and Grover, T.W. 2000. Geochronological and kinematic constraints on crustal shortening and escape in a two-sided oblique-slip collisional and magmatic orogen, Paleoproterozoic Taltson magmatic zone, northeastern Alberta. Canadian Journal of Earth Sciences, **37**: 1549-1573.

Mezger, K., Rawnsley, C.M., Bohlen, S.R., and Hanson, G.N. 1991. U-Pb Garnet, Sphene, Monazite, and Rutile Ages - Implications for the Duration of High-Grade Metamorphism and Cooling Histories, Adirondack Mts, New-York. Journal of Geology, **99**: 415-428.

Montel, J.M., Foret, S., Veschambre, M., Nicollet, C., and Provost, A. 1996. Electron microprobe dating of monazite. Chemical Geology, **131**: 37-53.

Morelli, R.M., Ansdell, K.M., Ashton, K.E., and Hartlaub, R.P. in prep. Geochemical discrimination and source characteristics of subalkaline and alkaline basaltic rocks from

the Paleoproterozoic Martin Group, Beaverlodge Domain, Rae Province. Canadian Journal of Earth Sciences

Parrish, R.R. 1990. U-Pb dating of monazite and its application to geological problems. Canadian Journal of Earth Sciences, **27**: 1431-1450.

Pattison, D.R.M. 2001. Instability of Al_2SiO_5 "triple-point" assemblages in muscovite+biotite+quartz-bearing metapelites, with implications. American Mineralogist, **86**: 1414-1422.

Pattison, D.R.M., Spear, F.S., and Cheney, J.T. 1999. Polymetamorphic origin of muscovite plus cordierite plus staurolite plus biotite assemblages: implications for the metapelitic petrogenetic grid and for P-T paths. Journal of Metamorphic Geology, **17**: 685-703

Pereira, M.D., and Bea, F. 1994. Cordierite-Producing Reactions in the Pena-Negra Complex, Avila Batholith, Central Spain - the Key Role of Cordierite in Low-Pressure Anatexis. Canadian Mineralogist, **32**: 763-780.

Sanborn-Barrie, M., Carr, S.D., and Theriault, R. 2001. Geochronological constraints on metamorphism, magmatism and exhumation of deep-crustal rocks of the Kramanituar Complex, with implications for the Paleoproterozoic evolution of the Archean western Churchill Province, Canada. Contributions to Mineralogy and Petrology, **141**: 592-612.

Scott, D.J. 1999. U-Pb geochronology of the eastern Hall Peninsula, southern Baffin Island, Canada: a northern link between the Archean of West Greenland and the Paleoproterozoic Torngat Orogen of northern Labrador. Precambrian Research, **93**: 5-26.

Scott, V.D., and Love, G. 1983. Quantitative Electron-Probe Microanalysis. Ellis Horwood Limited, Chichester, West Sussex.

Skulski, T., Sandeman, H.A., Sanborn-Barrie, M., MacHattie, T., Hyde, D., Johnstone, S., Panagapko, D., Byrne, D., 2002. Contrasting crustal domains in the Committee Bay Belt, Walker Lake-Arrowsmith River area, central Nunavut. Geological Survey of Canada, Current Res. 2002-C11.

Simonetti, A., Heaman, L.M., Creaser, R. and Hartlaub, R.P. 2004. U-Pb dating of detrital zircons by multiple ion counting LA-MC-ICP-MS. Goldschmidt Conference, Copenhagen.

Spear, F.S. 1995. Metamorphic Phase Equilibria and Pressure-Temperature-Time Paths, Mineralogical Society of America, Washington, D. C., 799 p.

Suzuki, K., and Adachi, M. 1991. Precambrian Provenance and Silurian Metamorphism of the Tsubonosawa Paragneiss in the South Kitakami Terrane, Northeast Japan,

Revealed by the Chemical Th-U-Total Pb Isochron Ages of Monazite, Zircon and Xenotime. Geochemical Journal, **25**: 357-376.

Stacey, J.S., Kramers, J.D. 1975. Approximation of terrestrial lead isotope evolution by a two-stage model. Earth Planet. Sci. Letters, **26**: 207-221.

Tera, F., and Wasserburg, J. 1972. U-Th-Pb Systematics in 3 Apollo 14 Basalts and Problem of Initial Pb in Lunar Rocks. Earth and Planetary Science Letters, **14**: 281-304.

Wheeler, J.O., Hoffman, P.F., Card, C.K., Davidson, A., Sanford, B.V., Okulitch, A.V., and Roest, W.R., 1996. Geological Map of Canada. Geological Survey of Canada, scale 1:5,000,000.

Williams, M.L., Jercinovic, M.J., and Terry, M.P. 1999. Age mapping and dating of monazite on the electron microprobe: Deconvoluting multistage tectonic histories. Geology, **27**: 1023-1026.

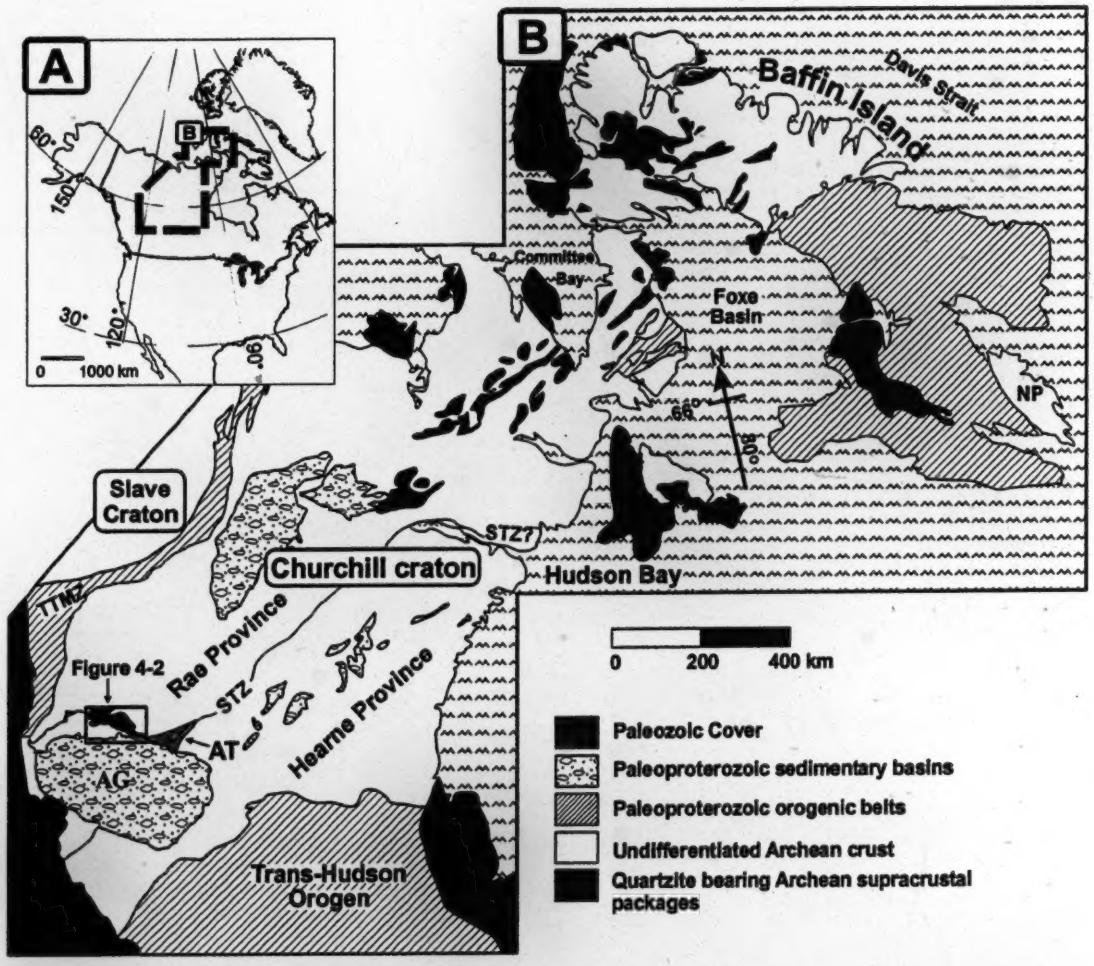

Figure 4-1. (A) Map of North America with the area of figure B indicated by a dashed box. (B) General geology of the Churchill craton and bounding tectonic entities. Quartzite-bearing greenstone sequences are highlighted in black (Modified after Jackson et al., 1990; Wheeler et al., 1996; Scott, 1999; and Skulski et al. 2002). The Beaverlodge Belt (Fig. 4-2) is highlighted on the north shore of Lake Athabasca. AG, Athabasca Group; AT, East Athabasca triangle, NP, Nain Province; STZ, Snowbird tectonic zone; TTMZ, Taltson-Thelon Magmatic Zone.

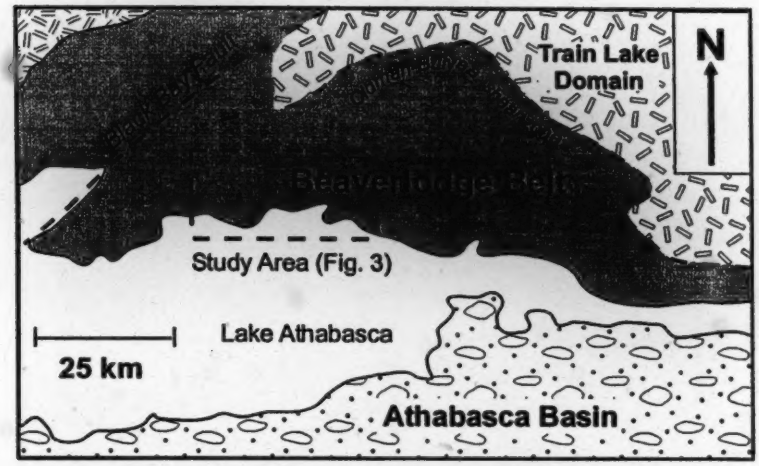

Figure 4-2. Geological map of the Beaverlodge Belt on the north shore of Lake Athabasca, Saskatchewan.

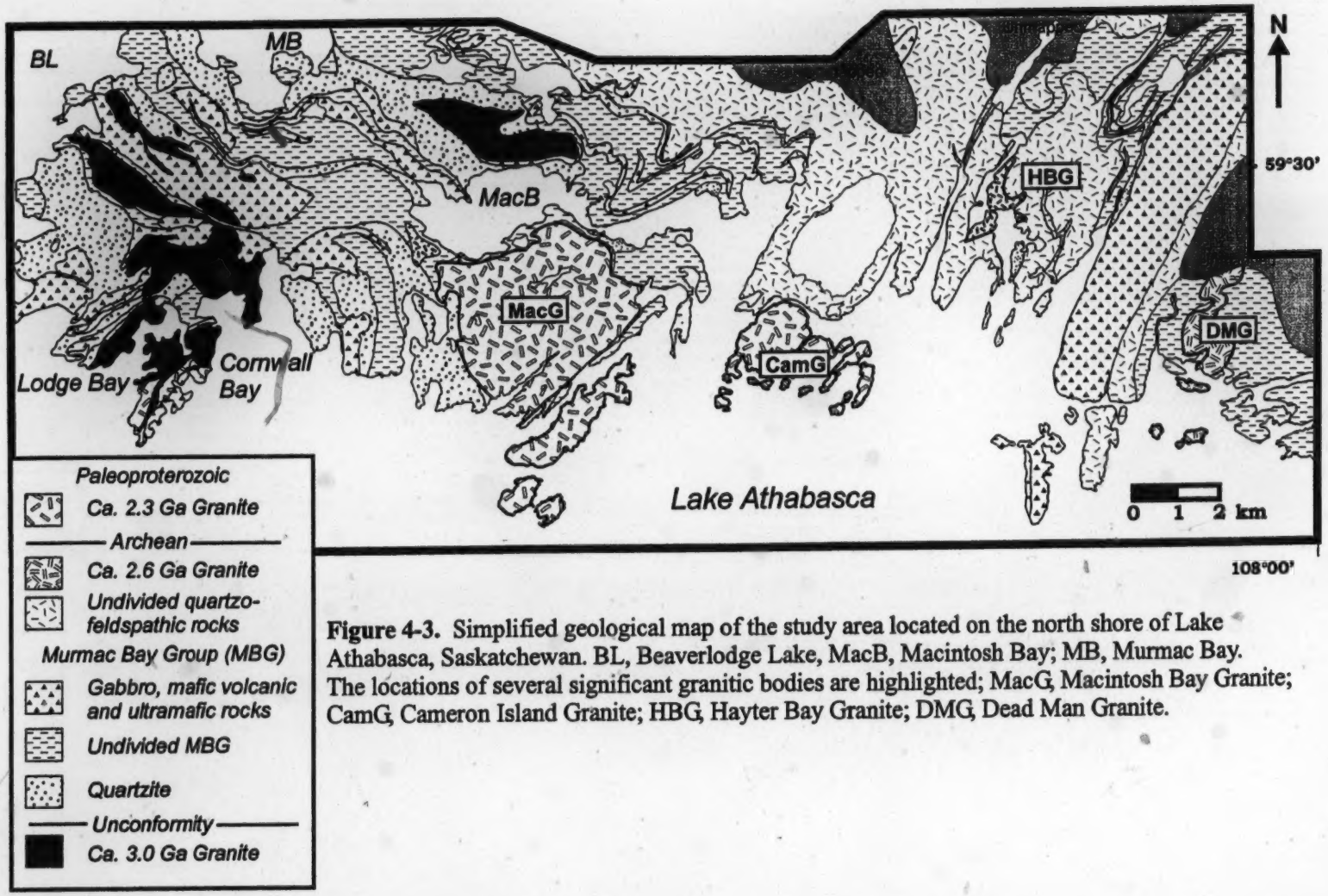

Figure 4-3. Simplified geological map of the study area located on the north shore of Lake Athabasca, Saskatchewan. BL, Beaverlodge Lake, MacB, Macintosh Bay; MB, Murmac Bay. The locations of several significant granitic bodies are highlighted; MacG, Macintosh Bay Granite; CamG, Cameron Island Granite; HBG, Hayter Bay Granite; DMG, Dead Man Granite.

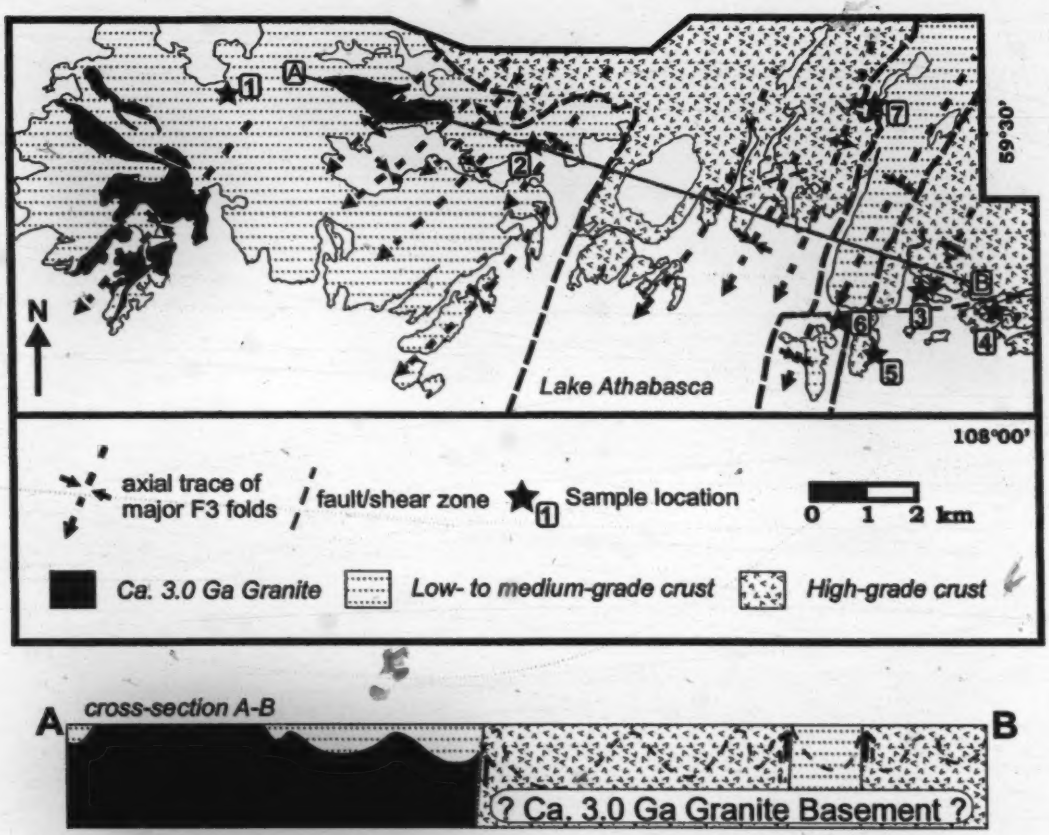

Figure 4-4. Metamorphic zonation map and cross-section sketch of the study area. Chemical and isotope geochronology sample locations include S-1, Andalusite-biotite schist (4700-6389); S-2, Fibrolite-biotite schist (RH98-465); S-3, Migmatitic garnet-sillimanite-biotite pelite (RH98-378); S-4, Garnet-biotite pelite diatexite (RH98-698); S-5, Cordierite-bearing granite neosome (RH98-543) and quartzofeldspathic migmatite (RH98-542); S-6, Amphibolite (RH98-521); S-7,Meta-volcanic (RH98-780). Cross-section displays 2X vertical exaggeration. Dark dashed lines represent foliation trends across the area.

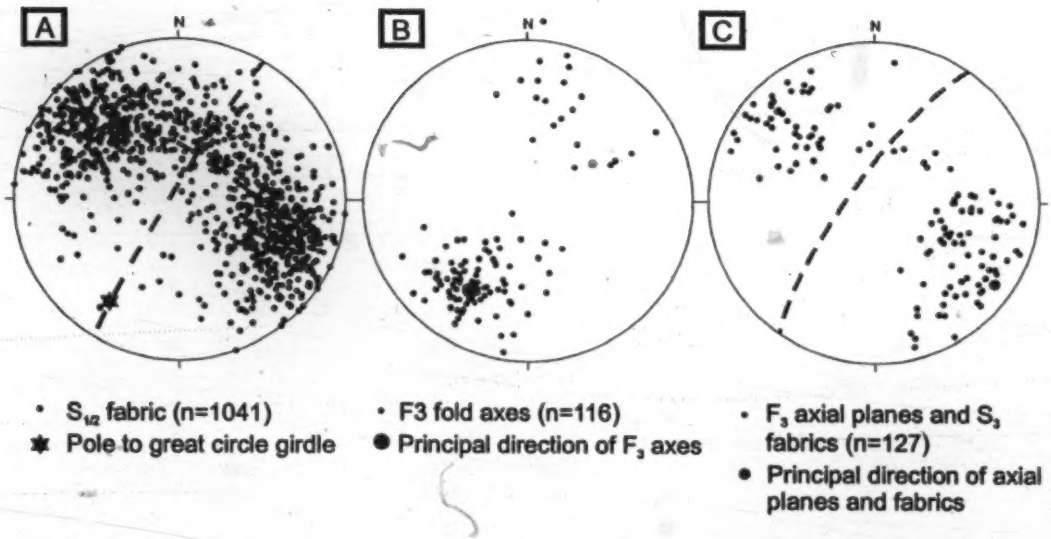

Figure 4-5. Lower hemisphere equal area stereographic projections of structural data from the area in figure 4-3: (A) Orientation of $S_{1/2}$ fabrics; (B) Measured F_3 fold axes; (C) Measured F_3 axial planes and S_3 fabrics. Plots were derived using Stereonett (Version 2.46) with principal directions and best fit girdles determined by eigenvector analysis.

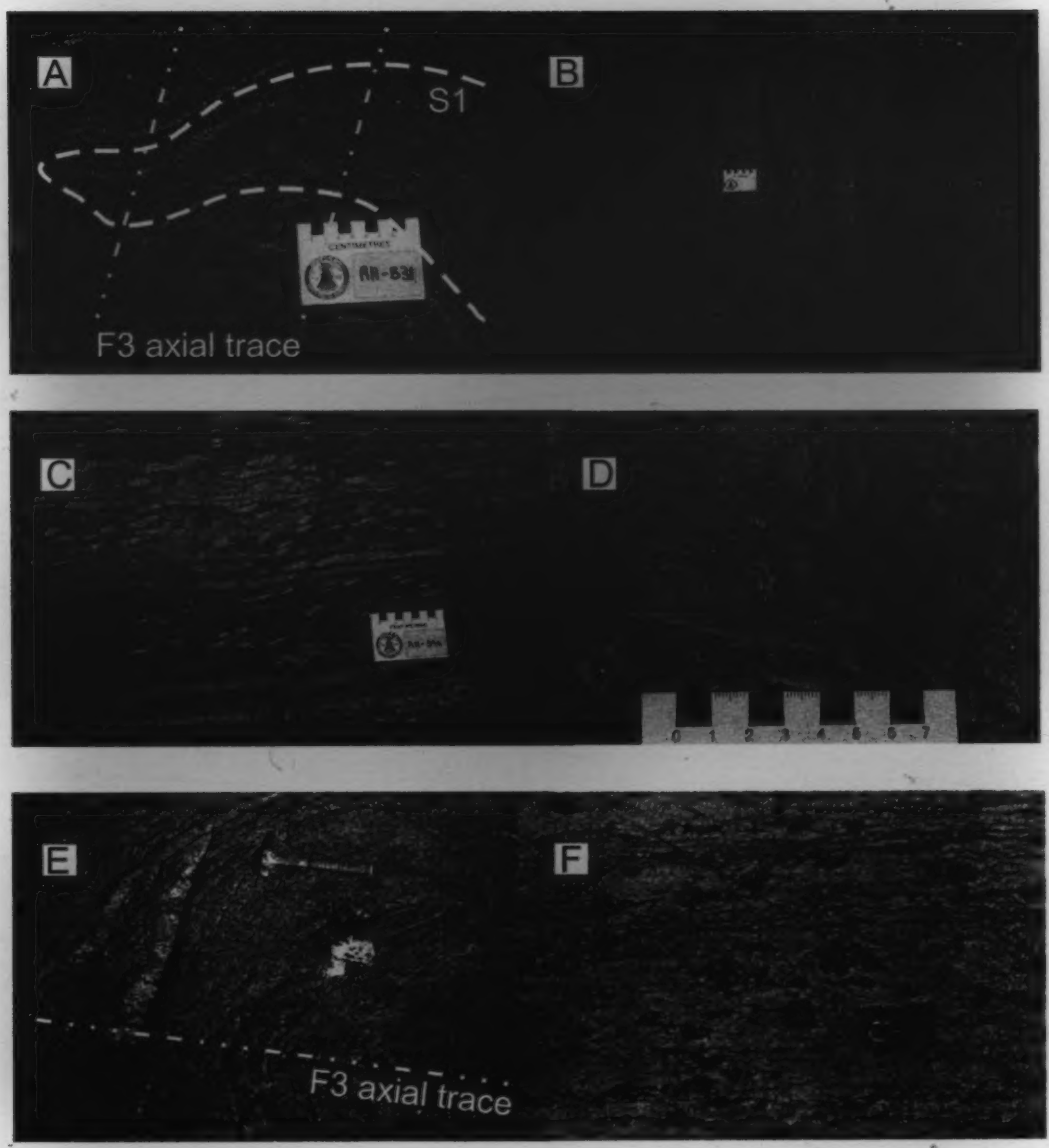

Figure 4-6. (A) Migmatite layering in a psammopelite which is deformed by a tight F_2 fold. This fold is, in turn, deformed by open F_3 folds. (B) Xenoliths of strongly foliated quartzofeldspathic gneiss within the ca. 2.3 Ga Gunnar Granite. (C) Quartz-sillimanite nodules that define a S_3 fabric which overprints the earlier S_2 fabric. (D) S_3 quartz-sillimanite nodules overprinting S_2 at the nose of a major F_3 fold. (E) Cordierite-bearing granite neosome which overprints the S_1 migmatite in a quartzofeldspathic rock. Cordierite in the late melt patches are axial planar to the open F_3 fold. (F) Biotite-cordierite overgrowths on garnet from the eastern margin of the study area. These overgrowths define a NE trending fabric that is parallel to the axial planes of F_3 folds.

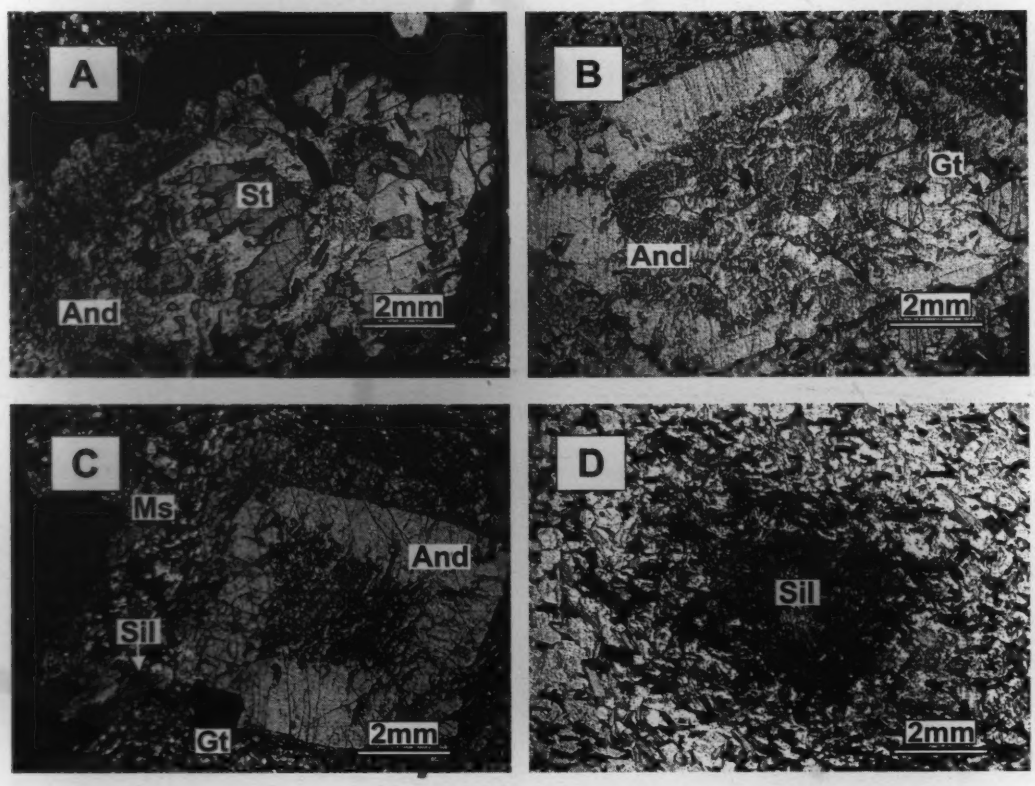

Figure 4-7. (A) Partial replacement of M_2 staurolite (St) by andalusite (And) in a low grade pelite from the western margin of the study area. XPL view. (B) M_2 assemblage of andalusite-garnet (Gt)-biotite. PPL view. (C) Partial replacement of (M_2) andalusite and garnet by later (M_3) muscovite (Ms) and sillimanite (Sil). XPL view. (D) M_3 intergrowth of fibrolite-sillimanite and quartz from a psammitic rock. PPL view.

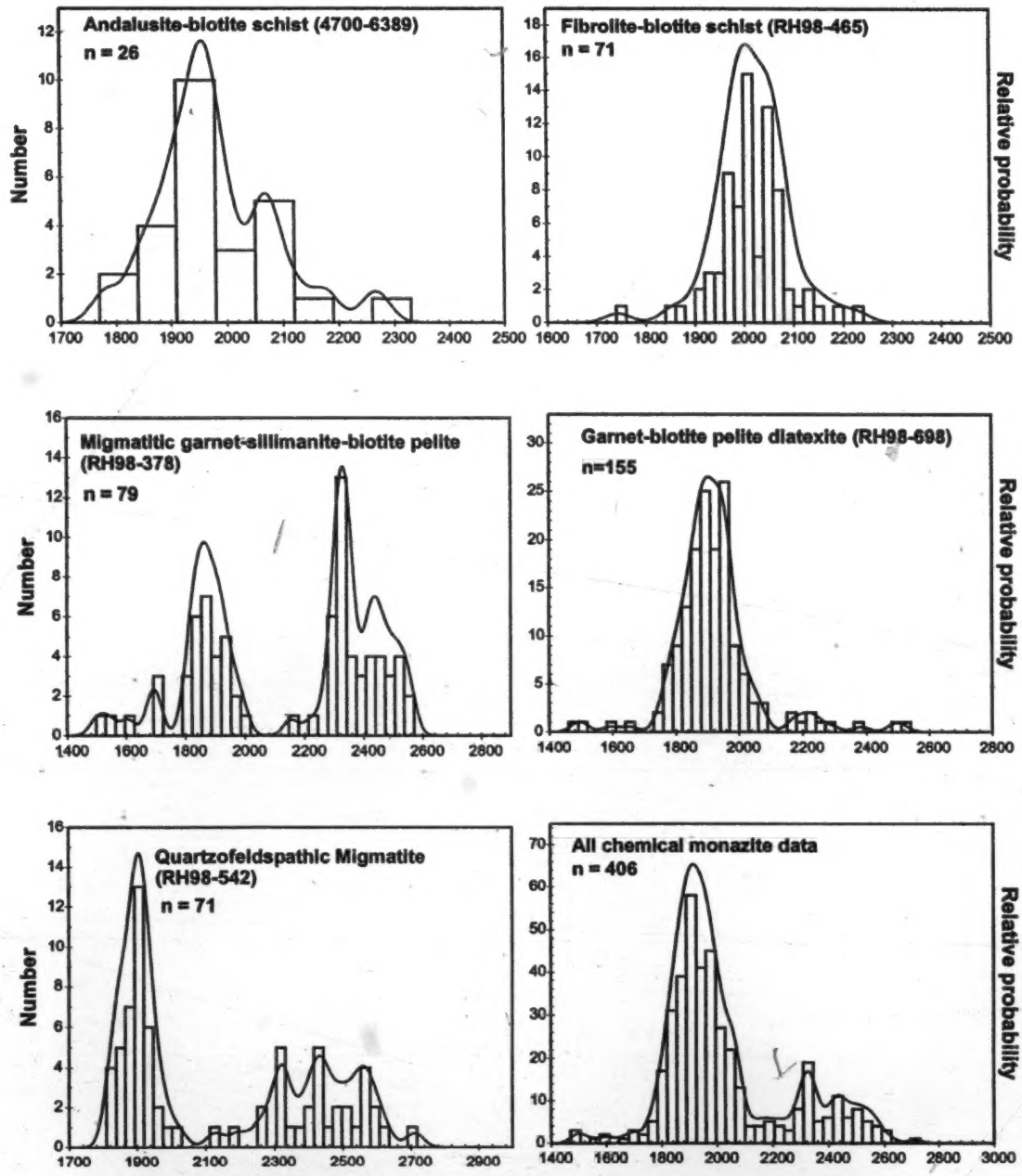

Figure 4-8. Chemical monazite ages from 5 samples compiled into histogram format with overlapping probability density plots. Plots were prepared utilizing Isoplot version 3.0 (Ludwig, 2003).

Figure 4-9. Backscatter electron images of monazite from migmatitic garnet-sillimanite-biotite pelite (RH98-378). The left image displays monazite encased with M1 garnet, whereas the right image displays a complexly zoned grain with an older core and younger rim.

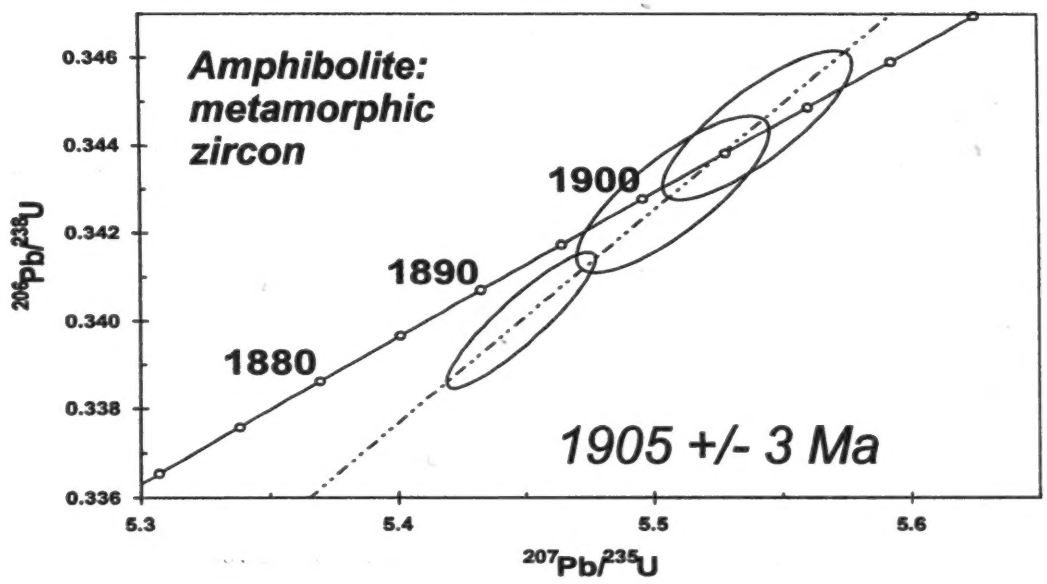

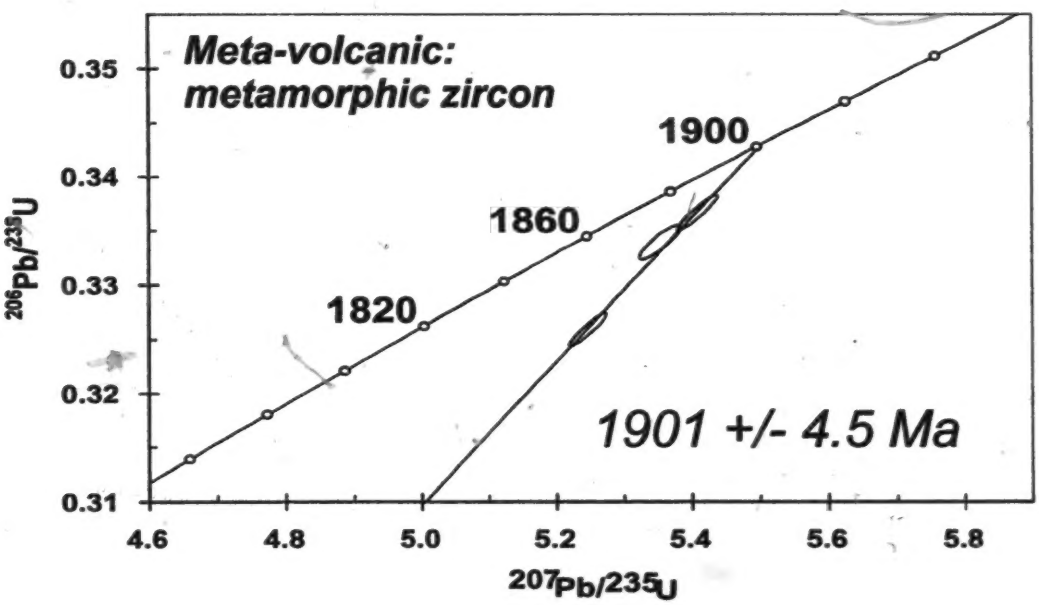

Figure 4-10. Concordia plots of metamorphic zircon from amphibolite (RH98-521, top) and meta-volcanic rock (RH98-780, bottom).

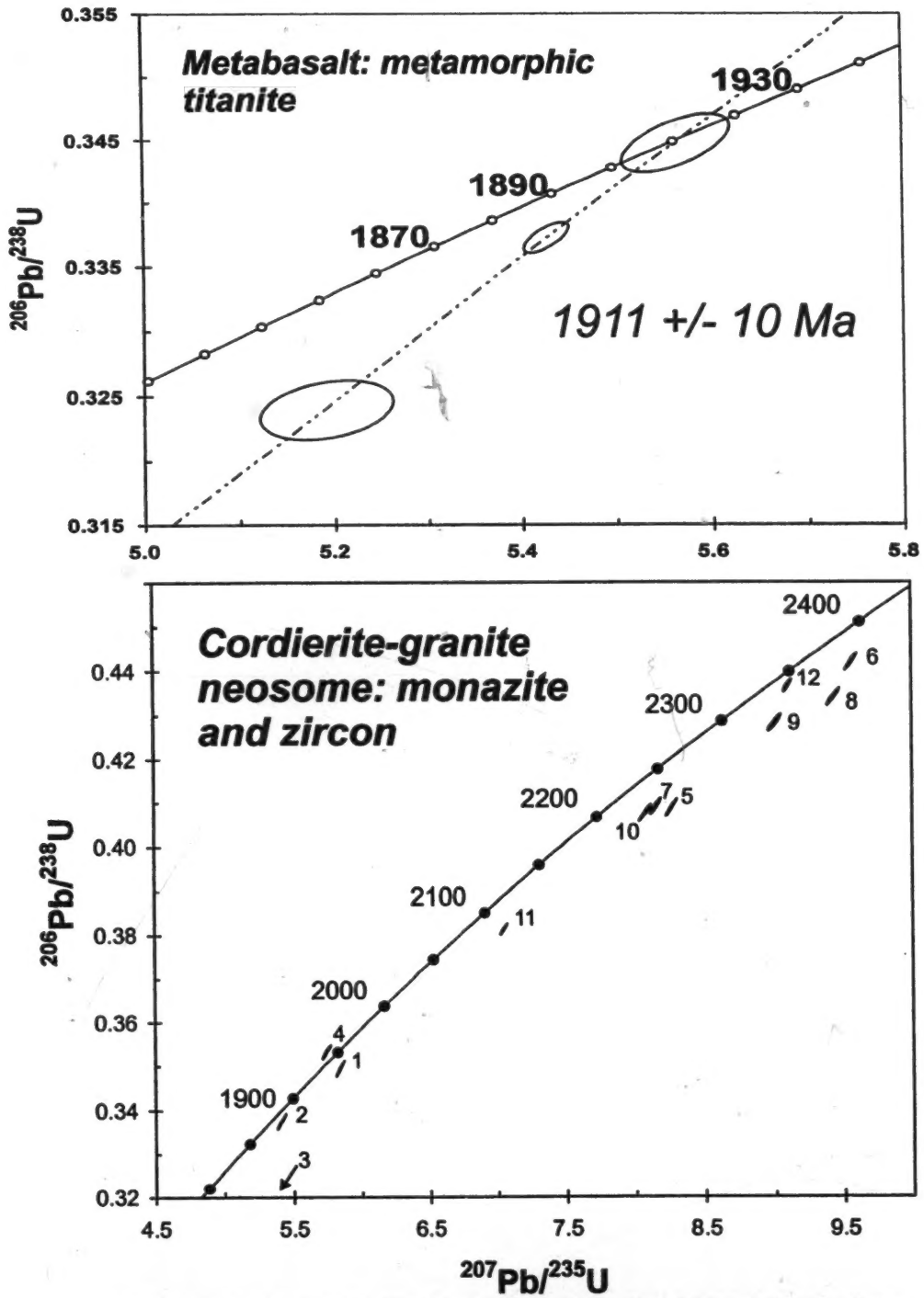

Figure 4-11. (Top) Concordia plot of metamorphic titanite from lower amphibolite-facies meta-basalt (4700-4541). (Bottom) Concordia plot of monazite and zircon from a cordierite-bearing granite neosome (RH98-543). Analyses 1-4 are monazite crystals. See text for a detailed description.

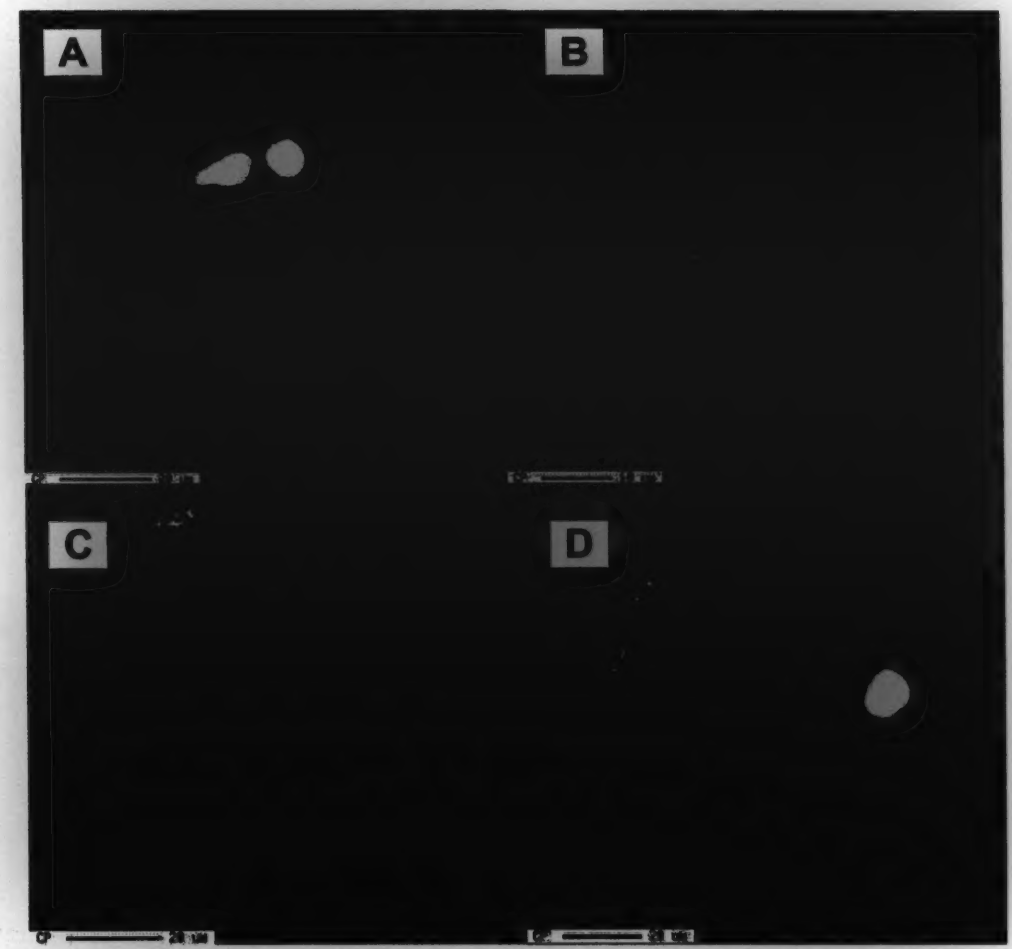

Figure 4-12. Backscatter electron images of selected metamorphic zircon crystals from a cordierite-bearing granite neosome (RH98-543). An early oscillatory zoned (xenocrystic?) component of zircon is seen in A, B and D. The volumetrically dominant component of the grains is massive zircon that is locally intergrown with white crystals of monazite (A and D). The massive cores are rimmed with younger altered zircon.

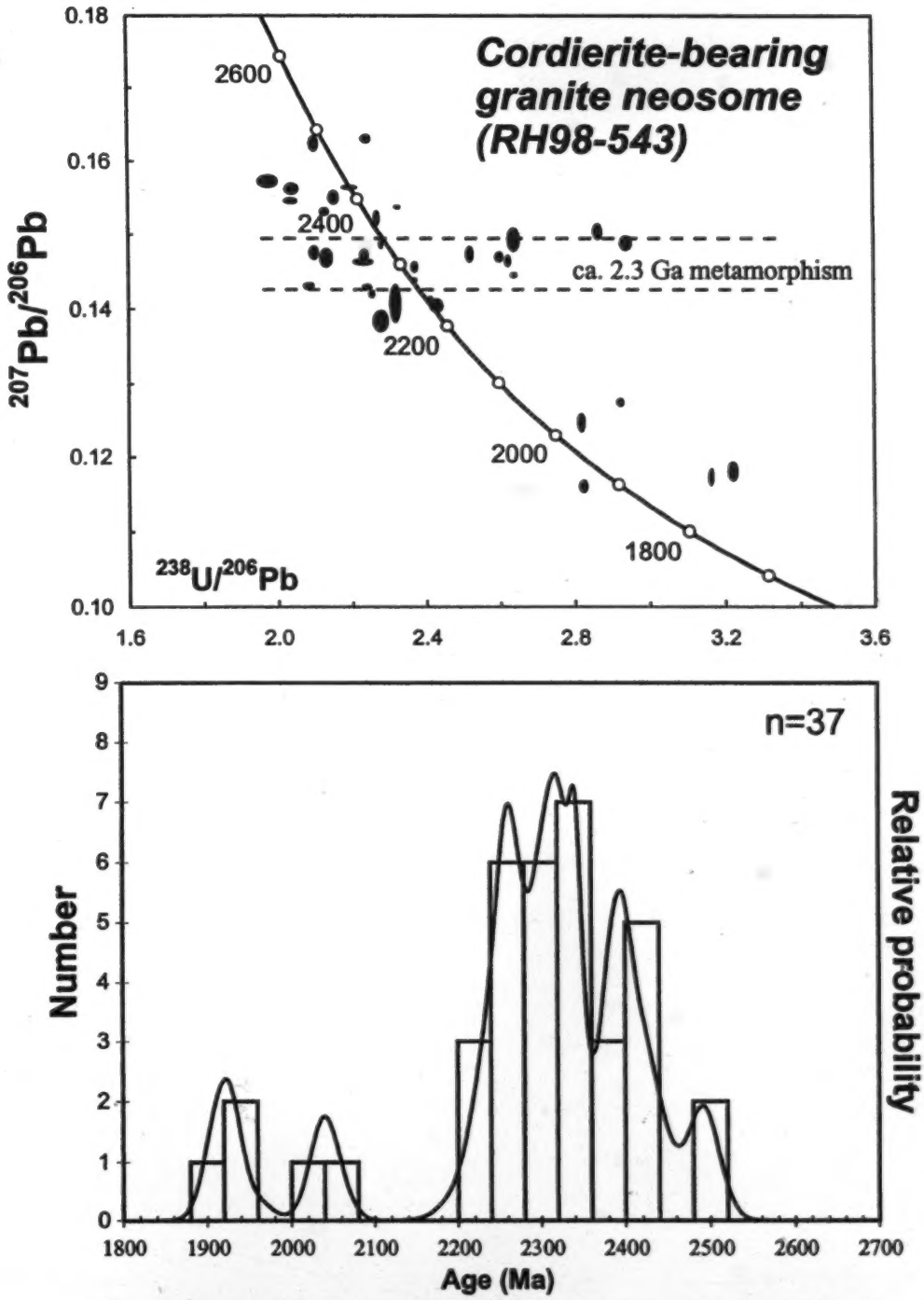

Figure 4-13. (Top) Tera-Wasserburg plot of zircon data from cordierite-bearing granite neosome. **(Bottom)** Age spot data from this sample compiled into histogram format with an overlapping relative probability distribution. The peak of age analyses spans a 100 Ma period, from 2250 to 2350 Ma.

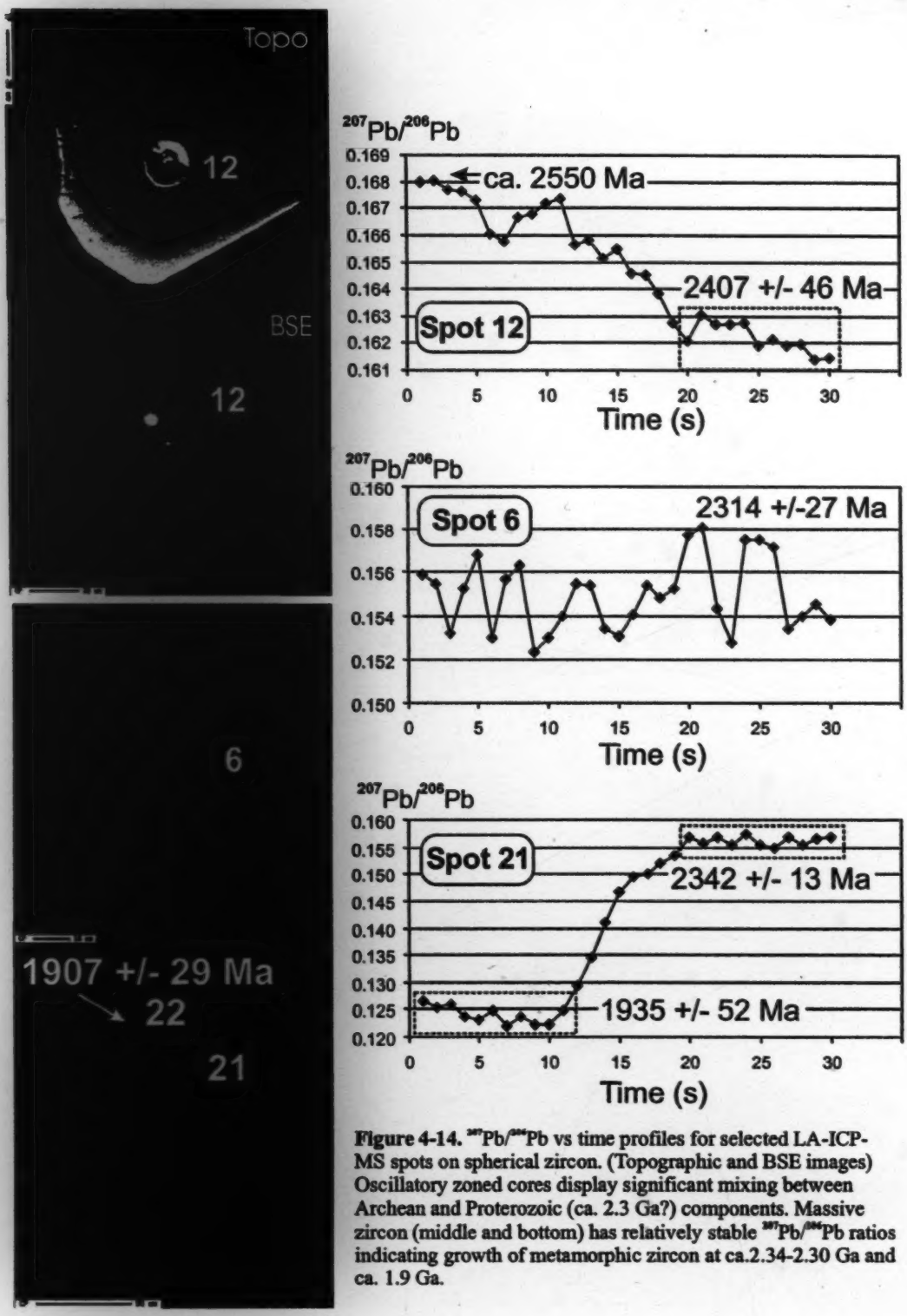

Figure 4-14. $^{207}Pb/^{206}Pb$ vs time profiles for selected LA-ICP-MS spots on spherical zircon. (Topographic and BSE images) Oscillatory zoned cores display significant mixing between Archean and Proterozoic (ca. 2.3 Ga?) components. Massive zircon (middle and bottom) has relatively stable $^{207}Pb/^{206}Pb$ ratios indicating growth of metamorphic zircon at ca.2.34-2.30 Ga and ca. 1.9 Ga.

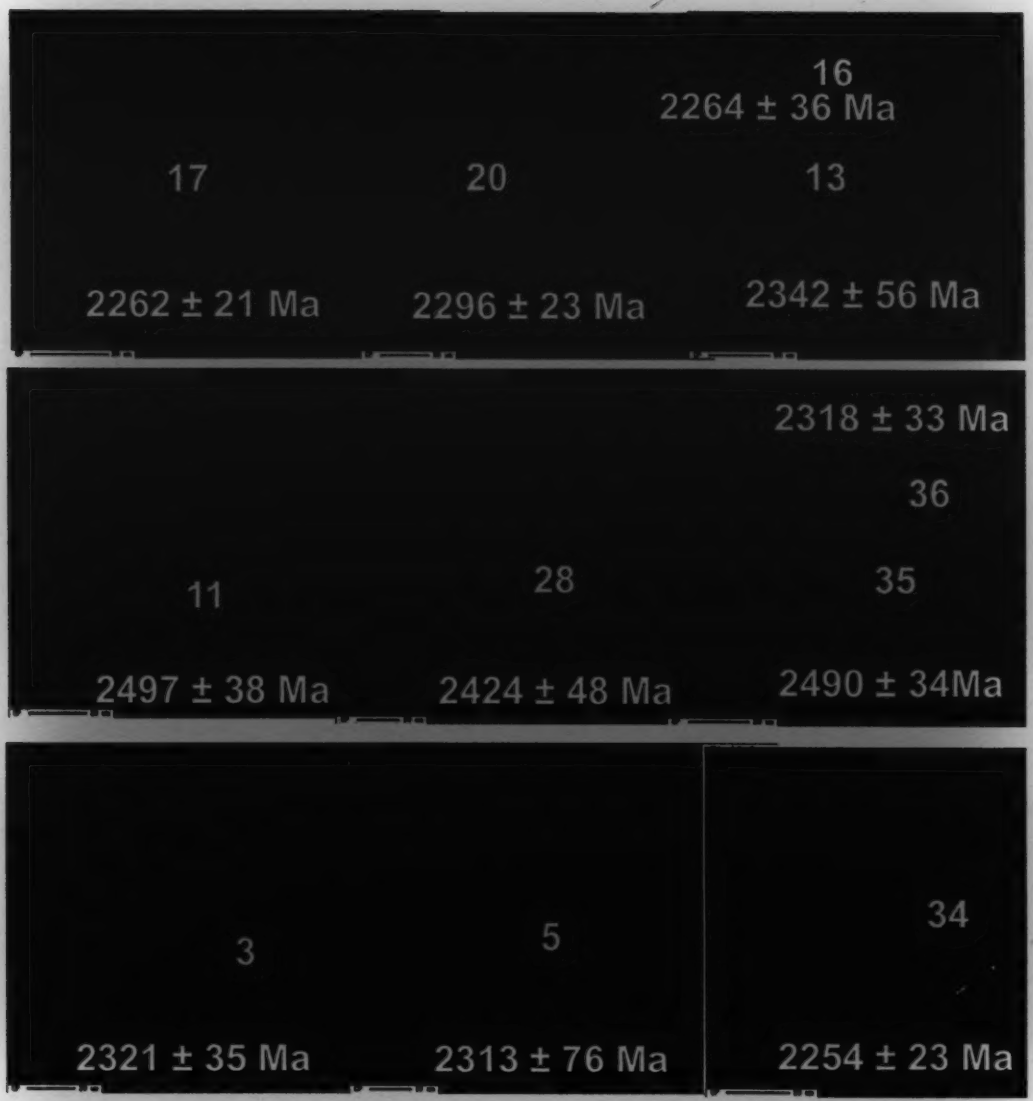

Figure 4-15. Backscatter electron images of selected metamorphic zircon crystals from a cordierite-bearing granite neosome (RH98-543). Individual U-Pb spot ages with errors (2σ) are identified. Laser spot size is 20 μm for all spots except 16 and 17; these two spots are 40 μm. The spherical grains (middle and bottom rows) contain an early oscillatory zoned component that yields mixed Neoarchean to Paleoproterozoic ages. The massive outer core that surrounds the oscillatory zoned component yields ca. 2.3 Ga ages similar to that for the large prismatic zircons (top row).

Table 4-1: Paleoproterozoic deformation and metamorphic history of the western Beaverlodge Belt.

High-grade zone	Medium-grade zone
Ca 2.34-2.30 Ga (coeval with the Blezardian Orogeny)	
Crustal thickening (D_1)	Shallow level emplacement of granites
Upper amphibolite-facies metamorphism (M_1)	D_1 deformation??
Late-stage (Syn- to post-orogenic) production of crustal melts	
Metamorphic zircon and monazite growth	
Ca. 1.98-1.92 Ga (coeval with the Taltson-Thelon Magmatic Zone)	
Tight to isoclinal folding (D2)	Tight to isoclinal folding (D2)
Upper amphibolite-facies conditions (M2)	Middle amphibolite-facies metamorphism (M2)
	Localized monazite growth
	Emplacement of leucogranites
Ca. 1.92-1.90 Ga (Late stage TTMZ)	
Open to tight folding (D3)	Open to tight folding (D3)
Low-pressure upper amphibolite-facies metamorphism (M3)	Middle amphibolite-facies metamorphism (M3)
Crystallization of monazite and zircon	Crystallization of monazite and zircon
Ca. 1.8 Ga (coeval with the Trans-Hudson Orogen)	
Greenschist-facies metamorphism (M4)	Greenschist-facies metamorphism (M4)
Gentle folding (D4)	Gentle folding (D4)
Brittle faulting	Brittle faulting
Lead loss in zircons	Lead loss in zircons

Table 4-2. Chemical monazite data (in wt%) and calculated spot ages.

Sample/grain/analysis	ThO2	UO2	PbO	Y2O3	time (Ma)	Sample/grain/analysis	ThO2	UO2	PbO	Y2O3	time (Ma)
4700-6389-g1	9.41	0.377	0.844	1.51	1781	4700-6389-g11-2	5.20	0.305	0.550	1.39	1965
4700-6389-g2	4.17	0.674	0.580	1.60	1961	4700-6389-g11-3	3.61	0.413	0.447	1.38	1963
4700-6389-g3	2.23	0.215	0.279	1.18	2071	4700-6389-g14	4.12	0.307	0.454	1.30	1954
4700-6389-g4	4.16	0.278	0.448	1.37	1951	4700-6389-g15	2.63	0.389	0.364	1.39	2012
4700-6389-g5-1	3.63	0.270	0.404	1.32	1971	4700-6389-g16	2.16	0.478	0.362	1.47	2061
4700-6389-g5-2	3.90	0.267	0.422	1.29	1953	4700-6389-g17	2.28	0.310	0.305	1.28	2004
4700-6389-g5-3	5.85	0.352	0.607	1.36	1922	4700-6389-g18	6.84	0.408	0.708	1.57	1921
4700-6389-g6	5.27	0.335	0.571	1.53	1980	4700-6389-g19	7.89	0.300	0.749	1.41	1889
4700-6389-g7	18.30	0.218	1.545	1.45	1840	4700-6389-g20	19.28	0.240	1.670	1.47	1882
4700-6389-g8	12.15	0.276	1.071	1.41	1849	4700-6389-g21	1.08	0.446	0.265	1.40	2175
4700-6389-g9	13.89	0.229	1.235	1.46	1903	4700-6389-g22	1.58	0.723	0.399	1.67	2118
4700-6389-g10	11.23	0.275	1.040	1.55	1926	4700-6389-g23	2.46	0.770	0.494	1.51	2078
4700-6389-g11-1	3.58	0.458	0.485	1.56	2063	4700-6389-g24	1.77	0.992	0.531	1.75	2266
RH98-465-g1	6.00	0.357	0.638	2.04	1970	RH98-465-g38	4.89	0.217	0.516	1.75	2044
RH98-465-g2-1	4.83	0.205	0.510	1.90	2058	RH98-465-g39	5.32	0.284	0.592	1.96	2091
RH98-465-g2-2	4.28	0.189	0.437	1.72	1983	RH98-465-g40	7.23	0.215	0.706	1.86	1989
RH98-465-g3	5.42	0.321	0.603	2.06	2055	RH98-465-g41	5.52	0.295	0.610	2.02	2077
RH98-465-g4	4.49	0.235	0.487	1.78	2049	RH98-465-g42	4.39	0.280	0.496	1.84	2059
RH98-465-g5	11.49	0.164	1.023	1.99	1920	RH98-465-g43	8.51	0.144	0.794	1.86	1989
RH98-465-g6	5.95	0.387	0.660	1.96	2016	RH98-465-g44	2.47	0.147	0.281	1.36	2095
RH98-465-g7	6.15	0.324	0.640	2.03	1970	RH98-465-g45	6.63	0.255	0.689	1.92	2053
RH98-465-g8	6.04	0.332	0.653	2.10	2026	RH98-465-g46	1.73	0.138	0.196	1.25	1978
RH98-465-g9	6.66	0.359	0.696	2.02	1969	RH98-465-g47-1	3.38	0.152	0.341	1.45	1956
RH98-465-g10	3.98	0.189	0.429	1.48	2067	RH98-465-g47-2	4.93	0.247	0.537	1.92	2069
RH98-465-g11	5.33	0.374	0.586	2.17	1972	RH98-465-g48	1.60	0.117	0.191	1.38	2105
RH98-465-g12	5.42	0.409	0.621	2.01	2017	RH98-465-g49	2.05	0.188	0.270	1.64	2190
RH98-465-g13	1.69	0.155	0.199	1.32	1983	RH98-465-g50-1	5.35	0.278	0.582	2.01	2055
RH98-465-g14	5.35	0.194	0.539	1.67	2009	RH98-465-g50-2	4.41	0.204	0.474	1.69	2067
RH98-465-g15	5.86	0.360	0.640	1.96	2008	RH98-465-g50-3	3.52	0.188	0.406	1.71	2160
RH98-465-g16	5.81	0.345	0.642	2.08	2041	Line 2 RH98-465-1	5.64	0.459	0.632	2.17	1947
RH98-465-g17-1	5.05	0.260	0.548	1.70	2055	Line 3 RH98-465-1	5.67	0.433	0.592	2.38	1849
RH98-465-g17-2	4.79	0.316	0.530	1.83	2005	Line 6 RH98-465-4	5.48	0.473	0.629	2.25	1965
RH98-465-g18	6.09	0.230	0.638	1.87	2071	Line 7 RH98-465-4	5.40	0.488	0.651	2.44	2032
RH98-465-g19	2.46	0.214	0.310	1.63	2133	Line 8 RH98-465-4	5.32	0.491	0.660	2.39	2076
RH98-465-g20	6.25	0.329	0.662	2.05	2002	Line 1 RH98-465-5	5.41	0.538	0.659	2.15	2005
RH98-465-g21	4.55	0.256	0.504	1.72	2066	Line 2 RH98-465-5	5.47	0.526	0.645	2.20	1964
RH98-465-g22	4.65	0.247	0.502	1.75	2035	Line 3 RH98-465-5	5.53	0.522	0.667	2.18	2013

Sample/grain/analysis	ThO2	UO2	PbO	Y2O3	time (Ma)
RH98-465-g23	2.53	0.197	0.298	1.64	2057
RH98-465-g24	7.08	0.248	0.712	1.89	2011
RH98-465-g25	5.96	0.287	0.622	1.95	2000
RH98-465-g26	6.38	0.374	0.705	1.92	2046
RH98-465-g27	4.78	0.228	0.496	1.75	1994
RH98-465-g28	5.23	0.315	0.570	1.97	2012
RH98-465-g29	5.51	0.361	0.624	1.90	2053
RH98-465-g30	3.47	0.138	0.348	1.63	1979
RH98-465-g31	4.59	0.378	0.550	2.07	2064
RH98-465-g32	6.24	0.378	0.698	1.99	2057
RH98-465-g34	1.22	0.179	0.181	1.48	2139
RH98-465-g35	2.79	0.211	0.316	1.50	1994
RH98-465-g36	5.04	0.185	0.507	1.80	2003
RH98-465-g37	1.89	0.195	0.262	1.54	2230
RH98-378-g1-1	5.47	0.156	0.512	3.28	1921
RH98-378-g1-2	6.30	0.247	0.576	0.60	1818
RH98-378-g1-3	5.71	0.271	0.563	0.90	1904
RH98-378-g1-4	8.94	0.983	1.296	0.27	2281
RH98-378-g1-5	7.24	0.835	1.147	0.83	2431
RH98-378-g1-6	6.11	0.295	0.583	0.87	1841
RH98-378-g1-7	7.78	0.822	1.142	0.73	2329
RH98-378-g1-8	7.04	0.995	1.212	0.80	2461
RH98-378-g1-9	13.23	0.367	1.492	0.12	2288
RH98-378-g1-11	7.90	1.173	1.407	1.32	2495
RH98-378-g4	13.11	0.546	1.585	0.10	2333
RH98-378-g6-2	1.43	0.148	0.163	0.24	1869
RH98-378-g6-3	0.06	0.109	0.041	0.04	2420
RH98-378-g7-1	3.94	0.170	0.372	0.24	1850
RH98-378-g7-2	3.59	0.122	0.329	0.16	1851
RH98-378-g8-1	6.46	0.568	0.961	0.63	2463
RH98-378-g8-2	5.90	0.130	0.699	0.46	2441
RH98-378-g8-3	6.88	0.230	0.820	1.07	2363
RH98-378-g8-4	12.65	0.507	1.506	0.06	2313
RH98-378-g8-5	12.86	0.457	1.500	0.05	2303
RH98-378-g9-1	17.68	0.519	2.046	0.09	2332
RH98-378-g9-2	19.11	0.553	2.182	0.09	2306
RH98-378-g9-3	14.06	0.634	1.723	0.06	2338
RH98-378-g9-4	13.77	0.582	1.661	0.07	2325

Sample/grain/analysis	ThO2	UO2	PbO	Y2O3	time (Ma)
Line 4 RH98-465-5	5.58	0.512	0.655	2.24	1977
Line 5 RH98-465-5	5.43	0.491	0.651	2.14	2023
Line 6 RH98-465-5	5.56	0.523	0.643	2.16	1941
Line 2 RH98-465-6	7.00	0.573	0.771	2.13	1915
Line 3 RH98-465-6	6.56	0.559	0.739	2.35	1937
Line 4 RH98-465-6	6.60	0.584	0.724	2.54	1875
Line 5 RH98-465-6	6.41	0.535	0.640	1.98	1743
Line 1 RH98-465-7	5.39	0.497	0.643	2.35	2005
Line 2 RH98-465-7	6.13	0.522	0.689	2.20	1934
Line 3 RH98-465-7	6.04	0.516	0.705	2.22	2001
Line 4 RH98-465-7	6.38	0.495	0.724	2.13	1990
Line 9 RH98-465-7	4.16	0.301	0.471	1.81	2013
Line 10 RH98-465-7	3.85	0.313	0.426	1.78	1927
RH98-378-g22-3	8.09	0.589	1.119	0.12	2406
RH98-378-g23	0.38	0.177	0.076	0.39	1695
RH98-378-g28	1.03	0.114	0.117	0.43	1834
RH98-378-g32-1	7.11	0.436	0.963	0.99	2438
RH98-378-g32-2	7.27	0.647	1.094	1.63	2482
RH98-378-g32-3	6.09	0.744	0.990	0.91	2447
RH98-378-g32-4	5.48	1.255	1.191	1.24	2532
RH98-378-g32-5	6.76	0.842	1.049	0.87	2338
RH98-378-g32-6	6.48	0.525	0.716	0.58	1924
RH98-378-g33	0.99	0.150	0.127	0.32	1864
RH98-378-g38-1	5.33	1.007	1.041	0.75	2486
RH98-378-g38-2	5.28	1.017	1.000	0.71	2407
RH98-378-g38-3	6.36	1.103	1.210	0.50	2507
RH98-378-g39	5.37	0.134	0.676	0.57	2555
RH98-378-g40-1	7.21	1.274	1.317	0.43	2406
RH98-378-g40-2	7.16	1.218	1.306	0.36	2435
RH98-378-g41	2.39	0.267	0.287	0.21	1923
RH98-378-g42	5.05	0.231	0.473	0.38	1823
RH98-378-g43	5.90	0.213	0.530	0.52	1806
RH98-378-g46	0.39	0.158	0.085	0.34	1972
RH98-378-g47-1	0.59	0.218	0.123	0.37	1990
RH98-378-g47-2	0.49	0.220	0.107	0.28	1868
RH98-378-g48-1	16.85	0.293	1.862	0.07	2325
RH98-378-g48-2	13.68	0.235	1.532	0.06	2356

Sample/grain/analysis	ThO2	UO2	PbO	Y2O3	time (Ma)
RH98-378-g10-1	6.76	1.739	1.541	1.31	2519
RH98-378-g10-2	6.78	1.197	1.317	1.00	2534
RH98-378-g10-3	6.22	1.105	1.223	0.93	2554
RH98-378-g10-4	13.93	0.521	1.640	0.06	2308
RH98-378-g10-5	14.32	0.532	1.707	0.09	2336
RH98-378-g11	0.74	0.149	0.095	0.11	1693
RH98-378-g13	1.01	0.203	0.150	0.18	1928
RH98-378-g14	0.77	0.177	0.119	0.17	1895
RH98-378-g15	0.36	0.173	0.086	0.12	1968
RH98-378-g17	0.74	0.195	0.123	0.22	1902
RH98-378-g18	0.41	0.212	0.112	0.41	2153
RH98-378-g19	3.15	0.401	0.492	0.07	2339
RH98-378-g20	1.78	0.217	0.191	0.22	1694
RH98-378-g21	1.24	0.170	0.153	0.24	1859
RH98-378-g22-1	6.04	0.140	0.540	0.13	1872
RH98-378-g22-2	5.72	0.156	0.520	0.26	1877

Sample/grain/analysis	ThO2	UO2	PbO	Y2O3	time (Ma)
RH98-378-g48-3	13.32	0.260	1.478	0.07	2317
RH98-378-g48-4	20.45	0.536	2.350	0.07	2340
RH98-378-g48-5	18.77	0.538	2.124	0.12	2289
RH98-378-g49	3.07	0.113	0.293	0.20	1906
RH98-378-g50-1	7.90	0.304	0.952	0.13	2350
RH98-378-g50-2	12.61	0.336	1.462	0.07	2356
RH98-378-g50-3	5.88	0.155	0.515	0.29	1817
RH98-378-g50-4	9.39	0.068	0.952	0.08	2223
RH98-378-g51	3.77	0.208	0.374	1.50	1873
RH98-378-g52	1.48	0.209	0.181	0.46	1830
RH98-378-g53-1	2.55	0.166	0.271	0.27	1939
RH98-378-g53-2	8.40	0.536	1.087	0.12	2325
RH98-378-g34	0.01	0.033	0.008	0.07	1606
RH98-378-g25	0.72	0.196	0.093	0.48	1499
RH98-378-g27	0.56	0.154	0.075	0.13	1541

Sample/grain/analysis	ThO2	UO2	PbO	Y2O3	time (Ma)
RH98-542-g1	6.80	0.260	0.658	2.38	1923
RH98-542-g2-1	14.85	0.888	1.998	0.88	2434
RH98-542-g2-2	8.11	0.241	0.734	2.54	1854
RH98-542-g2-3	22.37	0.650	2.488	0.27	2250
RH98-542-g3-1	10.24	0.184	0.898	0.09	1869
RH98-542-g3-2	8.47	0.261	0.767	0.48	1848
RH98-542-g4-1	9.06	0.214	0.809	0.25	1867
RH98-542-g4-2	1.67	0.120	0.222	0.06	2329
RH98-542-g5	8.97	0.315	0.820	0.90	1840
RH98-542-g6-1	30.71	0.736	3.452	0.09	2310
RH98-542-g6-2	10.07	0.172	0.869	0.30	1846
RH98-542-g6-3rim	10.56	0.194	0.908	0.26	1832
RH98-542-g6-4rim	12.34	0.247	1.076	0.86	1847
RH98-542-g7	6.41	0.212	0.606	0.32	1910
RH98-542-g8	8.91	0.311	0.811	0.65	1834
RH98-542-g9-2 (core)	8.99	0.205	0.787	0.22	1837
RH98-542-g10-1(inner core)	0.77	0.064	0.096	0.26	2127
RH98-542-g10-2 (rim 1)	8.87	0.332	0.833	0.98	1874
RH98-542-g10-3 (rim 1)	6.13	0.275	0.600	2.50	1903
RH98-542-g10-4 (outer rim)	4.30	0.207	0.433	2.73	1938
RH98-542-g12-1 (core)	17.08	0.808	2.213	0.74	2442

Sample/grain/analysis	ThO2	UO2	PbO	Y2O3	time (Ma)
RH98-542-g13-6 (outer rim)	8.51	0.237	0.791	2.32	1913
RH98-542-g14-1 (inner core)	13.42	0.657	1.842	0.20	2558
RH98-542-g14-2 (inner core)	13.31	0.731	1.829	0.51	2516
RH98-542-g14-3 (inner rim)	15.26	0.443	1.934	0.05	2535
RH98-542-g14-4 (inner rim)	15.01	0.471	1.966	0.12	2592
RH98-542-g14-5 (outer rim)	8.27	0.163	0.739	2.86	1891
RH98-542-g14-6 (outer rim)	8.90	0.183	0.856	2.47	2021
RH98-542-g14-7 (outer rim)	7.96	0.192	0.760	2.68	1985
RH98-542-g15-1	8.80	0.257	0.812	0.69	1891
RH98-542-g15-2	5.60	0.210	0.554	2.57	1966
RH98-542-g16-1	28.66	0.592	3.133	0.16	2276
RH98-542-g16-2	27.66	0.659	3.113	0.10	2314
RH98-542-g16-3	9.71	0.189	0.880	0.30	1919
RH98-542-g17	8.47	0.235	0.783	0.71	1902
RH98-542-g18-1	28.69	0.604	3.230	0.09	2336
RH98-542-g18-2	19.68	0.621	2.405	0.13	2433
RH98-542-g18-3	8.86	0.177	0.810	0.66	1932
RH98-542-g18-4	10.38	0.272	0.978	1.02	1946
RH98-542-g19-1	12.90	0.517	1.744	0.21	2593
RH98-542-g19-2	6.90	0.222	0.652	0.44	1917
RH98-542-g19-3	6.30	0.220	0.598	0.53	1907

Sample/grain/analysis	ThO2	UO2	PbO	Y2O3	time (Ma)
RH98-542-g12-2 (core)	16.16	1.177	2.329	1.18	2493
RH98-542-g12-3 (core)	15.17	0.936	2.081	0.72	2462
RH98-542-g12-4 (core)	16.79	0.723	2.179	0.34	2477
RH98-542-g12-5 (core)	25.42	0.674	2.894	0.09	2318
RH98-542-g12-6 (dark rim)	8.05	0.225	0.746	0.56	1906
RH98-542-g12-7 (dark rim)	9.69	0.282	0.894	0.51	1891
RH98-542-g12-8 (dark rim)	4.94	0.266	0.500	2.36	1913
RH98-542-g13-3 (rim)	2.73	0.162	0.266	0.24	1818
RH98-542-g13-4 (rim)	8.76	0.303	0.828	0.49	1901
RH98-542-g13-1 (core)	13.52	0.625	1.843	0.23	2563
RH98-542-g13-2 (core)	11.31	0.761	1.697	0.78	2623
RH98-542-g13-3 (core)	13.00	0.552	1.741	0.35	2553
RH98-542-g13-4 (inner rim)	20.55	0.674	2.493	0.12	2407
RH98-542-g13-5 (outer rim)	7.87	0.202	0.734	2.74	1932
RH98-542-g13-7 (outer rim)	9.59	0.177	0.849	0.36	1883

Sample/grain/analysis	ThO2	UO2	PbO	Y2O3	time (Ma)
RH98-542-g20-1	11.22	0.987	1.867	1.42	2711
RH98-542-g20-2	16.74	0.384	2.102	0.13	2566
RH98-542-g21-1	7.35	0.205	0.703	0.41	1964
RH98-542-g21-2	9.96	0.272	0.916	0.55	1896
RH98-542-g22	2.11	0.135	0.273	0.12	2326
RH98-542-g23-1	2.54	0.074	0.275	0.25	2194
RH98-542-g23-2	2.56	0.031	0.300	0.07	2505
RH98-542-g24-1	16.01	0.417	1.872	0.13	2380
RH98-542-g24-2	20.51	0.662	2.497	0.09	2419
RH98-542-g24-3	19.04	0.654	2.351	0.09	2434
RH98-542-g24-4	6.61	0.268	0.636	0.78	1900
RH98-542-g24-5	20.06	0.506	2.348	0.10	2388
RH98-542-g24-6	6.15	0.223	0.588	0.56	1911
RH98-542-g24-7	6.71	0.266	0.652	0.70	1921

Sample/grain/analysis	ThO2	UO2	PbO	Y2O3	time (Ma)
RH98-698-g1	3.30	0.127	0.300	0.09	1810
RH98-698-g1-2	2.04	0.070	0.182	0.09	1803
RH98-698-g1-3	4.21	0.150	0.389	0.11	1856
RH98-698-g3	3.16	0.013	0.274	0.33	1937
RH98-698-g4	3.97	0.170	0.360	0.13	1786
RH98-698-g5-1	0.73	0.062	0.062	0.03	1501
RH98-698-g5-2	2.34	0.125	0.231	0.08	1874
RH98-698-g5-3	2.48	0.145	0.255	0.09	1919
RH98-698-g5-4	2.03	0.110	0.204	0.20	1900
RH98-698-g6-1	2.03	0.151	0.216	0.13	1893
RH98-698-g6-2	1.87	0.147	0.208	0.28	1951
RH98-698-g7	1.10	0.141	0.140	0.05	1949
RH98-698-g8	1.44	0.041	0.132	0.22	1881
RH98-698-g9	1.77	0.083	0.163	0.40	1793
RH98-698-g10-1	0.62	0.128	0.095	0.07	1962
RH98-698-g10-2	1.41	0.149	0.173	0.10	1990
RH98-698-g10-3	0.47	0.160	0.095	0.08	2018
RH98-698-g11-1	2.19	0.139	0.222	0.10	1867
RH98-698-g11-2	2.25	0.110	0.230	0.11	1962
RH98-698-g11-3	1.78	0.053	0.195	0.03	2219
RH98-698-g13-1 (core)	0.62	0.092	0.082	0.23	1936
RH98-698-g13-2 (core)	0.45	0.040	0.043	0.31	1654

Sample/grain/analysis	ThO2	UO2	PbO	Y2O3	time (Ma)
RH98-698-g17-1	3.95	0.183	0.383	0.11	1881
RH98-698-g17-2	4.96	0.201	0.462	0.09	1844
RH98-698-g17-3	0.21	0.011	0.020	0.16	1790
RH98-698-g17-4	0.51	0.041	0.046	0.25	1591
RH98-698-g17-5	0.37	0.017	0.046	0.05	2382
RH98-698-g17-6	4.63	0.195	0.441	0.10	1874
RH98-698-g17-7	3.87	0.173	0.363	0.12	1831
RH98-698-g18-1	2.34	0.142	0.245	0.07	1936
RH98-698-g18-2	2.33	0.156	0.236	0.12	1848
RH98-698-g18-3 (rim)	2.21	0.123	0.205	0.30	1755
RH98-698-g19-1	2.56	0.091	0.235	0.13	1843
RH98-698-g19-2	4.22	0.155	0.387	0.08	1838
RH98-698-g19-3	2.24	0.117	0.216	0.23	1840
RH98-698-g20-1 (core)	2.12	0.084	0.204	0.07	1902
RH98-698-g20-2 (core)	1.88	0.110	0.188	0.11	1869
RH98-698-g20-3 (rim)	3.26	0.170	0.320	0.13	1871
Line 1 rh98-698-1	2.95	0.196	0.310	0.11	1912
Line 2 rh98-698-1	2.47	0.167	0.250	0.05	1840
Line 3 rh98-698-1	2.64	0.200	0.275	0.12	1848
Line 4 rh98-698-1	2.42	0.154	0.238	0.06	1814
Line 5 rh98-698-1	1.97	0.127	0.200	0.09	1866
Line 6 rh98-698-1	1.92	0.148	0.202	0.00	1857

RH98-698-g13-3 (core)	0.65	0.094	0.082	0.12	1865
RH98-698-g13-4 (rim)	1.60	0.096	0.161	0.17	1874
RH98-698-g13-5 (rim)	1.42	0.152	0.153	0.08	1766
RH98-698-g14-1	2.71	0.192	0.311	0.12	2046
RH98-698-g14-2	1.73	0.162	0.201	0.10	1948
RH98-698-g14-3	3.05	0.159	0.307	0.13	1915
RH98-698-g14-4	0.85	0.148	0.125	0.15	2012
RH98-698-g14-5	0.95	0.139	0.121	0.21	1880
RH98-698-g14-6	0.26	0.023	0.027	0.01	1779
RH98-698-g14-7	3.70	0.206	0.386	0.12	1955
RH98-698-g14-8	3.03	0.166	0.293	0.19	1832
RH98-698-g15	0.27	0.026	0.042	1.13	2512
RH98-698-g16-1	1.62	0.124	0.176	0.05	1914
RH98-698-g16-2	1.47	0.146	0.161	0.06	1820
RH98-698-g16-3	1.54	0.123	0.170	0.07	1931
RH98-698-g16-4	4.67	0.238	0.468	0.11	1912
RH98-698-g16-5	3.96	0.220	0.388	0.06	1847
RH98-698-g16-6	4.47	0.198	0.434	0.09	1893
Sample/grain/analysis	**ThO2**	**UO2**	**PbO**	**Y2O3**	**time (Ma)**
Line 8 RH98-698-2	0.31	0.014	0.023	0.05	1487
Line 9 RH98-698-2	0.40	0.025	0.045	0.03	2042
Line 10 RH98-698-2	1.09	0.074	0.109	0.14	1816
Line 11 RH98-698-2	3.72	0.227	0.375	0.12	1868
Line 12 RH98-698-2	2.78	0.277	0.302	0.15	1806
Line 1 RH98-698-3	1.31	0.207	0.181	0.02	1965
Line 3 RH98-698-3	1.57	0.192	0.198	0.05	1961
Line 4 RH98-698-3	1.84	0.164	0.218	0.04	2004
Line 5 RH98-698-3	2.43	0.236	0.277	0.08	1901
Line 6 RH98-698-3	2.59	0.200	0.280	0.05	1908
Line 7 RH98-698-3	2.65	0.221	0.305	0.07	1983
Line 8 RH98-698-3	2.64	0.231	0.300	0.06	1942
Line 1 RH98-698-4	0.79	0.123	0.115	1.49	2063
Line 2 RH98-698-4	0.86	0.102	0.120	1.45	2167
Line 3 RH98-698-4	3.08	0.181	0.326	0.51	1968
Line 4 RH98-698-4	0.36	0.207	0.095	0.01	1952
Line 5 RH98-698-4	0.28	0.236	0.093	0.05	1968
Line 7 RH98-698-4	0.26	0.242	0.100	0.04	2201
Line 8 RH98-698-4	0.28	0.234	0.094	0.05	2025
Line 9 RH98-698-4	0.28	0.249	0.104	0.05	2177
Line 7 rh98-698-1	2.09	0.190	0.219	0.08	1789
Line 8 rh98-698-1	2.17	0.131	0.214	0.13	1834
Line 9 rh98-698-1	2.12	0.135	0.208	0.06	1809
Line 10 rh98-698-1	2.18	0.110	0.217	0.10	1904
Line 11 rh98-698-1	2.26	0.117	0.214	0.09	1808
Line 12 rh98-698-1	2.10	0.125	0.217	0.10	1921
Line 13 rh98-698-1	2.24	0.114	0.219	0.09	1870
Line 14 rh98-698-1	2.01	0.119	0.202	0.09	1870
Line 15 rh98-698-1	2.15	0.094	0.208	0.08	1894
Line 16 rh98-698-1	2.20	0.136	0.222	0.11	1863
Line 17 rh98-698-1	2.28	0.130	0.223	0.09	1840
Line 18 rh98-698-1	2.19	0.132	0.230	0.11	1945
Line 19 rh98-698-1	2.88	0.205	0.299	0.10	1867
Line 1 RH98-698-2	2.79	0.173	0.286	0.11	1890
Line 2 RH98-698-2	4.01	0.236	0.374	0.11	1749
Line 4 RH98-698-2	0.62	0.047	0.073	0.04	2071
Line 6 RH98-698-2	0.45	0.050	0.053	0.04	1892
Line 7 RH98-698-2	0.42	0.039	0.050	0.00	1991
Sample/grain/analysis	**ThO2**	**UO2**	**PbO**	**Y2O3**	**time (Ma)**
Line 8 RH98-698-4	1.22	0.148	0.158	1.02	2008
Line 9 RH98-698-4	0.87	0.114	0.111	1.37	1938
Line 10 RH98-698-4	0.84	0.107	0.104	1.36	1901
Line 1 RH98-698-5-rim	3.48	0.093	0.317	1.44	1884
Line 2 RH98-698-5-rim	3.99	0.174	0.361	0.87	1777
Line 3 RH98-698-5-rim	4.82	0.286	0.494	0.16	1907
Line 4 RH98-698-5-rim	5.07	0.298	0.514	0.14	1888
Line 5 RH98-698-5-rim	5.26	0.300	0.536	0.17	1909
Line 6 RH98-698-5-rim	5.40	0.313	0.550	0.13	1903
Line 7 RH98-698-5-rim	5.67	0.336	0.576	0.16	1891
Line 8 RH98-698-5-rim	6.09	0.334	0.614	0.15	1900
Line 9 RH98-698-5-rim	6.37	0.360	0.646	0.14	1902
Line 1 RH98-698-5core	4.36	0.293	0.459	0.16	1911
Line 2 RH98-698-5core	4.23	0.277	0.453	0.13	1949
Line 3 RH98-698-5core	4.28	0.279	0.459	0.15	1956
Line 4 RH98-698-5core	4.21	0.279	0.457	0.14	1971
Line 5 RH98-698-5core	4.14	0.312	0.452	0.14	1934
Line 6 RH98-698-5core	4.16	0.285	0.453	0.10	1964
Line 7 RH98-698-5core	4.15	0.283	0.454	0.15	1974
Line 8 RH98-698-5core	4.10	0.221	0.451	0.17	2067

Sample/grain/analysis	ThO2	UO2	PbO	Y2O3	time (Ma)	Sample/grain/analysis	ThO2	UO2	PbO	Y2O3	time (Ma)
Line 10 RH98-698-4	0.25	0.235	0.108	0.04	2485	Line 9 RH98-698-5core	4.23	0.326	0.473	0.15	1965
Line 11 RH98-698-4	0.27	0.234	0.104	0.03	2291	Line 10 RH98-698-5core	4.31	0.307	0.467	0.18	1941
Line 12 RH98-698-4	0.27	0.233	0.102	0.00	2246	Line 11 RH98-698-5core	4.32	0.336	0.470	0.16	1914
Line 13 RH98-698-4	0.28	0.199	0.087	0.01	2036	Line 12 RH98-698-5core	4.31	0.310	0.470	0.12	1948
Line 14 RH98-698-4	0.26	0.187	0.088	0.05	2230	Line 13 RH98-698-5core	4.22	0.324	0.468	0.14	1952
Line 15 RH98-698-4	0.29	0.205	0.087	0.04	1973	Line 15 RH98-698-5core	4.27	0.312	0.456	0.15	1905
Line 16 RH98-698-4	0.63	0.213	0.123	0.11	1961	Line 16 RH98-698-5core	4.27	0.291	0.459	0.12	1944
Line 17 RH98-698-4	4.78	0.263	0.491	0.14	1932	Line 17 RH98-698-5core	4.33	0.314	0.456	0.14	1885
Line 18 RH98-698-4	5.10	0.279	0.509	0.21	1883	Line 18 RH98-698-5core	4.26	0.301	0.448	0.19	1892
Line 19 RH98-698-4	2.22	0.192	0.250	0.59	1929	Line 1 RH98-698-6	2.89	0.218	0.315	0.10	1930
Line 20 RH98-698-4	1.27	0.142	0.155	0.72	1952	Line 2 RH98-698-6	2.77	0.208	0.309	0.00	1972
Line 1 RH98-698-4	1.31	0.146	0.160	0.74	1950	Line 3 RH98-698-6	2.80	0.351	0.321	0.13	1786
Line 2 RH98-698-4	1.24	0.165	0.151	0.72	1852	Line 4 RH98-698-6	2.94	0.331	0.360	0.11	1952
Line 3 RH98-698-4	1.25	0.163	0.157	0.75	1921	Line 5 RH98-698-6	3.04	0.419	0.404	0.12	1981
Line 4 RH98-698-4	1.32	0.140	0.166	0.74	2027	Line 6 RH98-698-6	3.12	0.407	0.403	0.14	1965
Line 5 RH98-698-4	1.33	0.164	0.160	0.76	1877	Line 7 RH98-698-6	3.81	0.341	0.431	0.12	1924
Line 6 RH98-698-4	1.21	0.169	0.163	0.76	2000	Line 8 RH98-698-6	3.75	0.310	0.400	0.09	1856
Line 7 RH98-698-4	1.22	0.184	0.151	0.79	1806						

Table 4-3. U-Pb results

	Sample Description[a]	Weight (mg)	Concentrations (ppm) U	Th[b] model	Pb rad.	Th/U ratio	Common Pb (pg)[c]	Isotopic Ratios[d] $\frac{^{208}Pb}{^{204}Pb}$	$\frac{^{206}Pb}{^{238}U}$	$\frac{^{207}Pb}{^{235}U}$	$\frac{^{207}Pb}{^{206}Pb}$
Leucosome (RH98-543)											
1	Mzt (1)	0.005	7521	57746	7705	7.678	13	60190	0.3490±8	5.849±14	0.1216±1
2	Mzt (1)	0.006	10270	47085	7413	4.585	8	157175	0.3371±8	5.421±13	0.1167±1
3	Mzt (1)	0.004	8086	46394	5808	5.738	613	602	0.2029±39	3.3594±65	0.1201±2
4	Mzt, brown (1)	0.005	12884	60133	9768	4.667	9	144091	0.3529±7	5.752±12	0.1182±1
5	Zr, spherical (7)	0.011	1465	108	601	0.074	47	8474	0.4086±8	8.267±18	0.1468±1
6	Zr, spherical (1)	0.001	2207	183	990	0.083	14	6034	0.4418±8	9.559±19	0.1569±1
7	Zr, prismatic (1)	0.008	175	113	82	0.645	20	1937	0.4089±8	8.150±17	0.1446±1
8	Zr, spherical (1)	0.002	889	64	391	0.072	13	4417	0.4338±8	9.425±19	0.1576±1
9	Zr, spherical (1)	0.001	1395	44	596	0.032	7	3875	0.4281±8	9.003±18	0.1525±1
10	Zr, abr, spherical (1)	0.002	1190	42	481	0.035	7	10004	0.4073±8	8.077±17	0.1438±1
11	Zr, abr, spherical (1)	0.001	942	46	354	0.049	6	5020	0.3809±5	7.050±10	0.1342±1
12	Zr, abr, spherical (1)	0.001	819	70	361	0.085	11	2414	0.4364±6	9.098±12	0.1512±1
Amphibolite (RH98-521)											
1	Zr, spherical (1)	0.001	197	82	72	0.414	7	795	0.3429±7	5.508±15	0.1165±2
2	Zr, blocky (1)	0.003	119	47	44	0.396	9	715	0.3445±7	5.541±15	0.1167±2
3	Zr, Spherical (2)	0.04	124	45	44	0.368	5	2498	0.3400±6	5.448±12	0.1162±1
Altered Amphibolite (RH98-780)											
1	Zr, spherical (8)	0.001	568	80	189	0.140	5	1766	0.3340±6	5.354±13	0.1163±1
2	Zr, spherical (14)	0.001	628	111	213	0.177	5	3226	0.3366±7	5.409±12	0.1165±1
3	Zr, spherical (22)	0.002	411	59	134	0.145	5	3248	0.3259±6	5.247±11	0.1168±1
Meta-basalt (4700-4541)											
1	Ttn, Yellow (37)	0.069	26	1	8	0.053	62	619	0.3373±5	5.427±10	0.1167±2
2	Ttn, clear (37)	0.064	9	1	3	0.153	79	169	0.3240±9	5.192±29	0.1162±6
3	Ttn, Yellow (33)	0.067	32	4	11	0.125	188	263	0.3447±10	5.563±23	0.1170±4

Note: [a] Abreviations: Zr, zircon; Mzt, Monazite; Tnt, Titanite; abr, air abraded following the techniques of Krogh (1982). The number in parentheses identifies the number of grains or grain fragments analyzed.

[b] Model Th concentration calculated from $^{208}Pb/^{206}Pb$ ratio and $^{207}Pb/^{206}Pb$ age. [c] Total common lead in analysis. [d] Isotopic ratios corrected for 2.0 pg Pb and 0.5 pg U in blanks, fractionation, and initial common Pb (Stacey and Kramers, 1975). Uncertainties are reported at 1σ. [e] PD refers to the percent discordance along a chord to the origin.

Table 4-3. U-Pb results

	Apparent Ages (Ma)			
	$\frac{^{208}Pb}{^{238}U}$	$\frac{^{207}Pb}{^{235}U}$	$\frac{^{207}Pb}{^{206}Pb}$	PD[e]
Leucosome (RH98-543)				
1	1930	1954	1980±1	2.89
2	1873	1888	1906±1	2.00
3	1190	1495	1958±3	42.82
4	1948	1939	1930±1	-1.12
5	2208	2260	2309±1	5.12
6	2359	2393	2423±1	3.17
7	2210	2248	2283±1	3.78
8	2323	2380	2430±1	5.24
9	2297	2338	2375±1	3.88
10	2203	2240	2274±1	3.67
11	2081	2118	2154±1	3.98
12	2335	2348	2360±1	1.26
Amphibolite (RH98-521)				
1	1901	1902	1903±3	0.16
2	1908	1907	1906±3	-0.14
3	1887	1893	1899±2	0.74
Altered Amphibolite (RH98-780)				
1	1858	1878	1900±2	2.56
2	1870	1886	1904±1	2.01
3	1818	1860	1907±1	5.34
Meta-basalt (4700-4541)				
1	1873	1889	1906±2	1.99
2	1809	1851	1899±10	5.43
3	1909	1910	1912±6	0.13

Table 4-4: LA-MC-ICPMS results for sample RH98-543

	$^{206}Pb/^{238}U$	± (1σ)	$^{207}Pb/^{235}U$[1]	± (1σ)	$^{207}Pb/^{206}Pb$	± (1σ)	Ages (Ma)[2]	± Ma (2σ)
1	0.4294	0.0027	9.150	0.003	0.1538	0.0001	2397	20
2	0.3784	0.0064	7.830	0.006	0.1494	0.0006	2347	54
3	0.3843	0.0042	7.832	0.004	0.1471	0.0002	2321	35
4	0.3160	0.0024	5.143	0.002	0.1174	0.0004	1927	25
5	0.4474	0.0106	9.075	0.010	0.1464	0.0002	2313	76
6	0.3808	0.0032	7.731	0.003	0.1465	0.0003	2314	27
7	0.3786	0.0034	7.592	0.003	0.1447	0.0001	2293	29
9	0.4110	0.0071	8.007	0.007	0.1406	0.0004	2243	56
10	0.3963	0.0039	8.097	0.004	0.1474	0.0004	2325	32
11	0.4454	0.0054	10.068	0.005	0.1631	0.0002	2497	38
12	0.4900	0.0070	10.503	0.007	0.1547	0.0002	2407	46
13	0.3400	0.0059	7.014	0.006	0.1489	0.0004	2342	56
14	0.3488	0.0047	7.233	0.005	0.1505	0.0004	2350	43
15	0.4400	0.0028	9.287	0.003	0.1523	0.0004	2381	20
16	0.4452	0.0050	8.777	0.005	0.1430	0.0001	2264	36
17	0.4426	0.0029	8.718	0.003	0.1422	0.0002	2262	21
18	0.4214	0.0029	8.365	0.003	0.1440	0.0001	2275	22
19	0.4636	0.0052	9.968	0.005	0.1551	0.0004	2412	36
20	0.4211	0.0030	8.460	0.003	0.1458	0.0003	2296	23
21a	0.3103	0.0048	5.078	0.005	0.1182	0.0005	1937	52
21b	0.4377	0.0018	9.029	0.002	0.1489	0.0002	2342	13
22	0.3538	0.0041	5.697	0.004	0.1162	0.0003	1907	29
23	0.4306	0.0056	8.359	0.005	0.1409	0.0010	2237	42
24	0.4381	0.0078	8.410	0.008	0.1385	0.0005	2218	58
25	0.5049	0.0103	11.009	0.010	0.1573	0.0003	2436	65
26	0.4545	0.0078	9.857	0.008	0.1565	0.0001	2427	55
27	0.4468	0.0044	9.123	0.004	0.1473	0.0003	2324	32
28	0.4892	0.0074	10.594	0.007	0.1563	0.0003	2424	48
29	0.4683	0.0068	9.485	0.007	0.1470	0.0005	2310	47
30	0.3419	0.0038	6.043	0.004	0.1276	0.0002	2047	37
31	0.3544	0.0036	6.129	0.004	0.1248	0.0005	2035	33
32	0.4785	0.0051	9.444	0.005	0.1432	0.0002	2265	34
33a	0.4103	0.0041	7.972	0.004	0.1402	0.0002	2238	33
33b	0.4690	0.0049	9.957	0.005	0.1532	0.0002	2391	33
34	0.4139	0.0029	8.113	0.003	0.1414	0.0001	2254	23
35	0.4753	0.0051	10.701	0.005	0.1625	0.0004	2490	34
36	0.4754	0.0049	9.675	0.005	0.1477	0.0003	2318	33

[1] Calculated value based on $^{238}U/^{235}U = 137.88$.

[2] Upper intercept ages for analyses with a fixed lower intercept of 0.

Chapter 5: An ancient (Meso- to Paleoarchean) crustal block in the Rae Province, Saskatchewan: evidence from Sm-Nd and U-Pb constraints.

This chapter will form the basis of a paper to be submitted to the Canadian Journal of Earth Science or Precambrian Research. Co-authors are T. Chacko[a], R. Creaser[a], L.M. Heaman[a], and K.E. Ashton[b].
[a]Department of Earth and Atmospheric Sciences, 1-26 Earth Sciences Building, University of Alberta, Edmonton, Alta., Canada, T6G 2E3
[b]Saskatchewan Geological Survey, 2101 Scarth St., Regina, Sask., Canada, S4P 3V7

Introduction:

The Rae Province, northwestern Canada (Figure 5-1), comprises the western part of the Churchill craton, one of the largest exposures of Archean crust in the world. The Rae Province has an exposed extent greater than the combined area of Germany, Switzerland, and the United Kingdom, yet has received just a fraction of the scientific study. A basic requirement of any study of the Earth's crust is to understand the time(s) at which material was removed from the mantle to form the crust. This knowledge can help to decipher the nature of Earth's earliest crust (Nutman et al., 2000), aid crustal growth and recycling estimates (e.g. McCulloch and Bennett, 1994; Bowring and Housh, 1995), improve plate-reconstructions, and, from an economic point of view, focus diamond exploration activities (Helmstaedt and Gurney, 1995).

The present work relies heavily on the Sm-Nd isotope system to place basic crustal growth constraints on a large (~ 200 km) E-W transect across the Rae Province, north of Lake Athabasca, Saskatchewan (Figure 5-1). Sm-Nd isotope geochemistry is ideal for characterization of Archean crust due to the long half-life of ^{147}Sm, resistance to resetting (Barovich and Patchett, 1992), and low-cost when

compared to other radiogenic isotope systems. There are, however, relatively few Sm-Nd isotopic data available for the Rae Province, especially when compared to the adjacent Superior and Slave cratons. In addition to Nd isotope study, selected granitoid samples have been dated using U-Pb geochronology in order to place better constraints on the timing of magmatism in the Rae Province and in order to search for xenocrystic zircons that might hint at buried ancient crust. In this paper I show that a fragment of Mesoarchean (3.5-3.0 Ga) to Paleoarchean (4.4-3.5 Ga) crust occurs on the north shore of Lake Athabasca, Saskatchewan. Based on existing data, additional fragments of ancient crust may lie along the western margin of the Rae Province.

Regional Geology

The Beaverlodge Belt, Saskatchewan, Canada, (Figure 5-2) is a sub-domain of the Rae Province delineated by marginal shear zones and the presence of Archean supracrustal rocks of the Murmac Bay Group (Chapter 2). The area around Uranium City (Figure 5-2) has produced significant quantities of both gold and uranium. A recent effort to reassess the geology and mineral potential of this area has led to the production of maps and reports detailing the geology of the Beaverlodge Belt (Ashton and Card, 1998; Hartlaub and Ashton, 1998; Hartlaub, 1999; Ashton et al., 2000; Ashton et al., 2001). To the east of the Beaverlodge Belt, the Train Lake and Dodge Domains are dominated by Neoarchean granites that may represent the deeper crustal remnants of granite-geenstone belts. West of the Beaverlodge Belt, the Zemlak, Nolan and Ena Domains are granitoid-rich crustal blocks of unknown tectonic setting

that are distinguished from one another on the basis of lithological and structural differences.

Sample selection:

Samples of all the known suites of plutonic rocks were selected from recently mapped areas of the Beaverlodge Belt. To achieve a more regional and complete perspective on crustal evolution in this region, two different approaches were taken: 1) Supracrustal rocks from the region were collected in order to ascertain the average crustal residence time of their source rocks. These crustal residence times can be useful in determining regions of potential ancient crust (Jahn and Condie, 1995; Böhm et al., 2000). 2). Reconnaissance granitoid samples were collected from a transect extending at least 50 km to the north, east, and west of the Beaverlodge Belt.

Because Sm and Nd are low abundance trace elements, felsic and intermediate rocks with adequate proportions of minerals that partition these elements (e.g. biotite, hornblende, apatite, zircon) were preferentially chosen and quartzite was not collected. In addition, mafic and ultramafic rocks were not analyzed because of the difficulty in calculating meaningful Nd model ages for rocks with high Sm/Nd ratios.

Mesoarchean Basement (RH98-LBG, RH00-6336, RH98-125)

Three samples of known granitic basement to the Murmac Bay Group (Chapter 2) were collected from the Uranium City area for Sm-Nd isotope analysis; one sample each from the 3060 ± 40 Ma Lodge Bay Granite, the 2999 ± 6.8 Ma Cornwall Bay Granite, and an undated basement dome (Chapter 2).

Neoarchean granitoids

Several dated *circa* 2.6 Ga granitoids were selected from the area within and adjacent to the Beaverlodge Belt. These granitoids vary in composition from granodiorite to granite and generally contain up to 30% hornblende and/or orthopyroxene ± biotite. The petrology of the Deadman and Donaldson Lake granites is described in chapter 2. A sample of the Prince Lake Granite was chosen because it makes up a large component of the northern Beaverlodge Belt and, together with the Stephens Lake Granite, has > 40 km^2 of exposed extent. This orange to white granite is coarse-grained and locally contains metamorphic orthopyroxene and migmatitic layering. Orthopyroxene, where present, is overprinted by metamorphic biotite, garnet and hornblende. A poorly constrained 2440 +/- 57 Ma U-Pb zircon age (Bickford et al., 1987) was reported for the Stephens Lake portion of this granite.

In addition to dated Neoarchean granites, reconnaissance sampling of granitoid rocks was conducted northwestwards from the Beaverlodge Belt towards the Taltson-Thelon Magmatic Zone (TTMZ, Figure 5-1). Because most felsic magmatism in the core of the Rae Province appears to have occurred ca. 2.6 Ga (Davis et al., 2000), most of the samples of undated granitoid are likely of this age.

Ca. 1.9-2.0 Ga granites

Pink leucogranite that injects Archean basement is abundant within the Uranium City area. One of these granites has a poorly defined U-Pb age of 1994 ± 37 Ma (Persons, 1988). A foliated to gneissic granodiorite (4701-299) was collected from the western end of the Beaverlodge Belt (Ashton et al., 2001). This rock is a leucocratic granodiorite which grades into a migmatite that has injected hosting paragneisses. It contains 1-2% chlorite after biotite, 0-2% epidote in veins and as

alteration, and trace muscovite-sericite in fractures and as feldspar alteration. Leucocratic granitoids are also exposed in the area surrounding Uranium City (Fig. 2). The massive pink Uranium City granite (RH01-06) was collected within the town site of Uranium City and appears typical of this leucogranite suite.

Supracrustal rocks

Several samples of meta-sedimentary rocks were chosen for Nd analysis in order to determine the average crustal residence time of their source rocks; this included three pelitic to psammitic rocks from the Beaverlodge Belt and one pelite from close to the western margin of the Rae Province at Taylor Lake (RH01-20). Although none of these meta-sediments have been directly dated, those from the Beaverlodge Belt are interpreted to be part of the Neoarchean Murmac Bay Group (Chapter 2). A single sample of intermediate volcanic rock was also taken from the Murmac Bay Group (RH98-439). A sample of quartzofeldspathic gneiss from the Beaverlodge Belt (RH98-90) could have either a sedimentary or an igneous origin.

Methodology

The U-Pb procedures used in this paper are identical to those outlined in detail in chapter 4. All isotopic ratios were measured by a Daly photomultiplier detector in single collector mode on a VG354 mass spectrometer. All errors reported in Table 5-1 are 1σ and were calculated using an in-house program that numerically propagates all known sources of uncertainty. Regression calculations and age uncertainties were determined using Isoplot version 3.0 (Ludwig, 2003).

Sm-Nd samples were crushed and finely powdered in a tungsten-carbide shatterbox. Rock powder was mixed to ensure sample homogeneity and 0.05 to 0.6 grams, dependent on Sm concentration, of the powder was added to a pre-cleaned Savillex vial. A mixed ^{149}Sm-^{150}Nd spike, HF and HNO_3 were then added to the sample vial. The vial was placed on the hot plate for 6 days to ensure complete dissolution of all mineral grains. Samples were dried down and then converted to a 0.75N HCl solution. This solution was centrifuged and loaded onto a large cation column for REE separation. The collected REE solution was dried down and then converted to a 0.025N HCl solution. This solution was added to DEP columns to separate the Sm and Nd. The Sm and Nd were dried down and then converted to a nitric acid solution that was loaded onto separate Re filaments. Isotope ratios were measured entirely with Faraday collectors on a Micromass Sector 54 Thermal-Ionization Mass Spectrometer. All reported depleted mantle model ages (T_{DM}) are based on the mantle evolution model of Goldstein et al. (1984). Additional details of Sm-Nd geochemistry methods are reported in Unterschutz et al. (2002)

U-Pb results:

Prince Lake Granite (RH99-869)

The Prince Lake Granite contains numerous brown, prismatic, slightly resorbed zircons.

All 7 analyses were of single grains of near identical initial appearance. The similar U contents (280-700 ppm), Th/U ratios (0.16-0.45), and $^{207}Pb/^{206}Pb$ ages (2330-2567 Ma) for these grains (Table 5-1), is consistent with a single population of igneous

zircon. Although all grains underwent air abrasion prior to analysis, a much higher degree of air abrasion was used for grains 3-7. These highly abraded cores have a lower weight and less common lead than the weakly abraded grains (Table 5-1). Discounting analysis 3, which has more common lead and higher errors than analyses 4-7, a discordia line derived by the highly abraded grains has an upper intercept age of 2601 ±16 Ma and a lower intercept age of 1793 ± 130 Ma (MSWD=0.22; Figure 5-3). The upper intercept is interpreted to represent the crystallization age of the granite, whereas the lower intercept, which is identical to lower intercepts of other Neoarchean granites in the area (Chapter 2), corresponds to a period of Paleoproterozoic metamorphism.

Uranium City Granite (RH01-06)

The Uranium City Granite contains a mixed population of zircon grains that range from resorbed rounded varieties to colourless prismatic grains (Figure 5-4). Although the majority of grains are colourless, rare yellow grains are present and many grains are cloudy. Backscatter electron images of zircon from the sample indicates that the majority of grains contain massive structureless cores that have been overgrown by occilatory zoned zircon (Figure 5-4). These cores likely represent a xenocrystic component to the zircon in this sample. Analyses Nos. 1, 3 and 7 consist of single colourless ovoid zircons. Nos 1 and 7 are exceptionally clear grains whereas No. 3 is slightly cloudy. Analysis No. 2 is an extremely cloudy abraded prismatic zircon. Analysis No. 4 consists of a single exceptionally clear and colourless blocky zircon that was moderately abraded. Analyses No. 5 and 6 are both extremely clear

prismatic zircon but #5 was heavily abraded to a sphere, whereas #6 was moderately abraded.

Because of its distinct morphology and near concordance, the 1933 Ma $^{207}Pb/^{206}$ Pb age for analysis #4 may represent the crystallization age for the Uranium City Granite. However the high uranium content for this grain (2035 ppm) may indicate that this grain was derived by metamorphsim or crustal anatexsis. The 1933 Ma crystallization age is in good agreement with the petrologically similar Feil Lake granite and is consistent with formation coeval with the Taltson Magmatic Zone. Elsewhere in the Uranium City area, a gold-bearing pink leucogranite has a poorly defined U-Pb age of 1994 ± 37 Ma (Persons, 1988). Analysis No. 2 also has a high U content (1899 ppm) and, when taken together with analysis No.4, defines a chord with an upper intercept age of 1913 ± 4 Ma. An alternative interpretation is that the Uranium City Granite is Archean and has Proterozoic metamorphic zircon. The similar morphology and chemistry (Table 5-1) of analyses 1,3 and 7 is consistent with their derivation from a common source rock. A discordia line through these analyses and No. 4 has an upper intercept age of 3899 +/- 97 Ma (Figure 5-5). This upper intercept age may indicate that Paleoarchean crust was involved in the formation of this granite. Paleoarchean crust has been suspected in the region since the discovery of >3.7 Ga ages from detrital zircons in a quartzite ~10 km to the northeast (Chapter 2).

Feil Lake Granite (4701-299)

This sample contains a mixed zircon population consisting of colourless and slightly brown prismatic to acicular grains. Backscatter electron images reveal that

the sample contains highly altered grains with cores and overgrowth, as well as relatively pristine acicular grains. Analysis No. 1 represents an abraded clear and colourless acicular zircon grain that has a slighly lower Th/U ratio (0.14) than the other grains in the sample (Table 5-1). The concordant $^{207}Pb/^{206}Pb$ age of 1974 ± 5 Ma for this grain is considered a good estimate of the crystallization age for this granite. Analyses No. 2 and 3 consist of brown abraded prismatic grains. These two grains likely represent xenocrystic zircons from a protolith with a crystallization age of > 3.0 Ga. By plotting the analyses from the Feil Lake Granite with those of the Uranium City Granite (Figure 5-6) it is apparent that the two samples define a best-fit discordia line that has a Paleoarchean upper intercept age.

Sm-Nd Results:

Mesoarchean Basement

All three Mesoarchean basement samples have low concentrations of Sm (1-2 ppm) and Nd (5-16 ppm) (Table 5-2). The Nd model ages are also nearly identical, ranging from 3.12 to 3.33 Ga. These model ages are only slightly older than the ca. 3.0 Ga crystallization ages for the granites and, combined with the -1.0 to +1.7 ϵNdT values for these rocks, indicate that these granites are broadly juvenile in composition (Figure 5-7, 5-8). The relatively homogeneous zircon populations of the basement granites (Chapter 2) is consistent with this conclusion. Because granites do not form by direct melting of ultramafic rock (Pitcher, 1997), it is unlikely that the Mesoarchean granites are directly mantle-derived. It is possible, however, that the

source rocks for the granites were mantle derived mafic to intermediate igneous rocks of nearly the same age.

Neoarchean granitoids

All but one of the dated Neoarchean granitic rocks from this study have uniform Nd model ages ranging from 2.85 to 2.97 Ga and ϵNdT ranging from -1.2 to +1.7 (Table 5-2, Figure 5-7). Only the Donaldson Lake Granite is an exception. This granite has an average ϵNdT of -3.4 that indicates that it has been contaminated with, or was formed from, much older crustal material. The presence of numerous xenoliths of amphibolite, quartzite and pelite (Chapter 2) is consistent with contamination of this granite. In addition, although the majority of zircons in this granite have ca. 2.6 Ga cores, one zircon was extremely discordant and could be significantly older (Grain No. 4, Chapter 2).

All 7 undated granites of probable Neoarchean age have similar Sm and Nd concentrations (Table 5-2) and Nd model ages (2.83-2.99 Ga). The ϵNdT for 6 of the 7 granites at 2600 Ma is almost identical with a range between -0.1 and +1.3. A foliated granitoid gneiss has a slightly lower ϵNdT of -1.2 at 2600 Ma, within the range of the dated Neoarchean granites (-1.2 to +1.7) but possibly indicating some crustal contamination.

Ca. 1.9 Ga granite

The exceptionally leucocratic nature and low Sm (1.22 ppm) and Nd (8.63 ppm) concentrations of the Feil Lake Granite is significantly different from the Neoarchean granitoids, but almost identical to known Mesoarchean basement (Table 5-2). Its Nd composition (T_{DM} of 3.18 Ga, $\epsilon_{Nd}(t) = -14.3$) is consistent with an intra-

crustal mode of formation, also supported by the presence of entrained > 3.0 Ga zircon xenocysts. The Nd evolution of this granite (Figure 5-7), is identical to known ca. 3.0 Ga basement in the area, suggesting that this granite is entirely derived from older crust.

Supracrustal rocks

Supracrustal rocks from this study have a wide range of T_{DM} ages (2.75-3.21 Ga) and ϵ_{Nd} values at 2600 Ma (+2.3 to -4) (Figure 5-8). This range of values likely reflects the variety of source rocks from which these samples were derived. The samples with the lowest ϵ_{Nd} values are preferentially located in the western Beaverlodge Belt and may have been derived almost wholly from the Meso- to Paleoarchean basement in the area (Figure 5-2).

Discussion: Crust formation and recycling in the Rae Province

Ancient Archean crust

Paleoarchean crust is exceptionally rare in the rock record, yet yields direct evidence for Earth's earliest stages of formation (Condie, 1993). Estimates for the rate of crustal growth and recycling during Paleoarchean time are tied to the analysis of these ancient crustal remnants (Bowring and Housh, 1995). Great effort should be made, therefore, to find and describe this relict ancient crust. Evidence from the present work, and related studies (Chapter 2), indicates that ancient crust (>3.6 Ga) exists along the western edge of the Beaverlodge Belt, Rae Province, Canada. In this area, the ca. 2631 ± 12 Ma Donaldson Lake Granite has an ϵNdT of -3.7 and older xenocrystic zircons, the Uranium City granite has xenocrystic zircons with a possible

Paleoarchean crystallization age, and a quartzite contains >3.7 Ga detrital zircons. These data, in conjunction with the Nd T_{DM} ages reported in this study, suggest the outline of a Meso- to Paleoarchean crustal block in the southwestern Rae Province (Figure 5-2). The Black Bay shear zone comprises both cataclastic rocks and older mylonitic gneisses (Bergeron, 2000) that transect this old crustal block. It is possible that this major shear zone represents the surface expression of a suture between Mesoarchean and younger crust. If this is the case, a possible location for exposed ancient crust would be within this deformational zone. The lowest metamorphic grades in the region appear to be centered on this ancient crustal block (Chapter 4). Thus, the basement complex appears to have had an important influence on later metamorphism and deformation.

Elsewhere in the Churchill craton, evidence for ancient crust occurs primarily along the western margin of the Rae Province. Thériault et al. (1994) reported 3.0-3.9 Ga Nd model ages in the Queen Maud Block and immediately southeast of the MacDonald Fault (Figure 5-9). A 3300 Ma $^{207}Pb/^{206}Pb$ minimum age for a zircon xenocryst was described from the Campbell Granite in this same area (Henderson and Loveridge, 1990). To the south, but also along the western margin of the Rae Province, McNicoll et al. (2000) recorded numerous Mesoarchean Nd model ages within the basement to the Taltson Magmatic Zone. Ca. 3.7 Ga detrital zircons from Neoarchean supracrustal belts in the northern Rae Province (Eva Zaleski, pers. com., 2001; Tom Skulski, pers. com. 2002) also indicate that ancient crust must have been exposed at the surface by ca. 2.7 Ga. The significantly older nature of crust along the western margin of the Churchill craton would be consistent with the presence of a

thick mantle keel in this area. This region might, therefore, become an important target for diamond exploration activities.

3.0-3.3 Ga crust

Ca. 3.0-3.2 Ga crust appears to be widespread along the margins of the Rae Province (Figure 5-9). In addition to crust of this age exposed in the Uranium City area (Chapter 2), a 3129 +13/-10 Ma tonalite gneiss is located along the western margin of the Rae Province, south of the McDonald fault (Henderson and Thériault, 1994). Also along the western margin of the Rae Province, 3.2-3.1 Ga granite and tonalite gneiss occurs as basement to the Taltson Magmatic Zone (McNicoll et al., 2000). The ca. 3.15-3.3 Ga Chipman Batholith is located along the Snowbird Tectonic Zone (Hanmer et al. 1994a) at the boundary between the Rae and Hearne Provinces. The Nd isotopic composition of the 3.0 Ga crust in the Uranium City area suggests a relatively juvenile source (Figure 5-8). However, other examples of ca. 3.0-3.3 Ga crust from the Rae Province appear to have more evolved isotopic compositions (Figure 5-8). For example, a 3.08 Ga migmatitic tonalite gneiss from the Taltson Magmatic Zone basement has a T_{DM} of 3.73 Ga (McNicoll et al., 2000).

2.85 Ga crust

Ca. 2.85 Ga granitoid crust occurs sporadically throughout the Rae Province, primarily as basement to Neoarchean supracrustal sequences. 2.87 Ga granodiorite represents basement to the Woodburn Lake Group (Zaleski et al., 2001) and ca. 2.85 Ga trondhjemite-tonalite makes up part of the basement to the Mary River Group (Jackson et al., 1990). Interestingly, both ca. 2.85 and ca. 2.92 Ga granitoids are found along the eastern side of the Hall Peninsula on Baffin Island (Scott, 1997). The

similarity of these ages to that of known Rae Province basement indicates a possible link between the two. Because the eastern side of Baffin Island has been linked to the Nain Province, Greenland, (Scott, 1997) there may also be a connection between the Rae and Nain provinces.

Neoarchean magmatism

Voluminous, variably deformed granitic rocks with U-Pb ages between 2.58 and 2.64 Ga were first identified in the Rae Province by Ashton (1988). The regional extent, and strictly felsic composition, of these rocks was recognized shortly thereafter by LeCheminant and Roddick (1991). They also recognized the age and petrologic similarities between the Rae suite of granitoids and a granitic suite studied by van Breemen and Henderson (1988) in the Slave Province. The tectonic setting of these granitoids is one of the fundamental unknowns in the Rae Province (Relf and Hanmer, 2000; Davis *et al.*, 2000). Discounting those samples from this study that appear to be contaminated by Mesoarchean crust in the Uranium City area, the known and suspected Neoarchean granitoids from the Rae Province (n=17; this study; Dudas et al., 1991) have relatively similar ϵNd_T values that range between -1.2 and +1.7. This similarity in Nd compositions makes it difficult to explain their derivation as recycling of entirely older crust. The consistent T_{DM} and ϵNdT over such a large area of crust indicate a regional uniform reservoir. On the basis of a Sm-Nd isochron derived from these 17 samples, the reservoir would have had a $^{143}Nd/^{144}Nd$ ratio of approximately 0.50929 ± 0.00018 at 2.58 Ga and an ϵNd of ~0. The mantle evolution model of Goldstein et al. (1984) predicts an ϵNd of + 4.5 at 2580 Ma. Cousens et al. (2001) examined the geochemistry and Nd isotopic composition of a suite of

Proterozoic ultrapotassic rocks, the Christopher Island Formation, which were injected and erupted over a 240,000 km^2 area of the Churchill craton. From this work they suggested that an enriched lithospheric mantle has existed beneath much of the Churchill craton since the Neoarchean. This enriched lithospheric mantle would have had ϵNd of between -3 and +2 at 2600 Ma, similar to the average ϵNd of 0 for the Neoarchean granites in this study (Figure 5-8). It seems possible, therefore, that melts from such an enriched lithospheric mantle could have mixed with a juvenile crustal reservoir to produce the Neoarchean granites of the Rae Province. The lack of exposed coeval mafic and ultramafic igneous rocks makes this explanation, however, somewhat tenuous.

Proterozoic Magmatism

Voluminous ca. 2.3 Ga magmatic rocks are found along the entire western margin of the Rae Province (Chapter 3). The ϵNd values for six samples of this suite vary considerably and plot both above and below the evolution envelope for ca. 2.6 Ga granites (Figure 5-8). Because one sample plots above the evolution trend for the ca. 2.6 Ga granites, it seems likely that a more juvenile component was involved in the formation of this granite. The ca. 2.3 Ga granites that plot below the Nd evolution envelope for ca. 2.6 Ga magmatism (Figure 5-7) indicate that some Mesoarchean basement was involved in their origin, either through contamination or partial melting.

Two granites from this study, the Feil Lake granite and the Uranium City granite, have ages consistent with the timing of the 2.0-1.93 Ga Taltson Magmatic Zone (Figure 5-1). Interestingly, both of these granites are leucocratic and have

abundant xenocrystic zircons, consistent with formation by crustal melting (Miller et al. 2003). In addition, the Feil Lake granite has a crustal Nd signature (T_{DM} = 3.18 Ga, ϵNdT = -14.3) that can be best explained by derivation by melting of the local Mesoarchean basement. Granitoids from the Taltson Magmatic Zone have younger T_{DM} and higher ϵNdT(1.94 Ga) values (-3.4 to -9.8) (De et al., 2000) than those from this study. This difference can be explained by either a larger mantle component to the TMZ granites, or by their derivation from source rocks that have a lower average crustal residence time. The second explanation appears more likely due to the now known and suspected existence of Meso to Paleoarchean crust in the Uranium City area.

Conclusions

Evidence from the present work, and related studies (Chapter 2), indicates that ancient crust (>3.6 Ga) exists along the western edge of the Beaverlodge Belt, Rae Province, Canada. Previous study (Thériault et al., 1994) suggests that additional ancient crust may be found along the western margin of the Rae Province. The presence of ancient crust along the margin of Archean cratons may have important implications for the timing of ancient crustal fragmentation and dispersion. Paleoarchean crust has been documented at the margins of the Superior Craton (Goldich and Hedge, 1974; Böhm et al., 2000; David et al., 2003), Slave Craton (Bowring et al., 1989), Nain Province (Nutman et al., 1996) and Yilgarn Craton (Maas et al., 1992). The addition of the Churchill craton to this group is significant and raises an interesting question. Was there a single ancient (Paleoarchean) continent

that was rifted apart and dispersed during late Neoarchean time? The answer to this question may be difficult to resolve, but further exploration of the geochemical, isotopic and field characteristics of the ancient crust along the western margin of the Churchill craton will be critical in attempting to address this question. Ca. 3.0 Ga granites in the Beaverlodge belt are relatively juvenile and do not appear to have mixed extensively with this older crust. Ca. 1.9 Ga granites, alternatively, are crustal melts that were derived from, or mixed with, Meso- to Paleoarchean sources.

Acknowledgements:

Partial funding for Sm-Nd isotope work was provided for by a Geological Society of America Research Grant to the first author. Thanks to Colin Card for providing several samples from the eastern margin of the Beaverlodge Belt.

References

Ashton, K.E. 1988. Precambrian Geology of the southeastern Amer Lake area (66H/1), near Baker Lake, N.W.T.: a study of the Woodburn Lake group, an Archean orthoquartzite-bearing sequence in the Churchill Structural Province; Ph.D. thesis, Queens University, Kingston, Ontario, 335 p.

Ashton, K.E., and Card, C.D., 1998. Rae Northeast: A Reconnaissance of the Rae Province Northeast of Lake Athabasca. Sask. Geol. Surv. Misc. Rep. 98-4, 3-16.

Ashton, K.E., Kraus, J., Hartlaub, R.P., and Morelli, R., 2000. Uranium City revisited: A new look at the rocks of the Beaverlodge Mining Camp. Sask. Geol. Surv., Misc. Rep. 2000-4.2, 3-15.

Ashton, K.E., Boivin, D., and Heggie, G. 2001. Geology of the Southern Black Bay Belt, west of Uranium City, Rae Province. Sask. Geol. Surv., Misc. Rep. 2001-4.2. 50-63.

Barovich, K.M., and Patchett, P.J. 1992. Behavior of Isotopic Systematics During Deformation and Metamorphism - a Hf, Nd and Sr Isotopic Study of Mylonitized Granite. Contributions to Mineralogy and Petrology, **109**: 386-393.

Bergeron, J. 2000. The deformational history of the Black Bay Structure in Uranium City, Northern Saskatchewan. Unpublished M.Sc. thesis, University of Saskatchewan, Saskatoon, Saskatchewan.

Bickford, M.E., Van Schmus, W.R., Collerson, K.D., and Macdonald, R. 1987. U-Pb zircon geochronology project: New results and interpretations; *in* Summary of Investigations 1987, Saskatchewan Geological Survey, Sask. Energy Mines, Misc. Rep. 87-4, p76-79.

Böhm, C.O., Heaman, L.M., Creaser, R.A., and Corkery, M.T. 2000. Discovery of pre-3.5 Ga exotic crust at the northwestern Superior Province margin, Manitoba. Geology, **28**: 75-78.

Bowring, S.A., and Housh, T. 1995. The Earth's Early Evolution. Science, **269**: 1535-1540.

Bowring, S.A., Williams, I.S., and Compston, W. 1989. 3.96 Ga Gneisses from the Slave Province, Northwest-Territories, Canada. Geology, **17**: 971-975.

Condie, K.C. 1993. Plate tectonics and crustal evolution. Oxford, Pergamon Press Ltd, 492 p.

David, J., Parent, M., Stevenson, R., Nadeau, P., and Godin, L. 2003. The Porpoise Cove supracrustal sequence, Inukjuak area: a unique example of Paleoarchean crust (ca. 3.8 Ga) in the Superior Province. GAC-MAC-SEG joint annual conference. Vancouver, B.C.

Davis, W.J. and nine others. 2000. Regional Differences in the Neoarchean evolution of the Western Churchill Province: Can we make sense of it?, Geocanada 2000, Abstract volume

Dudas, F.O., LeCheminant, A.N., and Sullivan, R.W. 1991. Reconnaissance Nd isotopic study of granitoid rocks from the Baker Lake region, District of Keewatin, N.W.T., and observation on analytical procedures. *In* Radiogenic age and isotopic studies: Report 4. Geological Survey of Canada. Paper 90-2, pp. 101-112.

Goldich, S.S., and Hedge, C.E. 1974. 3,800-Myr Granitic Gneiss in Southwestern Minnesota. Nature, **252**: 467-468.

Hartlaub, R.P., 1999. New insights into the geology of the Murmac Bay Group, Rae Province, Northwest Saskatchewan. Sask. Geol. Survey, Misc. Rep. 99-4.2, 17-26.

Hartlaub, R.P. and Ashton, K.E., 1998. Geological investigations of the Murmac Bay Group, Lake Athabasca north shore transect. Sask. Geol. Surv., Misc. Rep. 98-4, 17-28.

Helmstaedt, H.H., and Gurney, J.J. 1995. Geotectonic Controls of Primary Diamond Deposits - Implications for Area Selection. Journal of Geochemical Exploration, **53**: 125-144.

Henderson, J.B., and Loveridge, W.D. 1990. Inherited Archean zircon in the Proterozoic Thelon Tectonic Zone: U-Pb geochronology of the Campbell granite, south McDonald fault, District of Mackenzie, Northwest Territories, Paper 98-2, Geological Survey of Canada, pp. 63-70.

Jackson, G.D., Hunt, P.A., Loveridge, W.D., and Parrish, R.R., 1990. Reconnaissance geochronology of Baffin Island, N.W.T.. Geol. Surv. Can., Pap. 89-2, 123-148.

Jahn, B.M., and Condie, K.C. 1995. Evolution of the Kaapvaal-Craton as Viewed from Geochemical and Sm-Nd Isotopic Analyses of Intracratonic Pelites. Geochimica Et Cosmochimica Acta, **59**: 2239-2258.

Ludwig, K.R., 2003. Isoplot/Ex, a geochronological toolkit for microsoft excel, Version 3.0. Berkely, California, Berkely Geochronology Center Special Publication 4.

Maas, R., Kinny, P.D., Williams, I.S., Froude, D.O., and Compston, W. 1992. The Earths Oldest Known Crust - a Geochronological and Geochemical Study of 3900-4200 Ma Old Detrital Zircons from Mt Narryer and Jack Hills, Western-Australia. Geochimica Et Cosmochimica Acta, **56**: 1281-1300.

McCulloch, M.T., and Bennett, V.C. 1994. Progressive Growth of the Earths Continental-Crust and Depleted Mantle - Geochemical Constraints. Geochimica Et Cosmochimica Acta, **58**: 4717-4738.

McNicoll, V.J., Theriault, R.J., and McDonough, M.R. 2000. Taltson basement gneissic rocks: U-Pb and Nd isotopic constraints on the basement to the Paleoproterozoic Taltson magmatic zone, northeastern Alberta. Canadian Journal of Earth Sciences, **37**: 1575-1596.

Miller, C.F., McDowell, S.M., and Mapes, R.W. 2003. Hot and cold granites? Implications of zircon saturation temperatures and preservation of inheritance. Geology, **31**: 529-532.

Nutman, A.P., McGregor, V.R., Friend, C.R.L., Bennett, V.C., and Kinny, P.D. 1996. The Itsaq Gneiss Complex of southern West Greenland; the world's most extensive record of early crustal evolution (3900-3600 Ma). Precambrian Research, **78**: 1-39.

Nutman, A.P., Bennett, V.C., Friend, C.R.L., and McGregor, V.R. 2000. The early Archaean Itsaq Gneiss Complex of southern West Greenland: The importance of field observations in interpreting age and isotopic constraints for early terrestrial evolution. Geochimica Et Cosmochimica Acta, **64**: 3035-3060.

Persons, S.S., 1988. U-Pb geochronology of Precambrian rocks in the Beaverlodge area, Northwestern Saskatchewan. M.Sc. Thesis, University of Kansas.

Pitcher, W.S., 1997. The nature and origin of granite. London, Chapman and Hall, 387 p.

Relf, C. and Hanmer, S. 2000. A speculative and critical summary of the current state of knowledge of the western Churchill Province; a NATMAP perspective. Geocanada 2000, Abstract volume

Scott, D.J. 1999. U-Pb geochronology of the eastern Hall Peninsula, southern Baffin Island, Canada: a northern link between the Archean of West Greenland and the Paleoproterozoic Torngat Orogen of northern Labrador. Precambrian Research, **93**: 5-26.

St-Onge, M.R., Scott, D.J., and Wodicka, N. 2001. Terrane boundaries within Trans-Hudson Orogen (Quebec-Baffin segment), Canada: changing structural and metamorphic character from foreland to hinterland. Precambrian Research, **107**: 75-91.

Thériault, R.J., Henderson, J.B., Roscoe, S.M., 1994. Nd isotopic evidence for early to mid-Archean crust from high grade gneisses in the Queen Maud Block and south of the McDonald Fault, western Churchill Province, Northwest Territories. Radiogenic age and isotopic studies: report 8, Geol. Surv. Can., 1994-F, 37-42.

Unterschutz, J.L.E., Creaser, R.A., Erdmer, P., Thompson, R.I., and Daughtry, K.L. 2002. North American margin origin of Quesnel terrane strata in the southern Canadian Cordillera: Inferences from geochemical and Nd isotopic characteristics of Triassic metasedimentary rocks. Geological Society of America Bulletin, **114**: 462-475.

van Breemen, O. and Henderson, J.B. 1988. U-Pb zircon and monazite ages from the southern Slave Province and Thelon Tectonic Zone, Artillery Lake area, N.W.T., *In* Radiogenic age and isotopic studies: Report 2, Geological Survey of Canada, Paper 91-2, pp. 17-24.

Zaleski E., Davis, W.J. and Sandeman, H.A., 2001. Continental extension, mantle magmas & basement/cover relationships. 4th International Archean Symposium 2001, Extended Abstracts. AGSO – Geoscience Australia, Record 2001/37, pp. 374-376.

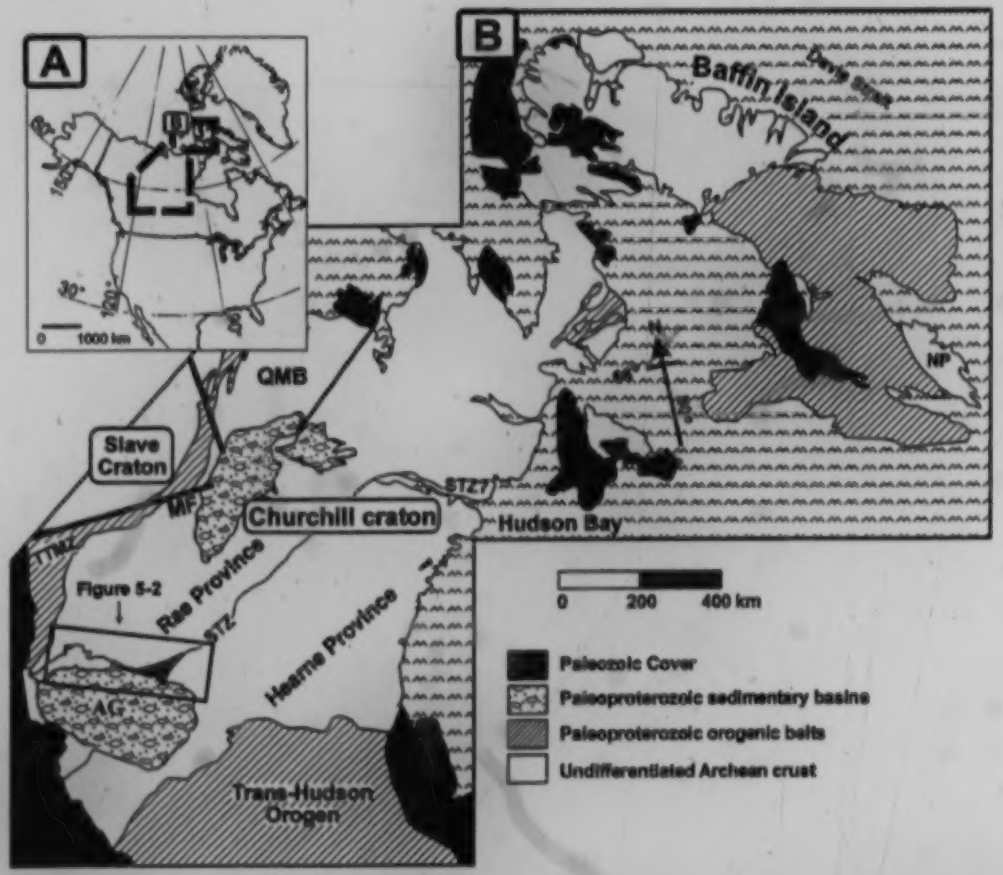

Figure 5-1. (A) Map of North America with the area of figure B indicated by a dashed box. (B)Simplified geology of the Churchill craton and bounding tectonic entities. (Modified after Jackson et al., 1990; Wheeler et al., 1996; Scott, 1999 ; and Skulski et al. 2002). The area of figure 5-2 is highlighted on the north shore of Lake Athabasca. AG, Athabasca Group; MF, McDonald Fault; NP, Nain Province; QMB, Queen Maud Block; STZ, Snowbird tectonic zone; TTMZ, Taltson-Thelon Magmatic Zone.

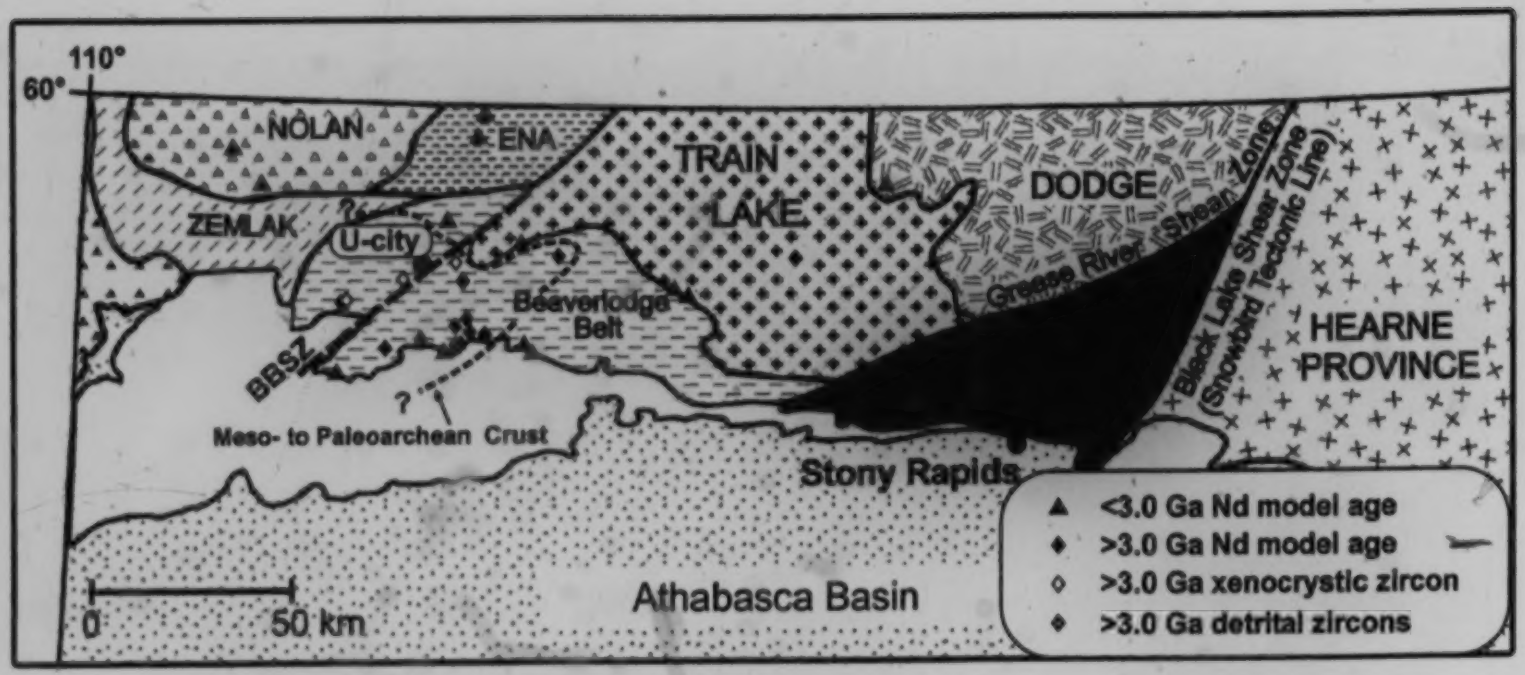

Figure 5-2. Simplified geological map of northwestern Saskatchewan. Old (>3.0 Ga) Nd TDM ages, xenocrystic zircons, and ancient detrital zircons highlight an area of Meso- to Paleoarchean crust. TDM ages are from this study and Chapter 3.

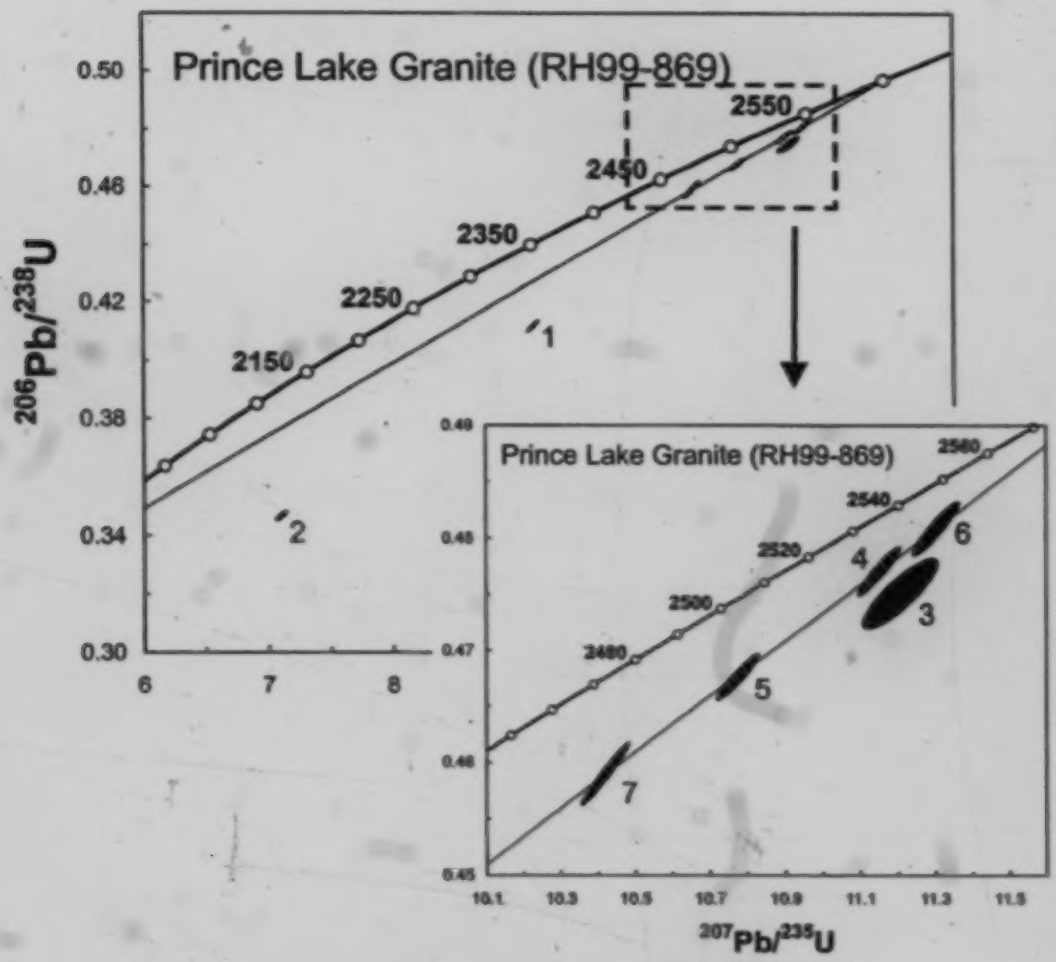

Figure 5-3. Concordia diagram for the Prince Lake Granite.

Figure 5-4. Backscatter electron images of zircon from leucogranites. The U-City Granite (RH01-06) contains zircon with Paleoarchean xenocrystic cores that are surrounded by occilatory zoned overgrowths. The Feil Lake Granite contains massive prismatic Paleoproterozoic zircon (4701-299b) in addition to grains with cores and overgrowths(4701-299a).

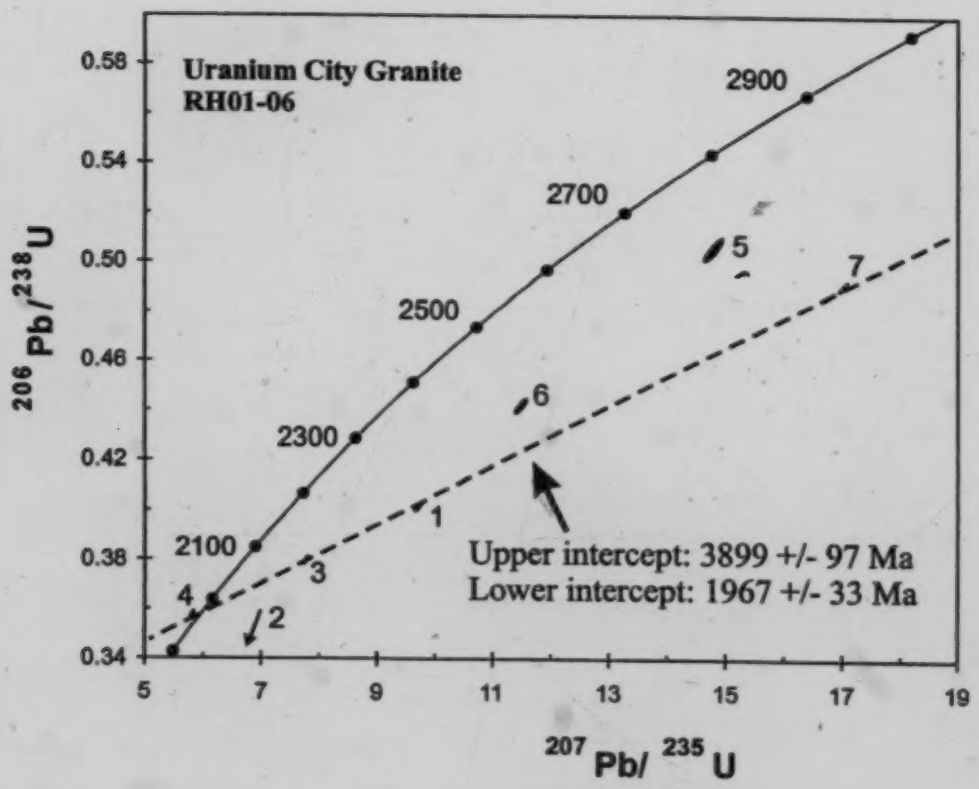

Figure 5-5. Concordia diagram for the Uranium City Granite.

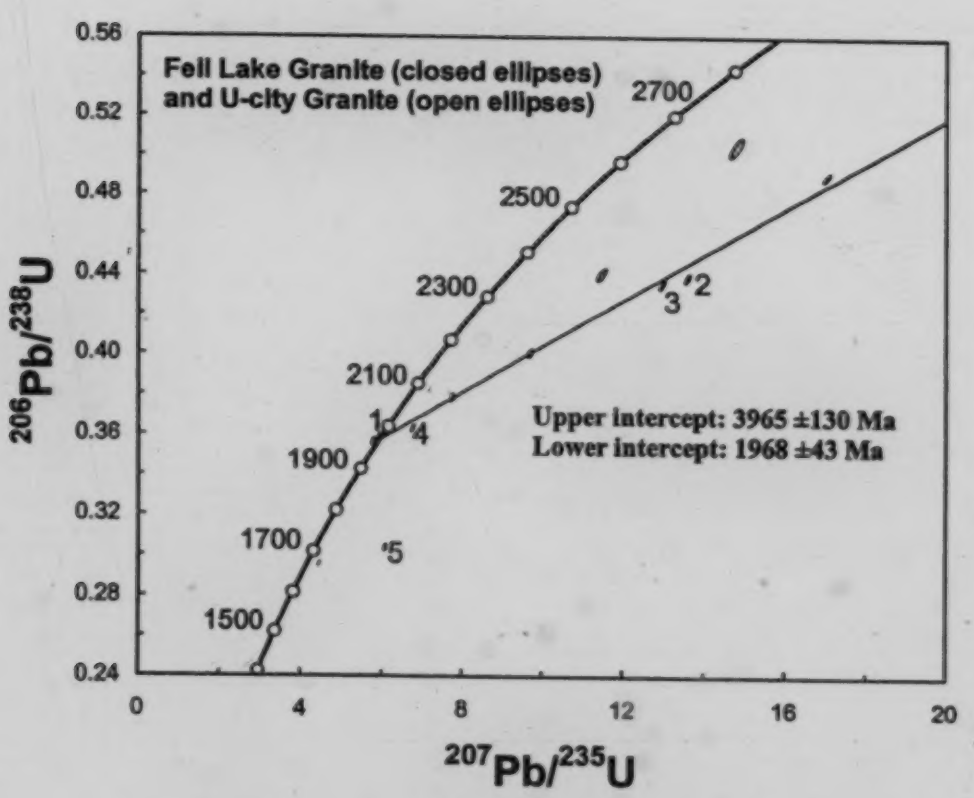

Figure 5-6. Concordia diagram for the Feil Lake and Uranium City granites.

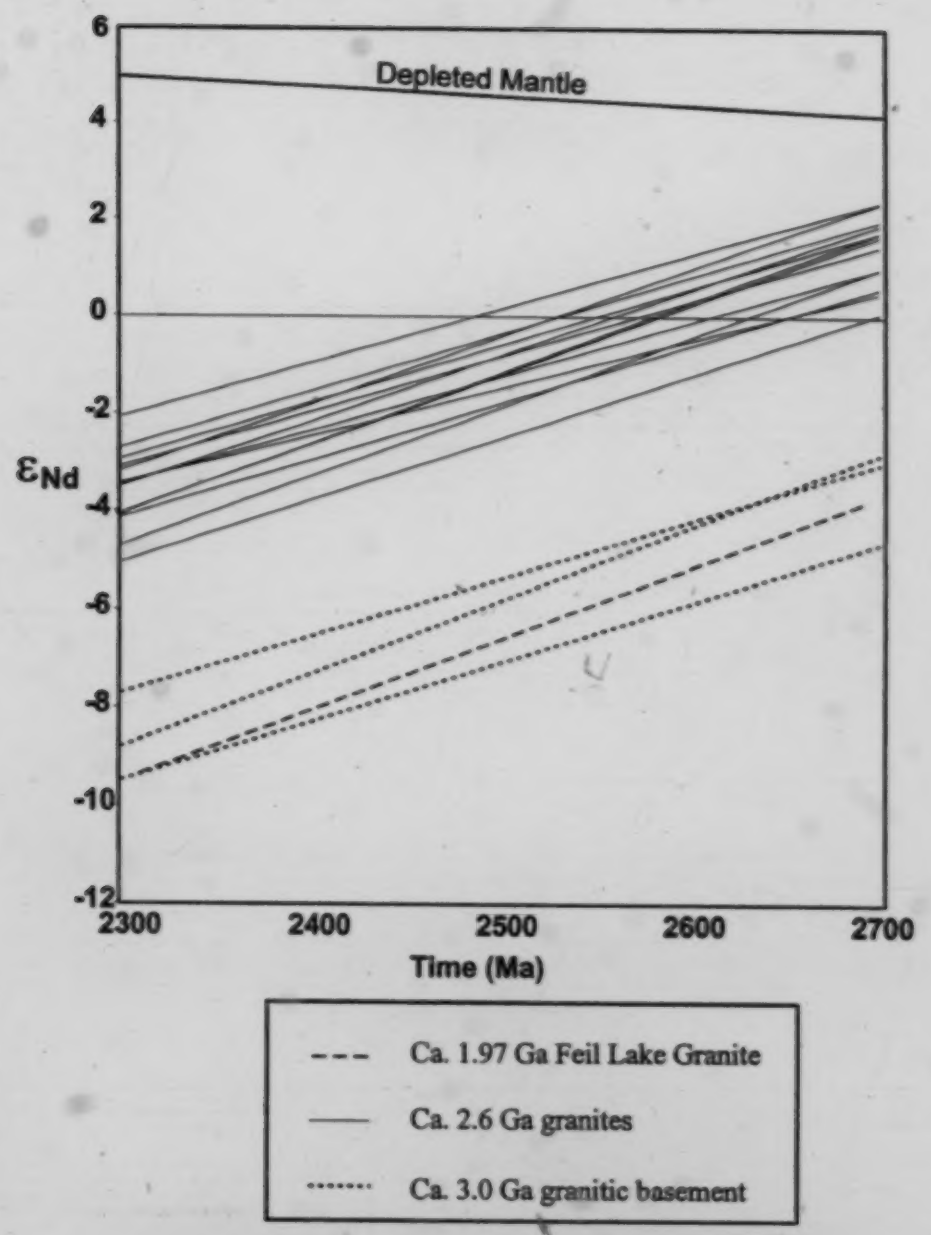

Figure 5-7. Nd evolution trend for granitic samples from this study. The ca. 1.97 Ga Feil Lake Granite has an evolution trend similar to known Mesoarchean basement. Plotted ca. 2.6 Ga granites are restricted to those outside the region of ancient crust (Figure 5-2).

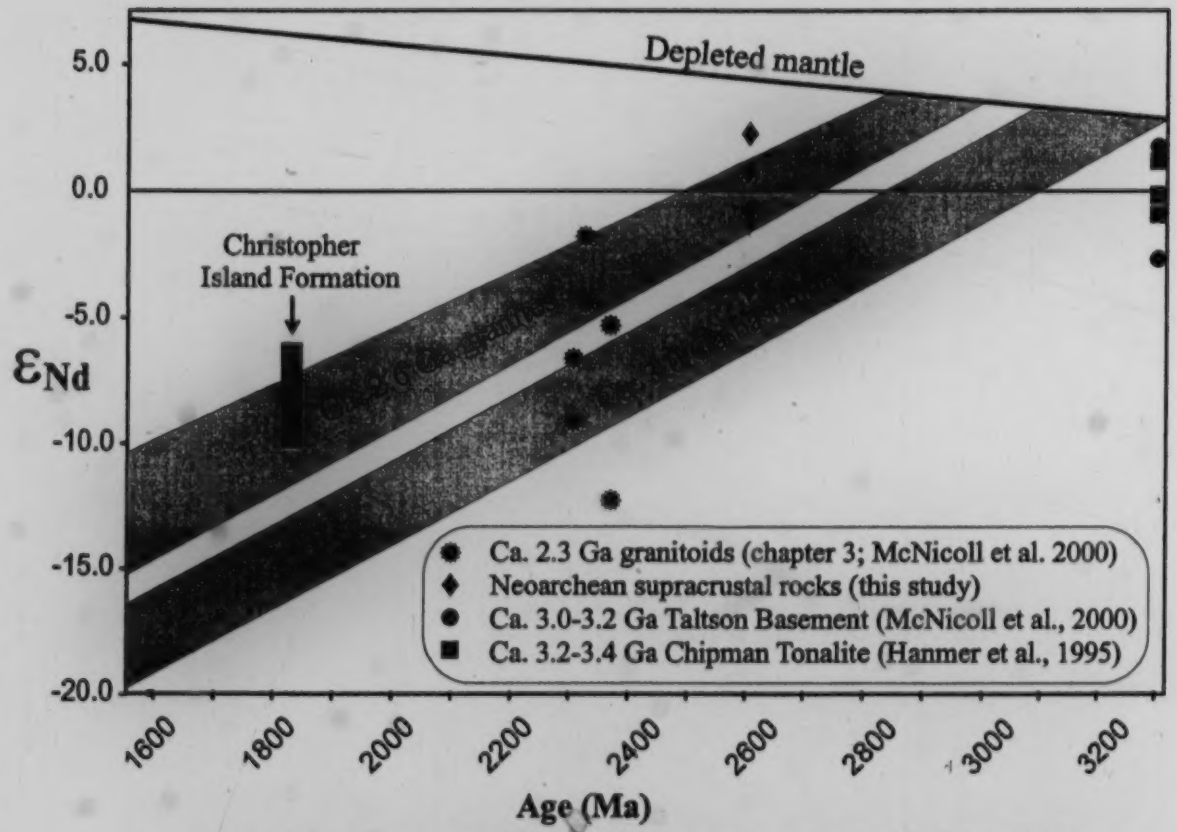

Figure 5-8. Nd evolution trends for ca. 2.6 and 3.0 Ga granites from this study. Plotted ca. 2.6 Ga granites are restricted to those outside the region of ancient crust (Figure 5-2). Depleted mantle trend is based on the evolution model of Goldstein et al. (1984). See text for a discussion of the other plotted samples.

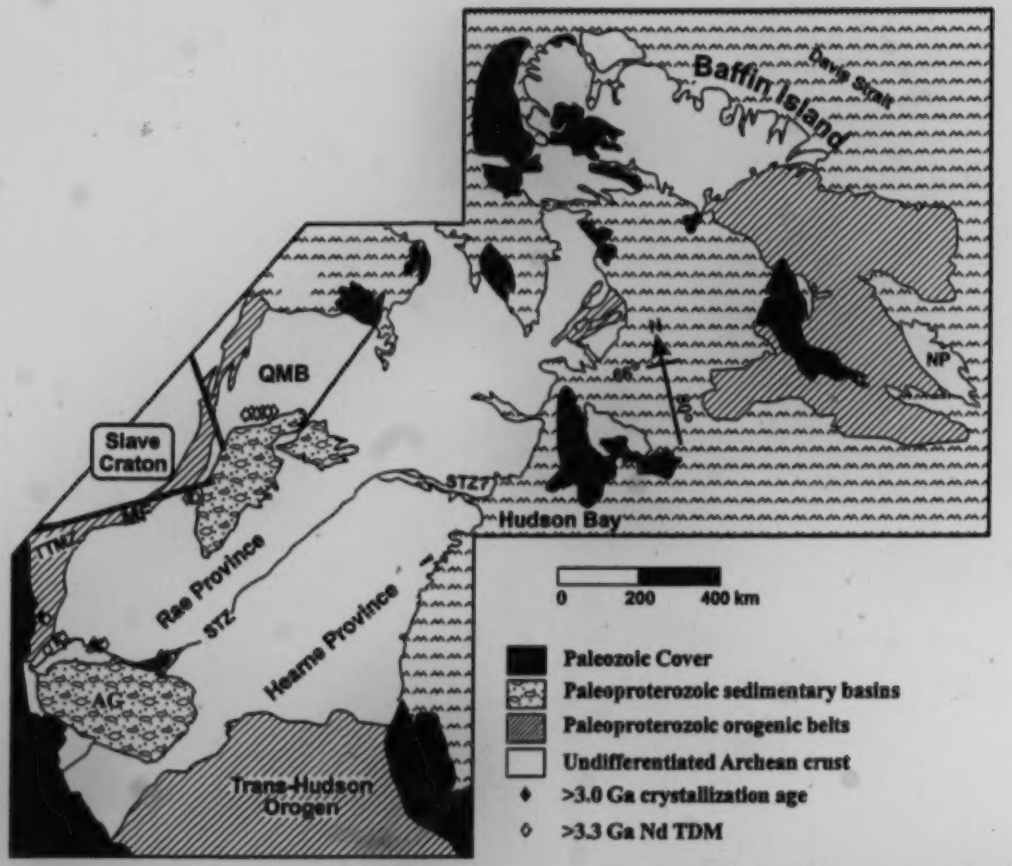

Figure 5-9. Simplified geology of the Churchill craton and bounding tectonic entities. (Modified after Jackson et al., 1990; Wheeler et al., 1996; Scott, 1999; and Skulski et al. 2002). U-Pb crystallization ages and TDM's from De et al., 2000; Dudas et al. 1991; Hanmer et al. 1994a,b; Henderson and Theriault, 1994; McNicoll et al., 2000; Theriault 1992; Theriault et al. 1994;TDM's restricted to those samples with 147Sm/144Nd < 0.14. AG, Athabasca Group;MF, McDonald Fault; NP, Nain Province; QMB, Queen Maud Block; STZ, Snowbird tectonic zone; TTMZ, Taltson-Thelon Magmatic Zone.

Table 5-1. U-Pb results

Sample Description[a]	Weight (mg)	Concentrations (ppm) U	Th[b] model	Pb rad.	Th/U ratio	Pb (pg)[c]	Isotopic Ratios[d] $^{206}Pb/^{204}Pb$	$^{206}Pb/^{238}U$	$^{207}Pb/^{235}U$	$^{207}Pb/^{206}Pb$	Apparent Ages (Ma) $^{206}Pb/^{238}U$	$^{207}Pb/^{235}U$	$^{207}Pb/^{206}Pb$	PD[e]
Prince Lake granite (RH99-869)														
1 Zr, abr (1)	0.005	696	110	298	0.16	44	2128	0.4116±7	9.136±18	0.1610±1	2222.4±3.3	2351.7±1.9	2465.8±1.0	11.66
2 Zr, abr (1)	0.004	392	131	146	0.33	65	513	0.3468±7	7.104±17	0.1486±2	1919.1±3.1	2124.5±2.4	2329.6±2.3	20.34
3 Zr, abr (1)	0.002	325	145	172	0.45	30	729	0.4746±12	11.188±33	0.1710±2	2503.8±5.3	2538.9±2.8	2567.1±2.3	2.97
4 Zr, abr (1)	0.003	406	149	212	0.37	17	2074	0.4770±9	11.149±23	0.1695±1	2514.3±3.9	2535.7±1.9	2552.9±1.0	1.83
5 Zr, abr (1)	0.003	284	114	147	0.40	18	1571	0.4676±8	10.775±22	0.1671±1	2473.0±3.6	2504.0±1.9	2529.1±1.1	2.67
6 Zr, abr (1)	0.002	269	80	139	0.30	8	2404	0.4810±10	11.303±25	0.1705±1	2531.4±4.2	2548.4±2.1	2562.0±1.1	1.44
7 Zr, abr (1)	0.002	644	213	320	0.33	5	8111	0.4591±12	10.417±27	0.1646±1	2435.6±5.2	2472.6±2.4	2503.2±0.8	3.24
Uranium City granite (RH01-06)														
1 Zr, (1)	0.001	248	75	108	0.30	15	440	0.4006±8	9.720±25	0.1760±3	2171.6±3.8	2408.6±2.4	2615.6±2.5	19.96
2 Zr, abr (1)	0.001	1899	935	609	0.49	81	619	0.2961±5	4.494±10	0.1101±2	1672.1±2.2	1729.9±1.9	1800.4±2.7	8.08
3 Zr, abr (1)	0.002	423	42	162	0.10	26	585	0.3787±7	7.779±17	0.1490±2	2070.1±3.2	2205.8±2.0	2334.4±2.0	13.22
4 Zr, abr (1)	0.000	2035	180	714	0.09	13	689	0.3566±6	5.823±13	0.1185±2	1965.9±3.0	1949.9±2.0	1932.9±2.7	-1.98
5 Zr, abr (1)	0.001	88	34	51	0.38	11	274	0.5047±20	14.788±68	0.2125±4	2633.8±8.6	2801.7±4.9	2922.4±3.4	12.10
6 Zr, abr (1)	0.001	321	234	171	0.73	10	452	0.4409±12	11.491±41	0.1890±4	2354.5±5.4	2563.8±3.3	2733.8±3.1	16.53
7 Zr, abr (1)	0.001	192	49	108	0.25	4	2187	0.4899±9	17.006±30	0.2518±1	2570.3±3.7	2935.2±1.7	3195.9±0.8	23.66
Feil Lake granite (4701-299)														
1 Zr, abr (1)	0.001	290	42	107	0.14	4.0	1118	0.3592±9	6.002±22	0.1212±3	1978.3±4.3	1976.1±3.3	1973.8±4.5	-0.3
2 Zr, abr (1)	0.001	519	145	256	0.28	2.0	4353	0.4391±8	13.594±23	0.2245±2	2346.7±3.4	2721.8±1.6	3013.4±1.0	26.3
3 Zr, abr (1)	0.001	191	77	96	0.41	1.3	4276	0.4362±11	12.990±32	0.2160±2	2333.5±4.8	2678.9±2.3	2951.1±1.2	24.9
4 Zr (1)	0.001	733	241	295	0.33	13	1045	0.3632±7	6.801±14	0.1358±2	1997.5±3.1	2085.8±1.8	2174.2±2.0	9.4
5 Zr (1)	0.001	994	363	335	0.37	6.1	1576	0.3039±5	6.109±12	0.1458±1	1710.8±2.7	1991.7±1.7	2297.2±1.3	29.0

Table 5-1. comments

[a] Abreviations: Zr, zircon; abr, air abraded following the techniques of Krogh (1982). The number in parentheses identifies the number of grains or grain fragments analyzed.

[b] Model Th concentration calculated from $^{208}Pb/^{206}Pb$ ratio and $^{207}Pb/^{206}Pb$ age. [c] Total common lead in analysis

[d] Atomic ratios corrected for 2.0 pg Pb and 0.5 pg U in blanks, fractionation, and initial common Pb (Stacey and Kramers, 1975). Uncertainties are reported at 1σ.

[e] PD refers to the percent discordance along a chord to the origin.

Table 5-2: Sm-Nd results

Sample#	Rock Type	UTM (E)	UTM (N)	Sm ppm	Nd ppm	$^{147}Sm/^{144}Nd$	$^{143}Nd/^{144}Nd$	uncert.	TDM[1]	~TMa[2]	eNdT
Mesoarchean basement											
RH98-LBG	Lodge Bay granite	634800	6591125	1.04	5.86	0.1071	0.510887	0.000009	**3.23**	**3060**	**1.2**
RH00-6336	Cornwall Bay granite	643625	6593625	2.13	15.69	0.0822	0.510455	0.000008	**3.12**	**3000**	**1.7**
RH98-125	Sheared granite	647875	6598750	1.71	9.97	0.1039	0.510748	0.000008	**3.33**	*3000*	**-1.0**
Neoarchean granites											
RH98-583	Dead Man granite	665500	6592775	11.93	64.49	0.1119	0.511247	0.000008	**2.85**	**2639**	**1.7**
RH99-869	Prince Lake granite	655675	6611450	6.75	37.03	0.1102	0.511170	0.000008	**2.92**	**2600**	**0.3**
4798-2085b*	Granodiorite	373116	6606407	2.02	13.03	0.0936	0.510898	0.000009	**2.86**	**2550**	**-0.1**
4798-2031c*	Granodiorite	374122	6602281	11.23	77.26	0.0879	0.510750	0.000008	**2.91**	**2550**	**-1.2**
4798-3029*	Granodiorite	403550	6613525	6.18	30.32	0.1232	0.511352	0.000009	**3.03**	2600	**-0.5**
4798-4012*	Granite	430735	6633875	7.23	40.98	0.1066	0.511063	0.000009	**2.97**	**2678**	**0.3**
RH01-08	Sheared leucogranite	643102	6623321	9.96	70.10	0.0859	0.510752	0.000008	**2.86**	*2600*	**0.3**
RH01-09	Granite w/inclusions	651832	6637204	12.64	83.98	0.0910	0.510875	0.000008	**2.83**	*2600*	**1.0**
RH01-10	Foliated granitoid gneiss	657764	6649286	6.38	39.02	0.0989	0.510899	0.000008	**2.99**	*2600*	**-1.2**
RH01-16	Megacrystic granodiorite	613430	6634746	6.56	45.26	0.0877	0.510780	0.000009	**2.86**	*2600*	**0.2**
RH01-17	Megacrystic granodiorite	603762	6643951	15.33	86.11	0.1076	0.511139	0.000008	**2.89**	*2600*	**0.6**
RH01-18	Sheared granite	580439	6706325	4.01	22.58	0.1073	0.511146	0.000009	**2.87**	*2600*	**0.8**
RH01-12	Granodiorite/tonalite	647274	6755121	11.09	59.86	0.1120	0.511180	0.000007	**2.95**	*2600*	**-0.1**
RH99-307a	Sheared granite	663700	6612400	1.54	9.60	0.0972	0.510841	0.000009	**3.02**	*2600*	**-1.8**
RH98-354	Donaldson Lake granite	645900	6609500	1.03	4.34	0.1430	0.511525	0.000025	**N/A**	**2640**	**-3.5**
RH98-354	Donaldson Lake granite	645900	6609500	1.09	4.68	0.1416	0.511529	0.000009	**N/A**	**2600**	**-3.2**
Ca. 1.9 Ga granite											
4701-0299	Feil Lake granite	619280	6600800	1.22	8.63	0.0855	0.510470	0.000009	**3.18**	**1970**	**-14.3**
Supracrustal rocks											
RH98-46	Psammite	653400	6594950	5.43	30.86	0.1063	0.510885	0.000009	**3.21**	*2600*	**-4.0**
RH98-465	Pelite	652750	6597400	5.77	33.73	0.1034	0.510974	0.000009	**3.00**	*2600*	**-1.2**
RH98-439	Intermediate volcanic	654850	6598200	3.98	17.63	0.1366	0.511563	0.000008	**3.14**	*2600*	**-0.9**
RH98-588	Migmatitic psammopelite	666100	6592375	6.26	37.75	0.1002	0.511101	0.000008	**2.75**	*2600*	**2.3**
RH98-90	Quartzofeldspathic gneiss	659550	6594960	5.30	38.14	0.0841	0.510519	0.000007	**3.09**	*2600*	**-3.7**
RH01-20	Psammopelite	568032	6722524	4.67	28.48	0.0991	0.510997	0.000009	**2.86**	*2600*	**0.7**

[1]TDM calculated using the mantle evolution model of Goldstein et al. (1984). N/A indicates Sm/Nd >0.14. [2]Ages in bold are aproximate ages based on U-Pb dating (Hartlaub, unpublished data). Ages in italics are assumed ages for the samples.All UTM's are recorded in zone 12 except sample numbers with a * which are recorded in zone 13.

Chapter 6: Concluding remarks

The Churchill craton of northwestern Canada represents one of the largest exposures of Archean crust in the world. However, most of this craton has been studied only at a reconnaissance scale. The preceding chapters place basic geological and chronological constraints on a small section of crust near the Churchill craton's western margin. This closing chapter attempts to place this new research in the context of the major unresolved craton-wide issues. Many of the conclusions raise new questions which provide avenues for future research.

Mesoarchean basement and its tectonic influences

The Meso- to Paleoarchean basement complex described in chapter 2 and 5 represents one of just a few known areas of >2.9 Ga crust in the Churchill craton. A highlight of chapter 2 is the discovery of new exposures of this basement complex. This basement lies unconformably beneath the Murmac Bay Group (MBG) and the only recognized exposures occur on the western side of the Beaverlodge Belt. The majority of Mesoarchean crust in the Churchill craton appears to be ca. 3.0-3.1 Ga granite. It is exposed along the western margin of the craton (Henderson and Theriault, 1994; McNicoll et al., 2000), within the study area, and within the southern Snowbird Tectonic Zone (Hanmer et al., 1994). The exciting discovery of >3.7 Ga detrital zircons in MBG sediments and Paleoarchean zircon xenocrysts in Paleoproterozoic granite (Chapter 2 and 5) indicates that there are ancient components of the Churchill basement that have yet to be discovered. Whether this ancient basement is currently exposed at the surface is

unclear, but initial results of Nd isotope work north of Lake Athabasca, Saskatchewan, indicate that the oldest crust may lie along the western margin of the Beaverlodge Belt (chapter 5). Because the Churchill craton is so large, a regional Nd study of Archean sediments and granites that incorporates the results from chapter 5 might prove to be the best method of probing the location and extent of the Meso and Paleoarchean crust.

The low metamorphic grade of rocks surrounding the exposed basement block is highlighted in chapter 4. Clearly the basement complex has had an important influence on later metamorphism and deformation. An interesting avenue for future research would be a study of the structural effects of the basement complex on surrounding crust. Such work would require a structural study of the entire western side of the Beaverlodge Belt and a detailed study of the timing and sense of early movement on the Black Bay Fault. Bergeron (2000) recorded multiple episodes of Proterozoic activation on the Black Bay Fault, but it is possible that the fault was initially activated in the basement block as an Archean structure.

Ca. 2.7 Ga rifting in the Rae Province

Chapter 2 places new constraints on the age and tectonic setting of the Murmac Bay Group. The >2.63 Ga and <2.77 Ga age constraints for deposition of the MBG are based on the timing of cross-cutting granites and unconformably underlying basement, as well as by the age of the youngest detrital zircon in psammite. There remains a need to better constrain the timing of MBG sedimentation and volcanism. Is the entire MBG the same age or can it be broken down further on the basis of unconformities or age differences? A potential future avenue for testing the age of MBG volcanism would be Sm-Nd dating of ultramafic and mafic rocks from the area. Potential crust-mantle mixing

in these rocks may, however, make this method untenable. The timing of sedimentation could be better constrained with a more extensive detrital zircon study. This question could be addressed by either a SHRIMP or LA-MC-ICPMS study, and would have the added bonus of providing information on the provenance of MBG detritus.

The similarities in lithology, timing, and tectonic setting between the MBG, the Woodburn Lake Group, the Prince Albert Group, and the Mary River Group is discussed at length in chapter 2. All three of the supracrustal packages have a significant component of quartzite and banded iron formation with interlayered mafic volcanic rock and komatiite. This distinctive assemblage is common in the Archean rock record and has been related to continental extension (e.g. Thurston et al., 1985; Hunter et al., 1998). The chemical composition of low-grade basaltic rocks from the Beaverlodge Belt is consistent with a rift origin but, like Phanerozoic equivalents, a mixed geochemical signal not distinctive of a single tectonic environment is recorded (chapter 2). An important discovery that stems from the work in chapter 2 is the identification of a distinctive population of ca. 3.7 Ga detrital zircon in the MBG sediments. This population has now been identified in all ca. 2.7 Ga Rae Province quartzite packages for which detrital zircon analysis has been done. This ca. 3.7 Ga detrital zircon component is not seen in Proterozoic supracrustal packages such as the Hurwitz (Davis et al., 2003) or Athabasca groups (Rainbird et al., submitted). The presence of ancient detritus in the ca. 2.7 Ga supracrustal packages is consistent with a continental setting for these rocks. The correlation of ca. 2.7 Ga extension-related packages in the Rae Province is one of the most provocative aspects of chapter 2. This correlation would imply the existence of a > 2000 km rift in Archean continental crust.

The ca. 2.6 Ga granite problem

Although this thesis touches only briefly, in chapters 2 and 5, on the topic of ca. 2.6 Ga granites, it is an important part of Churchill craton evolution that needs to be addressed. Ca 2.58-2.64 Ga granitoid magmatism appears to be widespread throughout both the Rae and Hearne provinces. This magmatism is not oriented in a linear belt, nor does it seem to be associated with regional deformation and metamorphism (Davis et al., 2000). The EMP dating of monazite in chapter 4 also indicates that there is no evidence for ca. 2.6 Ga metamorphism or deformation. This lack of crustal thickening associated with the granites makes a subduction related origin for these granites unlikely (Davis et al., 2000). Ongoing regional studies of the age, geochemistry, and isotopic composition of these granites may yield important constraints for their tectonic setting.

The Rae-Hearne connection

Although the nature of the Snowbird Tectonic Zone (STZ) is hotly debated, chapter 4 highlights how the ages of metamorphism and deformation along the structure is similar to ages recorded in the Beaverlodge Belt. Detailed study of the crustal history across this boundary may allow for the development of a robust model for the STZ, and clarify the interrelationship of the Rae and Hearne provinces. At this stage, one of the significant differences appears to be a lack of Archean quartzite packages on the Hearne side of the boundary. Further, ca. $\geq$3.0 Ga granitoid basement to supracrustal packages has not yet been documented from the Hearne Province. The presence of ca. 2.6 Ga granites on both sides of the STZ appears to be the first indication of a shared history for the Rae and Hearne provinces (Davis et al., 2000).

Paleoproterozoic metamorphism, deformation, and plutonism

In addition to the Archean granites discussed in chapter 2, there is a significant volume of Paleoproterozoic granite in the Beaverlodge Belt. Original U-Pb and Pb-Pb dating of these Paleoproterozoic granites (Persons, 1988; O'Hanley *et al.*, 1994) yielded a wide spectrum of ages that was due, in large part, to zircon inheritance and lead loss during later deformation. The data presented in chapter 3 places much tighter constraints on the age of these plutons and highlights how the ca. 2.3 Ga granites are not limited to the Beaverlodge Belt, but are part of a major craton-scale magmatic arc. This magmatic belt is interpreted to be related to subduction and collision along the western margin of the Churchill craton. This period is termed the Blezardian Orogeny after Stockwell (1982). Stockwell (1982) was the first to identify the abundance of ca. 2.3 Ga K-Ar ages in the Churchill craton, but he did not place a tectonic context on these ages or explain why they should be considered to be related to orogeny. The model presented in chapter 3 involves accretion of the Slave to the margin of the Churchill sometime between 2.34 and 2.26 Ga. This accretion closed the east-dipping subduction zone and brought the Blezardian Orogeny to an end. This new model explains the abundance of 2.4-2.26 Ga magmatic rocks on the western margin of the Churchill craton, the cessation of this magmatism by ca. 2.26 Ga, and the relict ca. 2.3 Ga isotopic ages in the Slave craton. A collision of the Slave and Churchill cratons at ca. 2.3 Ga would also explain the lack of arc-like petrology, isotopes, and geochemistry for granites (Chacko et al., 2000; De et al., 2000) from the Taltson-Thelon Magmatic Zone. To test further and improve the tectonic model presented in chapter 3, a detailed geochemical and isotope study of ca. 2.3 Ga magmatic rocks throughout the Churchill craton should be undertaken. New mapping and isotopic studies could be conducted along the western margin of the Churchill craton,

particularly along the Boothia Peninsula and in the Queen Maud Block (Fig. 3-1). A reconnaissance in-situ SHRIMP study of metamorphic monazite from the Queen Maud Block has recently discovered significant evidence for ca. 2.3 Ga metamorphism (Berman, personal communication).

Evidence for Blezardian tectonism in the Beaverlodge Belt is presented in chapter 4. The earliest phase of metamorphism and deformation (M_1/D_1) has been constrained, by monazite and zircon growth, to have occurred at ca. 2.3 Ga (chapter 4). Ca. 2.3 Ga deformation and metamorphism is coincident with the Paleoproterozoic magmatism identified and discussed in chapter 3. A regional study of in-situ metamorphic mineral growth could be conducted in rocks found along the paleo-margin between the western Churchill and Slave Provinces in order to determine the craton-wide effects of D_1/M_1. In particular, $^{40}Ar/^{39}Ar$ studies of muscovite and biotite growth could be conducted along regional shear zones and in-situ monazite and zircon dating could be conducted on metapelites. Since the age of fabrics in ca. 2.3 Ga granites may prove critical, *in-situ* Ar-Ar geochronology on the biotite defining these fabrics is suggested. It is possible, however, that the strong ca. 1.9 Ga overprint highlighted in chapter 4 may have reset this system.

The age of M_2/D_2 in the Beaverlodge Belt is less well constrained than M_1/D_1; however a best estimate for its timing is the ca. 2.0-1.92 Ga chemical ages for metamorphic monazite in the area. This timing is coeval with the intrusion of ca. 1.98-1.93 Ga crustally derived leucogranites in the Beaverlodge Belt (Chapter 5) and magmatism in the Taltson-Thelon Magmatic Zone (McDonough et al., 2000; Chacko et al., 2000).

A significant conclusion from chapter 4 is that in-situ monazite chemical dating and LA-MC- ICPMS isotopic dating is useful for resolving the history of polymetamorphic terranes. This method clearly has a better spatial resolution than the whole grain U-Pb ID-TIMS analyses of metamorphic monazite and zircon, allowing identification of several discrete periods of mineral growth in a single crystal. The 1.92-1.90 Ga low-pressure metamorphism (M_3) overprints the earlier Paleoproterozoic events in most of the studied samples. Exhumation of high-grade rocks in the Beaverlodge Belt and along the Snowbird Tectonic Zone at ca. 1.92-1.90 Ga occurred slightly after ca. 1.99-1.93 Ga plutonism in the Taltson-Thelon Magmatic Zone. Regional exhumation may, therefore, be related to the final phases of Churchill-Slave intracontinental collision.

References

Ashton, K.E., Boivin, D., Heggie, G., 2001. Geology of the Southern Black Bay Belt, west of Uranium City, Rae Province. Saskatchewan Geological Survey, Misc. Rep. 2001-4.2. 50-63.

Bergeron, J. 2000. The deformational history of the Black Bay Structure in Uranium City, Northern Saskatchewan. Unpublished thesis, University of Saskatchewan, Saskatoon, Saskatchewan.

Chacko, T., De, S.K., Creaser, R.A., and Muehlenbachs, K. 2000. Tectonic setting of the Taltson magmatic zone at 1.9-2.0 Ga: a granitoid-based perspective. Canadian Journal of Earth Sciences, 37: 1597-1609.

Davis, W.J. and nine others. 2000. Regional Differences in the Neoarchean evolution of the Western Churchill Province: Can we make sense of it?. Geocanada 2000, Calgary, Alberta, abstract volume

Davis, W.J., Aspler, L.B., Rainbird, R., and Chiarenzelli, J. 2000. Detrital zircon geochronology of the Proterozoic Hurwitz and Kiyuk Groups: A revised post-1.92 Ga age for deposition of the upper Hurwitz Group. Geocanada 2000, Calgary, Alberta, abstract volume.

De, S.K., Chacko, T., Creaser, R.A., and Muehlenbachs, K. 2000. Geochemical and Nd-Pb-O isotope systematics of granites from the Taltson Magmatic Zone, NE Alberta:

implications for early Proterozoic tectonics in western Laurentia. Precambrian Research, **102**: 221-249.

Hanmer, S., Parrish, R., Williams, M., and Kopf, C. 1994. Striding-Athabasca Mylonite Zone - Complex Archean Deep-Crustal Deformation in the East Athabasca Mylonite Triangle, Northern Saskatchewan. Canadian Journal of Earth Sciences, **31**: 1287-1300.

Henderson, J.B., Thériault, R.J., 1994. U-Pb zircon evidence for circa 3.1 Ga crust south of the McDonald Fault, northwestern Canadian Shield, Northwest Territories. Geological Survey of Canada, Current Res. 1994-F, 43-47.

Hunter, M.A., Bickle, M.J., Nisbet, E.G., Martin, A., and Chapman, H.J. 1998. Continental extension setting for the Archean Belingwe Greenstone Belt, Zimbabwe. Geology, **26**: 883-886.

McDonough, M.R., McNicoll, V.J., Schetselaar, E.M., and Grover, T.W. 2000. Geochronological and kinematic constraints on crustal shortening and escape in a two-sided oblique-slip collisional and magmatic orogen, Paleoproterozoic Taltson magmatic zone, northeastern Alberta. Canadian Journal of Earth Sciences, **37**: 1549-1573.

McNicoll, V.J., Thériault, R.J., and McDonough, M.R. 2000. Taltson basement gneisses: U-Pb and Nd isotopic constraints on the basement to the Taltson magmatic zone, Northeastern Alberta, Canadian Journal of Earth Sciences, **37**: 1575-1596.

O'Hanley, D.S., Kyser, K.T., and Sibbald, T.I.I., 1994. The age and origin of the North Shore Plutons in the Rae Province, Goldfields area, Saskatchewan; Canadian Journal of Earth Sciences, **31**: 1397-1406.

Persons, S.S., 1988, U-Pb geochronology of Precambrian rocks in the Beaverlodge area, Northwestern Saskatchewan. M.Sc. Thesis, Lawrence, University of Kansas, 68p.

Rainbird, R.H., Stern, R.A., Rayner, N., and Jefferson, C.W. Submitted. Age, provenance and regional correlation of the Athabasca Group constrained by igneous and detrital zircon geochronology. EXTECH IV Athabasca Uranium Multidisciplinary Study.

Thurston, P.C., Ayres, L.D., Edwards, G.R., Gelinas, L., Ludden, J.N., Verpaelst, P., 1985. Archean bimodal volcanism. In: Ayres, L.D., Thurston, P.C., Card, K.D., Weber, W. (Eds.), Evolution of Archean Supracrustal Sequences. Geological Association of Canada, Special Paper 28. 7-21.